Hydrothermal Treatment of Bitumen Froth at 250 °C:

Impact on Bitumen Properties and Role of Clay Minerals

by

Annapurna Sri Sowmya Turuga

A thesis submitted in partial fulfillment of the requirements for the degree of

Doctor of Philosophy

in

Chemical Engineering

Department of Chemical and Materials Engineering
University of Alberta

Abstract

Bitumen froth produced in the hot water extraction process of mined oil sands consists of about 60 wt % bitumen, 30 wt% water and 10 wt% mineral solids. To convert the bitumen in bitumen froth into a marketable product, the water and solids need to be separated. Solvent-based froth treatment processes are currently employed in industry to treat the bitumen froth. These processes are operated in the temperature range 30-85 °C. Depending on the process type (naphthenic vs. paraffinic froth treatment), the resultant bitumen product is either diluted and transported to a high conversion refinery, or fully upgraded to synthetic crude oil that can be processed in a conventional refinery. Partial upgrading of bitumen is a compromise between the two extremes of dilution and full upgrading.

In this context, a modified froth treatment process called 'hydrothermal treatment', in which the bitumen froth is directly heated without solvent addition to temperatures higher than those used in the current froth treatment processes, is investigated in this thesis. It is anticipated that application of higher temperature can promote reactions in the froth in the presence of water and mineral solids, leading to partial bitumen upgrading, in addition to assisting with froth separation. Previous research on hydrothermal treatment of bitumen froth focused on the separation characteristics of the process. In this thesis, the focus is on investigating the effect of hydrothermal treatment of bitumen froth at moderate conditions (250 °C) on changes in bitumen properties, and the possible role of mineral solids in this process.

Reactions performed with industrial bitumen froth indicated that hydrothermal treatment at 250 °C did not lead to partial upgrading of bitumen. Treatment of bitumen at 250 °C was beneficial only when bitumen was treated on its own. Among the properties tested, viscosity and total acid

number of bitumen increased significantly after hydrothermal treatment compared to untreated bitumen. An increase in the viscosity of bitumen samples was accompanied by an increase in their free radical content. Minerals, in particular, promoted an increase in the free radical content of bitumen after thermal treatment. Among the various hypotheses that were evaluated against experimental results, generation of additional free radicals by redox reactions and increased radical addition in the presence of minerals seemed to be a plausible explanation for the observed increase in bitumen viscosity. The increase in TAN after hydrothermal treatment was tentatively explained by base-catalyzed hydrolysis of esters and anhydrides, promoted by the bases in bitumen froth.

Further, free radical and acid-catalyzed (cationic) addition reaction pathways, which are potential ways by which the clay minerals in bitumen froth may promote heavier material formation were examined using model compounds α-methyl styrene (AMS) and 1-octene, instead of bitumen froth, at a reaction temperature of 250 °C. Pure thermal conversion of probe molecules was low compared to mineral related conversion. Dimerization of AMS and alkylation of 1-octene and toluene (used as solvent) were identified as major reactions in the presence of minerals, indicating that clay minerals promoted heavier material formation. Additional reactions performed in the presence of minerals and pyridine, used as surrogates for alkaline bitumen froth, and selectivity to different product isomers that enabled differentiation between free radical and cationic pathways, indicated that the mineral related conversion was predominantly cationic in nature. Some conversion of probe molecules to addition products was observed in the presence of minerals and pyridine suggesting that minerals could promote heavier material formation through cationic addition even under alkaline conditions. The possible occurrence of side reactions such as transfer hydrogenation and isomerization in the presence of clay minerals during hydrothermal treatment

was also indicated in this work. No evidence was provided in this study to support the claim that clay minerals promote free radical addition reactions.

This thesis sought to test whether the use of a new modified approach for bitumen froth treatment can contribute to partial bitumen upgrading. When that was proved not to be the case, it raised questions about the fundamental chemical mechanisms of organic molecules on clay minerals responsible for heavier material formation. Using model compounds, this study revealed, for the first time, that the clay minerals in bitumen froth can promote cationic addition reactions at a temperature of 250 °C, even under alkaline conditions.

Preface
(Mandatory due to collaborative work)

Chapter 3 of this thesis was published as "Turuga, A. S. S.; De Klerk, A. Hydrothermal Treatment of Bitumen Froth: Impact of Mineral Solids and Water on Bitumen Properties. *Energy Fuels* **2021**, *35*, 17536–17550". I was responsible for concept formation, experimental design, data collection and analysis as well as manuscript composition. I was also the corresponding author, and I was responsible for presenting portions of this work at the American Chemical Society (ACS) Spring Meeting 2021 (oral presentation), Future Energy Systems Digital Research Showcase 2020 (poster presentation) and Petrophase 2023 (oral presentation). Arno de Klerk acted as the supervisory author and was involved in the concept formation, data interpretation and manuscript composition.

Chapter 4 of this thesis was published as "Turuga, A. S. S.; De Klerk, A. Free Radical and Cationic Addition due to Clay Minerals Found in Bitumen Froth at 250 °C Probed with Use of α-Methylstyrene and 1-Octene. *Energy Fuels* **2022**, *36* (23), 14148–14162." I was responsible for concept formation, experimental design, data collection and analysis as well as manuscript composition. I was also the corresponding author, and I was responsible for presenting portions of this work at the American Chemical Society (ACS) Spring Meeting 2021 and Petrophase 2023 (oral presentation). Arno de Klerk acted as the supervisory author and was involved in the concept formation, data interpretation and manuscript composition.

Acknowledgements

First and foremost, I would like to thank my supervisor Dr. Arno de Klerk for his guidance and support through all these years. His detailed feedback and coaching in various tasks greatly contributed to my learning and motivated me to keep improving. He encouraged me to ask questions and think critically, which pushed me to try to better understand the way things work. Besides study-related matters, he always encouraged me to keep up with my hobbies and activities that I enjoy outside work, to have a well-rounded life.

Next, I thank my entire research team for their help, support and friendship throughout my campus life. They created a fun learning atmosphere in the labs and meeting rooms with their presence. I would like to specially thank a few: Natalia and Felipe, for their collaboration in some side projects during the initial months of my PhD. Working with them and discussing experimental strategies triggered new ideas. Giselle, Garima, Felix, Cloribel and Tudor, for training me on new lab equipment. Cibele, for being an amazing lab manager and helping me conduct research activities by ordering chemicals and microreactors in a timely manner. Joy, Kaushik, Glaucia and Lina, for engaging in technical conversations with me and clarifying my doubts.

I cannot imagine my PhD journey without my friends (and family) in Edmonton Mani, Hari and Shibashis who never let me feel lonely during the global pandemic; Sumanth, without whom I wouldn't be the person I am today. Thank you for always being there for me when I needed someone.

I am blessed to have my loving husband Bhargav in my life, and thank him for always believing in me, wanting me to be independent and cheering for me from thousands of miles away.

I am thankful to my parents, sister and extended family in India and USA for all of their love, support and blessings.

I would like to sincerely thank the University of Alberta, Edmonton, for supporting my graduate studies.

Table of Contents

List of Tables

xiv

List of Figures

Chapter 1. Introduction

1.1. Background

Petroleum, also called crude oil, or simply oil, is one of the most important raw materials that we have. Historically, oil has been the largest major energy source, contributing to about one-third of the global primary energy consumption.[1] Petroleum products made from crude oil are used for transportation, heating, electricity generation and production of thousands of intermediate and end-user goods such as plastics, synthetic materials and chemicals.

Canada, which consists over 26 billion cubic metres of oil reserves (as of December 2020) that are recoverable under current economic and technological conditions, is the fourth largest producer of oil in the world.[2] Oil reserves in Canada are classified into conventional oil and unconventional oil sands reserves. Generally speaking, the term 'unconventional oil' in the oil and gas industry refers to crude oils that cannot be produced or transported using traditional techniques, due to their unusual compositions or inaccessible placements.

Oil sands represent about 97 % of the proven oil reserves in Canada,[2] and are a key driver of Canada's economy. Oil sands are a mixture of mineral particles, water and the oil component called bitumen. Bitumen is the heaviest and thickest form of petroleum. Due to its high viscosity and poor fluidity at reservoir conditions and pipeline temperatures, bitumen cannot be recovered from the oil sand deposits using conventional recovery methods or transported in pipeline using conventional transportation methods.[3]

The depth at which the oil sand deposits are located determines the method used for bitumen extraction. Oil sand deposits located at a depth of 75 m or less can be recovered using surface

mining techniques,[4] and represent twenty percent of the recoverable oil sand reserves in Canada.[2] Bitumen from deeper deposits (>75 m) is recovered by in-situ methods. The current research is relevant only to bitumen production by mining.

The mined oil sands ore is transported to a processing plant, where it is crushed and then mixed with a large volume of warm water to produce a slurry. The slurry is pumped to the main extraction plant through a conditioning pipeline, called hydrotransport line, where shear forces act on the oil sand lumps and break them apart, releasing bitumen droplets. The bitumen droplets attach to free air bubbles in the flow, which are produced from the air entrained in the ore or added to the pipeline.[5,6] In addition, sodium hydroxide is sometimes added to increase the pH to about 8.5 and aid in the release of bitumen from the sand grains.[6] When the conditioned slurry reaches the main extraction unit, a gravity-based separation process is used to separate the components. Bitumen attached to air bubbles or aerated bitumen is lighter due to its high air content and rises to the top of the unit, while the heavy solid particles sink to the bottom. However, recovering pure bitumen in the extraction process is difficult due to complex interactions between the components. As a result, some fine solids, clay particles and emulsified water still linger with the aerated bitumen, and the mixture is collectively known as the bitumen froth. As aerated froth cannot be pumped easily, the air bubbles are removed from froth by sparging with steam. Deaerated bitumen froth, produced this way in the hot water extraction process, is a mixture consisting of 45-65 wt % bitumen, 20-35 wt % water and 5-15 wt % mineral solids,[7] and bitumen froth is the material of interest in this thesis.

Currently, in the oil sands industry, the bitumen froth is further cleaned through the addition of a light hydrocarbon solvent. In this step, called the froth treatment, solvent addition aids in the removal of mineral solids and water from bitumen froth by reducing the viscosity of bitumen. Two

2

different technologies for froth treatment, called the naphthenic froth treatment (NFT) and paraffinic froth treatment (PFT) are employed in industry, based on the two types of solvents (naphtha and paraffinic solvent respectively) used, and they are operated at temperatures below 80 °C.[6] Solvent is recovered from the resultant bitumen-solvent product stream in a solvent recovery unit and recycled back. The commercial froth treatment processes are described in more detail in Chapter 2 (Literature Review).

After the solvent is recovered from the bitumen-solvent product stream of froth treatment, the remaining bitumen product is very viscous at ambient conditions and cannot be transported by pipeline. The pipeline specifications for crude oil transportation are 0.5 vol % maximum content of bottom solids and water, and a viscosity of 350 cSt (3.5×10^{-4} m^2/s) at pipeline temperature.[6] The bitumen product from NFT doesn't meet these specifications, whereas the product from PFT meets the bottom solids and water specification, but not the viscosity targets.

Upgrading and dilution are the two main strategies that are currently used in industry to enhance the fluidity of bitumen generated in froth treatment and enable pipeline transport to refineries, where useful products such as petrochemicals and transportation fuels are produced.

Upgrading is achieved through removal of undesirable components from bitumen using chemical separation processes and/or application of high temperature reactions to reduce the heavy fractions of bitumen as well as lower the sulfur and nitrogen contents.[6] The product of upgrading is a light synthetic crude oil (SCO), which is slightly better in quality than conventional crude oil and can be processed in a conventional refinery.[6] However, upgrading bitumen requires significant investment and its economics depends mainly on the price difference between light synthetic and

heavy crude that needs to offset the capital, maintenance and operating costs of the upgrading facilities.

In the case of dilution, the low-quality bitumen is mixed with a solvent such as natural gas condensate or naphtha. Diluted bitumen is much lower in quality compared to SCO,[8] and is transported to a high conversion refinery, which is capable of processing heavier feedstocks. At the refinery, the diluent is recovered and returned to the bitumen production facility for reuse. The diluent makes up about one-third of the diluted bitumen product, limiting pipeline capacity and driving up costs, as the overall cost of transporting bitumen would include the cost of purchasing and transporting the diluent.[9]

The solution to the economic constraints to upgrading and the use of dilution may lie in partial upgrading. Partial upgrading is the middle ground between the two extremes of full upgrading and dilution, in which the quality of bitumen is improved just to the level sufficient enough to reduce or eliminate diluent addition and meet pipeline specifications. Reduction or elimination of diluent allows freeing up pipeline capacity, and the capital and operating costs in partial upgrading are lower compared to SCO production.

A potential way to achieve partial upgrading as part of froth treatment and address bitumen fluidity earlier in the process is to perform the froth treatment at higher temperatures to promote reactions in the froth. To be clear, unlike the current practice of upgrading bitumen after the separation of water and solids in froth treatment, the proposed modification explored in this thesis aims to partially upgrade bitumen while it is still present along with the mineral solids and water in the froth through the application of high temperature. In addition, increasing the operating temperature

(>80°C) may assist with the separation of water and solids from bitumen. This alternate approach to froth treatment has been called hydrothermal treatment.[10,11]

Hydrothermal treatment is the direct heating of bitumen froth, produced in the hot water extraction process, without solvent addition. Previous work on hydrothermal treatment mainly focused on the separation characteristics of bitumen froth in the temperature range 300-420 °C.[10] At the studied conditions, the modified process effectively removed fine solids and water from bitumen resulting in amounts as low as 0.08 wt% solids and 0.03 wt % water in the bitumen product.[10]

One of the important questions that still remains unanswered is whether hydrothermal treatment of bitumen froth results in partial upgrading of bitumen. In other words, would the combination of bitumen, water (hydro), high temperature (thermal) and mineral solids in the hydrothermal froth treatment process improve the quality of bitumen?

Conversion of bitumen in the presence of 4-8 wt% of native mineral solids and 8-12 wt% water at 425-510 °C was patented by Sankey, et al.[12] It was found that the patented process gave better results in terms of viscosity reduction and removal of sulfur and heavy metals, compared to the conventional thermal conversion of bitumen on its own. Similar studies were performed with heavy oils to reduce their viscosity in the presence of water and solid catalysts, including minerals, and the process was known as catalytic aquathermolysis.[13] Aquathermolysis of heavy oil in the temperature range 160-280 °C in the presence of minerals resulted in up to 30 % viscosity reduction.[13] Literature on the catalytic properties of minerals and the physical and chemical effects of water in thermal upgrading reactions are discussed in more detail in Chapter 2.

So far, no work was conducted with bitumen froth to study the impact of mineral solids and water on the thermal conversion of bitumen. Further, the test conditions used in the above mentioned

studies including bitumen, minerals and/or water were severe (> 300 °C), and whether the same benefits could be obtained at less severe conditions or not, hasn't been evaluated.

In literature, there is evidence that free radical reactions and macroscopic changes can occur in bitumen at temperatures as low as 200 °C,[14,15] which is below the thermal cracking temperature of most of the organic molecules in bitumen. However, these studies were performed using bitumen and asphaltenes (a fraction of bitumen) after the removal of bulk solids and water. In the froth treatment process investigated in this thesis, the reaction system contains two liquid phases (water and bitumen) and an order of magnitude higher solids content. It is of interest to explore the physical and chemical changes in bitumen caused by hydrothermal treatment in the temperature range 200-300 °C.

Further, little work was done to understand the chemistry that takes place on the surface of the solids and how it affects bitumen conversion. In this context, investigating the role of clay minerals can be useful, as they are known to exhibit redox properties and function as acid catalysts.[16-20] Clay minerals in bitumen froth constitute 40-70 wt% of the total solids in the froth, and are expected to influence bitumen conversion during hydrothermal treatment, potentially by promoting free radical reactions. Additionally, although the froth is slightly alkaline in nature (pH ~ 8.3), the contribution of the surface acidity of clays to the reaction chemistry cannot be ignored.

1.2. Objectives and Scope of Work

The main objective of the current work is to investigate the impact of mineral solids on bitumen upgrading in the hydrothermal froth treatment process and understand the reaction chemistry taking place in the presence of solids. To achieve this, the following sub-objectives were identified:

a) To investigate hydrothermal treatment of bitumen froth, i.e. treatment of bitumen in the presence of both mineral solids and water as potential process for bitumen upgrading

b) To determine the individual and collective effects of water and mineral solids on the physical and chemical changes in bitumen upon thermal treatment

c) To understand the nature of reactions that are promoted by the mineral solids in bitumen froth.

The development of experimental work conducted in this thesis benefited from previous literature works mainly related to froth treatment, thermal conversion of bitumen, catalytic aquathermolysis of heavy oils and organic-clay interactions, which were critically reviewed and discussed in Chapter 2.

The approach that was taken to meet the objectives of this work was to first evaluate the role of hydrothermal froth treatment on bitumen upgrading (Chapter 3). The benefits of hydrothermal treatment of bitumen froth at less severe temperature (250 °C), which were not investigated before, was evaluated in this study. This is a temperature that could be achieved by steam heating without the need to use a furnace, and also at which conversion reactions can occur. In Chapter 3, analysis of bitumen properties was performed to determine the individual and collective impact of water and minerals on bitumen conversion at 250 °C.

Chapter 4 focused on investigating the nature of reactions promoted by the clay minerals that potentially led to the viscosity changes observed in the bitumen phase in Chapter 3. Free radical reaction vs. cationic reaction (initiated by the acid sites) pathways occurring in the presence of the clay minerals kaolinite and illite were explored. These two reaction pathways were distinguished using an organic base to reduce the contribution of cationic reactions, and to mimic the alkaline nature of the bitumen froth.

The main conclusions and recommendations for future research can be found in Chapter 5.

1.3. References

(1) Statistical Review of World Energy - All Data, 1965-2021. *BP Statistical Review of World Energy* [Online]; London, 2022. https://www.bp.com/en/global/corporate/energy-economics/statistical-review-of-world-energy.html (accessed Nov 5, 2022).

(2) *Energy Fact Book 2021-2022*; ISSN 2370-3105; Natural Resources Canada; Canada, 2021; pp 96–146.

(3) De Klerk, A. Unconventional Oil: Oilsands. In *Future Energy: Improved, Sustainable and Clean Options for Our Planet*, 3rd ed.; Letcher, T. M., Eds.; Elsevier: Amsterdam, Netherlands, 2020; pp 49–65.

(4) Strausz, O. P.; Lown, E. M. 2003. *The Chemistry of Alberta Oil Sands, Bitumens and Heavy Oils*; Alberta Energy Research Institute: Calgary, Canada, 2003; p 24.

(5) Masliyah, J.; Zhou, Z. J.; Xu, Z.; Czarnecki, J.; Hamza, H. Understanding Water-Based Bitumen Extraction from Athabasca Oil Sands. *Can. J. Chem. Eng.* **2004**, *82* (4), 628–654.

(6) Gray, M. R. *Upgrading Oilsands Bitumen and Heavy Oil*; Pica Pica Press: Edmonton, Canada, 2015; pp 5–238.

(7) Czarnecki, J.; Masliyah, J.; Xu, Z.; Dabros, M. *Handbook on Theory and Practice of Bitumen Recovery from Athabasca Oil Sands - Volume 2: Industrial Practice*; Kingsley Knowledge Publishing: 2013; p 214.

(8) Gray. M. R. Fundamentals of Partial Upgrading of Bitumen. *Energy Fuels* **2019**, *33* (8), 6843–6856.

(9) De Klerk, A. Processing Unconventional Oil: Partial Upgrading of Oilsands Bitumen. *Energy Fuels* **2021**, *35* (18), 14343–14360.

(10) Chen, Q.; Stricek, I.; Cao, M.; Gray, M. R.; Liu, Q. Influence of Hydrothermal Treatment on

Filterability of Fine Solids in Bitumen Froth. *Fuel* **2016**, *180*, 314–323.

(11) Zhao, J.; Liu, Q.; Gray, M. R. Characterization of Fine Solids in Athabasca Bitumen Froth

Before and After Hydrothermal Treatment. *Energy Fuels* **2016**, *30* (3), 1965–1971.

(12) Sankey, B. M.; Maa, P. S.; Bearden, R., Jr. Conversion of the Organic Component from Tar

Sands to Lower Boiling Products. U.S. Patent 5,795,464, August 18, 1998.

(13) Fan, H.; Zhang, Y.; Lin, Y. The Catalytic Effects of Minerals on Aquathermolysis of Heavy

Oils. *Fuel* **2004**, *83*(14–15), 2035–2039.

(14) Yañez Jaramillo, L. M.; De Klerk, A. Partial Upgrading of Bitumen by Thermal Conversion

at 150–300° C. *Energy Fuels* **2018**, *32* (3), 3299–3311.

(15) Naghizada, N.; Prado, G. H. C.; De Klerk, A. Uncatalyzed Hydrogen Transfer during 100–

250 °C Conversion of Asphaltenes. *Energy Fuels* **2017**, *31* (7), 6800–6811.

(16) Solomon, D. H. Clay Minerals as Electron Acceptors and/or Electron Donors in Organic

Reactions. *Clays Clay Miner*. **1968**, *16* (1), 31–39.

(17) Worasith, N.; Ninlaphurk, S.; Mungpayaban, H.; Wen, D.; Goodman, B. A. Characterization

of Paramagnetic Centres in Clay Minerals and Free Radical Surface Reactions by EPR

Spectroscopy. In *Clays and Clay Minerals: Geological Origin, Mechanical Properties and

Industrial Applications*, Wesley, L. R.; Eds.; Nova Science Publ.: New York, NY, 2014; pp

336–359.

(18) Gorski, C. A.; Aeschbacher, M.; Soltermann, D.; Voegelin, A.; Baeyens, B.; Marques

Fernandes, M.; Hofstetter, T. B.; Sander, M. Redox Properties of Structural Fe in Clay

Minerals. 1. Electrochemical Quantification of Electron-Donating and -Accepting Capacities

of Smectites. *Environ. Sci. Technol.* **2012**, *46* (17), 9360–9368.

(19) Nagendrappa, G. Organic Synthesis Using Clay Catalysts. *Reson.* **2002**, *7* (1), 64–77.

(20) Soma, Y.; Soma, M. Chemical Reactions of Organic Compounds on Clay Surfaces. *Environ. Health Perspect.* **1989**, *83*, 205–214.

Chapter 2. Literature Review

2.1. Introduction

As mentioned in Chapter 1, bitumen froth is a complex mixture consisting of about 45-65 wt % bitumen, 20-35 wt % water and 5-15 wt % mineral solids.[1] To investigate the role of hydrothermal froth treatment for converting bitumen in the presence of mineral solids and water, it is essential to understand the basic characteristics and behavior of each of these froth components.

Bitumen has been extensively characterized (details can be found in the book by Strausz and Lown).[2] An overview of some of the basic properties of bitumen, which are considered important for this thesis, is provided in this chapter. Although characterization of froth solids in literature was not performed as extensively as bitumen, some information is available in literature. Each of the studies had a different purpose behind conducting froth solids characterization, but they were generally related to the investigation of separation efficiency of the hot water extraction and froth treatment processes for bitumen recovery. In addition, different methods were used to isolate the mineral solids from the froth for characterization. Finally, characterization of the water phase in bitumen froth has not been reported in literature until recently.

Before proposing hydrothermal treatment as a potential modified process intensification method of froth treatment, an overview of the state-of-the-art knowledge of the current industrial froth treatment operations, highlighting the main differences between the two types of solvent-based froth treatment (naphthenic and paraffinic), and on-going research, is provided with an aim to identify gaps and offer recommendations for future research. Considering bitumen froth as a whole, the presence of water-in-oil emulsions poses challenges for separating the water and solids from the bitumen froth. This phase separation problem and the factors contributing to the stability

of emulsions are briefly highlighted in the current chapter to justify the role of froth treatment processes in bitumen recovery.

Hydrothermal froth treatment, which is the direct thermal processing of bitumen froth in the absence of a hydrocarbon solvent, involves the application of higher temperatures (> 85 °C) than those used in the current froth treatment processes with an anticipation to promote partial bitumen upgrading. Due to this, the thermal and hydrothermal characteristics of the froth components are summarized in this chapter. First, the thermal behavior of bitumen in the absence of bulk solids and water, and in the ≤ 400 °C temperature range, in terms of the physical and chemical property changes and free radical chemistry, is discussed. Later, the behavior of high-temperature water and studies performed using both water and mineral solids at hydrothermal conditions are reviewed. Thermal alteration of mineral solids and potential reaction pathways, especially in the presence of clay minerals, are described.

To summarize, the purpose of this literature review is to gain an understanding of the key elements of the oil sands bitumen froth characterization and treatment processes, as well as the behavior of the froth components at hydrothermal conditions. The literature review is divided into four subtopics: 1. characteristics of the bitumen froth components, which are the bitumen, water and mineral solids; 2. froth treatment processes – types, challenges and research opportunities; 3. thermal conversion behavior of bitumen, mainly at lower temperatures (100−400 °C); 4. characteristics of hydrothermal conversion, and the behavior of mineral solids and water, with special focus on the clay minerals, at hydrothermal conditions

The knowledge gained from the review of existing scientific literature was used for experimental planning, and in the analysis of the reaction products and interpretation of the data generated in this thesis.

2.2. Bitumen Froth and its Components

The basic characteristics of bitumen, and the composition of mineral solids and water in the bitumen froth, are separately summarized in this section.

2.2.1. Characteristics of Bitumen

As mentioned in Chapter 1, bitumen is the heaviest and thickest form of petroleum, with a density > 1000 kg/m^3 (API gravity < 10 °API) and viscosity > 10^2 Pa.s, at the standard temperature of 15 °C.[2] The information presented in this section on the bitumen characteristics, was mainly extracted from Refs. (1) and (2).

The elemental composition of bitumen is in the range: carbon 83.1 ± 0.5 wt %, hydrogen 10.3 ± 0.3 wt %, nitrogen 0.4 ± 0.1 wt %, oxygen 1.1 ± 0.3 wt % and sulfur 4.6 ± 0.5wt %.[2] Bitumen contains lower hydrogen to carbon (H/C) ratios (1.45-1.6) than conventional crude oil, with H/C ratios up to 2.0,[2] which indicates the lower paraffinic and higher naphthenic and aromatic nature of bitumen. In addition, bitumen contains higher heteroatom (N, S, O) content and higher metals content than most conventional crude oils. The properties of Athabasca bitumen are compared with West Texas Intermediate (WTI) in Table 2-1.[3] WTI is a benchmark in crude oil pricing i.e. it serves as a reference price used by sellers and buyers of crude oil.

Table 2-1. Physical and Chemical Properties of Conventional Crude Oil vs. Bitumen.[3]

Crude Oil	Density (kg/m^3)	Viscosity (m^2/s ×10^6) at 40°C	Sulfur (wt %)	Nitrogen (wt %)	Metals (ppm by weight)
West Texas Intermediate	821	4	0.3	0.08	3.2
Athabasca Bitumen	1007	7000	4.9	0.5	280

Heavy oils and bitumen are a result of microbial degradation of light crude oil, which occurs under the action of aerobic and anaerobic heterotrophic bacteria (bacteria that use organic carbon for growth).[4] Such biodegradation results in enrichment of sulfur and metals, and preferential removal of light, saturated hydrocarbons, making the oil (bitumen) heavy and rich in heavy organic compounds.[4]

Figure 2-1 contains some illustrative hydrocarbon and heteroatom-containing organic compounds in bitumen. Hydrocarbons in bitumen can be classified into three main types: paraffinic, naphthenic and aromatic. Strausz and Lown reported the occurrence of the majority of sulfur in petroleum and bitumen in the rings of cyclic, mainly aromatic compounds.[2] These include thiophenic sulfur species and cyclic organic sulfides. Lesser amounts of sulfur are present in the form of linear chain sulfides and sulfoxides. Next, nitrogen in petroleum and bitumen is present in two main forms: basic pyridine derivatives and non-basic pyrrole derivatives. Additionally, metalloporphyrin structures containing nitrogen and the metals Ni and V also commonly occur in bitumen. In Alberta bitumens, oxygen mainly occurs in the form of carboxylic acid groups, and is also present in alcoholic hydroxyl groups and carbonyl groups of esters, ethers and ketones. Naphthenic acids, which comprise of naphthenic structures attached to carboxylic acid groups, account for ~1-2 wt % of bitumen, and are responsible for an important property of bitumen called total acid number (TAN). Finally, the most abundant metals found in the mineral-free bitumen are Al, Fe, Na, K, Ni, V and Ti (Ca and Mg were not reported). The metals Ni and V are considered to play an important role in obtaining information about the depositional environment and origin of the crude oil.[2] These metals are reported to mainly occur in the form of porphyrins, as shown in Figure 2-1.
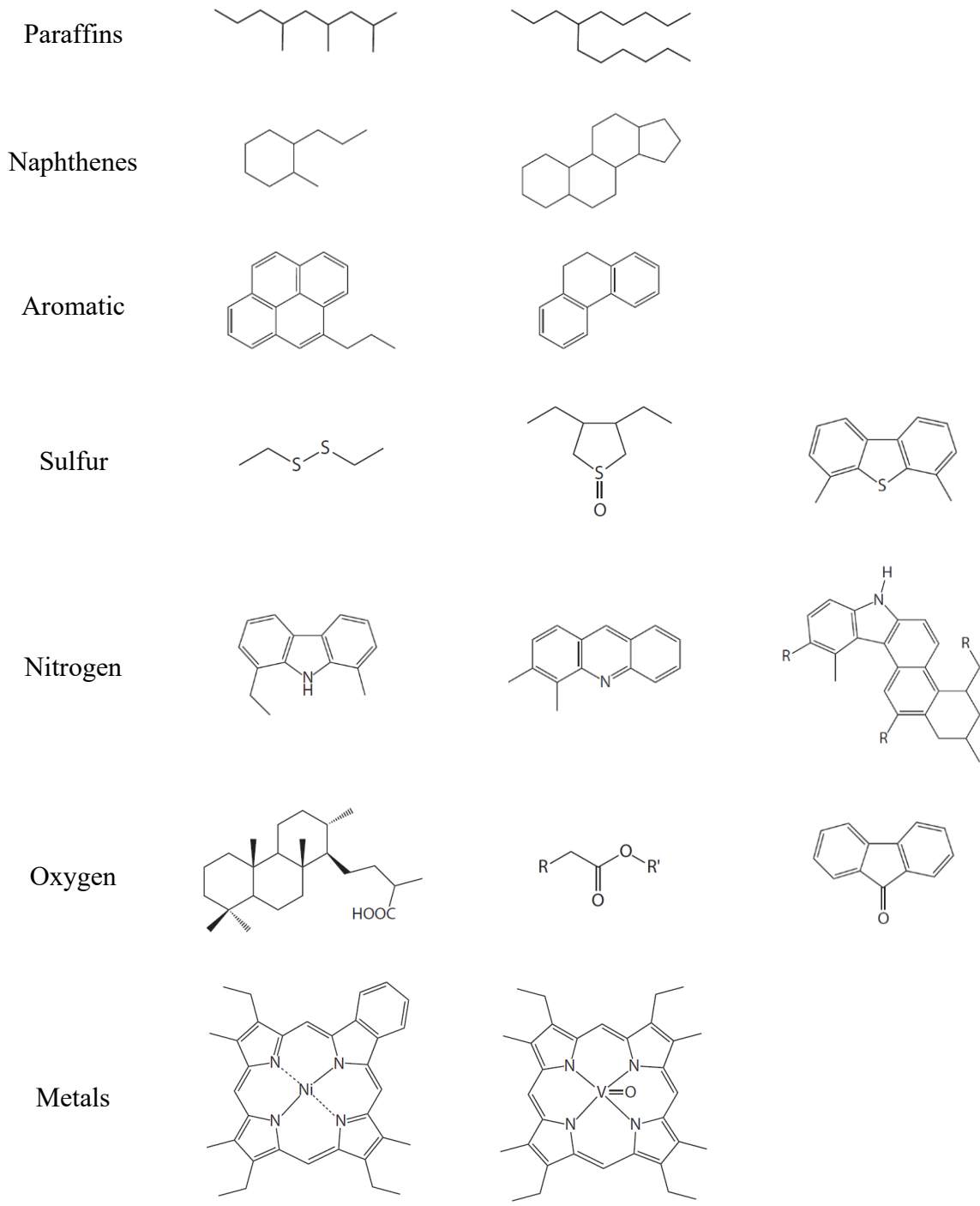
Figure 2-1. Representative Compounds in Petroleum and Bitumen.[3]

The fraction of bitumen with boiling point greater than 524 °C is called vacuum residue.[2] Bitumen contains about 50 vol% of vacuum residue.[3] Most of the physical properties in bitumen can be correlated with its chemical composition.[2,3] For example, the densities of Alberta bitumens and heavy oils can be correlated with their elemental composition using Eq 2-1.[3]

$$\rho = 1033 - 13.69H + 13.85S + 115.7N \qquad \text{Eq 2-1}$$

where ρ is the density in kg/m^3, and H, S, N are the hydrogen, sulfur and nitrogen contents in wt%.

Boduszynski, based on his Continuum Model, proposed many rules to relate boiling point to the molar mass and elemental composition of petroleum species. For a homologous series of compounds belonging to a particular class (e.g. paraffins), the boiling point increases with an increase in molecular weight. While this is true for all homologous series, compounds containing naphthenic rings, heteroatom-functionalities or fused aromatic moieties are offset to higher boiling point. In other words, for a given carbon number range, increased aromaticity and presence of heteroatom functionalities increases the boiling point. To summarize, the model dictates that any defined boiling point range contains compounds of a broad molecular weight range, with paraffins as the highest molecular weight compounds, followed by naphthenic compounds, aromatic species, heteratom-containing compounds, and finally polyaromatic species. Boduszynski concluded that the composition of petroleum progresses gradually and continuously in molecular weight, aromaticity and heteroatom content as a function of increasing boiling point.[5]

SARA fractionation is a common classification method used to fractionate bitumen into four classes based on their solubility or adsorption characteristics. These classes are saturates, aromatics, resins and asphaltenes.[2] Bitumen is composed of the following amounts of SARA

16

fractions: saturates 15-21 wt%, aromatics 18-19 wt%, resins 44-48 wt% and asphaltenes 14-20 wt%.[2]

Asphaltenes are a complex fraction of bitumen and are defined operationally as insoluble in *n*-paraffinic solvents such as *n*-pentane and *n*-heptane, but soluble in aromatic solvents such as toluene.[6] Based on the choice of paraffinic solvent used as precipitant, e.g. *n*-pentane or *n*-heptane, the precipitated asphaltenes are designated as *n*-pentane-asphaltenes or *n*-heptane-asphaltenes respectively.[2] In literature, it is argued that asphaltenes, being a solubility class, cannot be defined by characteristics such as molecular weight, polarity and heteroatom content.[7] Instead, the asphaltenes are a heterogenous fraction containing molecules that simply belong to the continuum of molecules in petroleum and span a wide range of molecular weights.[7] In literature, two contrasting molecular structures of asphaltenes were proposed: i) archipelago structure, in which several aromatic moieties are interconnected by aliphatic chains,[8,9] and ii) island structure, in which one fused aromatic ring system (core) contains many aliphatic side chains.[10,11] Regardless of the perspective on the structure of asphaltene molecules, they can self-assemble to form nanoaggregates at low concentrations (50-200 mg/L) in solvents, including toluene.[12,13] These nanoaggregates form clusters or flocs at higher concentrations (1-10 g/L).[12,13] Asphaltenes contain a significant portion of heteroatoms (N, S, O) and heavy metals such as Ni and V in bitumen.[2] Rejection of a portion of asphaltenes in a solvent deasphalting process produces a partially upgraded bitumen product, known as deasphalted oil.[14]

In its native state, bitumen is known to contain free radicals, of the order of 10^{18} spins/g.[15] Free radical chemistry is used to explain the physicochemical changes in bitumen during thermal conversion, and is described in section 2.4.

The viscosity, density, TAN, H/C ratio, and the amounts of heteroatoms (N, S, O), metals, asphaltenes and free radicals are important properties of bitumen in the first part of this thesis, in which the role of hydrothermal froth treatment in partial bitumen upgrading is investigated.

2.2.2. Characterization of Froth Solids

Mineral solids in bitumen froth, obtained from the oil sands in Alberta, were characterized in some studies (Table 2-2).[16-21] Properties of froth solids that were measured include mineralogical composition, elemental distribution, surface functional groups, particle size distribution and surface wettability. Table 2-2 lists the studies in which the froth solids were characterized and the analytical techniques used to characterize the mineral solids.

In the above-mentioned studies, no single method was used to isolate the solids from bitumen froth, and different studies employed different procedures to separate the solids. Dilution of bitumen froth with toluene,[17,18,21] naphtha[19] or heptol[20], followed by room temperature centrifugation[18-22] or filtration,[17] and Dean-Stark analysis involving refluxing bitumen froth with toluene,[16] were some methods that were used to separate the mineral solids from bitumen froth. In all the methods, the solids were commonly cleaned or washed with toluene to remove the toluene-soluble organics coated on the solids surface.

Table 2-2. Characterization of Froth Solids in Literature

Property	Analytical Technique	Ref.
Mineral identification	X-ray diffraction (XRD)	16-21
Elemental analysis	CHNS elemental analysis	17,18,23
	X-Ray Fluorescence (XRF)	24, 25
Surface morphology and elemental mapping	Scanning electron microscopy with energy dispersive X-ray spectroscopy (SEM-EDX)	17-21
Surface elemental composition	X-ray photoelectron spectroscopy (XPS)	17,18,21
Functional groups of adsorbed organics	Fourier-transform infrared (FTIR) spectroscopy	20,21
	^{13}C solid state NMR spectroscopy	24, 25
Particle size distribution (PSD)	Laser diffraction Analysis	16,21
	Wet Sieving and Centrifugation	16
	Focused beam reflectance measurement (FBRM)	17
Surface wettability (contact angle measurement)	Washburn method	18,21
	Sessile drop method	22

XRD analysis of the froth solids indicated that the solids are composed of the clay minerals kaolinite and illite, and non-clay minerals quartz, siderite, pyrite, anatase and rutile.[16-20] Hematite, maghemite, microcline, mica, zircon, feldspar, plagioclase, chlorite and lepidocrocite are some other non-clay minerals that were found to be present in the froth solids in some studies.[16,17,19,20] Their elemental composition and classification into light and heavy minerals based on density are shown in Table 2-3. Constituting about 40-70 wt% of the total solids in bitumen froth,[17,18] the clay minerals are known for their role as important industrial minerals, and their classification, principal characteristics and applications are widely reported in literature.[26,27, 28]

Table 2-3. Formulae of Minerals found in Bitumen Froth.[2,19,29,30]

Light Minerals (Density < 2960 kg/m^3)	
Kaolinite	$Al_2Si_2O_5(OH)_4$
Illite	$K_{0.8}Al_{2.8}Si_{3.2}O_{10}(OH)_2$
Quartz	SiO_2
Siderite	$FeCO_3$
Plagioclase	$(Na,Ca)Al(Si,Al)Si_2O_8$
Microcline	$KAlSi_3O_8$
Chlorite	$Mg_{2.5}Fe_{2.5}Al_2Si_3O_{10}(OH)_8$
Heavy Minerals (Density > 2960 kg/m^3)	
Pyrite	FeS_2
Rutile	TiO_2
Anatase	TiO_2
Hematite	Fe_2O_3
Maghemite	Fe_2O_3
Zircon	$ZrSiO_4$
Lepidocrocite	$FeO(OH)$

The total organic carbon content of the toluene-washed froth solids was reported to be about 15-26 wt % from the CHNS elemental analysis.[17,18,23] XPS analysis of the froth solids, which

specifically measured the surface concentration of carbon, indicated that the solids were still associated with toluene-insoluble organic matter post separation.[17,18,21] The relative atomic concentration of carbon was measured to be about 1 wt % C / (wt %, Al + Si + Fe) on the solids, at a 7-10 nm surface depth, by Zhao, et al.[18] The presence of organics on the surface of the froth solids was also suggested by the appearance of peaks characteristic of the methyl and methylene groups at around 2900-2800 cm^{-1} in the FTIR spectra.[21] A broad peak from 1515-1338 cm^{-1} was noticed, which could be a concomitant result of C$-$H bending in methyl and methylene groups,[21] as well as the vibrational modes of carbonate ions in the carbonate minerals (1470-1475 cm^{-1}).[31] Although it was not highlighted, the peaks at ~736 and ~866 cm^{-1}, corresponding to the in-plane and out-of-plane bending vibrations of carbonate ions in siderite,[32] were shown in the fingerprint region of the FTIR spectra of the raw and washed solids of the bitumen froth.[21]

Additionally, Axelson, et al. characterized the organic coated solids obtained from high-water content (> 5%) and low-water content (< 5%) containing bitumen froth using ^{13}C NMR spectroscopy and found that the high-water content froth solids contained a significant amount of carbonyl carbon component with a chemical shift ~176 ppm,[24] corresponding to acid carboxy carbon group (170-182 ppm),[33] which was not the case with the low-water content froth solids. Interestingly, the high-water content froth solids were also composed of significantly higher amounts of iron compared to the low-water content froth solids, and this iron was found to be present in the form of iron carbonates and hydroxides instead of pyrite.[24] Similar observations were noted for the high-water content (> 7%) froth solids in comparison with the low-water content (< 5%) froth solids by Mikula, et al.[25] These results also indicate that high-water content bitumen froth likely originates from the presence of hydrophilic organic matter attached to the surface of solids and heavy metal minerals.

Different types of mechanisms were proposed to explain the association between the mineral surface and organic matter.[20,34] Mechanisms which may bind the active sites on the mineral surface to polar organic functional groups are cation bridging, acid-base interactions and hydrogen bonding.[20,34,35] Ren, et al. proposed formation of a chemical bond (Si/Al−OOCR) on the surface of weathered clay minerals to explain the strong effect of weathering on the surface wettability of solids.[36] Prior to weathering, the solids are likely hydrolyzed by the formation water to result in surface silanol (Si−OH) and aluminol (Al−OH) groups, which may form hydrogen bonds with the heteroatom-containing species in the surrounding organic matter. Under weathering conditions, dehydration leading to the loss of formation water may lead to chemical binding of heteroatom functional groups like R−COOH with the solids surface as a result of direct contact. Further, physical entanglement of some organic macromolecules with the mineral surfaces may also occur.[37,38]

In addition to the surface carbon, XPS signals of the mineral lattice ions indicated that the surface organic coating was not continuous. [17,18,21] The irregular surface morphology and elemental mapping of froth solids in the SEM-EDX technique also revealed the heterogeneous distribution of elements carbon, oxygen, nitrogen, sulfur, aluminium and iron on the surface of the solids.

The discontinuous organic coating can explain the variability in the contact angle measurements in different studies. Contact angles in the range 44 to 94° were reported in literature for the froth solids, [17,18,21,22] indicating their intermediate surface wettability (contact angle typically between 50 and 130°).[39] In literature, it is widely believed that surface wettability of solids is an important property in determining the stability of water/oil emulsions.[21] Compared to either oil-wet or water-wet solids, bi-wettable solids with intermediate wettability would tend to accumulate at the oil-water interface and increase the stability of emulsions, making it difficult to demulsify.

One of the properties of froth solids that was measured using a variety of techniques was the PSD.[16,17,21] In oil sands industry, particles of diameter lesser than 44 μm are called fine solids and those of diameter greater than 44 μm are called coarse solids.[26] Another common classification used for categorizing grains based on particle size is the Wentworth scale. In this scale, particles of size smaller than 2 μm are referred to as the 'clay fraction' and those in the size range 2-62.5 μm as the silt fraction.[2] Although a major portion of the clay fraction of bitumen froth is comprised of the clay minerals (mainly kaolinite and illite), the clay fraction also contains non-clay minerals.[16,20]

Based on the wet sieving work of Kaminsky, et al.,[16] nearly half of the solid particles in the froth were found to be fine solids as shown in Table 2-4, and the clay fraction accounted for about 14 wt% of the total solids in the froth. In the study by Chen, et al.,[17] the chord length distribution was determined for the froth solids using FBRM technique. Approximately 85% of the solids were reported to have chord lengths smaller than 10 μm. Wang, et al.[21] found that while the froth solids exhibited a broad range of PSD from 0 to 1000 μm by laser diffraction, the median particle size (D_{50}) of the solids was around 11.5 μm.

Table 2-4. PSD of Mineral Solids in Bitumen Froth [16]

	> 45 μm [a]	< 45 μm [a]	< 2 μm [b]	< 0.2 μm [b]
Froth Solids (wt %)	51.5	48.5	14.4	3.6

[a] Determined using Wet Sieving

[b] Determined using Centrifugation

The inconsistencies among the results of the different particle size measurement techniques are because each of these techniques defines the size of a particle in a different way. For example, sieving defines the particle diameter based on whether the particle can pass through a certain mesh or not, and laser diffraction measures the volume of the particle and reports the diameter of a sphere

with the same volume. FBRM records the length of the straight line between two points located on the edge of the particle (chord length). These techniques neglect the shape of the particles, which is why microscopy coupled with image analysis could be a better method of determining particle sizes of irregularly shaped particles. According to Roostaei, et al., the deviation among different particle size measurement techniques increases with an increase in the fines content.[40] However, the studies mentioned above, describing the PSD of froth solids, can be used qualitatively to commonly indicate that the fine solids account for a significant portion of the froth solids.

Couillard, et al. attempted to link the mineral type to the wettability characteristics of the solids within the 0.2-2 μm clay size fraction of bitumen froth.[19] They performed toluene-water partitioning of these solids and conducted quantitative XRD analysis of the partitioned clay solid fractions. It was found that the biwettable clays, which remained at the toluene-water interface, contained significantly larger amounts of the mineral phases pyrite, rutile, anatase, zircon, chlorite and siderite+iron-oxide-hydroxite compared to the hydrophilic clays, which partitioned into the aqueous phase, and were found to have more amounts of quartz+amorphous silica and the clay minerals kaolinite and illite-smectite, as shown in Table 2-5. Additionally, a decrease in the mass ratio of kaolinite to illite-smectite from hydrophilic clays (~1.8) to biwettable clays(~1.2) was also highlighted. Further, the total toluene-unextractable organic carbon content was measured to be 3.6 wt% and 27.4 wt% respectively in the hydrophilic and biwettable clays respectively. However, a similar examination of the total froth solids was not conducted.

Table 2-5. Quantification of Mineral Phases in the Clay Solids Separated from Bitumen Froth[19]

Mineral Phase	Phase Concentration (wt %)			
	Hydrophilic Clays		Biwettable Clays	
	Concentration	Standard Uncertainty	Concentration	Standard Uncertainty
Quartz + Amorphous Silica	13.2	0.03	3.2	0.03
Illite-Smectite	25.6	0.02	9.1	0.02
Kaolinite	47.0	0.1	11.3	0.1
Pyrite	0.8	0.01	7.2	0.03
Zircon	0.01	0.0	0.2	0.0
Rutile	0.4	0.3	1.5	0.3
Anatase	0.6	0.3	2.3	0.3
Siderite + Amorphous iron oxide-hydroxide ($Fe(OH)_3$ or $FeO(OH)\cdot H_2O$)	2.0	1.2	11.0	0.03
Chlorite	0.1	0.0	5.4	0.1

2.2.3. Water Composition

As mentioned earlier, characterization of the water phase in bitumen froth has not been reported in literature until recently. Wang, et al.[21] measured the pH, and examined the type of ions and their concentrations in the aqueous phase of the bitumen froth using inductively coupled plasma-mass spectrometry and ion chromatography. The pH of the aqueous phase was found to be 7.9 ± 0.1, indicating its slightly alkaline nature. Na^+ (646 ppm), Ca^{2+} (~ 20 ppm), K^+ (~ 14 ppm) and Mg^{2+} (~ 5 ppm) were identified as the major cations, whereas Cl^- (~ 640 ppm) and SO_4^{2-} (~ 130 ppm) were the major anions present in the water phase of the bitumen froth.

The origin of these ions mainly lies in the industrial recycle process water, which accounts for 85 % of the total water usage in the hot water extraction process of oil sands,[41] briefly described in Chapter 1. Similar to the results of the aqueous phase characterization from bitumen froth, it has

been reported that the process water predominantly contains Na^+, Cl^-, HCO_3^- and SO_4^{2-}, while divalent ions Ca^{2+} and Mg^{2+} are present in smaller concentrations, as shown in Table 2-6. The process water is basic in nature,[42] with pH in the range 7.8 to 8.5.[41]

The water originally contained within the oil sands deposit (commonly referred to as the connate water), process aids added during the extraction process and treatment of tailings (e.g. NaOH), ion-exchange reactions of the clay minerals, and to a lesser extent, the local surface water, all contribute to the overall concentration of ions in the recycle process water. [41]

The composition of ions contained in the connate water of high grade (bitumen content 12-16 wt %) and low grade (bitumen content 6-9 wt %) oil sand ores is listed in Table 2-6. Normally, the connate water composition is measured by adding boiling (100°C) distilled water in amounts equal to the weight of the oil sands sample, followed by bitumen separation and centrifugation.[26] The concentration of ions in the connate water is expressed as mg per kg of oil sands instead of mg/L, as it may be unclear whether the volume in units mg/L refers to the volume of the connate water or the collected test water sample. Significant differences in the concentration of ions between a high grade and a poor grade ore can be observed in Table 2-6, with the concentration of divalent ions (Mg^{2+}, Ca^{2+}, SO_4^{2-}) being much higher in the poor grade ore. Sodium and chloride are the dominant ions in the connate water of Alberta oil sands. pH values of the connate water, that have been reported in the literature,[2,41] range from 7 to 8.5, indicating that it is basic in nature.

During the hot water extraction of bitumen from oil sands, the recycle process water is combined with fresh make-up water from the Athabasca river, which is alkaline in nature and has a much lower concentration of ions, especially Na^+ and Cl^-, compared to that in the recycle process water, as indicated in Table 2-6.

Table 2-6. Composition of Ions in Athabasca River Water, Industrial Recycle Process Water and

Connate Water of Oil Sands [26,41]

	Ions (mg/L)		Ions (mg per kg of oil sand)	
	Industrial Recycle Process Water	Athabasca River	Connate Water (High Grade Ore)	Connate Water (Low Grade Ore)
Na^+	494-617	13	62.4	18.1
K^+	14-20	1	5.2	19.8
Mg^{2+}	15-22	9	0.1	18.4
Ca^{2+}	27-48	31	0.3	32
Cl^-	368-513	11	308.3	1.1
NO_3^-	0-4	- [a]	- [a]	- [a]
SO_4^{2-}	63-115	25	13.5	118.4
HCO_3^-	597-649	121	22.9	37.8
pH	7.8-8.5	7.9	7	7.4

[a] Not Reported

2.3. Froth Treatment

2.3.1. The Phase Separation Problem

Separation of water and mineral solids from bitumen froth is important as their presence is detrimental for pipeline transport, and for the downstream upgrading and refining operations. Mineral solid particles can deposit in the pipeline, increasing pressure drop, and contribute to equipment wear and plugging of reactor beds in subsequent operations.[3,26] On the other hand, dissolved salts in water may cause fouling or lead to corrosion during pipeline transport and downstream operations. Chlorides are the most problematic of these, as they make their way into downstream upgrading and into the refinery operations, causing serious corrosion problems.[1] Due to their hydrolysis behavior in the presence of steam at elevated temperatures during refinery operations, the chlorides can be converted to the corrosive hydrochloric acid.[3] As an example, the

hydrolysis reaction of $CaCl_2$ is shown in Eq 2-2.[3] The aqueous hydrogen chloride solution formed upon condensation can lead to corrosion. The hydrochloric acid can also react with traces of ammonia gas released from the nitrogen-containing compounds in crude oil, forming solid ammonium chloride (Eq 2-3.) which can contribute to fouling in equipment.[3]

$$CaCl_{2\,(s)} + H_2O_{(g)} \xrightarrow{\;>200\,°C\;} CaClOH_{(s)} + HCl_{(g)} \qquad\qquad \text{Eq 2-2.}$$

$$HCl_{(g)} + NH_{3\,(g)} \longrightarrow NH_4Cl_{(s)} \qquad\qquad \text{Eq 2-3.}$$
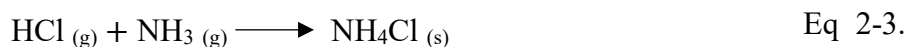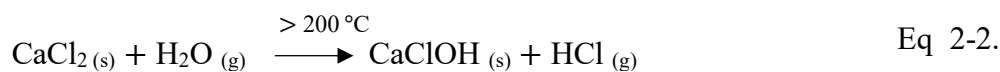
Presence of stable water-in-oil (w/o) emulsions in bitumen froth is a primary factor affecting the separation of solid and aqueous phases from the organic phase.[43] Based on literature, following are some of the factors contributing to the stability of w/o emulsions.

a) Asphaltenes, which are a solubility class, have been primarily shown to stabilize w/o emulsions.[44] Asphaltenes form a viscoelastic film around the water droplets, which prevents the droplets from coalescing.[45] Electronegative elements such as O, N, S in the asphaltene molecules can form hydrogen bonds with the H atom in the water molecule, which becomes a major driving force for the asphaltene molecules to accumulate at the oil-water interface.[46] Further, Singh, et al. concluded that that the asphaltene molecules are oriented at the interface in such a way that the interaction between the water phase and the heteroatom is maximized.[47] In addition, self-aggregation of asphaltenes to form nanoaggregates and clusters at the oil-water interface is said to result in the formation of thick films, that sterically stabilize emulsions. Complex intermolecular interactions such as π-π stacking, hydrogen bonding and acid-base interactions are said to be involved in the aggregation of asphaltenes.[46] Although the link between self-association of asphaltenes to emulsion stability has mostly been indirect, Rocha, et al. confirmed that the least

soluble or most self-associated portion of asphaltenes, which is only a sub-fraction, was mainly responsible for the stability of the emulsions.[48]

b) Fine solids, mainly clays, can stabilize emulsions by adsorbing onto the oil-water interface and forming a protective interfacial film. For this reason, the higher amounts of fine solids and clays in the low-grade oil sand ores (6-9 % bitumen) compared to the high-grade oil sand ores (> 12% bitumen) are said to have a detrimental effect on bitumen extraction from low-grade ores and subsequent froth treatment.[49,50] Various factors influence the role of fine solids in contributing to the stability of emulsions, including the size and concentration of the solids, their wettability, asphaltenes, and water chemistry, among others.[45,34]

The size and concentration of solid particles indirectly affect emulsion stability by influencing the droplet size of the dispersed phase.[45] Based on a correlation presented by Binks and Lumsdon,[51] between the emulsion droplet size (radius) and the solid particles' size (radius) and concentration, the smaller the size of the particles and higher the fines content, the smaller are the droplets of the dispersed phase formed in the emulsification process.

Wettability of solids plays an important role in determining the partitioning of solids in the emulsion onto the oil-water interface.[45] It is generally accepted that biwettable solids of intermediate wettability (contact angle close to 90°) could stabilize both water-in-oil and oil-in-water emulsions.[52]

In the study about the influence of bitumen components on the stability of water-in-oil emulsions,[44] the role of fine solids in the stabilization of emulsions was found to be minor in the presence of asphaltenes, which appeared to act as the primary stabilizers. The competitive adsorption of asphaltenes and fine solids at the oil-water interface was illustrated in the review by Velayati, et al.[45]

An example of the influence of water chemistry on the emulsion stabilization role of solids is the effect of pH of the aqueous phase on the contact angle (wettability) of the clays and the clay coverage at the oil-water interface.[53] Yan and Masliyah reported that the variation of contact angle of kaolinite particles, treated with asphaltenes, with pH could be represented by an inverted U-shaped curve with a peak (or maximum) contact angle occurring at a certain pH (~6 in their oil-water emulsion system).[53] Similarly, the clay coverage (mass of clays adsorbed at the oil-water interface ÷ total mass of clays in the emulsion) versus pH curve was also shown to have the same shape.[53] They attributed these observations to the formation of cationic species resulting from the reaction between asphaltene zwitterions and hydronium ions, and anionic species from the reaction between asphaltene zwitterions and hydroxyl ions, both reactions increasing the hydrophilicity of the clay surface.[53] In the same study, it was also shown that the oil droplet diameter increased with the pH of the aqueous phase.[53] Although these results are specific to oil-in-water emulsions, they may still be of value to water-in-oil emulsions.

c) Although, caustic addition (mostly sodium hydroxide) during extraction increases the pH of the solution and aids in bitumen liberation from the sand grains, it can have a detrimental impact on bitumen recovery due to emulsification of bitumen droplets in water.[54,55] The sodium hydroxide (NaOH) can react with the organic acids present in bitumen, releasing natural surfactants into the water phase.[50,54] These natural surfactants adsorb at the oil-water interface and lower the interfacial tension between bitumen and water.[55] At the same time, raising pH by addition of caustics increases the hydrophilicity of solids by enhancing hydrolyses and causes the solids to carry negative surface charges due to deprotonation, resulting in increased repulsion between the solids and bitumen.[55] While these phenomena facilitate bitumen liberation from the sand grains, lowering bitumen-water interfacial tension is anticipated to emulsify bitumen droplets in water, leading to

poor aeration. [55] Hence, there is an optimum amount of NaOH (normally 0.01 to 0.2 wt% of oil sands ore) added during oil sands bitumen extraction, to achieve an operating slurry of pH~8.5 and optimum bitumen recovery. [55] The study by Flury, et al. using different types of caustics in bitumen extraction, gives the impression that the above effects are attributed to pH control, rather than the use of a specific base such as NaOH.[55] In their study, a similar bitumen recovery was obtained using NaOH and ammonium hydroxide (NH_4OH) at pH=8.5.

Romanova, et al.[49] studied the effect of NaOH addition in extraction process on the performance of froth treatment process. Compared to bitumen recovery after froth treatment following bitumen extraction without NaOH addition, optimum NaOH addition (0.1 wt%) in the extraction process (at 80 °C) significantly increased bitumen recovery after both the *n*-heptane-diluted bitumen froth treatment (paraffinic solvent method) and toluene-diluted bitumen froth treatment (toluene was used instead of naphtha in the sense that all of the bitumen constituents are soluble in the solvent), both conducted at 60 °C. It appeared that NaOH addition during bitumen extraction promoted coalescence of the water droplets in bitumen froth, giving rise to a better phase separation.[49]

2.3.2. Commercial Froth Treatment Processes

In industry, separation of water and mineral solids from bitumen froth is achieved through a process called froth treatment. In froth treatment, a hydrocarbon solvent is used to reduce the viscosity of bitumen and increase the density difference between bitumen and water, thus enabling separation of the components. As mentioned in Chapter 1, the two types of froth treatment processes are naphthenic froth treatment (NFT) and paraffinic froth treatment (PFT), based on the solvent type.

In the NFT process, the bitumen froth is blended with a hydrocarbon solvent in the boiling range 76-230 °C, commonly referred to as a naphtha diluent.[56] In the PFT process, paraffinic solvents,

mainly *n*-pentane and *n*-hexane rich materials are blended with the bitumen froth.[3, 56] In both the processes, the diluted bitumen froth is directed to a settler, where gravity separation of the froth components occurs. Some additional features of the NFT and PFT processes are summarized in Table 2-7.

Table 2-7. Characteristics of Naphthenic and Paraffinic Froth Treatment Processes [3,43,45]

Characteristics	NFT	PFT
Solvent Type	Naphtha	Paraffinic (typically $n-C_5$ and $n-C_6$)
Solvent Density (kg/m^3)	750−800	625−670
S/B ratio (wt/wt)	0.6−0.8	≥ 1.5
Operating Temperature (°C)	75−85	30, 70

The solvent used in the NFT process is denser than that used in the PFT process, and higher solvent-to-bitumen (S/B) ratios are used in the PFT process compared to the NFT process. The commercial froth treatment processes are operated at temperatures 85 °C and lower, with the operating pressure being dependent on the solvent added and the operating temperature, such that the solvent remains in liquid phase during the process. Further, a major difference between the NFT and PFT processes is that the addition of paraffinic solvent at typically higher S/B ratios (≥1.5) in the PFT process results in partial precipitation of asphaltenes in the bitumen, whereas the asphaltenes are mostly retained in the diluted bitumen in the NFT process.

Four separate layers are said to form in the froth treatment (Figure 2-2),[45,57] with the diluted bitumen (dilbit) being separated as the top layer. As mentioned above, higher concentrations of water and solids are present in the dilbit resulting from NFT, which is a diluted water-in-oil

emulsion. The clear portion of the separated water phase is another layer, below which the sunken fine solids form a tailings layer consisting of solids and water, which in the case of PFT also includes the precipitated asphaltenes. Between the dilbit layer and the separated clear water phase layer is the so-called rag layer which is an emulsion of hydrocarbons, water and fine solids. The rag layer was also referred to as a 'skin emulsion' by Bichard,[57] and contains much higher amounts of water and solids than those in the dilbit.
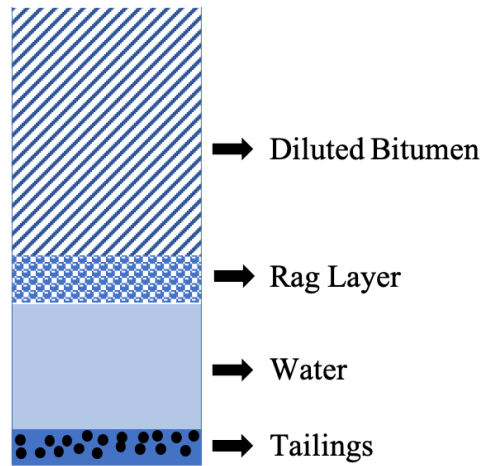
Figure 2-2. Four Phase System of Gravity Separated Bitumen Froth

It is relatively difficult to perform separation in the NFT process compared to the PFT process, which is why a demulsifier is added to the settling unit in the NFT process to enhance the separation efficiency.[58] In addition, inclined plates, centrifugation and cyclones are used in the NFT plant to aid the phase separation, [43] as shown in Figure 2-3. However, the resultant bitumen product from the NFT process still contains 2-5 wt % water and 0.5-1 wt % fine solids.[43] The bitumen product from the NFT process is processed in an adjacent upgrader, that is designed to accept bitumen feed with some solids and water, to synthetic crude oil. Bitumen upgrading in proximity to the froth treatment also produces the naphtha diluent which is used in the NFT process.
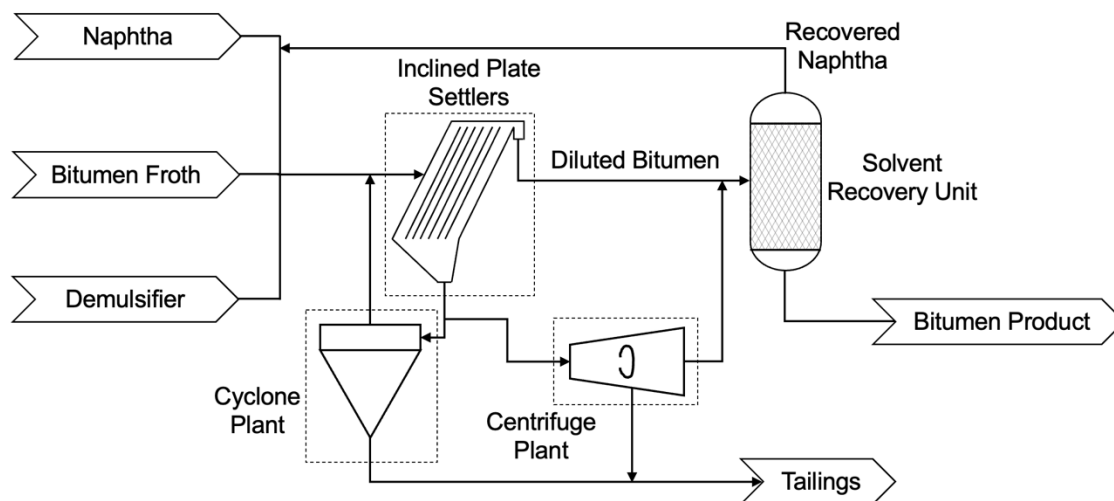
Figure 2-3. Simplified Process Flow Diagram of the NFT Process

On the other hand, due to precipitation of asphaltenes in the paraffinic solvent used in the PFT process, the fine mineral solids and water droplets bind together with the precipitated asphaltenes and form aggregates that settle easily. Nearly complete removal of solids and water can be achieved in the PFT process and the final paraffin diluted bitumen product is suitable for pipeline transport. This allows delinking the bitumen upgraders from the extraction plants.

Despite the benefits of the PFT process, a significant portion (7-9 wt %) of the bitumen is lost due to asphaltenes precipitation.[3] Hence, the hydrocarbon recovery is lower for PFT compared to the NFT process. Moreover, the PFT process requires about 2-3 times more volume of solvent than the NFT process (Table 2-7). The volume of solvent needed (S/B ratio) to achieve a certain level of asphaltene rejection in the PFT process is determined by the type of solvent used.[59,60] For example, Zhao and Wei measured the residual asphaltenes content in DAO as a function of S/B ratio using *n*-pentane and *n*-hexane, in the temperature range 20-160 °C.[58] They found that at any given temperature, a higher S/B ratio of *n*-hexane than that of *n*-pentane was required to achieve the same residual asphaltenes content in DAO. In other words, *n*-pentane was more effective at asphaltenes rejection compared to *n*-hexane. Similar observation was noted in the work of Turuga

and De Klerk in which the yields of asphaltenes precipitated in the solvent deasphalting process of bitumen at ambient conditions using n-pentane (n-C_5), n-hexane (n-C_6) and n-heptane (n-C_7) at different S/B ratios in the range 3:1 to 40:1 were measured.[61] It was shown that at any given S/B ratio the yields of n-C_5-, n-C_6- and n-C_7-asphaltenes followed the order: n-C_5-asphaltenes $> n$-C_6-asphaltenes$> n$-C_7-asphaltenes, indicating that the carbon number of linear chain paraffinic solvents from C_5 to C_7 influenced asphaltenes rejection.

NFT was the only commercial froth treatment process for over thirty years from 1970s to early 2000s until the PFT process was commercialized. The original Suncor and Syncrude operations employed NFT process for froth cleaning. Later, the PFT process was employed by mines that did not have an onsite upgrader, with the intention of producing high quality diluted bitumen which can be transported through a pipeline over large distance to the market. The PFT process, being relatively newer, is used in fewer commercial projects compared to the NFT process.[43]

Post froth treatment, the naphtha or paraffinic solvent that remains in the dilbit is recovered in a solvent recovery unit (SRU). Solvent is also recovered from the froth treatment tailings using a tailings solvent recovery unit (TSRU). Figure 2-4 schematically shows the solvent recovery process in a bitumen froth treatment plant carried out using the SRU and TSRU. While SRU is an established technology in the oil sands industry, various research developments regarding TSRU took place, which are presented in the review by Rao and Liu.[43]
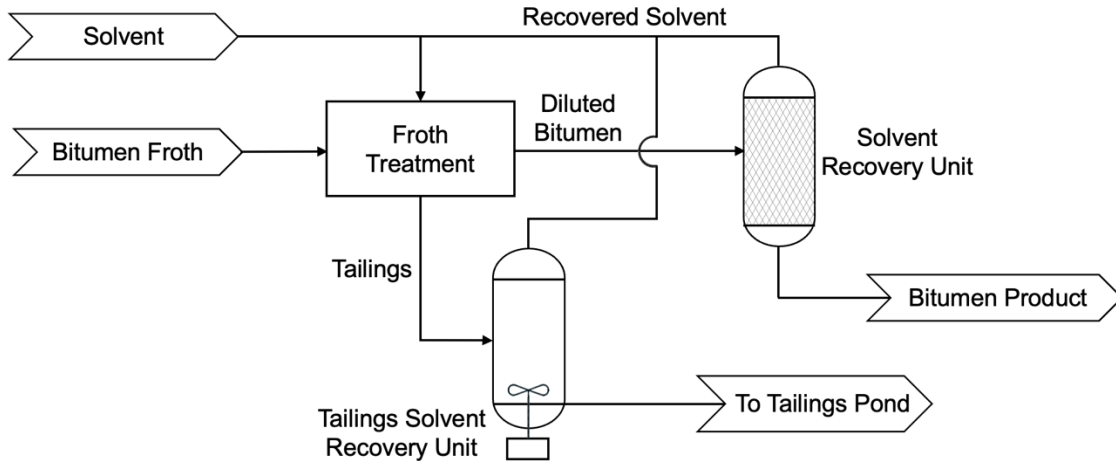
Figure 2-4. Schematic Representation of Solvent Recovery in a Froth Treatment Plant

2.3.3. Prior Research and Future Research Opportunities

As mentioned in section 2.2.2., maximizing bitumen recovery from froth, and at the same time, achieving low concentrations of solid and water impurities in the bitumen product are important outcomes for froth treatment. Most of the reported research in the area of froth treatment was concerned with investigating the factors contributing to the stability of emulsions, such as asphaltenes and fine solids, and testing various demulsification methods, including chemical (inorganic and organic) addition, solvent washing, ultrasonics, microwave irradiation and electrostatics, especially in the NFT process.[44,45,48,58,62-64]

Other interesting topics related to froth treatment, that were explored, include a) investigation of the effect of extraction conditions, such as NaOH dosage, mixing energy, and temperature on the froth treatment efficiency;[49] b) conducting froth treatment using a blend of naphtha and paraffinic solvent to achieve the benefits of both NFT and PFT processes, i.e. obtaining a bitumen product, virtually free of residual solids and water, with increased bitumen recovery due to asphaltenes retention;[65] c) investigation of the effect of temperature (80-150 °C) on bitumen recovery and product quality in NFT and PFT processes;[66] d) a novel froth cleaning device in which, the

36

naphtha-diluted bitumen froth is washed by introducing it into aqueous phase as drops, using a distributor, and the top organic phase is circulated continuously back into the same aqueous phase, to facilitate separation of water and solids from bitumen.[67]

Shelfantook investigated the impact of increasing the operating temperature on the NFT and PFT processes.[66] It was found that increasing the operating temperature in the range 80-150 °C resulted in a dramatic improvement in the percentage of hydrocarbon in the product of the NFT process (S/B ratio = 0.6-0.9 kg/kg), which increased from approximately 94.5 wt% to approximately 99 wt %. On the other hand, for the PFT process (S/B ratio = 2.0-2.9 kg/kg), increasing temperature in the same range improved bitumen recovery from approximately 91 % to approximately 96 % (i.e., loss of asphaltenes to the tailings was reduced) with only a slight decrease in the product quality (measured as percentage of hydrocarbon in the product). Further, the ratio of tailings-to-product concentrations for Ni and V increased from around 2 to 4 in the PFT process when the temperature was increased from 50 to 150 °C, indicating that the concentration of metalloporphyrins in the bitumen reporting to the tailings was not only higher than that in the product bitumen but also increased with temperature. In their study, the operating temperature was kept below 150 °C due to equipment limitations. [66] Based on these results, high temperature operation of the solvent based NFT and PFT processes was claimed to have benefits that can offset the increase in operating cost associated with the increased energy requirements, although no cost assessment was presented in their work. [66]

Previous studies also explored a process called hydrothermal treatment, which is a modified method of froth treatment, in which the froth is directly heated at higher temperatures without solvent addition.[17,18] The temperatures used in these studies were in the range 300-420 °C. The focus of these studies,[17,18] similar to the previously mentioned studies in this section, was on

enhancing the overall separation efficiency of the process. However, this process may act as a potential way to achieve partial bitumen upgrading as part of froth treatment, in the presence of water and mineral solids, by promoting reactions at high temperature.

So far, no work was conducted with bitumen froth to study the impact of mineral solids and water on the thermal conversion of bitumen. The current work is focused on the hydrothermal treatment process and the role of water and mineral solids in the bitumen conversion. Before reviewing the hydrothermal characteristics of the froth components i.e., bitumen, water and mineral solids (section 2.5), the thermal behavior of bitumen in the absence of bulk solids and water is discussed in section 2.4 to describe the role of temperature on bitumen conversion.

2.4. Thermal Behavior of Bitumen

In industry, bitumen is thermally treated as part of the upgrading processes, to improve its quality and flow characteristics. Typically, after production, the bitumen feedstock undergoes atmospheric and vacuum distillation to recover the lighter hydrocarbons based on their boiling points, and the remaining vacuum residue (+524 °C boiling range) is upgraded.[3]

During thermal upgrading of vacuum residue without the addition of hydrogen gas and the presence of a catalyst, temperature is the key driver for converting the heavier molecules of the vacuum residue into lighter molecules through cracking reactions. Visbreaking and coking are two such processes that are employed in industry, and these thermal conversion processes are operated in the temperature ranges 430-500 °C (visbreaking) and 500-550 °C (coking).[3]

Cracking is the thermal breakage of chemical bonds in hydrocarbons which is used to break down and convert heavier molecules into lighter molecules. The major bonds of interest in the primary upgrading processes are the $C-C$, $C-H$ and $C-S$ bonds. Different types of bonds have different bond dissociation energies (BDE) which indicate the difficulty of breaking those bonds. For

example, aliphatic C−S bond is the weakest covalent bond commonly found in bitumen with a BDE around 285 kJ/mol. BDEs for aliphatic C−C and C−H bonds are mostly in the ranges of 320−375 kJ/mol and 370−425 kJ/mol respectively.[68] In the absence of a catalyst the primary upgrading processes must be operated above 420 °C to achieve thermally induced breakage of C−C bonds at useful reaction rates.[3]

Dissociation of chemical bonds during cracking reactions results in the formation of highly chemically reactive intermediates called free radicals, which are atoms or molecules consisting of an unpaired electron. These free radicals participate in chain reaction processes yielding significant conversions of the feed. During thermal cracking of bitumen fractions, olefins are also formed, which further react with radicals to generate addition reactions. The mechanisms of thermal cracking reactions are described in the book by Gray.[3]

Formation of a solid byproduct called coke is a limitation to thermal upgrading processes for producing valuable distillable liquids. The term coke is loosely used to describe toluene-insoluble carbon-rich deposits formed during thermal conversion.[69] With complex individual reactions occurring in a complex mixture like bitumen, the chemistry associated with bitumen conversion processes is quite complex. It is postulated that coke formation during thermal treatment occurs by a combination of insolubility and hydrogen depletion.[69] During conversion, one potential explanation is that the coke precursors by self-associating and phase separating form a second liquid phase which ultimately leads to solid coke formation. The process for coke formation was described by Wiehe,[70] which provides useful information about the thermal conversion chemistry of complex molecules. This description is not universally accepted.[71]

As the focus of this thesis is on the lower temperature conversion of bitumen, the studies on thermal conversion behavior of bitumen at ≤ 400 °C were reviewed and are discussed in the following sub-sections.

2.4.1. Viscosity Changes

Viscosity changes of bitumen were particularly investigated in previous studies on thermal conversion of bitumen in the temperature range 150-400 °C.[69,72,73] At each of the studied temperatures, the relationship between viscosity and reaction time was complex. Regardless, following thermal treatment at temperatures 250 °C and above, the viscosity of the treated bitumen products was lower compared to the viscosity of the bitumen feed. [72,73] On the other hand, thermal treatment at 150 and 200 °C negatively impacted the viscosity as the treated bitumen viscosity was greater than that of the feed.[72]

It was possible to achieve two orders of magnitude lower viscosity compared to that of the bitumen feed by performing visbreaking at 360-400 °C.[73] The meaningful improvement in the viscosity reduction of bitumen achieved in these studies indicated that mild visbreaking may have benefit as a partial upgrading technology that could be used to reduce the diluent requirements for meeting the Canadian pipeline viscosity specification. However, to fully unlock the potential of lower temperature thermal conversion of bitumen, there are other properties (e.g. olefin content) that need to be evaluated to consider the other pipeline specifications.

Another interesting finding in a study by Zachariah and De Klerk was that continued thermal conversion of bitumen at 400 °C resulted in unproductive changes in viscosity.[69] Although visbreaking of bitumen at 400 °C resulted in productive changes in viscosity, as the reaction progressed, the viscosity of treated bitumen product not only increased after 180 min, but approached the viscosity of the bitumen feed around 360 min reaction time.[69] This implied that

mild visbreaking at 400 °C still had a limited reaction period in the course of which actual upgrading benefits can be achieved.

Changes in the viscosity of bitumen were attributed to various factors in literature. For example, the viscosity increase at 150 and 200 °C, followed by a viscosity decrease at 250 and 300 °C was related to the relative rates of the free radical addition and cracking reactions.[72] The transition from higher rate of free radical addition to higher rate of free radical cracking, which occurs in the temperature range 200-250 °C for many substances, implied that the observed increase in the viscosity of bitumen at 150 and 200 °C was likely contributed by heavier material formation due to addition reactions.[72] Based on literature, Wang, et al. interpreted the viscosity decrease in low temperature visbreaking (340-400 °C) to be resulting from the decrease in effective volume fraction occupied by the aggregates in bitumen.[73] It was proposed that weak physical and chemical interactions, holding the aggregating species and clustered asphaltenes in bitumen, could be disrupted during low temperature conversion, resulting in disaggregation and/ or a possible decrease in the boundary layer volume surrounding the aggregates. Two other factors that were highlighted in literature as sources of viscosity changes were: a) an increase in excluded volume accompanied by a parallel increase in viscosity and a slight decrease in density; b) phase behavior changes in treated bitumen products influenced by the chemical changes taking place during thermal conversion.[72] Further, viscosity was poorly correlated with the *n*-pentane insoluble content of bitumen in these studies.[72,73] However, a simpler explanation that can be offered to explain the viscosity decrease at higher temperatures is the dilution effect created by the formation of lighter molecules of lower viscosity produced by thermal cracking.

In addition to the studies using bitumen, low temperature conversion of vacuum residue deasphalted oil (VR DAO) at 280-400 °C was investigated.[74] At the studied temperatures (280,

320, 360, 400 °C), the viscosity of VR DAO was reduced upon thermal treatment, although, the decrease in viscosity observed at 280 and 320 °C was minor and of little value for upgrading VR DAO.

2.4.2. Solids Deposition

Formation of coke-like particles during low temperature conversion of bitumen was detected in previous studies.[69,72] When Cold Lake bitumen was treated at 150 and 200 °C, no notable increase in solids yield was found, although indication of product instability with respect to phase behavior was observed at longer reaction times.[72] A significant increase in the solids yield was observed within 1 h of reaction at 250 ° C.[72] This temperature is below the thermal cracking temperature of most organic compounds in bitumen, which indicates that there were also other mechanisms that were responsible for reactions leading to solids deposition. Further, visual inspection of filtered solids obtained from thermal conversion of Cold Lake bitumen at 300 °C after 8 h reaction, indicated the formation of distinct fine coke-like solid particles, providing indirect evidence of a possible second phase formation. [72] The particle size of most of these solids was less than 10 μm. Presence of these fine particles also made the separation of solids from liquid products by filtration a time-consuming process. This work provides empirical evidence to suggest that solids separation is influenced by conversion temperature in the range 150-250 ° C. [72]

Zachariah and De Klerk characterized the solids after thermal conversion of Long Lake bitumen at 400 °C.[69] The bitumen feed initially contained ~1 wt % of mineral matter, which appeared as platelets in the microscopic images of the solids (Figure 2-5) at 0 min reaction time. Upon thermal treatment, these mineral solids acted as repositories for organic matter deposition, even before the onset of bulk coking. The platelet structures which initially appeared, transformed into fine coke-like particles at 240 min reaction time, and finally into larger structures after 300 min reaction

time, as shown in Figure 2-5. Further, in addition to the yield and appearance, the filtration characteristics of the solids formed after thermal conversion at 400 °C also varied with the reaction time. As the temperature used in this study (400 °C) was high enough for thermal cracking reactions, the role of solids in promoting these reactions cannot be ruled out.
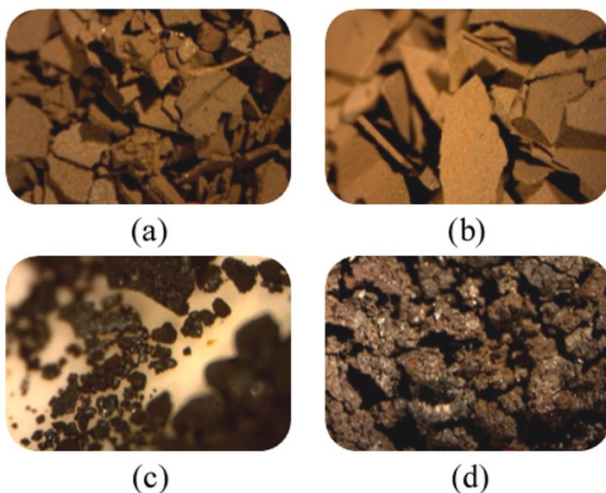
Figure 2-5. Microscopic Images of Solids Isolated from Long Lake Bitumen Following Treatment at 400 °C for a Reaction Time of (a) 0 min (b) 60 min (c) 240 min (d) 300 min [69]

The above studies were performed with bitumen which had ~1 wt % mineral solids. [69,72] The role of solids in upgrading and the effect of thermal conversion on the separation of solids was not investigated using bitumen froth, which consists of order of magnitude higher content of solids and two liquid phases.

2.4.3. Free Radical Reaction Chemistry

The chemistry of free radical-based thermal conversion can be generally divided into three stages: initiation, propagation and termination.[68]

Initiation is most often described as homolytic cleavage of bonds to produce free radicals, as represented by Eq 2-4. BDEs determine the thermal energies that are required to break the chemical bonds.

$$R_1 - R_2 \rightarrow R_1{}^{\bullet} + R_2{}^{\bullet}$$ Eq 2-4.

In addition to homolytic bond dissociation, bimolecular interaction of two non-radical species could produce two free radical products due to hydrogen transfer. An example is shown in Figure 2-6.
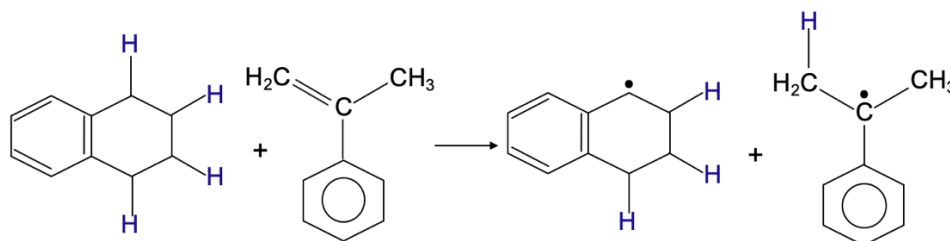
Figure 2-6. Illustration of Molecule-Induced Homolysis, Involving Transfer of Hydrogen Atoms from Tetralin to α-Methyl Styrene, Generating Free Radicals

However, bitumen in its native state already contains free radicals, of the order of 10^{18} spins/g,[15] which means that initiation is not necessary for free radical reactions to proceed. Qualitative and quantitative analysis of free radicals is widely performed using electron spin resonance (ESR) spectroscopy. Naghizada, et al.,[75] in their work with industrial asphaltenes, observed measurable changes in the overall aromatic hydrogen content after conversion for 1 h at 120 °C (too low for homolytic bond dissociation), which suggested that free radical species originally present in the asphaltenes feed participated in free radical hydrogen transfer reactions.

Free radical reactions are chain reactions. When heated, radicals initially present in bitumen or those which are generated by initiation reactions can propagate in various ways to generate new

free radicals. Hydrogen transfer through hydrogen abstraction (Eq 2-5.), cracking (Eq 2-6) and addition of the radicals to double bonds (Eq 2-7) are often involved in propagation steps. Additionally, intramolecular free radical isomerization (Figure 2-7), typically 1,5 or 1,6 transfer, is another type of propagation reaction. In transfer reactions, reference is usually made to hydrogen transfer. However, transfer of methyl group is also possible. Each of these propagation reaction types was described in some more detail with examples by De Klerk.[68]

$$R-CH_2-CH^\bullet-R'+R''-CH_2-CH_2-R''' \rightarrow R-CH_2-CH_2-R'+R''-CH_2-CH^\bullet-R''' \qquad \text{Eq 2-5.}$$

$$R-CH_2-CH^\bullet-R' \rightarrow R^\bullet + CH_2=CH-R' \qquad \text{Eq 2-6.}$$

$$R-CH_2-CH^\bullet-R'+R''-CH=CH-R''' \rightarrow \begin{array}{c} R-CH_2-CH-R' \\ | \\ R''-CH^\bullet-CH-R''' \end{array} \qquad \text{Eq 2-7.}$$
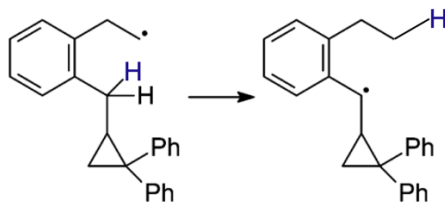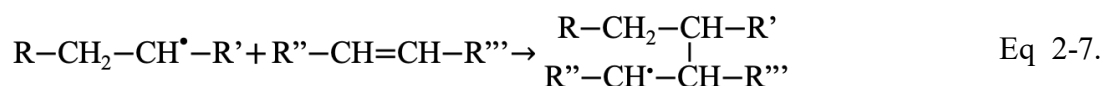
Figure 2-7. Example of Free Radical Isomerization Taking Place by Intramolecular 1,5 Hydrogen Transfer (Adapted from DeZutter, et al.[76])

In literature, the reactivity of bitumen and asphaltenes for hydrogen transfer reactions at 250 °C was demonstrated by making use of model compounds.[75,77] In other studies, occurrence of hydrogen and methyl transfer reactions in the temperature range 150-300 °C was indicated by measurements such as the aliphatic and aromatic hydrogen contents, and the ratio of methylene ($-CH_2-$) to methyl ($-CH_3$) groups in converted bitumen, as well as the amounts of methane gas generated during bitumen conversion.[72]

Finally, termination of free radical chain reactions takes place when two free radicals react to produce non-radical species. Termination occurs either through the combination of two free radicals (Eq 2-8.) or by disproportionation, which involves hydrogen transfer (Eq 2-9.) or methyl transfer between two free radicals.

$$R-CH_2-CH^{\bullet}-R'+R''-CH_2-CH^{\bullet}-R''' \rightarrow \begin{array}{c} R-CH_2-CH-R' \\ | \\ R''-CH_2-CH-R''' \end{array} \qquad \text{Eq 2-8.}$$

$$R-CH_2-CH^{\bullet}-R'+R''-CH_2-CH^{\bullet}-R''' \rightarrow R-CH_2-CH_2-R'+R''-CH=CH-R''' \qquad \text{Eq 2-9.}$$
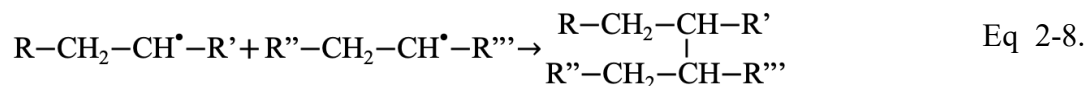
In the work by Naghizada, et al.,[75] the observed increase in the *n*-heptane insolubles content of the products of industrial asphaltenes treated at 140-150 °C was tentatively attributed to free radical combination reactions.

2.5. Hydrothermal Conversion

Hydrothermal treatment can generally be defined as the physical and chemical transformation of a feedstock into valuable products using a combination of water ('*hydros*' in Greek) and heat ('*thermos*' in Greek).[78] According to Byrappa, et al.,[78] the term 'hydrothermal' was first used by Sir Roderick Murchison (1792–1871), a British geologist, to describe the action of high temperature, pressurized water in causing changes in the earth's crust, giving rise to the formation of various minerals and rocks.

Hydrothermal methods have been tested for treatment of various unconventional hydrocarbon resources, such as heavy oil,[79-81] oil sands bitumen,[82-84] biomass [84-86] and oil shale,[87] in the presence or absence of catalytic materials. In some studies, in literature, the term 'aquathermolysis' was used to refer to thermal conversion, especially of heavy oils, in the presence of high temperature water.[88] As the focus of this thesis is on the hydrothermal treatment of bitumen froth, which is a

complex mixture of bitumen, water and mineral solids, a review on the behavior of water and mineral solids at hydrothermal conditions is presented in the following sub-sections.

2.5.1. Role of High-Temperature Water

Water under hydrothermal conditions can be divided into sub-critical water (100–320 °C), near-critical water (320–374 °C) and supercritical water (T ≥ 374 °C, P ≥ 22.1MPa), as shown in the phase diagram of water (I) in Figure 2-8.[79]

Previously, application of water at hydrothermal conditions for heavy oil upgrading was investigated. At the studied conditions of sub-critical water (160-300 °C), the water was shown to contribute to the reduction of heavy oil viscosity and to a slight removal of sulfur from the heavy oil. [79,88] Between 200 and 300 °C, small amounts of light hydrocarbons with carbon numbers C_1-C_7 in the gas phase were also formed upon treatment of heavy oil with water. [79,88] On the other hand, heavy oil was significantly upgraded in the presence of near-critical and supercritical water, which resulted in a major reduction in the heavy oil viscosity accompanied by significant changes in the amounts of SARA components and heteroatom (especially sulfur) content.[79] Further, hydrothermal treatment of bitumen at temperatures ≥ 300 °C was investigated. Some of the characteristics that were shown to be affected by the treatment were sulfur removal, asphaltenes conversion to maltenes and coke suppression.[82] While all these works studied the contribution of water to the changes in heavy oil and bitumen relative to their raw (untreated) state, the action of water was unsubstantiated compared to the action of temperature by performing a control experiment of thermal treatment in the absence of water. Only in the work by Fan, et al., a control experiment was performed, in which the treatment of heavy oil at 240 °C in the absence of water did not lead to any change in the viscosity of heavy oil, whereas the viscosity was reduced by 14-28% when the same treatment was performed in the presence of 10-50 wt% water.[88]

Physical properties of water (II) such as dielectric constant, density, inorganic solubility and hydrocarbon solubility, change with an increase in temperature from sub critical state to near supercritical state, and finally to supercritical state, as shown in Figure 2-8.[79] Due to a decrease in the dielectric constant of water with increasing temperature, water gradually loses its polarity and turns into a good solvent for organic species and light gases such as O_2, N_2, CO_2, CO, NH_3. Moreover, the ionic product ($K_W = [H^+] [OH^-]$) of water at 300 °C and 34.5 MPa (sub-critical region) is around 10^{-11} compared to the value of 10^{-14} at the standard conditions (25 °C and 101.3 kPa)[89] due to the endothermic character of water self-dissociation. This phenomenon results in higher concentrations of H^+ and OH^- ions, which may provide a good environment for acid- or base- catalyzed reactions like hydrolysis.[80,90] However, as the critical point approaches, the ionic product of water starts to decrease and water is said to no longer act as an efficient acid-base catalyst. [80,90]
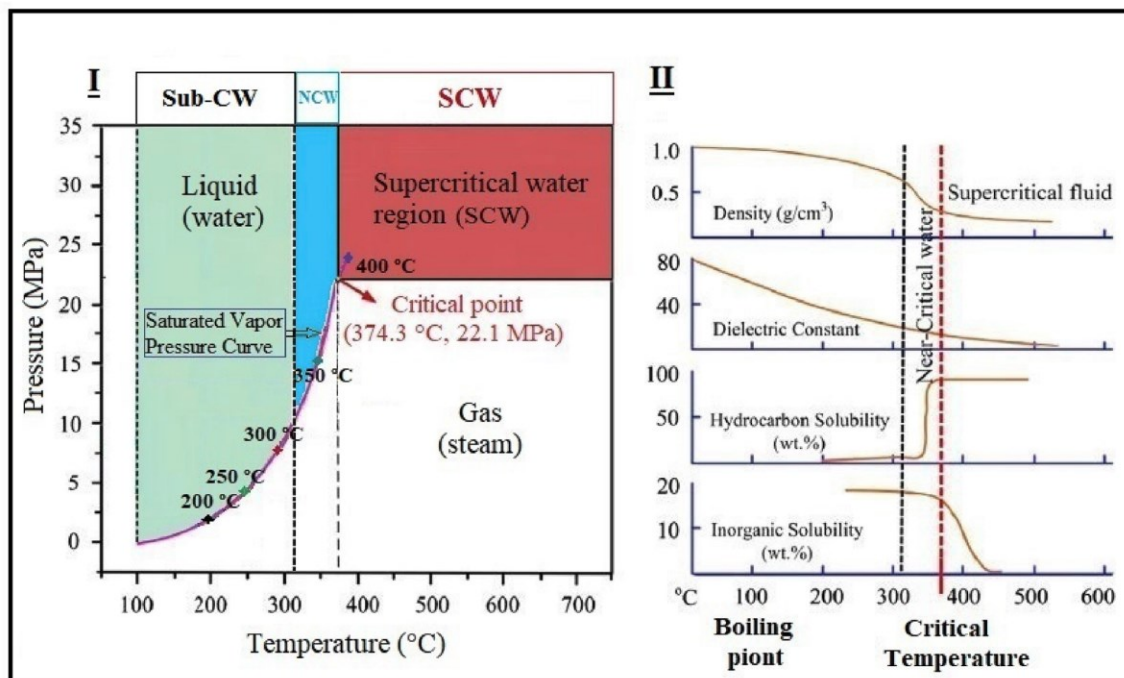
Figure 2-8. Phase Diagram of Water (I) and Changes in the Physical Properties of Water with Increasing Temperature in the Sub-Critical, Near-Critical and Super-Critical States (II) [79]

Upgrading of oil sands bitumen and coal tar using supercritical water (SCW) as a reaction medium was investigated previously.[91,92] Significant increase in the asphaltenes conversion and maltenes yield of coal tar pyrolysis in the presence of SCW in comparison with those obtained in the presence of N_2 was noted by Han, et al., which led to the hypothesis that the H and OH radicals from SCW quenched the free radicals generated from thermal cracking of asphaltenes during the decomposition of coal tar, producing a higher yield of maltenes.[92] Experiments were conducted using model compounds benzyl phenyl ether ($C_{13}H_{12}O$), quinoline (C_9H_7N) and dibenzyl suphide ($C_{14}H_{14}S$) to further assist with understanding the reaction chemistry which likely occurred between asphaltenes and SCW. [92] Formation of lighter products from the model compound pyrolysis in SCW was explained using free radical chemistry that involved breakage of $C-S$, $C-N$ and $C-O$ bonds and the participation of H and OH radicals from SCW to quench some of the free radicals formed during these reactions. [92] However, no specific proof of the generation of free radicals from SCW was presented in this work.

The primary reaction representing the homolytic dissociation of water ($\Delta H = 492$ kJ/mol)[93] for the generation of hydroxyl radical (OH$^\bullet$) and hydrogen radical (H$^\bullet$) is shown in Eq 2-10. In literature, radiolysis is reported as a method for producing free radicals via exposure of water to high energy radiation, in which alpha particles and gamma rays are commonly used.[94] As the generated radicals are short lived and swiftly recombine, techniques like spin trapping combined with electron spin resonance spectroscopy may be used to detect such radicals.[95] The possibility of splitting water into free radicals by mere application of high temperature, especially in the range 400-480 °C, that was used in the coal tar pyrolysis study, is barely reported in literature.

$$H_2O \rightarrow OH^\bullet + H^\bullet$$ Eq 2-10.

Morimoto, et al. considered that the chemical effects of SCW on bitumen upgrading were small based on the analysis of gas products.[83] Based on the gaseous products analysis and H/C ratio measurements of the heavier products (distillation residue and coke), they found no evidence that the participation of SCW in steam reforming and water-gas shift reactions (Eq 2-11. and Eq 2-12 respectively), or as a radical capping agent played a major role in bitumen conversion. Steam-methane reforming (shown in Eq 2-11) is highly endothermic requiring a high temperature (typically 750-950 °C) and a high pressure (typically1.4-4 MPa) in the presence of a catalyst (Ni-based catalysts are most widely used).[96] On the other hand, the water-gas shift reaction (shown in Eq 2-12.), which is an intrinsic inclusion into the steam reforming process, is moderately exothermic. Although lower temperatures favor the formation of products in the water-gas shift reaction, the reaction kinetics are slow or sluggish.[97,98] At the temperature and pressure conditions (440 °C and 10–30 MPa) used in the study on bitumen upgrading in supercritical water in the absence of a catalyst, the steam reforming and water-gas shift reactions would probably not be meaningful to produce hydrogen that could participate in the bitumen conversion. Such high pressures are likely to shift the equilibrium of the steam reforming reaction to the left, generating fewer moles of gases according to the Le Chatelier's principle.

$$CH_4 + H_2O \rightleftharpoons CO + 3H_2 \quad \Delta H° = +206 \text{ kJ/mol} \qquad \text{Eq 2-11.}$$

$$CO + H_2O \rightleftharpoons CO_2 + H_2 \quad \Delta H° = -41 \text{ kJ/mol} \qquad \text{Eq 2-12.}$$
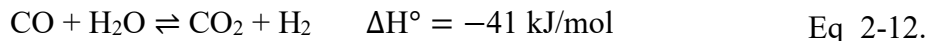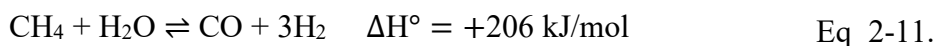
Instead, it was proposed that the effect of SCW on the conversion of oil sands bitumen was primarily physical in nature, and that the SCW likely dispersed the heavier components of bitumen, which prevented recombination reactions after radical formation and the so-called cage-effect from occurring.[91]

In this thesis, the focus is on performing hydrothermal treatment at conditions corresponding to the sub-critical state of water.

Table 2-8. Synthetic Organic Reactions Occurring in the Presence of High Temperature (200-350 °C) Aqueous Solutions [99]

Reaction Type	Starting Material	Products	Medium	Yield (%)	Temperature/ Time
Hydrolysis	*n*-hexyl acetate	hexanol, acetic acid	water	94	295 °C/180 min
Decarboxylation	indole-2-carboxylic acid	indole	water	100	255 °C/20 min
	2-carbethoxyindole	indole	water	20	255 °C/20 min
	2-carbethoxyindole	indole	0.2 M NaOH	93	255 °C/20 min
Hydration of Alkenes and Alkynes	phenylacetylene	acetophenone	water	51	250 °C/5 days
	phenylacetylene	acetophenone	0.5 M H_2SO_4	90	280 °C/60 min
Isomerization	carvone	carvacrol	water	95	250 °C/10 min
Intramolecular Aldol Condensation	2,5-hexanedione	3-methyl cyclopent-2-enone	0.01 M NaOH	81	200 °C/15 min

Various examples of synthetic organic reactions, such as hydrolysis, decarboxylation, hydration of alkenes and alkynes, isomerization and condensation, occurring in the presence of high temperature (200-350 °C) aqueous solutions were presented by An, et al. [99] Some of these reactions are listed in Table 2-8.[99]

Hydrolysis ("hydro" = water and "lysis' = break) is a chemical reaction in which water is consumed to break a larger molecule into two smaller molecules (reverse of condensation). Ester hydrolysis reactions are catalyzed by both acids and bases.[100] Decarboxylation involves removal of a carboxyl group from an organic compound, generating CO_2 as the by-product. Decarboxylation reactions were shown to occur in the presence of high temperature water, and the addition of water to a carboxylic acid group is said to be catalyzed by acidic solutions through a carbocation mechanism.[101] In the conversion of 2-carbethoxyindole to indole (Table 2-8) in water, ester hydrolysis of 2-carbethoxyindole to indole-2-carboxylic acid was considered to be the intermediate step, followed by decarboxylation to indole.[99] The overall reaction, when carried out in a basic NaOH solution, as compared to reaction in pure water, yielded higher amounts of indole. It was concluded that ester hydrolysis was the rate-limiting step, and the overall decarboxylation of 2-carbethoxyindole to indole was catalyzed by the base. Hydration reaction of alkenes and alkynes is the addition of water to the double- and triple- bonded carbon atoms, resulting in the formation of an alcohol and ketone (from tautomerization of enol) respectively. These reactions are also said to be catalyzed by dilute acidic solutions like sulfuric acid and proceed through formation of a carbocation intermediate.[99,102] Isomerization of carvone to cavacrol, which occurs at high temperature water, was also shown to be acid-catalyzed through a carbocation mechanism.[103] Intramolecular Aldol Condensation, during which an organic compound containing

two carbonyl functionalities yields a ring product, occurs in the presence of a base such as NaOH.[104]

In addition, studies conducted to investigate the reactivity of model organic compounds in water in the temperature range 200-350 °C, with pressures varying from 4 MPa (at 200 °C) to 17 MPa (at 350 °C), indicated that ionic chemistry predominates over thermal free radical routes.[105] Examples such as ester hydrolysis of methyl-1-naphthoate followed by decarboxylation,[100] intramolecular rearrangement reactions and cleavage of 4-phenoxyphenol,[100] and cleavage of cyclohexyl phenyl compounds containing oxygen, sulfur or nitrogen links,[106] which did not appear to occur under thermal conditions (via free radical routes) but preferentially occurred under aqueous conditions, were given.[105] Further, using 3-substituted oxygenated pyridine compounds (acid, aldehyde and hydroxymethyl), it was shown that water-soluble reaction products generated upon direct cleavage or indirect condensation reactions of these compounds, such as formaldehyde and formic acid, auto catalyzed reactions.[105,107] These studies indicated that water can act as an effective acidic or basic catalyst, and that the water-soluble products can reinforce its reactivity through auto-catalysis. The ability of water to affect selective ionic chemistry in some of the hydrolysis, condensation and cleavage reactions, that are not accessible thermally, was largely attributed to the changes in the properties of water at high temperatures, which become more compatible with organic reactions.[105]

Thus, literature on the role of high temperature water suggests that presence of water may be beneficial for upgrading bitumen. However, most studies that were performed using bitumen were conducted at severe conditions ≥ 300 °C, and in the absence of solids. Hence, further information is required to understand the role of water in the lower temperature conversion of bitumen.

2.5.2. Role of Minerals under Hydrothermal Conditions

2.5.2.1. Impact on Heavy Oil/Bitumen Properties

Conversion of bitumen in the presence of 4-8 wt% of native mineral solids and 8-12 wt% water at 425-510 °C and 100-1500 psig was patented by Sankey, et al.[108] Compared to conventional visbreaking, the patented process gave better results in terms of viscosity reduction, vacuum residue conversion and removal of sulfur and heavy metals, as indicated in Table 2-9. These benefits were attributed to the deposition of coke on the surface of solids and the role of solids in adsorbing heteroatoms and metals from bitumen.

Table 2-9. Comparison of Bitumen Properties in Conventional Visbreaking Process and Patented Process of Thermal Treatment in the Presence of Mineral Solids and Water [108]

Property of Bitumen	Feed	Conventional Visbreaking	Patented Process
Density (kg/m^3) at 15.6 °C	1014	993	966
Viscosity (cSt/38 °C)	30000	260	30
Sulfur (wt%)	4.9	4.4	3.7
Metals (Ni+V) (ppm)	300	300	126
+525°C content (wt%)	54	38	25

In a study by Fan, et al., heavy oil was mixed with 10 wt% water and 10 wt% mineral solids (~10 wt% clay minerals and 90 wt% non-clay minerals) and subjected to aquathermolysis in an autoclave at 240 °C for 24 h.[109] After reaction in the presence of both water and minerals, the viscosity of the heavy oil was reduced by approximately 25 %, whereas about 12 % reduction in viscosity was observed in the presence of only water (without solids addition).[109] In another study

by Fan, et al., heavy oil was mixed with 30 wt% water and 10 wt% mineral solids (~10 wt% clay minerals and 90 wt% non-clay minerals) and subjected to aquathermolysis in an autoclave at 240 °C for 48 h.[88] After reaction in the presence of both water and minerals, the viscosity of the heavy oil was reduced by approximately 37 %, whereas about 26 % reduction in viscosity was observed in the presence of only water (without solids addition).[88]

Xian, et al. studied the individual effects of different clay and non-clay minerals on viscosity of heavy oils in aquathermolysis.[110] The minerals used in that study were illite, kaolinite, montomorillonite, quartz, potassic feldspar and plagioclase. The amount of water in the reaction feed was maintained at 30 wt%. The viscosity of heavy oil was not only reduced in the presence of minerals but clear differences in the degree of viscosity reduction were identified between the minerals as a function of temperature (160−260 °C), reaction time (0−48 h) and dosage of minerals (0-30 wt%). For example, the degree and rate of viscosity reduction was higher for kaolinite when compared to quartz. The optimal conditions for viscosity reduction in this process were different for different minerals. It can be inferred that nature of minerals is an important factor in this process. In the same study,[110] the clay minerals illite, kaolinite and montmorillonite showed higher viscosity reduction compared to other minerals, at any particular temperature, reaction time or mineral dosage.

Fan, et al. proposed that the transition metal species such as Ni and V present in heavy oils can be adsorbed on the surface of clays due to their negative charge.[88] It was said that this assembly of transition metal on silica-alumina support acts as a catalyst similar to industrial hydrocracking catalyst.[88] However, no experiment proof of metal (Ni and V) reduction in the heavy oil due to adsorption on mineral surface was provided in this study.

In a different study,[111] Nhieu, et al. reported that removal of fine solids from the Athabasca vacuum tower bottoms, significantly decreased the onset of coke formation during thermal conversion at 410 °C. The increase in the induction time in the presence of solids, at the conditions used in this study, was attributed to the solids aiding dispersion of coke precursors and preventing them from agglomerating, decreasing the rate of coke formation.

So far, research on oil-mineral interactions has mainly focused on the adsorption behavior of oil fractions on the surfaces of solids (described in sections 2.5.2.3.) or on the thermal alteration of solids (section 2.5.2.2.). Limited work was conducted to understand the mechanism by which solids affect the reaction chemistry of bitumen conversion, especially in the hydrothermal froth treatment process. For example, the clay minerals may participate in the bitumen conversion chemistry by virtue of their acidic and/or redox characteristics of clay minerals, influencing the physical and chemical properties of bitumen during hydrothermal froth treatment.

2.5.2.2. Thermal Alteration of Mineral Solids

As mentioned in section 2.2.2., mineral solids in bitumen froth are associated with toluene-insoluble organic matter. Wettability alteration of the solids after hydrothermal froth treatment at 392 °C was reported by Zhao, et al.[18] Contact angle measurements suggested that hydrothermal treatment transformed the wettability of solids and made them more hydrophobic, most likely due to accumulation of organic components on the surface of solids. Due to this, most of the froth solids stayed in the organic phase after hydrothermal treatment, contributing to destabilization of water-in-oil emulsions in bitumen froth. Moreover, the organic layer which was originally patchy on the mineral surfaces in bitumen froth, became more continuous after hydrothermal treatment. It was hypothesized that the organics that were initially trapped within the mineral were released during hydrothermal treatment due to disruption of these aggregates, which led to a redistribution

of organic material on the surface of solids, changing their surface properties.[17] According to the review by Chen and Liu, the patchy nature of bitumen coating on clay particles was reported in several recent works.[34]

Additionally, under the conditions of hydrothermal treatment process, it is possible that minerals undergo decomposition and changes in crystal structures. For example, dehydroxylation of kaolinite (Eq 2-13) occurs in the temperature range 350-700 °C during which the chemically bonded water molecules are lost resulting in the formation of metakaolin.[112] Chen, et al. reported that, compared to untreated kaolinite, the adsorption density (mg/m^2) and surface coverage of asphaltenes on the dehydroxylated kaolinite, after multiple contacts, were higher, and increased with an increase in the degree of dehydroxylation (function of treatment temperature and measured as TGA weight loss).[113] This observation was attributed to the strained structures on dehydroxylated kaolinite after the release of water molecules, which may act as active binding sites for adsorption of organic substances.[113] From this, it can be inferred that, the affinity of clay minerals to hydrocarbons may be strengthened during thermal processing. Further, as the minerals in oil sands are already covered with organic matter, it may affect the degree of dehydroxylation of the clay and its adsorption behavior.

$$Al_2Si_2O_5(OH)_4 \rightarrow Al_2O_3 \cdot 2SiO_2 + 2H_2O \qquad \text{Eq 2-13.}$$

Another example that was reported in literature is the formation of pyrrhotite from pyrite in coal when heated above 450 °C.[114] Pyrite (FeS_2) decomposes into pyrrhotite and sulfur.[115] It was reported that during this transformation not all of the sulfur is emitted but some sulfur gets trapped in the organic matrix.[116] In the characterization of solids after hydrothermal treatment at 392 °C, although no significant changes in the composition of clays were found, a significant amount of

pyrrhotite ($Fe_{(1-x)}S$; x=0-0.17) was formed from pyrite and siderite,[18] indicating that the formation of pyrrhotite can occur at temperatures below 450 °C.

Additionally, a change in the crystal structure of quartz occurs at 573 °C due to transformation of α-quartz to β-quartz.[117] Decomposition of carbonate minerals in the thermogravimetric analysis of oil shales was also reported in the 600-850 °C temperature range,[118,119] according to Eq 2-14. and Eq 2-15. for calcite ($CaCO_3$) and dolomite ($CaMg(CO_3)_2$) respectively.[118]

$$CaCO_3 \rightarrow CaO + CO_2 \qquad \text{Eq 2-14.}$$
$$[Ca, Mg]CO_3 \rightarrow [Ca, Mg]O + CO_2 \qquad \text{Eq 2-15}$$

Thus, upon heating, decomposition and changes in crystal structures of minerals can occur. Although an initial mass loss under 200 °C can occur due to moisture loss,[120,121] decomposition and structural changes were reported for most minerals at temperatures above 400 °C. This aspect is important for hydrothermal froth treatment during which the solids in the froth are heated, especially at temperatures exceeding 400 °C. Moreover, the organic coating on the surface of mineral solids in bitumen froth might affect the degree of thermal alteration of solids during hydrothermal treatment as compared to pure inorganic solids.

2.5.2.3. Mineral-Organic Interactions

The various ionic reactions of model organic compounds in high temperature water, that were mentioned in section 2.5.1., were reported to be accelerated in the presence of clay minerals.[105] The role of clays in organic reactions was mainly attributed to their acidic properties.

Clays may function as Bronsted acids or Lewis acids or both. A substance that can donate protons or H^+ ions is called a Bronsted acid, where as a substance that can accept an electron pair is known as a Lewis acid. To explain the acidic characteristics of clay minerals in the following lines, Figure

2-9 is used as an example. In Figure 2-9, the lattice structure of a 2:1 (T-O-T) clay, with an octahedral (O) gibbsite [$Al_2(OH)_6$] sheet sandwiched between two tetrahedral (T) silicate [SiO_4]$^{4-}$ sheets, and the interlayer spacing of the clay structure are shown. Most of the acid characteristics described below are applicable to kaolinite and illite, which are 1:1 (T-O) and 2:1 (T-O-T) clays respectively.
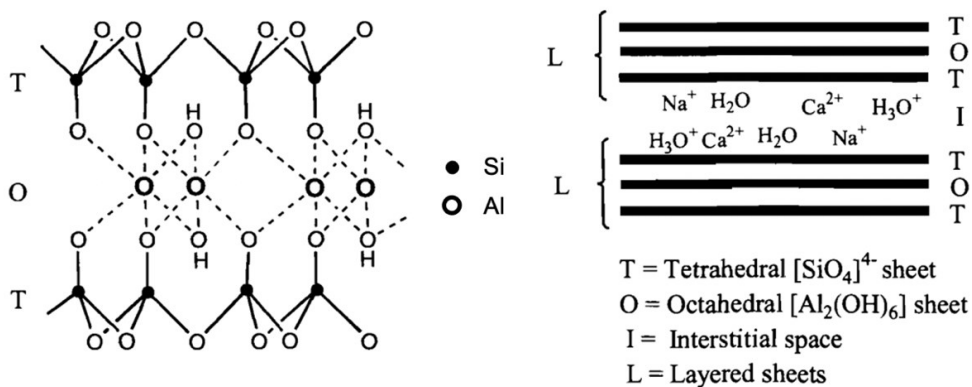
Figure 2-9. Clay Structure (2:1 Clay)[122]

The Bronsted acidity of clay minerals is either due to dissociation of coordinated water molecules in the interlayer spacing caused by the polarizing effect of the exchangeable cations (Eq 2-16) or due to hydroxyl groups in specific sites at the layer edges which dissociate into reactive protons.[122-125]. Termination at the layer edges results in broken bonds, which may be compensated by the formation of hydroxyl groups.[124] For example, the rupture of the siloxane bond ($\equiv$Si$-$O$-$Si$\equiv$) in the tetrahedral sheet and reaction with water (Eq 2-17.) would result in the formation of a Bronsted acidic silanol (Si-OH) group, which could release protons (Eq 2-18).[124,126] On the other hand, unsaturated or incompletely coordinated Al^{+3} ions located at the edges act as Lewis acid sites.[122,123] Due to the presence of an vacant d-orbital, Al^{+3} can accept an electron pair, thus acting as a Lewis acid. These acid sites in clay minerals can initiate ionic reactions of organic compounds, mainly through the formation of a carbocation intermediate. [122,123]

$$[M(H_2O)_n]^{3+} \leftrightarrows [M(H_2O)_{n-1}(OH)]^{2+} + H^+ \qquad \text{Eq 2-16.}$$

$$\text{Si–O–Si (SiO* + Si*)} + H_2O \rightarrow \text{Si-OH} \qquad \text{Eq 2-17.}$$

$$\text{Si-OH} \rightarrow \text{SiO}^- + H^+ \qquad \text{Eq 2-18.}$$
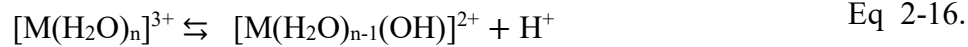
In the current research, the clay minerals in bitumen froth are not chemically modified by external addition of acid. Exchangeable base cations such as Ca^{2+}, Mg^{2+}, K^+ and Na^+ would be the counter-ions present in clays, not H^+, and diminish the acidity of clays. Therefore, it could be relevant to explore whether the clay minerals in bitumen froth can catalyze cationic organic reactions at the alkaline conditions of the bitumen froth (pH of the aqueous phase $= 7.9 \pm 0.1$)[21] during hydrothermal treatment.

Clay minerals are also said to exhibit redox properties.[127-132] Their redox behavior is generally attributed to the structurally bound iron (Fe) present in the majority of clay minerals.[130,131] For example, formation of phenoxyl-type radicals, under ambient conditions, by adsorption of phenol on Fe(III)-Montmorillonite and reduction of Fe^{3+} to Fe^{2+} was reported.[132] Thus, redox reactions between the clay minerals and organic compounds could lead to the formation of reactive radical intermediates, which further participate in reactions.

Like clays, non-clay minerals can act as adsorbents and catalysts. For example, terminal and bridged hydroxyl groups on the surface of titanium dioxide behave as Lewis base and Lewis acid centers respectively.[133] Carbonate minerals have a higher affinity towards acidic components.[20,134,135] Surface silanol (Si-OH) groups in quartz may act as adsorption sites by hydrogen bonding.[136,137] However, very little is reported in literature about the catalytic effects of non-clay minerals as compared to acidic clay mineral catalysis.

Adsorption is a key step in catalysis, in which the reactants are adsorbed on the surface of the catalyst. The following paragraphs summarize the literature on adsorption of oil fractions on the surfaces of different solids.

Adsorption of nC_6-asphaltenes obtained from crude oil on calcium carbonate at room temperature was investigated by Subramanian, et al.[138] Post adsorption from asphaltene-toluene mixtures, the adsorbed asphaltenes were extracted in two steps – first, using tetrahydrofuran (THF) at 45 °C, and second, using acid digestion with HCl solution at room temperature. After the first step of desorption with THF, a significant amount of asphaltenes (~20 wt%) remained on the surface of $CaCO_3$, which could not be removed easily using organic solvent extraction, indicating that this asphaltene sub-fraction had strong affinity to $CaCO_3$. This sub-fraction, which was called the 'irreversibly adsorbed asphaltenes' sub-fraction, was shown to contain the highest concentrations of carbonyl and carboxylic acid groups and derivates. After acid treatment in the second step, nearly 98-99 % of the initial asphaltene material was recovered by dissolution of $CaCO_3$ attached to the asphaltenes based on Eq 2-19. The choice of acid used in the second step – HCl vs. acetic acid, had negligible impact on the recovery of asphaltenes and their characteristics. In this study, the adsorption behavior of asphaltenes was fit to the Langmuir equation (Eq 2-20), assuming monolayer adsorption. However, the irreversible nature of adsorption and the need for the destruction of mineral matter by acid digestion suggests that the adsorption of asphaltenes on the surface of $CaCO_3$ was probably not just a physical adsorption following a Langmuir isotherm, but rather a chemical adsorption.

$$CaCO_3 + 2\ HCl \rightarrow CaCl_2 + H_2O + CO_2 \uparrow \qquad\qquad \text{Eq 2-19}$$

$$q = q_{max}\frac{K_L C_e}{1 + K_L C_e}$$

Eq 2-20

where:

q = amount adsorbed (mg/m^2)

q_{max} = maximum adsorption capacity (mg/m^2)

K_L = Langmuir equilibrium adsorption constant (l/g)

C_e = equilibrium asphaltene concentration in solution (g/l)

The linear form of the above Langmuir model is given by Eq 2-21.

$$\frac{C}{q} = \frac{1}{q_{max}K_L} + \frac{C}{q_{max}}$$

Eq 2-21

Similarly, adsorption of nC$_5$-asphaltenes obtained from bitumen onto sodium exchanged kaolinite and illite minerals from clay-toluene mixtures was investigated by Tu, et al.[139] The adsorption isotherms were in agreement with the Langmuir equation (Eq 2-20. and Eq 2-21.), indicating monolayer adsorption. The adsorbed layer was again reported to be patchy and discontinuous. In another study, adsorption of nC$_7$-asphaltenes obtained from bitumen onto γ-Al$_2$O$_3$ nanoparticles from asphaltene-toluene mixtures in the temperature range 298-328 K indicated that the adsorption was exothermic ($\Delta H°_{ads}<0$), i.e., adsorption decreased with increase in temperature, and that it was spontaneous ($\Delta G°_{ads}<0$) in nature.[140] A positive value for $\Delta S°_{ads}$ was noted, which corresponds to an increase in the randomness upon asphaltenes adsorption at the solid-liquid interface. These thermodynamic parameters were determined using Eq 2-22. and Eq 2-23. Further, the resultant adsorption isotherms were in good agreement with the Langmuir model (Eq 2-20. and Eq 2-21.). Thermodynamics of adsorption can be complex, and the description provided in this section might be an over-simplification. The negative Gibbs free energy, which is the driving force for the

asphaltenes adsorption could have been contributed by a number of forces or interactions from the bulk to the solid-liquid interface.

In the same study, the effect of water content on asphaltenes adsorption was studied, in which it was found that the asphaltenes adsorption decreased linearly with increasing water content in the range 0.1-0.25 vol%. This was attributed to the competitive adsorption between the asphaltenes and water, and increase in the hydrophilicity of nanoparticle surface which drives away asphaltenes from the surface and decreases their adsorption.

$$\Delta G°_{ads} = -RT \ln(K_{ads}) \qquad\qquad \text{Eq 2-22.}$$

$$\ln(K_{ads}) = -\frac{\Delta H°_{ads}}{RT} + \frac{\Delta S°_{ads}}{R} \qquad\qquad \text{Eq 2-23.}$$

where:

$\Delta G°_{ads}$ = standard Gibbs free energy change (J mol^{-1})

R = ideal gas constant (8.314 J mol^{-1} K^{-1})

T = temperature (units K)

K_{ads} = adsorption equilibrium constant (dimensionless), calculated as $K_L C_S$, where K_L is the Langmuir equilibrium adsorption constant and C_S is the solvent (toluene) molar concentration

$\Delta H°_{ads}$ = standard change in enthalpy (J mol^{-1})

$\Delta S°_{ads}$ = standard change in entropy (J mol^{-1} K^{-1})

Previously, even Freundlich adsorption isotherm model (Eq 2-24.) was used to describe the behavior of asphaltene adsorption on certain solid surfaces, suggesting multilayer adsorption of asphaltenes on heterogeneous surfaces.[141,142]

$$N_{ads} = K_F C_E^{1/n}$$ Eq 2-24.

where:

N_{ads} = mass adsorbed per unit mass of adsorbent (mg/g)

K_F = Freundlich constant ((mg/g)(L/mg)$^{1/n}$)

C_E = equilibrium concentration (mg/L)

$1/n$ = adsorption intensity factor (dimensionless)

Giraldo, et al. proposed a different model, called the Dubinin−Astakhov model (Eq 2-25.), to predict the adsorption behavior of asphaltenes onto different surfaces.[143] They found that the Dubinin−Astakhov model represented the experimental data obtained for asphaltene adsorption better than the Freundlich or Langmuir adsorption models.

$$N_{ads} = N_{ads,max} \exp\left[-\left(\frac{A}{E}\right)^n\right]$$ Eq 2-25.

where:

N_{ads} = mass adsorbed per unit mass of adsorbent (mg/g)

$N_{ads,max}$ = maximum adsorbed amount (mg/g)

A = adsorption potential (KJ/mol)

E = adsorption energy (KJ/mol)

n = parameter representing surface heterogeneity

Li, et al. investigated the affinity of the SARA fractions in bitumen to different minerals using the Quartz Crystal Microbalance with Dissipation monitoring (QCM-D) tests, in which the desorption of pre-adsorbed oil fractions from minerals through water flushing was studied.[144] The amount desorbed (on weight basis), and desorption rate constant (s^{-1}) were used as indicators of the affinity between the oil fraction and the mineral. It was shown that the desorption behavior was different for different SARA fractions and different minerals. Among the minerals investigated in this study

(silica, kaolinite and calcium carbonate), the amounts of the oil fractions desorbed followed the order saturates > aromatics > resins > asphaltenes for silica and kaolinite, and saturates ≈ aromatics > resins > asphaltenes for calcium carbonate. Particularly, calcium carbonate showed the highest affinity among all the minerals, as it was found that the desorption amount was low (10% and below) for all the oil fractions on the calcium carbonate surface. The amount of asphaltenes that desorbed from the minerals was close to zero, indicating that the asphaltenes adsorbed strongly on the minerals, irrespective of the mineral type. Using the kinetics of desorption, spontaneous desorption from the mineral surfaces was noticed only for the saturate and aromatics fractions. On the other hand, based on the mineral type, the affinity of oil fractions to minerals in aqueous solutions was given as: calcium carbonate > kaolinite > silica. Although the interactions between the asphaltenes and minerals were partly explained by hydrogen bonding interactions, acid-base interactions likely played a role. It was observed in this study that the asphaltenes possessed the highest TAN values (~8 mg KOH/g) among the SARA fractions. Calcium carbonate, being a base, can chemically react with the acid groups in the asphaltenes, which can explain the highest affinity of asphaltenes to calcium carbonate. Silica (SiO_2), in the absence of water to create the silanol groups, can be considered neutral which might explain its least affinity to the asphaltenes. Finally, the relatively amphoteric character of kaolinite, due to the presence of Al-OH groups, might explain its moderate affinity to the asphaltenes in this work.

On the other hand, Mamonov, et al. identified that sandstone material containing a sufficient amount of clay mineral (8-16 wt% illite) preferentially adsorbed basic compounds from crude oil in a crude oil-brine-rock system, based on acid and base number analysis of effluent remaining after adsorption), whereas the sandstone material containing mainly quartz and having an insignificant amount of clay minerals (2.5 wt% kaolinite), did not show a marked tendency to

adsorb organic matter or preference for basic or acidic compounds.[145] It was explained that the charges of polar organic acidic and basic compounds depend on the pH of the aqueous phase, which influences the adsorption of those compounds on the charged surfaces of minerals. At acidic pH (< 7) conditions, polar organic bases are positively charged, while at alkaline pH (> 7), they are neutral, as shown in Eq 2-26. On other hand, polar organic acids are negatively charged at alkaline pH and neutral at acidic pH, as shown in Eq 2-27.

$$R_3N: + H_2O \rightleftarrows R_3NH^+ + OH^- \qquad\qquad \text{Eq 2-26.}$$

$$RCOOH + H_2O \rightleftarrows RCOO^- + H_3O^+ \qquad\qquad \text{Eq 2-27.}$$

The above studies on adsorption involve oil fractions which are not thermally treated. Carbognani, et al. and Lopez-Linares, et al. investigated the adsorption characteristics of visbroken vacuum residue and its asphaltenes.[146,147] Both the studies concluded that the adsorption (mg/g) of severely visbroken vacuum residue (conversion = 28.5 % after visbreaking for 300 min at 380 °C) and its asphaltenes on kaolin increased compared to the untreated vacuum residue and its asphaltenes. However, the same was not true for adsorption of asphaltenes from the severely visbroken vacuum residue on Na- and Ca-montmorillonites, on which the adsorption decreased compared to the untreated vacuum residue asphaltenes.[147] A possible explanation for these observations could be the release of CO and CO_2 during conversion of bitumen from the decomposition of some of the oxygenate functional groups, producing a product that has a lower TAN and will be less reactive towards basic minerals. In addition, Carbognani, et al. reported that passing the thermally cracked residua through the kaolin packed bed improved their intrinsic stability through adsorption of unstable molecules from the visbroken residua.[147] Further, Lopez-Linares, et al. also found that the adsorption of asphaltenes was not governed by the surface area of the solids studied, but instead correlated with the pore volume and pore diameter of the adsorbents.[147] These studies suggest that

thermal modification of bitumen components may influence their adsorption on the surface of mineral solids and that the solids may have the potential to selectively adsorb unstable molecules and promote upgrading of unstable vacuum residues. However, the role of solids during thermal conversion of bitumen is still not clear.

In hydrothermal froth treatment, it is possible that both physical adsorption and chemisorption occur. As physical adsorption is a weaker interaction than chemisorption, physically adsorbed species can more readily be desorbed by an increase in temperature or displaced by other species.[145] Competitive adsorption, which is the ability of species to displace other species, [148] is therefore dependent on the nature of competing species, type of adsorption and temperature. In minerals that are unlikely to have any catalytic activity, competitive adsorption between physisorbed species can occur, which is also a function of temperature and the nature of competing species. The penetrating ability of species through the liquid medium to reach the solid surface is subject to mass transport limitations.[148] Therefore, reaction time and temperature must be considered as important variables in this process to study adsorption. In addition, the pore constraints of minerals must be taken into consideration. For example, solids with narrow pores might pose a constraint for the adsorption of larger molecules, limiting their adsorption capacities. To summarize, research on oil-mineral interactions has mainly focused on the adsorption characteristics of oil fractions on the surfaces of mineral solids. Limited work was done to understand the mechanisms by which the clay and non-clay minerals could affect the reaction chemistry influencing bitumen conversion following on adsorption.

2.6. References

(1)   Czarnecki, J.; Masliyah, J.; Xu, Z.; Dabros, M. *Handbook on Theory and Practice of Bitumen Recovery from Athabasca Oil Sands - Volume 2: Industrial Practice*; Kingsley Knowledge Publishing: 2013; p 214.

(2)   Strausz, O. P.; Lown, E. M. 2003. *The Chemistry of Alberta Oil Sands, Bitumens and Heavy Oils*; Alberta Energy Research Institute: Calgary, Canada, 2003; pp 29–636.

(3)   Gray, M. R. *Upgrading Oilsands Bitumen and Heavy Oil*; Pica Pica Press: Edmonton, Canada, 2015; pp 2–477.

(4)   Hollerbach, A. Influence of Biodegradation on the Chemical Composition of Heavy Oil and Bitumen. In *Exploration for Heavy Crude Oil and Natural Bitumen*; Meyer, R. F.; AAPG Studies in Geology Series No. 25; American Association of Petroleum Geologists: Tulsa, OK, 1987; pp 243–248.

(5)   Chacón-Patiño, M. L.; Rowland, S. M.; Rodgers, R. P. The Compositional and Structural Continuum of Petroleum from Light Distillates to Asphaltenes: The Boduszynski Continuum Theory as Revealed by FT-ICR Mass Spectrometry. In *The Boduszynski Continuum: Contributions to the Understanding of the Molecular Composition of Petroleum;* Ovalles, C.; Moir, M. E.; ACS Symposium Series 1282; American Chemical Society: Washington DC, USA, 2018; pp 113–171.

(6)   Speight, J. G. Petroleum Asphaltenes - Part 1: Asphaltenes, Resins and the Structure of Petroleum. *Oil Gas Sci. Technol.* **2004**, *59* (5), 467–477.

(7)   Moir, M. E. Asphaltenes, what art thou? Asphaltenes and the Boduszynski Continuum. In *The Boduszynski Continuum: Contributions to the Understanding of the Molecular Composition of Petroleum*; Ovalles, C.; Moir, M. E.; ACS Symposium Series 1282;

American Chemical Society: Washington DC, USA, 2018; pp 3–24.

(8)   Alshareef, A. H.; Scherer, A.; Tan, X.; Azyat, K.; Stryker, J. M.; Tykwinski, R. R.; Gray, M. R. Formation of Archipelago Structures During Thermal Cracking Implicates a Chemical Mechanism for the Formation of Petroleum Asphaltenes. *Energy Fuels* **2011**, *25* (5), 2130–2136.

(9)   Acevedo, S.; Castro, A.; Negrin, J. G.; Fernández, A.; Escobar, G.; Piscitelli, V.; Delolme, F.; Dessalces, G. Relations Between Asphaltene Structures and Their Physical and Chemical Properties: The Rosary-Type Structure. *Energy Fuels* **2007**, *21* (4), 2165–2175.

(10)   Sabbah, H.; Morrow, A. L.; Pomerantz, A. E.; Zare, R. N. Evidence for Island Structures as the Dominant Architecture of Asphaltenes. *Energy Fuels* **2011**, *25* (4), 1597–1604.

(11)   Ruiz-Morales, Y.; Mullins, O. C. Polycyclic Aromatic Hydrocarbons of Asphaltenes Analyzed by Molecular Orbital Calculations with Optical Spectroscopy. *Energy Fuels* **2007**, *21* (1), 256–265.

(12)   Mullins, O. C.; Sabbah, H.; Eyssautier, J.; Pomerantz, A. E.; Barré, L.; Andrews, A. B.; Ruiz-Morales, Y.; Mostowfi, F.; McFarlane, R.; Goual, L.; Lepkowicz, R. Advances in asphaltene science and the Yen–Mullins model. *Energy Fuels* **2012**, *26* (7), 3986–4003.

(13)   Ollinger, J. On Mimicking Nano-particulate Behaviors of Asphaltenes in Solution and at Interfaces. M.S. Thesis, University of Alberta, Edmonton, Canada, 2015.

(14)   Zachariah, A.; De Klerk, A. Partial Upgrading of Bitumen: Impact of Solvent Deasphalting and Visbreaking Sequence. *Energy Fuels* **2017**, *31* (9), 9374–9380.

(15)   Tannous, J. H.; De Klerk, A. Quantification of the Free Radical Content of Oilsands Bitumen Fractions. *Energy Fuels* **2019**, *33* (8), 7083–7093.

(16)   Kaminsky, H. A. W.; Etsell, T. H.; Ivey, D. G.; Omotoso, O. Distribution of Clay Minerals

in the Process Streams Produced by the Extraction of Bitumen from Athabasca Oil Sands. *Can. J. Chem. Eng.* **2009**, *87* (1), 85–93.

(17)   Chen, Q.; Stricek, I.; Cao, M.; Gray, M. R.; Liu, Q. Influence of Hydrothermal Treatment on Filterability of Fine Solids in Bitumen Froth. *Fuel* **2016**, *180*, 314–323.

(18)   Zhao, J.; Liu, Q.; Gray, M. R. Characterization of Fine Solids in Athabasca Bitumen Froth Before and After Hydrothermal Treatment. *Energy Fuels* **2016**, *30* (3), 1965–1971.

(19)   Couillard, M.; Tyo, D. D.; Kingston, D. M.; Patarachao, B.; Zborowski, A.; Ng, S.; Mercier, P. H. J. Structure and Mineralogy of Hydrophilic and Biwettable Sub-2 μm Clay Aggregates in Oil Sands Bitumen Froth. *Miner.* **2020**, *10* (11), 1040.

(20)   Adegoroye, A.; Wang, L.; Omotoso, O.; Xu, Z.; Masliyah, J. Characterization of Organic-Coated Solids Isolated from Different Oil Sands. *Can. J. Chem. Eng.* **2010**, *88* (3), 462–470.

(21)   Wang, D.; Qiao, C.; Zhao, Z.; Yang, W.; Chen, H.; Yin, T.; Yan, Z.; Wu, M.; Mao, X.; Santander, C.; Liu, Q.; Liu, Q.; Nikrityuk, P. A.; Tang, T.; Zeng, Hongbo. Understanding the Properties of Bitumen Froth from Oil Sands Surface Mining and Treatment of Water-in-Oil Emulsions. *Energy Fuels* **2021**, *35* (24), 20079–20091.

(22)   Adegoroye, A.; Uhlik, P.; Omotoso, O.; Xu, Z.; Masliyah, J. A Comprehensive Analysis of Organic Matter Removal from Clay-Sized Minerals Extracted from Oil Sands Using Low Temperature Ashing and Hydrogen Peroxide. *Energy Fuels* **2009**, *23* (7), 3716–3720.

(23)   Kotlyar, L. S.; Sparks, B. D.; Woods, J. R.; Chung, K. H. Solids Associated with the Asphaltene Fraction of Oil Sands Bitumen. *Energy Fuels* **1999**, *13* (2), 346–350.

(24)   Axelson, D. E.; Mikula, R. J.; Potoczny, Z. M. Characterization of Oil Sands Mineral Components and Clay-Organic Complexes. *Fuel Sci. Technol. Int.* **1989**, *7* (5–6), 659–673.

(25)   Mikula1, R. J.; Axelson, D. E.; Sheeran, D. Mineral Matter and Clay-Organic Complexes in Oil Sands Extraction Processes. *Fuel Sci. Technol. Int* **1993**, *11* (12), 1695–1729.

(26)   Masliyah, J.; Czarnecki, J.; Xu, Z. *Handbook on Theory and Practice of Bitumen Recovery from Athabasca Oil Sands - Volume 1: Theoretical Basis*; Kingsley Knowledge Publishing: 2011; pp 177–192.

(27)   Wypych, F.; De Freitas, R. A. Clay minerals: Classification, structure, and properties. In *Clay Minerals and Synthetic Analogous as Emulsifiers of Pickering Emulsions*; Developments in Clay Science; Elsevier: Amsterdam, Netherlands, 2022; Vol. 10, pp 3–35.

(28)   Murray, H. H. Overview—Clay Mineral Applications. *Appl. Clay Sci.* **1991**, *5* (5-6), 379–395.

(29)   University of South Alabama. Mineral Chemical Groups and Formulae for Rock Forming Minerals. https://www.southalabama.edu/geography/allison/GY111/MineralFormulaTable.pdf (accessed April 17, 2023).

(30)   Reausser College of Natural Resources, UC Berkeley. Chemical Formulae for Minerals and Gems. https://nature.berkeley.edu/classes/eps2/wisc/mineral.html (accessed April 17, 2023).

(31)   Vinoth Kumar, K. C.; Jani Subha, T. FT-IR Spectroscopic Analysis of Seasonal Impact of Mineral Assemblage in Coastal Soil Samples and its Structural Study. *Int. J. Adv. Sci. Res. Manage.* **2019**, *4* (4), 245–252.

(32)   Hao, H.; Li, L.; Yuan, Z.; Patra, P.; Somasundaran, P. Adsorption Differences of Sodium Oleate on Siderite and Hematite. *Miner. Eng.* **2019**, *137*, 10–18.

(33)   Rakhmatullin, I. Z.; Efimov, S. V.; Klochkov, A. V.; Gnezdilov, O. I.; Varfolomeev, M.
        A.; Klochkov, V. V. NMR Chemical Shifts of Carbon Atoms and Characteristic Shift
        Ranges in the Oil Sample. Pet. Res. **2022**, *7* (2), 269–274.

(34)   Chen, Q.; Liu, Q. Bitumen Coating on Oil Sands Clay Minerals: A Review. *Energy Fuels*
        2019, *33* (7), 5933–5943.

(35)   Liu, J.; Xu, Z.; Masliyah, J. Role of Fine Clays in Bitumen Extraction from Oil Sands.
        AIChE J. **2004**, *50* (8), 1917–1927.

(36)   Ren, S.; Dang-Vu, T.; Zhao, H.; Long, J.; Xu, Z.; Masliyah, J. Effect of Weathering on
        Surface Characteristics of Solids and Bitumen from Oil Sands. *Energy Fuels* **2009**, *23* (1),
        334–341.

(37)   Pignatello, J. J. Soil Organic Matter as a Nanoporous Sorbent of Organic Pollutants. *Adv.*
        Colloid Interface Sci. **1998**, *76–77*, 445–467.

(38)   Golchin, A.; Baldock, J. A.; Oades, J. M. A Model Linking Organic Matter Decomposition,
        Chemistry, and Aggregate Dynamics. In *Soil Processes and the Carbon Cycle*, 1st ed.; Lal,
        R.; Kimble, J. M.; Follett, R. F.; Stewart, B. A., Eds.; CRC Press: Boca Raton, FL, 1998;
        pp 245–266.

(39)   Aveyard, R.; Binks, B. P.; Clint, J. H. Emulsions Stabilised Solely by Colloidal Particles.
        Adv. Colloid Interface Sci. **2003**, *100-102*, 503–546.

(40)   Roostaei, M.; Hosseini, S. A.; Soroush, M.; Velayati, A.; Alkouh, A.; Mahmoudi, M.;
        Ghalambor, A.; Fattahpour, V. Comparison of Various Particle-Size Distribution-
        Measurement Methods. *SPE Reservoir Eval. Eng.* **2020**, *23* (04), 1159–1179.

(41)   Zhao, H.; Dang-Vu, T.; Long, J.; Xu, Z.; Masliyah, J. H. Role of Bicarbonate Ions in Oil
        Sands Extraction Systems with a Poor Processing Ore. *J. Dispers. Sci. Technol.* **2009**, *30*

(6), 809–822.

(42)   Allen, E. W. Process Water Treatment in Canada's Oil Sands Industry: I. Target Pollutants and Treatment Objectives. *J. Environ. Eng. Sci.* **2008**, *7* (2), 123–138.

(43)   Rao, F.; Liu, Q. Froth Treatment in Athabasca Oil Sands Bitumen Recovery Process: A Review. *Energy Fuels* **2013**, *27* (12), 7199–7207.

(44)   Kloet, J. V.; Schramm, L. L.; Shelfantook, B. The Influence of Bituminous Froth Components on Water-in-Oil Emulsion Stability as Determined by the Micropipette Technique. *Colloids Surf., A* **2001**, *192* (1–3), 15–24.

(45)   Velayati, A.; Habibi, A.; Nikrityuk, P.; Tang, T.; Zeng, H. Emulsions in Bitumen Froth Treatment and Methods for Demulsification and Fines Removal in Naphthenic Froth Treatment: Review and Perspectives. *Energy Fuels* **2022**, *36* (16), 8607–8623.

(46)   Ma, J.; Yang, Y.; Li, X.; Sui, H.; He, L. Mechanisms on the Stability and Instability of Water-in-Oil Emulsion Stabilized by Interfacially Active Asphaltenes: Role of Hydrogen Bonding Reconstructing. *Fuel* **2021**, *297*, 120763.

(47)   Singh, M. B.; Rampal, N.; Malani, A. Structural Behavior of Isolated Asphaltene Molecules at the Oil–Water Interface. *Energy Fuels* **2018**, *32* (8), 8259–8267.

(48)   Rocha, J. A.; Baydak, E. N.; Yarranton, H. W. What Fraction of the Asphaltenes Stabilizes Water-in-Bitumen Emulsions? *Energy Fuels* **2018**, *32* (2), 1440–1450.

(49)   Romanova, U. G.; Valinasab, M.; Stasiuk, E. N.; Yarranton, H. W.; Schramm, L. L.; Shelfantook, W. E. The Effect of Oil Sands Bitumen Extraction Conditions on Froth Treatment Performance. *J. Can. Pet. Technol.* **2006**, *45* (09), 36–45.

(50)   Masliyah, J.; Zhou, Z. J.; Xu, Z.; Czarnecki, J.; Hamza, H. Understanding Water-Based Bitumen Extraction from Athabasca Oil Sands. *Can. J. Chem. Eng.* **2004**, *82* (4), 628–654.

(51) Binks, B. P.; Lumsdon, S. O. Pickering Emulsions Stabilized by Monodisperse Latex Particles: Effects of Particle Size. *Langmuir* **2001**, *17* (15), 4540–4547.

(52) Binks, B. P.; Lumsdon, S. O. Influence of Particle Wettability on the Type and Stability of Surfactant-Free Emulsions. *Langmuir* **2000**, *16* (23), 8622–8631.

(53) Yan, N.; Masliyah, J. H. Effect of pH on Adsorption and Desorption of Clay Particles at Oil–Water Interface. *J. Colloid Interface Sci.* **1996**, *181* (1), 20–27.

(54) Bakhtiari, M. T. Role of Sodium Hydroxide in Bitumen Extraction: Production of Natural Surfactants and Slime Coating. Ph.D. Dissertation, University of Alberta, Edmonton, Canada, 2015.

(55) Flury, C.; Afacan, A.; Tamiz Bakhtiari, M.; Sjoblom, J.; Xu, Z. Effect of Caustic Type on Bitumen Extraction from Canadian Oil Sands. *Energy Fuels* **2014**, *28* (1), 431–438.

(56) Van Der Merwe, S.; Diep, J. K. Q.; Shariati, M. R.; Hann, T. Process and System for Solvent Addition to Bitumen Froth. U.S. Patent 10,041,005, Aug 7, 2018.

(57) Bichard, J. A. *Oil Sands Composition and Behaviour Research*; AOSTRA Technical Publication Series, No. 4; Canada, 1987; p 9–2

(58) Feng, X.; Behles, J. A. Understanding the Demulsification of Water-in-Diluted Bitumen Froth Emulsions. *Energy Fuels* **2015**, *29* (7), 4616–4623.

(59) Xu, Y. Asphaltene Precipitation in Paraffinic Froth Treatment: Effects of Solvent and Temperature. *Energy Fuels* **2017**, *32* (3), 2801–2810.

(60) Zhao, Y.; Wei, F. Simultaneous Removal of Asphaltenes and Water from Water-in-Bitumen Emulsion: I. Fundamental Development. *Fuel Process. Technol.* **2008**, *89* (10), 933–940.

(61) Turuga, A. S. S. Effect of Solvent Deasphalting Process on the Properties of Deasphalted

Oil and Asphaltenes from Bitumen. M.S. Thesis, University of Alberta, Edmonton, Canada, 2017

(62) Telmadarreie, T.; Berton, P.; Bryant, S. L. Treatment of Water-in-Oil Emulsions Produced by Thermal Oil Recovery Techniques: Review of Methods and Challenges. *Fuel* **2022**, *330*, 125551.

(63) Poindexter, M. K.; Marsh, S. C. Inorganic Solid Content Governs Water-in-Crude Oil Emulsion Stability Predictions. *Energy Fuels* **2009**, *23* (3), 1258–1268.

(64) Jiang, T.; Hirasaki, G. J.; Miller, C. A.; Ng, S. Effects of Clay Wettability and Process Variables on Separation of Diluted Bitumen Emulsion. *Energy Fuels* **2011**, *25* (2), 545–554.

(65) Hristova, E. J.; Stoyanov, S. R. Bitumen Froth Treatment in the Transition Region Between Paraffinic and Naphthenic Process Conditions. *Fuel* **2021**, *286*, 119385.

(66) Shelfantook, W. E. A Perspective on the Selection of Froth Treatment Processes. *Can. J. Chem. Eng.* **2004**, *82* (4), 704–709.

(67) Gu, G.; Zhang, L.; Xu, Z.; Masliyah, J. Novel Bitumen Froth Cleaning Device and Rag Layer Characterization. *Energy Fuels* **2007**, *21* (6), 3462–3468.

(68) De Klerk, A. Thermal Conversion Modeling of Visbreaking at Temperatures Below 400°C. *Energy Fuels* **2020**, *34* (12), 15285–15298.

(69) Zachariah, A.; De Klerk, A. Thermal Conversion Regimes for Oilsands Bitumen. *Energy Fuels* **2016**, *30* (1), 239–248.

(70) Wiehe, I. A. A Phase-Separation Kinetic Model for Coke Formation. *Ind. Eng. Chem. Res.* **1993**, *32* (11), 2447–2454.

(71) Yañez Jaramillo, L. M.; De Klerk, A. Is Solubility Classification a Meaningful Measure

in Thermal Conversion?. *Energy Fuels* **2022**, *36* (16), 8649–8662.

(72)   Yañez Jaramillo, L. M.; De Klerk, A. Partial Upgrading of Bitumen by Thermal
         Conversion at 150–300° C. *Energy Fuels* **2018**, *32* (3), 3299–3311.

(73)   Wang, L.; Zachariah, A.; Yang, S.; Prasad, V.; De Klerk, A. Visbreaking Oilsands-Derived
         Bitumen in the Temperature Range of 340–400° C. *Energy Fuels* **2014**, *28* (8), 5014–5022.

(74)   Castillo, J.; De Klerk, A. Visbreaking of Deasphalted Oil from Bitumen at 280–400° C.
         Energy Fuels **2018**, *33* (1), 159–175.

(75)   Naghizada, N.; Prado, G. H. C.; De Klerk, A. Uncatalyzed Hydrogen Transfer during 100–
         250 °C Conversion of Asphaltenes. *Energy Fuels* **2017**, *31* (7), 6800–6811.

(76)   DeZutter, C. B.; Horner, J. H.; Newcomb, M. Rate Constants for 1, 5-and 1, 6-Hydrogen
         Atom Transfer Teactions of Mono-, Di-, and Tri-Aryl-Substituted Donors, Models for
         Hydrogen Atom Transfers in Polyunsaturated Fatty Acid Radicals. *J. Phys. Chem. A* **2008**,
         112 (9), 1891–1896.

(77)   Payan, F.; De Klerk, A. Hydrogen Transfer in Asphaltenes and Bitumen at 250° C. *Energy
         Fuels* **2018**, *32* (9), 9340–9348.

(78)   Byrappa, K.; Adschiri, T. Hydrothermal Technology for Nanotechnology. *Prog. Cryst.
         Growth Charact. Mater.* **2007**, *53* (2), 117–166.

(79)   Al-Muntaser, A. A.; Varfolomeev, M. A. Suwaid, M. A.; Yuan, C.; Chemodanov, A. E.;
         Feoktistov, D. A.; Rakhmatullin, I. Z.; Abbas, M.; Domínguez-Álvarez, E.;
         Akhmadiyarov, A. A.; Klochkov, V. V.; Amerkhanov, M. I. Hydrothermal Upgrading of
         Heavy Oil in the Presence of Water at Sub-Critical, Near-Critical and Supercritical
         Conditions. *J. Pet. Sci. Eng.* **2020**, *184*, 106592.

(80)   Canıaz, R. O.; Erkey, C. Process Intensification for Heavy Oil Upgrading Using

Supercritical Water. *Chem. Eng. Res. Des.* **2014**, *92* (10), 1845–1863.

(81)   Arcelus-Arrillaga, P.; Pinilla, J. L.; Hellgardt, K.; Millan, M. Application of Water in

Hydrothermal Conditions for Upgrading Heavy Oils: A Review. *Energy Fuels* **2017**, *31*

(5), 4571–4587.

(82)   Vilcáez, J.; Watanabe, M.; Watanabe, N.; Kishita, A.; Adschiri, T. Hydrothermal

Extractive Upgrading of Bitumen Without Coke Formation. *Fuel* **2012**, *102*, 379–385.

(83)   Morimoto, M.; Sugimoto, Y.; Sato, S.; Takanohashi, T. Bitumen Cracking in Supercritical

Water Upflow. *Energy Fuels* **2014**, *28* (2), 858–861.

(84)   Liu, Z.; Li, Y.; Yu, F.; Zhu, J.; Xu, L. Co-Pyrolysis of Oil Sand Bitumen with

Lignocellulosic Biomass Under Hydrothermal Conditions. *Chem. Eng. Sci.* **2019**, *199*,

417–425.

(85)   Tekin, K.; Karagöz, S.; Bektaş, S. A Review of Hydrothermal Biomass Processing.

Renewable Sustainable Energy Rev. **2014**, *40*, 673–687.

(86)   Pavlovic, I.; Knez, Z.; Skerget, M. Hydrothermal Reactions of Agricultural and Food

Processing Wastes in Sub-and Supercritical Water: A Review of Fundamentals,

Mechanisms, and State of Research. *J. Agric. Food Chem.* **2013**, *61* (34), 8003–8025.

(87)   Djimasbe, R.; Varfolomeev, M. A.; Kadyrov, R. I.; Davletshin, R. R. Khasanova, N. M.;

Saar, F. D.; Al-Muntaser, A. A.; Suwaid, M. A.; Mukhamedyarova, A. N. Intensification

of Hydrothermal Treatment Process of Oil Shale in the Supercritical Water Using

Hydrogen Donor Solvents. *J. Supercrit. Fluids* **2022**, *191*, 105764.

(88)   Fan, H.; Zhang, Y.; Lin, Y. The Catalytic Effects of Minerals on Aquathermolysis of Heavy

Oils. *Fuel* **2004**, *83* (14–15), 2035–2039.

(89)   Holzapfel, W.B. Effect of Pressure and Temperature on the Conductivity and Ionic

Dissociation of Water up to 100 Kbar and 1000°C. *J. Chem. Phys.* **1969**, *50* (10), 4424–4428.

(90) Tumanyan, B. P.; Petrukhina, N. Y. N.; Kayukova, G. P.; Nurgaliev, D. K.; Foss, L. E.; Romanov, G. V. Aquathermolysis of Crude Oils and Natural Bitumen: Chemistry, Catalysts and Prospects for Industrial Implementation. *Russ. Chem. Rev.* **2015**, *84* (11), 1145.

(91) Morimoto, M.; Sugimoto, Y.; Saotome, Y.; Sato, S.; Takanohashi, T. Effect of Supercritical Water on Upgrading Reaction of Oil Sand Bitumen. *J. Supercrit. Fluids* **2010**, *55* (1), 223–231.

(92) Han, L.; Zhang, R.; Bi, J. Experimental Investigation of High-Temperature Coal Tar Upgrading in Supercritical Water. *Fuel Process. Technol.* **2009**, *90* (2), 292–300.

(93) Estacio, S. G.; Couto, P. C. D.; Guedes, R. C.; Cabral, B. J. C.; Simões, J. A. M. Homolytic Dissociation in Hydrogen-Bonding Liquids: Energetics of the Phenol O–H Bond in Methanol and the Water O–H Bond in Water. *Theor. Chem. Acc.* **2004**, *112*, 282–289.

(94) Das, S. Critical Review of Water Radiolysis Processes, Dissociation Products, and Possible Impacts on the Local Environment: A Geochemist's Perspective. *Aust. J. Chem.* **2013**, *66* (5), 522–529.

(95) Marriott, P. R.; Perkins, M. J.; Griller, D. Spin Trapping for Hydroxyl in Water: A Kinetic Evaluation of Two Popular Traps. *Can. J. Chem.* **1980**, *58* (8), 803–807.

(96) Zhang, H.; Sun, Z.; Hu, Y. H. Steam Reforming of Methane: Current States of Catalyst Design and Process Upgrading. *Renewable Sustainable Energy Rev.* **2021**, *149*, 111330.

(97) Idriss, H.; Scott, M.; Subramani, V. Introduction to Hydrogen and its Properties. In *Compendium of Hydrogen Energy: Hydrogen Production and Purification*; Subramani, V.;

Basile, A.; Veziroğlu, T. N.; Eds.; Woodhead Publishing: Boston, MA, 2015; Vol. 1, pp 3–19

(98)   Cui, X.; Su, H. Y.; Chen, R.; Yu, L.; Dong, J.; Ma, C.; Wang, S.; Li, J.; Yang, F.; Xiao, J.; Zhang, M.; Ma, D.; Deng, D.; Zhang, D. H.; Tian, Z.; Bao, X. Room-Temperature Electrochemical Water–Gas Shift Reaction for High Purity Hydrogen Production. *Nat. Commun.* **2019**, *10* (86), 1–8.

(99)   An, J.; Bagnell, L.; Cablewski, T.; Strauss, C. R.; Trainor, R.W. Applications of High-Temperature Aqueous Media for Synthetic Organic Reactions. *J. Org. Chem* **1997**, *62* (8), 2505–2511.

(100)   Siskin, M.; Brons, G.; Vaughn, S. N.; Katritzky, A. R.; Balasubramanian, M. Aqueous Organic Chemistry. 3. Aquathermolysis: Reactivity of Ethers and Esters. *Energy Fuels* **1990**, *4* (5), 488–492.

(101)   Mundle, S. O.; Kluger, R. Decarboxylation via Addition of Water to a Carboxyl Group: Acid Catalysis of Pyrrole-2-Carboxylic Acid. *J. Am. Chem. Soc.* **2009**, *131* (33), 11674–11675.

(102)   Liu, X. Alkenes and Alkynes. *Organic Chemistry I;* Kwantlen Polytechnic University: Surrey, Canada, 2021; pp 332–366.

(103)   Kjonaas, R. A.; Mattingly, S. P. Acid-Catalyzed Isomerization of Carvone to Carvacrol. *J. Chem. Educ.* **2005**, *82* (12), 1813.

(104)   Fox, M. A.; Whitesell, J. K. Substitution Alpha to Carbonyl Groups: Enolate Anions and Enols as Nucleophiles. In *Organic Chemistry*, 3rd ed.; Eds.; Jones and Bartlett Publishers: Sudbury, Massachusetts, 2004; p 651.

(105)   Siskin, M.; Katritzky, A. R. Reactivity of Organic Compounds in Superheated Water:

General Background. *Chem. Rev.* **2001**, *101* (4), 825–836.

(106)   Siskin, M.; Brons, G.; Katritzky, A. R.; Murugan, R. Aqueous Organic Chemistry. 2. Crosslinked Cyclohexyl Phenyl Compounds. *Energy Fuels* **1990**, *4* (5), 482–488.

(107)   Katritzky, A. R.; Lapucha, A. R.; Murugan, R.; Luxem, F. J.; Siskin, M.; Brons, G. Aqueous High-Temperature Chemistry of Carbo-and Heterocycles. 1. Introduction and Reaction of 3-Pyridylmethanol, Pyridine-3-Carboxaldehyde, and Pyridine-3-Carboxylic Acid. *Energy Fuels* **1990**, *4* (5), 493–498.

(108)   Sankey, B. M.; Maa, P. S.; Bearden, R., Jr. Conversion of the Organic Component from Tar Sands to Lower Boiling Products. U.S. Patent 5,795,464, August 18, 1998.

(109)   Fan, H. F.; Liu, Y. J.; Zhong, L. G. Studies on the Synergetic Effects of Mineral and Steam on the Composition Changes of Heavy Oils. *Energy Fuels* **2001**, *15* (6), 1475–1479

(110)   Zhang, X.; Liu, Y.; Fan, Y.; Che, H. Effects of Reservoir Minerals and Chemical Agents on Aquathermolysis of Heavy Oil During Steam Injection. *China Pet. Process. Petrochem. Technol.* **2010**, *12* (3), 25–31.

(111)   Nhieu, P.; Liu, Q.; Gray, M. R. Role of Water and Fine Solids in Onset of Coke Formation During Bitumen Cracking. *Fuel* **2016**, *166*, 152–156.

(112)   Chen, Q. Organically-Modified Clay Minerals in Oil Sands: Characterization and Effect of Hydrothermal Treatment. Ph.D. Dissertation, University of Alberta, Edmonton, Canada, 2017.

(113)   Chen, Q.; Gray, M. R.; Liu, Q. Irreversible Adsorption of Asphaltenes on Kaolinite: Influence of Dehydroxylation. *Energy Fuels* **2017**, *31* (9), 9328–9336.

(114)   Shiley, R. H.; Konopka, K. L.; Hinckley, C. C; Smith, G. V.; Twardowska, H.; Saporoschenko, M. *Effect of Some Metal Chlorides on the Transformation of Pyrite to*

Pyrrhotite. Technical Report Number PB-82-255506; Illinois Department of Energy and Natural Resources, August 1982.

(115)   Lambert, J. M., Jr.; Simkovich, G.; Walker, P. L., Jr.; The Kinetics and Mechanism of the Pyrite-to-Pyrrhotite Transformation. *Metall. Mater. Trans. B* **1998**, *29* (2), 385–396.

(116)   Stewart, I.; Whiteway, S. G.; Cleyle, P. J.; Caley, W. F. Decomposition of Pyrite in a Coal Matrix During the Pyrolysis of Coal. In *Mineral Matter and Ash in Coal*; Vorres, K. S., Eds.; ACS Symposium Series; American Chemical Society: Washington, DC, 1986; Vol. 301, pp 485–499.

(117)   Ringdalen, E. Changes in Quartz During Heating and the Possible Effects on Si Production. *JOM* **2015**, *67* (2), 484–492.

(118)   Yu, X.; Zhai, C.; Jing, Y.; Sang, S.; Wang, Y.; Regenauer-Lieb, K.; Sun, Y.. Investigation of the Temperature Dependence of the Chemical–Mechanical Properties of the Wufeng–Longmaxi Shale. *ACS Omega* **2022**, *7* (49), 44689–44697.

(119)   Gougazeh, M.; Alsaqoor, S.; Borowski, G.; Alsafasfeh, A.; Hdaib, I. I. The Behavior of Jordanian Oil Shale during Combustion Process from the El-Lajjun Deposit. *J. Ecol. Eng.* **2022**, *23* (8), 133–140.

(120)   Wang, H.; Li, C.; Peng, Z.; Zhang, S. Characterization and Thermal Behavior of Kaolin. *J. Therm. Anal. Calorim.* **2011**, *105* (1), 157–160.

(121)   Araújo, J. H. D.; Silva, N. F. D.; Acchar, W.; Gomes, U. U. Thermal Decomposition of Illite. *Mater. Res.* **2004**, *7*, 359–361.

(122)   Nagendrappa, G. Organic Synthesis Using Clay Catalysts. *Reson.* **2002**, *7* (1), 64–77.

(123)   Soma, Y.; Soma, M. Chemical Reactions of Organic Compounds on Clay Surfaces. *Environ. Health Perspect.* **1989**, *83*, 205–214.

(124) Lambert, J. F.; Poncelet, G. Acidity in Pillared Clays: Origin and Catalytic Manifestations. *Top. Catal.* **1997**, *4* (1–2), 43–56.

(125)   Liu, D.; Yuan, P.; Liu, H.; Cai, J.; Tan, D.; He, H.; Zhu, J.; Chen, T. Quantitative Characterization of the Solid Acidity of Montmorillonite using Combined FTIR And TPD Based on the NH_3 Adsorption System. *Appl. Clay Sci.* **2013**, *80,* 407–412.

(126)   D'Souza, A. S.; Pantano, C.G. Mechanisms for Silanol Formation on Amorphous Silica Fracture Surfaces. *J. Am. Chem. Soc.* **1999**, *82* (5), 1289–1293.

(127) Solomon, D. H. Clay Minerals as Electron Acceptors and/or Electron Donors in Organic Reactions. *Clays Clay Miner.* **1968**, *16* (1), 31–39.

(128) Worasith, N.; Ninlaphurk, S.; Mungpayaban, H.; Wen, D.; Goodman, B. A. Characterization of Paramagnetic Centres in Clay Minerals and Free Radical Surface Reactions by EPR Spectroscopy. In *Clays and Clay Minerals: Geological Origin, Mechanical Properties and Industrial Applications*, Wesley, L. R.; Eds.; Nova Science Publ.: New York, NY, 2014; pp 336–359

(129) Hoving, A. L.; Sander, M.; Bruggeman, C.; Behrends, T. Redox Properties of Clay-Rich Sediments as Assessed by Mediated Electrochemical Analysis: Separating Pyrite, Siderite and Structural Fe in Clay Minerals. *Chem. Geol.* **2017**, *457*, 149–161.

(130) Gorski, C. A.; Aeschbacher, M.; Soltermann, D.; Voegelin, A.; Baeyens, B.; Marques Fernandes, M.; Hofstetter, T. B.; Sander, M. Redox Properties of Structural Fe in Clay Minerals. 1. Electrochemical Quantification of Electron-Donating and -Accepting Capacities of Smectites. *Environ. Sci. Technol.* **2012**, *46* (17), 9360–9368.

(131) Pentráková, L.; Su, K.; Pentrák., M.; Stucki, J. W. A Review of Microbial Redox Interactions with Structural Fe in Clay Minerals. *Clay Miner.* **2013**, *48* (3), 543–560.

(132) Nwosu, U. G.; Roy, A.; Dela Cruz, A. L. N.; Dellinger, B.; Cook, R. Formation of Environmentally Persistent Free Radical (EPFR) in Iron (III) Cation-Exchanged Smectite Clay. *Environ. Sci.: Processes Impacts* **2016**, *18* (1), 42–50.

(133) Lanin, S. N.; Vlasenko, E. V.; Kovaleva, N. V.; Zung, F. T. The Adsorption Properties of Titanium Dioxide. *Russ. J. Phys. Chem. A* **2008**, *82* (12), 2152–2155.

(134) Mohammed, M.; Babadagli, T. Wettability Alteration: A Comprehensive Review of Materials/Methods and Testing the Selected Ones on Heavy-Oil Containing Oil-Wet Systems. *Adv. Colloid Interface Sci.* **2015**, *220*, 54–77.

(135) Thomas, M. M.; Clouse, J. A.; Longo, J. M. Adsorption of Organic Compounds on Carbonate Minerals: 1. Model Compounds and Their Influence on Mineral Wettability. *Chem. Geol.* **1993**, *109* (1–4), 201–213.

(136) Bandura, L.; Woszuk, A.; Kołodyńska, D.; Franus, W. Application of Mineral Sorbents for Removal of Petroleum Substances: A Review. *Miner.* **2017**, *7* (3), 37.

(137) Stoffyn-Egli, P.; Lee, K. Formation and Characterization of Oil–Mineral Aggregates. *Spill Sci. Technol. Bull.* **2002**, *8* (1), 31–44.

(138) Subramanian, S.; Simon, S.; Gao, B.; Sjöblom, J. Asphaltene Fractionation Based on Adsorption onto Calcium Carbonate: Part 1. Characterization of Sub-Fractions and QCM-D Measurements. *Colloids Surf., A* **2016**, *495*, 136–148.

(139) Tu, Y.; Kingston, D.; Kung, J.; Kotlyar, L. S.; Sparks, B. D.; Chung, K. H. Adsorption of Pentane Insoluble Organic Matter from Oilsands Bitumen onto Clay Surfaces. *Pet. Sci. Technol.* **2006**, *24* (3–4), 327–338.

(140) Nassar, N. N. Asphaltene Adsorption onto Alumina Nanoparticles: Kinetics and Thermodynamic Studies. *Energy Fuels* **2010**, *24* (8), 4116–4122.

(141)   Cortés, F. B.; Mejía, J. M.; Ruiz, M. A.; Benjumea, P.; Riffel, D. B. Sorption Of Asphaltenes onto Nanoparticles of Nickel Oxide Supported on Nanoparticulated Silica Gel. *Energy Fuels* **2012**, *26* (3), 1725–1730.

(142)   Franco, C.; Patiño, E.; Benjumea, P.; Ruiz, M. A.; Cortés, F. B. Kinetic and Thermodynamic Equilibrium of Asphaltenes Sorption onto Nanoparticles of Nickel Oxide Supported on Nanoparticulated Alumina. *Fuel* **2013**, *105*, 408–414.

(143)   Giraldo, J.; Nassar, N. N.; Benjumea, P.; Pereira-Almao, P.; Cortés, F. B. Modeling and Prediction of Asphaltene Adsorption Isotherms using Polanyi's Modified Theory. *Energy Fuels* **2013**, *27* (6), 2908–2914.

(144)   Li, X.; Bai, Y.; Sui, H.; He, L. Understanding Desorption of Oil Fractions from Mineral Surfaces. *Fuel* **2018**, *232*, 257–266.

(145)   Mamonov, A.; Aslanidis, P.; Fazilani, N.; Puntervold, T.; Strand, S. Influence of Sandstone Mineralogy on the Adsorption of Polar Crude Oil Components and Its Effect on Wettability. *Energy Fuels* **2022**, *36* (18), 10785–10793.

(146)   Carbognani, L.; González, M. F.; Lopez-Linares, F.; Stull, C. S.; Pereira-Almao, P. Selective Adsorption of Thermal Cracked Heavy Molecules. *Energy Fuels* **2008**, *22* (3), 1739–1746.

(147)   Lopez-Linares, F.; Carbognani, L.; Stull, C. S.; Pereira-Almao, P.; Spencer, R. J. Adsorption of Virgin and Visbroken Residue Asphaltenes over Solid Surfaces. 1. Kaolin, Smectite Clay Minerals, and Athabasca Siltstone. *Energy Fuels* **2009**, *23* (4), 1901–1908.

(148)   Zhong, J.; Wang, P.; Zhang, Y.; Yan, Y.; Hu, S.; Zhang, J. Adsorption Mechanism of Oil Components on Water-Wet Mineral Surface: A Molecular Dynamics Simulation Study. *Energy* **2013**, *59*, 295–300.

Chapter 3. Hydrothermal Treatment of Bitumen Froth: Impact of Mineral Solids and Water on Bitumen Properties

Abstract

Hydrothermal treatment, i.e., thermal treatment of bitumen in the presence of water and solids, as a potential approach for combined froth treatment and upgrading was investigated in this work. Reactions were performed in batch reactors at 250 °C with the bitumen, water and solid phases separated from industrially obtained bitumen froth, and the impact of the presence or absence of water and/or solids on the bitumen conversion was studied. Statistical analysis of bitumen properties revealed that the hydrothermal treatment of the bitumen froth at 250 °C did not lead to upgrading of the bitumen. Treatment at the conditions used in this study was beneficial only when the bitumen was converted on its own. Water and/or mineral solids contributed to an increase in viscosity, which was accompanied by an increase in free radical content. These observations were tentatively explained based on the generation of free radicals by redox reactions and heavier product formation promoted by free radical addition reactions. While the treatment did not significantly impact the density of bitumen, changes in H/C ratio, *n*-heptane insoluble content and metal content of bitumen were noted. The total acid number (TAN) of bitumen increased in the presence of water and mineral solids. Base-catalyzed hydrolysis of esters and anhydrides in bitumen might be responsible for increase in TAN, and the solids and water appeared to promote these reactions.

Keywords: Hydrothermal treatment, bitumen froth, froth treatment, thermal conversion, upgrading

3.1. Introduction

Bitumen recovery from mined oilsands ore goes through a series of processing steps as shown in Figure 3-1.[1] Extraction of bitumen from mined oilsands is achieved through a water-based gravity separation process. Hot water, accompanied by the addition of sodium hydroxide to control the pH at around 8.5,[2] is used for bitumen liberation from the mineral particles in the oilsands ore. The mixture is aerated to assist with the separation. The liberated bitumen droplets attach to the free air bubbles and rise to the top of the gravity separation vessel as froth. In the extraction process, co-production of water and solids (small mineral particles) along with bitumen in the froth takes place due to complex interactions that occur among various oilsand components, water and air bubbles.[3] Deaerated froth typically contains about 60wt% bitumen, 30wt% water and 10wt% mineral solids.[4] The bitumen is recovered from the deaerated froth in the froth treatment unit, which is the unit of interest in this work.

As the bitumen in the bitumen froth is viscous and has a density similar to water, water does not separate readily from bitumen. Presence of small water droplets emulsified into the oil phase presents another problem for phase separation.[5] Bi-wettable fine solids found at the oil-water interface of these droplets contribute to the stability of water-in-oil emulsions in froth.[6]

In the commercial froth treatment processes, a naphthenic or a paraffinic solvent is added,[4] as indicated in Figure 3-1. Addition of solvent to the deaerated froth reduces the viscosity of bitumen and increases the density difference between water and bitumen, facilitating the separation of the two liquid phases. The phase separation between the diluted bitumen and the mixture of water and mineral solids is performed at a temperature below 80 °C.[1]
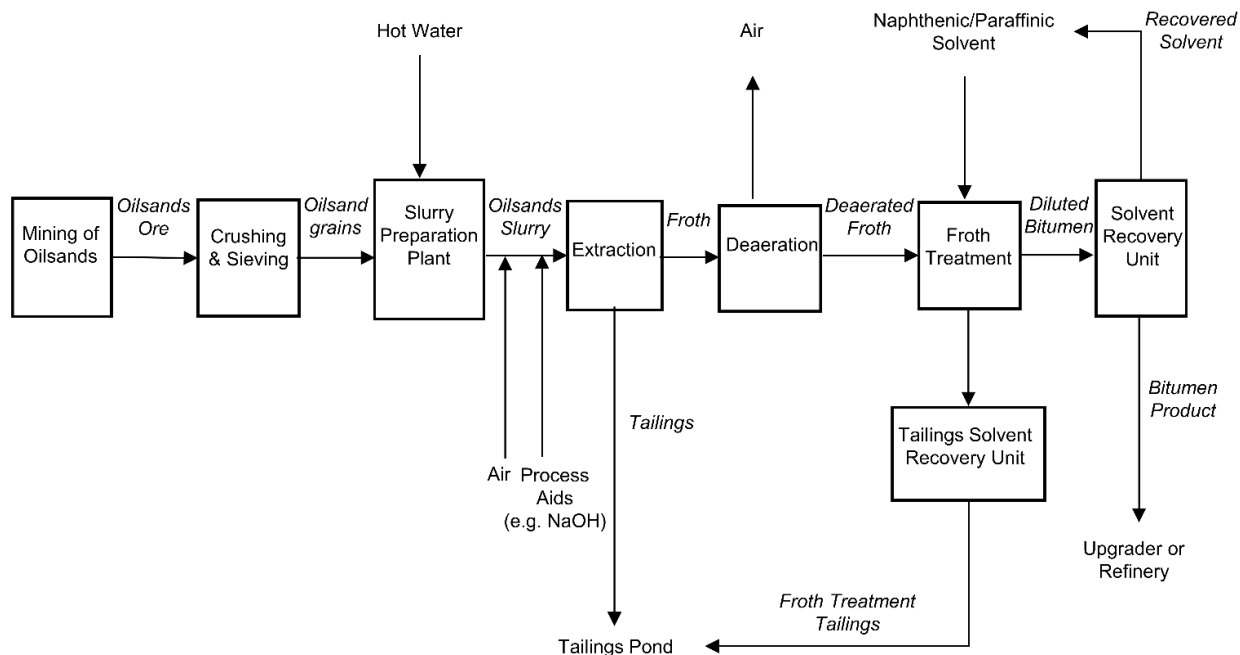
Figure 3-1. Process Flow Diagram of Bitumen Recovery from Mined Oilsands

Maximizing bitumen recovery from froth, and at the same time, achieving low concentrations of solid and water impurities in the bitumen product are essential for froth treatment. Recently, an alternative approach, called hydrothermal froth treatment was investigated by Chen, et al.[7] Hydrothermal treatment is the direct thermal processing of bitumen froth at higher temperatures. As temperature affects the viscosity of bitumen and the densities of both the bitumen phase and water phase, it is expected to influence the removal of solids and water from froth. At ~400 °C, hydrothermal treatment of froth resulted in a bitumen product containing about 0.03 wt% residual water and 0.08 wt% residual solids. In addition, the process resulted in thermal alteration of solids, due to which they became more hydrophobic. Bi-wettable fine solids, originally present at the oil-water interface in the froth, migrated to the bitumen phase due to increase in their hydrophobicity. This phenomenon contributed to destabilization of emulsions and facilitated separation of solids and water.

So far, studies on hydrothermal froth treatment have focused on enhancing the overall separation efficiency of the process. The upgrading of the bitumen that takes place as the operating temperature is increased has not been extensively investigated.

According to literature, some work was performed to study the effect of water and mineral solids on heavy oil or bitumen upgrading.[8-12] Presence of water in some thermal conversion processes called aquathermolysis and supercritical water treatment gave rise to benefits such as viscosity reduction, decrease in coke yield, increase in the yield of light components, increase in H/C ratio, decrease in the asphaltenes content, and decrease in the average molecular weight of oil.[8,9,11] Some researchers believed that water had chemical effects on upgrading reactions, while others explained that the effect was mainly physical.[11-13] Addition of reservoir minerals such as kaolinite, illite, quartz, feldspar, calcite, in the aquathermolysis of heavy oil, increased some of these benefits, and also contributed to sulfur and heavy metal removal in the thermal conversion of bitumen.[8,10] The effects of minerals were attributed to their catalytic and adsorption properties.

The physical and chemical effects of water on upgrading reactions, and the catalytic and adsorption properties of mineral solids, are expected to influence the conversion chemistry during froth treatment, thereby influencing the properties of bitumen. If partial upgrading of bitumen is possible in hydrothermal froth treatment, it would enable combining froth separation and thermal treating for bitumen upgrading into a single step operation.

The focus of the current work was to evaluate bitumen upgrading during hydrothermal treatment of bitumen froth, as well as to evaluate the impact of water and mineral solids on the resulting bitumen properties. This was done by performing reactions using industrially obtained bitumen froth, and measuring the properties of bitumen before and after reaction. A temperature of 250 °C was chosen for this study, because it is a temperature that is low enough to be achieved using steam

heating (instead of a furnace), but it is a temperature at which the bitumen can still undergo some conversion.[14,15]

3.2. Experimental

3.2.1. Materials.

The oilsands bitumen froth used in this study was obtained from the Athabasca region, courtesy of Suncor Energy. Based on Dean-Stark extraction, the bitumen froth contained approximately 21 wt% water and 8.5 wt% mineral solids. Characterization of the bitumen froth was performed by isolating the bitumen, water and solids from froth using the method described in Section 4.2.2.1, and analyzing them separately. The material balance of the separation and characterization of each of the froth phases are presented in the results section. The chemicals and cylinder gases used in this study are listed in Table 3-1.

Table 3-1. Chemicals and Cylinder Gases Employed in this Study

Compound	Formula	CASRN[a]	Purity (%)[b]	Supplier
Chemicals				
Toluene	C_7H_{16}	108-88-3	99.9	Fisher Scientific
n-heptane	C_7H_{16}	142-82-5	96	Fisher Scientific
Electrolyte 1M LiCl in ethanol	LiCl / C_2H_5OH			Fisher Scientific
0.1 N alcoholic potassium hydroxide	KOH/ iso- C_3H_8O			Metter Toledo
2-propanol	C_3H_8O	67-63-0	99.9	Fisher Scientific
2,2-diphenyl-1-picrylhydrazyl	$C_{18}H_{12}N_5O_6$	1898-66-4	~90	Sigma-Aldrich
Hydranal Composite-1				Sigma-Aldrich
Tetrahydrofuran	C_4H_8O	109-99-9	99.9	Fisher Scientific

Carbon Disulfide	CS_2	75-15-0	99.99	Fisher Chemical
Reference Material 5010		64742-53-6		Separation Systems Inc.
Polywax 655				Sigma-Aldrich
Ultra Pure Water Standard	H_2O			Anton Paar
Ethanol	C_2H_5OH	64-17-5	95	Sigma-Aldrich
Multi-Element Organometallic Oil Standard for ICP				Agilent
Multi-Element Standard Solution for ICP TraceCERT				Sigma-Aldrich
Cylinder Gases				
Nitrogen	N_2	7727-37-9	99.999	Praxair
Air	O_2 / N_2	132259 - 10 - 0	100	Praxair
Compressed Gas, Oxidizing	O_2 / Ar		19.96% O_2, Balance Ar	Praxair
Argon, Compressed	Ar		99.999	Praxair
Hydrogen, Compressed	H_2		99.999	Praxair
Helium, Compressed	He		>99	Praxair

[a] CASRN = Chemical Abstracts Services registry number.

[b] This is the purity guaranteed by the supplier.

3.2.2. Equipment and Procedure.

3.2.2.1. Isolation of bitumen, water and solid phases from the froth.

The bitumen froth was separated into bitumen, water and solids for characterization and to enable control over phase composition during the study.

Bitumen froth, originally present in a 2 L jar, was a thick semi-solid-like mixture at room temperature with some free water floating on the top. The free water was carefully collected with a 50 mL Thermo Scientific Target All-Plastic disposable syringe. The remaining mixture was pre-heated to about 60°C and mixed thoroughly with a spatula to homogenize it. The pre-heated mixture was diluted with toluene at a 1:3 (froth : toluene) volume ratio. In order to separate the solids, centrifugation of the diluted mixture was performed in an Eppendorf Centrifuge 5430 at 7000 rpm for 30 min, followed by vacuum filtration using a 0.22 μm filter to remove the solids not removed by centrifugation. The solids were washed with about twenty times excess fresh toluene in a beaker and strained using the vacuum filtration system. Then they were dried overnight in a vacuum oven at temperature 60 °C and absolute pressure 7.7 kPa to remove toluene. Bitumen was separated from the filtrate (bitumen, emulsified water and toluene mixture) by rotary evaporation at temperature 60 °C, speed 80 rpm and absolute pressure 7.7 kPa. The condensate obtained in the rotary evaporation operation was allowed to stand, during which the toluene and water layers separated due to density difference. The free water collected from froth and the water phase obtained in rotary evaporation were combined. In this manner, the bitumen, water and solids were isolated from the froth. The efficacy of these separation methods was tested by analyzing the residual amount of solids, water and toluene in bitumen, as well as the phase contamination in the water and solid phases of froth. This data will be presented in the results section.

3.2.2.2. Thermal Treatment in Microreactors.

Stainless steel (Type 316) micro batch reactors were used in the experiments. The reactors were constructed from tubing and fittings supplied by Swagelok, and equipped with a pressure gauge and thermocouple. The four types of reactions, each performed in triplicate in this study, are specified in Table 3-2. In this chapter, each type of reaction system is denoted by a notation for

easy reference. These notations contain the letters 'B', 'W' and 'S', which stand for bitumen, water and solids respectively. The reactor dimensions and amounts of reactants (g) used are also mentioned in Table 3-2. A reactor of slightly different dimensions was used for the B+W reactions due to non-availability of the reactor used for the remaining reactions. The pictures of the micro batch reactors can be found in Figure A. 1 of Appendix A.

Table 3-2. Reactions performed in this study [a]

Reaction Type	Reactor Dimensions [b]			Identifier	Mass of Feed (g)			Final Pressure (MPa)
	l (cm)	i.d. (cm)	t (cm)					
Hydrothermal treatment of bitumen froth	15.2	2.2	58.5	B+W+S	20			8.5
					Mass of Reactants (g) [c]			
					B	W	S	
Thermal treatment of bitumen	15.2	2.2	58.5	B	~15	-	-	6.5
Thermal treatment of (bitumen + water)	15.8	1.8	58.5	B+W	~15	~ 4	-	8.5
Thermal treatment of (bitumen + solids)	15.2	2.2	58.5	B+S	~15	-	~1.4	6.5

[a] Reaction Temperature = 250 °C, Initial pressure = 4.5 MPa

[b] Length (l) and internal diameter (i.d.) of reactor, and total length of the reactor tubing (t)

[c] Exact mass of each reactant was recorded for each experiment

The reactors were purged with nitrogen and tested for a gas leak. After ensuring that the leak test was successful, they were pressurized with nitrogen to an initial pressure of 4.5 MPa at room

temperature. The micro batch reactors were placed in a fluidized sand bath heater (Omega Fluidized Bath FSB-3), which was preheated to the intended reaction temperature 250 °C. The reactions were performed for a duration of 2 h, which was measured from the point in time when the internal temperature reached 250 °C.

The final pressures of the reaction systems at 250 °C are listed in Table 3-2. The vapor pressure of pure water at 250 °C is about 4 MPa,[16] and would be less in the presence of bitumen and solids in the reaction mixture. An initial pressure of 4.5 MPa was used to suppress the boiling of water at the final reaction temperature (vapor pressure < surrounding pressure), so that most of the water would remain in the liquid phase. Thereby it reduced the potential contribution of the phase change of water to any separation that may be observed during experiments. Although performing evaluation by keeping water in liquid phase was the main intention, it is also preferable from an economic point of view due to the energy consumption associated with water evaporation.

In addition to the experimental investigations conducted on the isolated components of bitumen froth (bitumen, water, and solids) in microreactors, insights into the behavior of bitumen froth as a whole when subjected to direct thermal treatment were also sought. In this context, an experiment was conducted wherein bitumen froth was treated as a unified system, without separating its constituents, and subjected to thermal exposure at 250°C for a duration of 5 h. This experiment was conducted in a larger-scale reactor, allowing for a more comprehensive assessment of the bitumen froth's response to elevated temperatures over an extended period. Further details regarding this experiment can be found in Appendix C.

3.2.2.3. Collection of Bitumen Products.

Post reaction, the reactors were removed from the sand bath and cooled to room temperature, after which they were depressurized. The products were removed from the reactor with the aid of toluene as solvent. The water phase separated from diluted bitumen product after reactions B+W and B+W+S was collected with a plastic syringe. The products still contained some dissolved gas, and bubbles appeared on the surface of the liquid products. To remove the gas, the products were ultrasonicated at room temperature for about 1 h. From the reaction systems that contained mineral solids (B+W+S and B+S), centrifugation (7000 rpm or 5752×g, 30 min) and vacuum filtration (0.22 μm filter) were used for the separation of solids from diluted bitumen products. Toluene and residual water were then removed from the bitumen products by rotary evaporation (60 °C, 80 rpm and absolute pressure 7.7 kPa). The product from the reaction B was used as is for analyses without further separation, since bitumen was the only phase present.

3.2.3. Analyses.

The analytical techniques used in the characterization of the bitumen isolated from froth before reactions, and the bitumen products of reactions B+W+S, B+W, B+S and B are described in this section. Additionally, the residual solids, water and toluene contents of the bitumen feed and product samples were analyzed to determine the bitumen phase contamination. Some analyses of the solid and water phases were also performed.

To determine the water content of bitumen samples (wt%) Karl Fischer (KF) titration of bitumen was carried out in a KF titrator V20S apparatus which was equipped with a DM-143 SC electrode. The method is a modified version of the procedure used by Carbognani, et al. for the determination of water content vacuum residua and bitumen using THF.[17] The application measurement range is 100 ppm to 100% water. About 0.5 g of bitumen sample was dissolved in 10 ml of THF to form

a homogeneous mixture that can be titrated. The sample weight and solvent (THF) weight in each sample mixture were noted. Known amount of sample mixtures were titrated with Hydranal composite 1, which was added from a burette into the titration vessel while stirring. During titration, a change in the electrical potential of the system is detected by the electrode due to a chemical reaction between the reagent and water in the sample. The end point is reached when the reaction is complete, and the water content is calculated from the amount of titrant added. As the calculation also requires knowing the moisture content of THF, which is the solvent used to dilute the samples, KF titration of THF was performed initially, before titrating the samples.

Residual toluene (wt %) in bitumen samples was determined using simulated distillation (simdis) and TGA. A method for the measurement of toluene content in bitumen-toluene mixtures using the boiling point distribution curve from simdis was developed by spiking Athabasca bitumen with known amounts of toluene. Athabasca bitumen on its own has no material with a boiling point below 250 °C,[1] which was also confirmed by simdis. Simdis analysis was performed by following the standard method ASTM D7169-11. The equipment used for this analysis was Agilent 7890B Gas Chromatograph (GC) with DB-HT Simdis column of dimensions 5m x 0.53mm x 0.15µm (length x inner diameter x film thickness) and the detector used was flame ionization detector (FID). Reference material 5010 was used to determine the detector response factor, and the Polywax 655 for the retention time calibration. 0.1±0.005g of the bitumen-toluene mixture was weighed and diluted with carbon disulphide to 10ml. It was found that the amount of toluene in a bitumen-toluene mixture can be obtained from the point where the slope of the curve changes, as shown in Figure A. 2(a) in Appendix A. TGA can also be used to determine the residual toluene content, as shown in Figure A. 2(b)) in Appendix A. The total mass lost (Initial mass – Mass remaining) until the point of change in slopes of the TGA curve is used to calculate the amount of

toluene in the sample. As the results of both analyses were found to be similar, TGA analysis was used to estimate the toluene content for all the bitumen samples in this study. Note that the bitumen samples in this study may also contain residual water as mentioned earlier. As the boiling point of water is less than toluene, the material lost in TGA, that is being considered for estimation of toluene content, is expected to include the water. Therefore, the toluene content in samples was calculated by subtraction of the amount of water already determined in the samples by KF titration.

The ash content of bitumen was determined by thermogravimetric analysis using Mettler Toledo TGA/DSC-1. Approximately 10mg of the sample was heated in a 70µL alumina crucible, in the presence of nitrogen gas flow (100 ml/min) from 25°C to 600°C at a rate of 10°C/min, and left for 1 h at 600°C The flow rate of the nitrogen gas was controlled using the Mettler Toledo GC 10 gas controller. The residue formed was further heated to 900 °C in the presence of air flow (100 ml/min) at a rate of 10°C/min, to produce ash. TGA was also used to measure the water, toluene and total organic content of mineral solids before and after reactions. The solids were heated from 25 °C to 900 °C at a rate of 10°C/min in the presence of air flowing at 100ml/min. The mass lost until 120 °C was considered to be due to water and/or toluene, and the remaining mass lost was reported as the amount of organic matter in the solids.

The solids separated from froth and those remaining in the water phase were visually observed with a Carl Zeiss StereoMicroscope Discovery V2.0 using a planapochromatic lens. The microscope lens had a zoom range of 20:1 and magnification upto 345X. Images of the froth solids were taken at 80X magnification, whereas those of the water samples were taken at 120X magnification.

Density of water samples was calculated by measuring the weight of 500 μL of the samples. An AV-600 Accumax variable volume pipette (100-1000 μL), whose measurement uncertainty is ±5 μL and imprecision is ±2 μL, was used for this purpose.

Metal determination in water and bitumen was carried out with an Agilent ICP-OES 5100. Elements analyzed were Al, B, Ca, Cu, Fe, Mg, Mn, Na, Ni, V, Si, Ti and Zn. Water samples were passed through a 0.22 μm syringe filter to remove as many suspended solids as possible and were diluted by a factor of 2 using Milli-Q water. A multi-element calibration standard containing 100 mg/L metal concentration in a 5 wt% nitric acid solution, supplied by Agilent, was used in the analysis of elements other than Ca, Mg, Fe, Na and K in the aqueous samples. A multi-element calibration standard containing 500 mg/L concentration of Ca, Mg, Fe, Na and K in a 5 wt% nitric acid solution, supplied by Agilent, was used for the aqueous samples. About 0.1 g of bitumen was dissolved in ~5 g of toluene in a glass vial, and the metal content was determined by using toluene as a blank. A multi-element organometallic oil standard containing 500 mg/kg analyte concentration, supplied by Agilent, was used for calibration in the analysis of bitumen samples. ICP analysis of both water and bitumen samples was performed using ultrahigh purity compressed argon gas. In the case of bitumen samples, a blend of argon (80%) and oxygen (20%) gases was supplied as auxiliary flow into the torch to enhance the carbon combustion, minimize the formation of deposits on the parts of the instrument and minimize the polyatomic interference. The operating parameters used for ICP-OES analysis of aqueous and organic samples are listed in the work by Chauhan and De Klerk.[18]

pH and conductivity of water samples were measured with an OAKTON PC 700 pH/mV/Conductivity/ºC/ºF Bench Meter. The pH range of the instrument is -2.00 to 16.00, and the conductivity range is 0.0-200 mS/cm. The pH calibration was performed using buffer solutions

of pH 4.00, 7.00, 10.00, supplied by Fisher Scientific, and the factory default settings for automatic conductivity calibration were applied.

Viscosity of the bitumen samples was measured using an Anton Paar RheolabQC viscometer. Approximately 4 g of bitumen sample was filled in a concentric cylinder (CC17/QC-LTD) measuring cup of diameter 18.080 mm. The bob diameter was 16.645 mm, resulting in a gap size of about 0.72 mm, and its length was 24.987 mm. The viscosity readings were taken at a constant shear rate 10 s^{-1}, at three different temperatures 20 °C, 40 °C and 60 °C. A Julabo F25-EH refrigerated/heating circulator was used to control the temperature and maintain it within $\pm$0.2 °C of the measurement temperature.

Density of bitumen was measured using an Anton Paar DMA 4500M at three different temperatures 20 °C, 40 °C and 60 °C. The claimed density and temperature measurement uncertainty of the instrument are 0.00005 g/cm³ and 0.02 °C respectively. The instrument was calibrated with an ultra pure water standard (reference density value = 0.99820 g/cm^3) supplied by Anton Paar, at 20.0 °C, to verify the accuracy of the device. The measured value of the density of the standard was 0.99821 g/cm^3.

Elemental analysis of bitumen was performed to determine the hydrogen-to-carbon ratio, nitrogen-to-carbon ratio and sulphur-to-carbon ratio, using a Thermo Flash 2000 Elemental Analyzer, by the Analytical and Instrumentation Laboratory of the Department of Chemistry at University of Alberta.

The *n*-heptane insoluble content of bitumen was determined by mixing 1 g of sample with 40 ml of *n*-heptane. The mixture was stirred on a magnetic stirrer for 1 h at ambient conditions, and left undisturbed in a dark place for a further 24 h. Then, the mixture was filtered under vacuum through a pre-weighed 0.22 μm filter paper. The membrane filter, upon which the precipitated solids were

collected, was placed in an aluminium weighing dish, and left to dry in the fumehood for about 48 h until no change in the weight due to solvent loss was observed. The *n*-heptane insoluble material was not further solvent fractionated with toluene.

The total acid number (TAN) of bitumen was determined using a Mettler Toledo T50 titration apparatus. The titration was carried out with a DG116-Solvent combined glass pH electrode, consisting of 1 M LiCl in ethanol as the refillable reference electrolyte. The electrode was calibrated with commercial aqueous pH 4, pH 7, and pH 11 buffer solutions. A titration solvent was prepared by mixing 5 mL $\pm$ 0.2 mL of water, 495 mL $\pm$ 5 mL of anhydrous 2-propanol and 500 mL $\pm$ 5 mL of toluene together. About 2.5 g of bitumen sample was dissolved in the titration solvent, and titrated with a solution of 0.1 N alcoholic potassium hydroxide (KOH in isopropanol).

The free radical content in the bitumen samples was measured using an Active Spectrum Micro-ESR. ~100 mg of bitumen was diluted with 1 ml of toluene (concentration of sample ~ 10 wt%) in a Norell® EPR tube of outer diameter 5 mm and length 177.8 mm for this analysis. For each sample, seven scans were performed at ambient conditions, with a sweep delay of 30 ms between each scan. Measurements were performed using the following instrument parameters: 1.2 Gauss coil amplitude, a microwave power of 15 mW and a digital gain of 12 dB. For each ESR spectrum, a double integrated intensity (DII) value for the organic radical peak was obtained in the microESR software. The free radical concentration (spins/g) of the bitumen-in-toluene solutions was determined using the calibration curve generated by Tannous and De Klerk,[19] using 0-7 mM solutions of 2,2-diphenyl-1-picrylhydrazyl (DPPH) in toluene. The calibration equation in their work was applied to convert the DII value to free radical concentration in spins/ml of the diluted bitumen sample, which was then divided by the concentration of bitumen in the solution (g/ml) to

obtain the solvent-free spins/g value of bitumen sample. The values are semi-quantitative and should be used only as relative measures for comparing samples.

A Mettler Toledo XS105 DualRange balance was used to determine the weights of substances in the TGA, KF titration, density, TAN and ESR analyses. The scale's capacity was 41 g with 0.01 mg readability in the fine range, and 120 g capacity with 0.1 mg readability in the full range. A Mettler Toledo NewClassic MF ML3002E balance was used for determining weights required for viscosity measurements. The capacity of the instrument was 3200 g and the readability was 0.01 g. A Mettler Toledo ME 204 analytical balance of maximum capacity 220 g and readability 0.0001 g was used for measuring weights related to ICP, asphaltenes content and simdis analyses.

3.3. Results

3.3.1. Material balances.

3.3.1.1. Froth Separation.

As described in section 4.2.2.1., the froth separation included many stages. Figure 3-2 contains a schematic diagram of the step-wise separation of froth into its component phases, with the input (subscript 'in') and output (subscript 'out') streams of the materials or components (Froth, bitumen 'B', solids 'S', water 'W' and toluene 'T') marked, for the calculation of material balance.

$T_{in} = T_{in(1)} + T_{in(2)}$

$T_{out} = T_{out(1)} + T_{out(2)} + T_{out(3)}$

$B_{out} = B_{out(1)} + T_{out(2)} - T_{in(2)}$
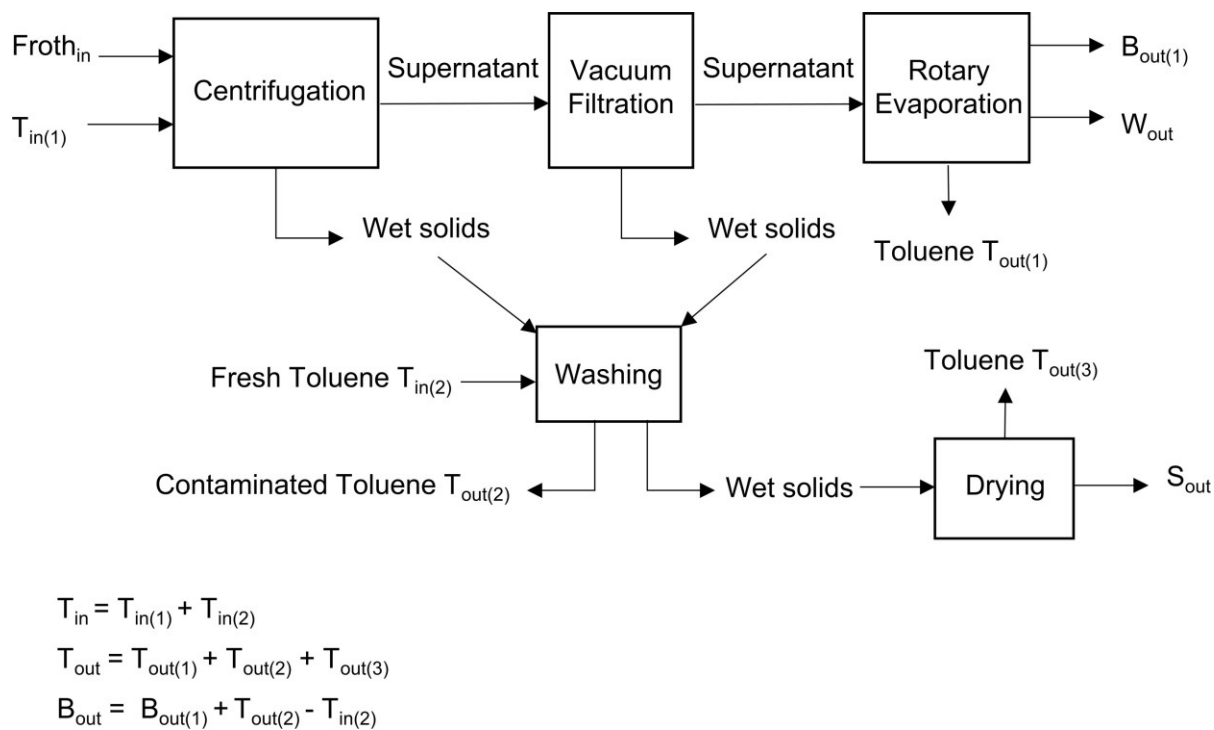
Figure 3-2. Schematic Diagram of Froth Separation

As mentioned earlier, the industrial froth used in this study contained some free water floating on the top, which was separated with a plastic syringe. As the physical nature of the froth was semi-solid-like at room temperature and highly viscous, heating it to 60 °C and solvent addition were both essential in order to separate the froth into its component phases. The separation of solids phase from diluted froth was the most onerous. Solids (unwashed) removed by centrifugation accounted for about 75% of the total wet solids that settled as brown-colored chunks with trapped bitumen at the bottom of the centrifuge tubes, and a significant portion of solids still remained in the supernatant. Vacuum filtration of the remaining solids was a slow process and required repeated replacement of filter papers. The weights of materials at each stage were measured, and the total material balance was calculated as shown in Table 3-3. On average, ~99% material

balance was obtained in froth separation. The major losses appeared to be due to the evaporation of toluene during the separations.

Table 3-3. Material balance for froth separation

Material	wt % (on the basis of total input) [a]	
	x	s
Input		
Froth$_{in}$	15.60	0.11
T$_{in}$	84.40	0.11
Total Input (Basis)	100	
Output		
B$_{out}$	11.18	0.15
W$_{out}$	3.49	0.03
S$_{out}$	1.24	0.04
T$_{out}$	82.85	0.27
Total Output	98.75	0.33

[a] Average (x) and standard deviation (s) of separations in triplicate

Due to the challenges associated with froth separation, it was likely that the bitumen obtained from froth still contained some trapped toluene, solids and/or water, that could affect the properties measured in this study. Similarly, it was possible that the solid and water phases were also contaminated with bitumen. The extent of phase contamination of each phase isolated from the froth was tested, and the results are presented in section 4.3.2.

3.3.1.2. Thermal Treatment.

Material balance for the different types of thermal treatment of bitumen, including hydrothermal froth treatment, is given in Table 3-4.

Table 3-4. Material balance for different types of thermal treatment of bitumen

Material	wt % (on the basis of total feed) [a]							
	B		B+W		B+S		B+W+S	
	x	s	x	s	x	s	x	s
Feed								
Froth	0.0	0.0	0.0	0.0	0.0	0.0	88.8	1.2
Bitumen	84.4	0.4	72.0	1.1	78.6	0.3	-[b]	-[b]
Solids	0.0	0.0	0.0	0.0	7.3	0.1	-[b]	-[b]
Water	0.0	0.0	19.2	0.2	0.0	0.0	-[b]	-[b]
Gas	15.6	0.4	8.8	1.3	14.1	0.4	11.2	1.2
Total Feed (Basis)	100.0	0.0	100.0	0.0	100.0	0.0	100.0	0.0
Product								
Liquid	82.9	3.6	90.5	3.6	79.9	0.1	89.4	0.9
Gas	16.1	3.5	7.7	2.0	18.0	1.0	9.4	1.6
Total Product	98.9	0.2	98.2	1.9	97.9	0.2	98.8	0.4

[a] Average (x) and standard deviation (s) of reactions in triplicate

[b] Composition as determined in Table 3-3 as the froth mixture itself was used in the reaction

The calculated overall material balance in the reactions was ≥ 98 % on the basis of total feed. As the reactors were pressurized with nitrogen gas before reactions, the increase in the weight of the reactors due to pressurization was included as the gas feed. The gas feed values are influenced by the free volume available in the reactors. In some cases, the product mixture in the reactor contained gas bubbles, indicating that some gas dissolved in the liquid phase and increased its

weight. The weights of materials and reactor setup at each step were noted down, and the gas leak test was performed before reactions, making it difficult to comment on the nature of losses that have occurred.

3.3.1.3. Separation of Products.

Similar to the froth separation, the material balance for the products separation was calculated using the input streams $Product_{in}$ and T_{in}, and output streams B_{out}, W_{out} and S_{out}. As shown in Table 3-5, about 97 to 99 % material balance was obtained in the products separation.

Table 3-5. Material balance for products separation

Material	wt % (on the basis of total input) [a]							
	B		B+W		B+S		B+W+S	
	x	s	x	s	x	s	x	s
Input								
$Product_{in}$	19.0	0.3	22.9	0.3	20.4	0.02	24.8	0.3
$Toluene_{in}$	81.0	0.3	77.1	0.3	79.6	0.02	75.2	0.3
Total Input (Basis)	100.0		100.0		100.0		100.0	
Output								
B_{out}	18.2	0.4	18.3	0.3	18.3	0.2	17.2	0.3
W_{out}	0.0	0.0	4.5	0.04	0.0	0.0	4.9	0.1
S_{out}	0.0	0.0	0.0	0.0	1.7	0.01	2.1	0.005
T_{out}	79.2	0.1	75.2	0.6	77.1	0.1	74.9	0.3
Total Output	97.4	0.4	98.1	0.4	97.1	0.3	99.1	0.03

[a] Average (x) and standard deviation (s) of reactions in triplicate

3.3.2. Phase Contamination.

3.3.2.1. Bitumen phase.

As mentioned earlier, it is expected that the bitumen, solid and water phases obtained from froth as well as the reaction products contain impurities. The amounts of residual toluene, water and solids in bitumen isolated from froth (called untreated bitumen in this study), and from the products of different reaction types, were measured and tabulated in Table 3-6.

Table 3-6. Residual solids, water and toluene content in bitumen from froth and reaction products

Reaction Products	Solids (wt %) [a]		Water (wt %) [a]		Toluene (wt %) [a]	
	x	s	x	s	x	s
Untreated bitumen	0.30	0.28	- [b]	-	4.25	0.57
B+W+S	1.37	1.44	0.32	0.01	1.50	0.33
B+W	0.49	0.33	0.42	0.23	4.22	1.17
B+S	1.15	1.52	- [b]	-	1.35	0.07
B	0.54	0.25	- [b]	-	4.10	0.28

[a] Analysis of three samples; average (x) and standard deviation (s)

[b] Below Detection Limit

As shown in Table 3-6, about 0.3 wt % solids, on an average, still remained in the untreated bitumen after froth separation, although having a large standard deviation. An increase in the mass of solids was observed upon treatment of bitumen (B). The B+W+S and B+S reactions, where solids were externally added to the bitumen and treated, resulted in bitumen products containing more residual solids.

Compared to solids and toluene, the water content in most bitumen samples analyzed was negligible. The water content in untreated bitumen was below the detection limit of the application (100 ppm). Only in the reactions where water was externally added to bitumen (B+W and B+W+S), residual water of up to 0.42 wt% on average, still remained in the bitumen products.

The amount of residual toluene in the bitumen samples was greater than the amounts of residual solids and water. Untreated bitumen, and the products of B+W and B contained between 4 and 4.5 wt % toluene, whereas the bitumen products of B+W+S and B+S reactions contained less than 2 wt % toluene. These differences in the residual toluene content among the bitumen samples would make the comparison of their properties inaccurate. To avoid this, toluene was added in some samples such that all the samples contained the same amount of residual toluene. Before dilution of samples, the highest amount of residual toluene, equal to 5 wt%, was found in one of the B+W samples. Therefore, other samples were diluted with toluene so that all the bitumen samples now had 5 wt% toluene in them. This dilution of samples, of course, decreased the amounts of residual solids and water in the samples compared to Table 3-6 and the recalculated values are shown in Table 3-7.

Table 3-7. Calculated values of bitumen, residual water and residual solids (wt %) in diluted

bitumen samples (~5 wt% toluene)

Diluted Bitumen Samples	Bitumen (wt %) [a]	Toluene (wt %) [b]	Water (wt %) [a]	Solids (wt %) [a]
Untreated bitumen	94.71	~5.00	- [c]	0.29
B+W+S	93.38	~5.00	0.31	1.31
B+W	94.09	~5.00	0.42	0.49
B+S	93.90	~5.00	- [c]	1.10
B	94.47	~5.00	- [c]	0.53

[a] Average of three samples

[b] The uncertainty introduced by the variation in toluene addition was not measured

[c] Below Detection Limit in the original measurements

3.3.2.2. Solids phase.

A stereomicroscope image of the solids (80X) isolated from bitumen froth (Figure 3-3) shows the

presence of organic coating (dark colored bituminous material) on various portions of the solid

matter. The stereomicroscopic images of water isolated from bitumen froth (Figure 3-3), both in

its untreated state and after undergoing thermal treatment (B+W and B+W+S), revealed intriguing

differences. In the treated water, the images indicated the continued presence of fine particles of

solids and suspended bitumen droplets, suggesting that the thermal treatment process may not have

completely eliminated these contaminants. Moreover, a notable observation was the distinct

orangish hue exhibited by the thermally treated water, in stark contrast to the untreated water from

bitumen froth. The change in color from the untreated water from bitumen froth to an orangish hue

in the thermally treated water likely indicates a chemical alteration or dissolution of more bitumen compounds during the thermal treatment process.
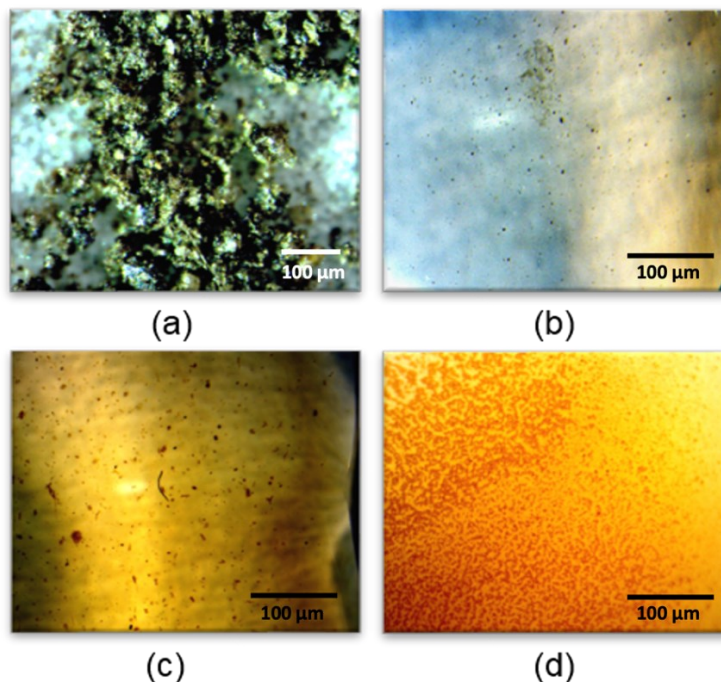
Figure 3-3. Stereomicroscope Images of (a) solids isolated from froth (b) water sample from untreated froth (c) water sample from B+W reaction (d) water sample from B+W+S reaction

In the TGA analysis (25 to 900 °C) of mineral solids isolated from froth, the amount of material that volatilized was about 16.5 wt%. About 0.2 wt % of these solids volatilized under 120 °C in the TGA, due to evaporation of residual toluene and/or water. After treatment, the amount of material that was released upon heating the solids obtained from B+W+S and B+S reactions increased to about 28.8 wt % and 26.3 wt % respectively, of which the amounts volatilized under 120 °C were equal to 1.3 wt % and 0.1 wt % respectively. The increase in the mass lost from treated solids in the TGA analysis compared to the untreated solids can be attributed to an increase in the organic content associated with the mineral solids upon thermal treatment.

3.3.2.3. Water phase.

The density of water samples was measured at 20 °C to check for differences due to dissolved organics and suspended solids as shown in Table 3-8. The densities were greater than the density of pure water, and increased upon thermal treatment comparing to the raw froth water. The density of water followed the order: untreated froth < B+W < B+W+S.

Table 3-8. Density of water samples [a] (20.00±0.05 °C)

Description of Water Sample	Density (kg/m^3)	
	x	s
Milli-Q water	998.23	0.02
Untreated froth	1004.54	0.23
B+W	1006.64	0.23
B+W+S	1008.48	0.40

[a] Analysis of three samples; average (x) and standard deviation (s)

Suspended solids in water samples were visually observed using a stereomicroscope at 120X magnification. As shown in Figure 3-3, small particles and bitumen droplets are suspended in the water phase separated from untreated froth and treated products. The color of the water from treated samples was more orangish compared to that from the untreated froth.

3.3.3. Characterization of Bitumen.

In this section the characterization data of bitumen samples (~5 wt% toluene) obtained from the reaction products of B, B+W+S, B+W and B+S is described. Various physical and chemical properties of bitumen from different types of thermal treatment were compared among the samples. The results are expressed on the basis of diluted bitumen sample (bitumen + toluene, wt % toluene = 5 wt%).

3.3.3.1. Viscosity.

As mentioned in the introduction, the viscosity of bitumen in the current study was expected to decrease upon thermal treatment in the presence of solids and/or water at 250 °C. To test this, the viscosity of bitumen samples obtained after treatment of the four reaction systems was measured as shown in Table 3-9. It was of interest to see whether the product samples followed the same viscosity vs. measurement temperature relationship as that of the untreated bitumen. For this reason, viscosity of each sample was measured at three temperatures: 20 °C, 40 °C and 60 °C.

Table 3-9. Viscosity (Pa.s) of the Bitumen Samples measured at 20 °C, 40 °C and 60 °C before and after reaction [a] (1 Pa.s = 1000 cP)

Bitumen Sample	20 °C		40 °C		60 °C	
	x	s	x	s	x	s
untreated bitumen	28.0	1.9	3.5	0.2	0.7	0.05
Reaction System						
B+W+S	40.5	3.3	4.5	0.4	0.9	0.1
B	22.4	3.1	3.1	0.4	0.6	0.1
B+W	40.6	8.0	4.6	0.8	0.9	0.1
B+S	100.7	38.2	9.1	2.9	1.5	0.4

[a] Average (x) and sample standard deviation (s) of experiments in triplicate.

These viscosity measurements exhibit a notable divergence from the values reported in previous literature. The data in Table 3-9 indicate a substantial reduction in viscosity when compared to the previously reported figures, which were approximately 90 Pa.s at 40°C and 9 Pa.s at 60°C.[14,20,21] A likely explanation for these disparities could be attributed to the inclusion of toluene and water in the current sample composition.

3.3.3.2. Density.

Thermal treatment of bitumen is expected to affect the molecular composition and size of its components. Therefore, the density of bitumen, which is influenced by the size and composition of its components, is also expected to change upon thermal treatment. In this study, the density of bitumen samples obtained after thermal treatment of the four reaction systems was measured and compared with the untreated bitumen as shown in Table 3-10. Densities were measured at three different temperatures (20 °C, 40 °C and 60 °C) to know whether all the samples show the same pattern under temperature changes.

Table 3-10. Density (kg/m^3) of the Bitumen Samples measured at 20 °C, 40 °C and 60 °C before and after reaction [a]

Bitumen Sample	20 °C		40 °C		60 °C		$d\rho/dT$
	x	s	x	s	x	s	
untreated bitumen	1005.86	1.18	994.47	1.26	983.36	1.33	-0.5626
B+W+S	1006.34	0.65	994.98	0.72	983.95	0.77	-0.5598
B	1005.36	0.47	993.94	0.49	982.79	0.47	-0.5643
B+W	1006.74	0.57	995.40	0.61	984.34	0.66	-0.5600
B+S	1009.46	0.03	998.25	0.03	987.32	0.01	-0.5537

[a] Average (x) and sample standard deviation (s) of experiments in triplicate.

3.3.3.3. Elemental Composition (C, H, N, S).

Elemental analysis was performed to determine the wt % of elements C, H, N and S in the bitumen samples. As mentioned in the introduction, changes in heteroatom content and H/C ratio are expected to occur on thermal treatment. Small differences in the average elemental composition

of bitumen samples, accompanied by large standard deviations, can be observed in Table 3-11. The calculated molar element ratios H/C, N/C and S/C are also listed in Table 3-11.

Table 3-11. Elemental (C, H, N, S) Composition (wt %) and Molar element ratios of Bitumen Before and After Reaction [a]

Bitumen Sample	C		H		N		S	
	x	s	x	s	x	s	x	s
untreated bitumen	83.85	0.07	10.17	0.21	0.52	0.02	4.56	0.28
B+W+S	83.79	0.01	10.33	0.07	0.50	0.004	4.82	0.01
B	83.43	0.55	10.37	0.02	0.48	0.0005	4.79	0.13
B+W	82.25	0.71	10.33	0.02	0.50	0.01	4.85	0.01
B+S	83.59	0.03	10.36	0.01	0.51	0.03	4.76	0.37
Bitumen Sample	H/C		N/C		S/C	
	x	s	x	s	x	s
untreated bitumen	1.46	0.03	0.005	0.0002	0.020	0.001
B+W+S	1.48	0.01	0.005	0.00004	0.022	0.0001
B	1.49	0.008	0.005	0.00004	0.022	0.0007
B+W	1.51	0.009	0.005	0.00003	0.022	0.0002
B+S	1.49	0.001	0.005	0.0003	0.021	0.002

[a] Average (x) and sample standard deviation (s) of experiments in triplicate

3.3.3.4. *n*-Heptane Insoluble Content.

As mentioned in the introduction, there are a few reasons why the asphaltenes content of bitumen is expected to change upon thermal treatment of bitumen in the presence of water and/or mineral solids. To study how the hydrothermal treatment of bitumen froth and thermal treatment of

bitumen in the presence of water or solids influences asphaltenes content, the *n*-heptane insoluble content in the bitumen samples was determined and compared as shown in Table 3-12. The *n*-heptane insoluble content obtained by this method also includes mineral solids.

Table 3-12. *n*-Heptane Insoluble Content of Bitumen Before and After Reaction [a]

	x	s
untreated bitumen	18.61	3.67
B+W+S	22.11	0.58
B	16.09	1.99
B+W	22.35	1.50
B+S	15.46	0.41

[a] Average (*x*) and sample standard deviation (*s*) of experiments in triplicate.

Samples contained ~ 5 wt% toluene.

3.3.3.5. Total Acid Number.

The total acid number (TAN) is an important quality measurement of crude oil. It is a measure of the quantity of acidic components in an oil sample and indicates the potential of corrosion problems in crude oil refineries. TAN of bitumen before and after thermal treatment was measured in this study for different reaction systems (Table 3-13).

Table 3-13. Total Acid Number (TAN) of Bitumen Before and After Reaction

Bitumen Sample	TAN (mg KOH/g) [a]	
	x	s
untreated bitumen	3.8	0.2
B+W+S	4.8	0.2
B	4.3	0.2
B+W	4.3	0.1
B+S	4.4	0.02

[a] Average (x) and sample standard deviation (s) of experiments in triplicate.

Samples contained ~ 5 wt% toluene.

3.3.3.6. Free Radical Content.

It is known that bitumen, in its natural form, contains free radicals which at high temperature can react in different ways leading to chemical changes in bitumen, as well as impacting its physical properties. Moreover, free radical content of bitumen is indicative of its storage stability. In this study, electron spin resonance spectrometry was used to determine the free radical content in the samples, expressed as spins/g (Table 3-14). The average g-values for the organic radical peak in the samples were also measured and included in Table 3-14. The g-values of the samples ranged between 2.0007 to 2.003. Differences in the g-factor help to identify differences in the samples.

Table 3-14. Free Radical Content (spins/g) and g-values in Bitumen Before and After Reaction

Bitumen Sample	Free Radical Content (spins/g) [a]		g-values [a]	
	x	s	x	s
untreated bitumen	3.1×10^{17}	1.1×10^{16}	2.0023	0.0003
B+W+S	3.4×10^{17}	8.7×10^{15}	2.0030	0.0014
B	3.2×10^{17}	7.4×10^{16}	2.0022	0.0004
B+W	4.2×10^{17}	1.1×10^{16}	2.0007	0.0004
B+S	3.7×10^{17}	6.7×10^{16}	2.0014	0.0005

[a] Average (x) and sample standard deviation (s) of experiments in triplicate.
Samples contained ~ 5 wt% toluene.

3.3.3.7. Metals.

As mentioned earlier, metals in bitumen and water can participate in processes such as adsorption and ion-exchange reactions, decreasing or increasing their concentration in the liquid phases. The effect of thermal treatment of bitumen in the presence of both water and solids on the concentration (ppm or μg/g) of metals in bitumen was studied, as shown in Table 3-15. Similar to analysis of feed water, the elements analyzed are the ones mainly present in the bitumen, water and mineral solid phases of oil sands.

Table 3-15. Metal Concentration ($\mu g/g$) in Bitumen Before and After Reaction [a]

Element	Untreated bitumen x	s	B+W+S x	s	B x	s	B+W x	s	B+S x	s
Al	65	0.3	43	1	65	2	47	0.3	45	1
B	13	0.1	4	0.1	12	0.3	11	0.1	4	0.1
Ca	13	0.1	8	0.2	13	0.3	13	0.1	13	0.2
Cu	2	0.02	1	2	0.1	0.02	1	0.01	1	0.01
Fe	51	0.2	38	1	51	0.2	42	0.2	36	1
K	-[b]	-[b]	-[b]	-[b]	-[b]	-[b]	-[b]	-[b]	-[b]	-[b]
Mg	8	0.03	6	0.1	8	0.1	6	0.03	9	0.2
Mn	1	0.01	1	0.02	1	0.03	1	0	3	0.04
Na	46	0.2	21	1	45	1	22	0.1	36	1
Ni	99	0.4	82	2	101	3	95	1	99	2
P	1	0.03	-[c]	-[c]	-[c]	-[c]	-[c]	-[c]	-[c]	-[c]
Si	100	1	67	2	99	3	74	0.4	69	1
Ti	14	0.1	11	0.2	14	0.4	12	0.1	11	0.2
V	241	1	203	4	241	6	226	1	233	4
Zn	2	0.01	2	0.04	2	0.1	2	0.02	3	0.04

[a] Analysis of three samples; average (x) and standard deviation (s).

Samples contained ~ 5 wt% toluene.

[b] Absent in the calibration standard

[c] Below Detection Limit

Changes in the metal concentration (ppm or μg/g) in aqueous samples were also determined, as shown in Table 3-16.

Table 3-16. Metal Concentration ($\mu g/g$) in Aqueous Phase Before and After Reaction [a]

Element	Untreated Froth		B+W+S		B+W	
	x	*s*	*x*	*s*	*x*	*s*
Al	1	0.02	1	0.01	0.03	0
Ca	8	0.02	0.1	0.1	1	0.1
Cu	-[b]	-[b]	-[b]	-[b]	-[b]	-[b]
Fe	0.3	0	0.02	0.02	0.02	0
K	28	0.1	16	18	4	0.3
Mg	6	0.01	0.03	0.1	1	0.1
Mn	-[b]	-[b]	-[b]	-[b]	-[b]	-[b]
Na	722	2	252	5	226	14
Ni	0.1	0	0.04	0.01	0.1	0.01
Ti	0.1	0.02	0.1	0.02	0.02	0.02
V	0.02	0	0.01	0	0	0
Zn	-[b]	-[b]	-[b]	-[b]	-[b]	-[b]
pH	8.3	0.1	8.2	0.02	8.2	0.04
Conductivity (mS/cm)	1.7	0.5	0.5	0.1	0.4	0.02

[a] Analysis of three samples; average (*x*) and standard deviation (*s*)

[b] Below detection limit

3.3.4. Correcting for Bitumen Phase Contamination.

As mentioned earlier, the bitumen samples analyzed in this study were contaminated with solids, water and residual toluene (~5 wt%). Evaluation of hydrothermal treatment on bitumen upgrading based on the properties of contaminated bitumen samples could be inaccurate as the presence of contaminants might influence the properties of bitumen. Therefore, the properties of the contaminated bitumen samples were corrected to calculate the corresponding property values of pure bitumen.

In literature, various theoretical models are available to predict the viscosity of different mixtures such as suspensions, bitumen-organic solvent mixtures and water-in-oil (W/O) emulsions.[22-33] Some of these models were used to correct the measured viscosity of the contaminated bitumen in this study. Their corresponding equations and assumptions based on which these equations are applicable can be found in Section S5 (Table A. 4 and Table A. 5 of Appedix A).

The final corrected viscosity values of bitumen (η_b) obtained from different types of thermal treatment are listed in Table 3-17. As the solids and water were sufficiently removed from the untreated and treated bitumen samples prior to analysis (volume concentration of solids $\phi_s \leq 0.003$ and water $\phi_w \leq 0.004$), their presence did not affect the viscosity measurement significantly (percentage change < 1%) after applying the Einstein equation for suspensions and emulsions.[22,25] The major change in viscosity occurred after correction for toluene.

Table 3-17. Corrected Viscosity (Pa.s) of the Bitumen Samples at 20 °C, 40 °C and 60 °C before and after reaction [a] (1 Pa.s = 1000 cP)

Bitumen Sample	20 °C		40 °C		60 °C		Slope	R^2
	x	s	x	s	x	s		
untreated bitumen	255	1	24.4	0.034	4.0	0.002	-3.17	1
Reaction System								
B+W+S	417	28	34.8	2.8	5.4	0.4	-3.20	1
B	194	31	21.4	0.3	3.3	0.6	-3.19	0.999
B+W	410	104	35.4	8.0	5.6	1.1	-3.15	1
B+S	1341	625	86.4	34.3	11.2	3.9	-3.23	1

[a] Average (x) and sample standard deviation (s) of corrected values of each individual measurement in Table 3-9.

The corrected viscosity values of the bitumen samples follow the linear relationship $\ln[\ln(\mu)]$ α $\ln(T)$ in accordance with the literature,[1] where μ is the viscosity in mPa.s and T is the measurement temperature in K. The slopes and R^2 values of the $\ln[\ln(\mu)]$ vs. $\ln(T)$ curves were also determined (Table 3-17).

Similar to viscosity, theoretical equations were used for correction of densities of contaminated bitumen samples (Table A. 6 of Appendix A).

The corrected densities of bitumen obtained after performing these calculations are reported in Table 3-18.

Table 3-18. Corrected Density (kg/m^3) of the Bitumen Samples at 20 °C, 40 °C and 60 °C before and after reaction [a]

Bitumen Sample	20 °C		40 °C		60 °C		dρ/dT	R^2
	x	s	x	s	x	s		
untreated bitumen	1013	1	1002	1	991	1	-0.5334	0.9999
B+W+S	1007	8	996	8	986	8	-0.5296	0.9999
B	1005	10	994	10	983	10	-0.5345	0.9999
B+W	1013	1	1002	1	991	1	-0.5303	1
B+S	1010	6	999	6	999	6	-0.5229	0.9999

[a] Average (x) and sample standard deviation (s) of corrected values of each individual measurement in Table 3-10.

The densities of the bitumen samples decreased linearly with an increase in the measurement temperature from 20 to 60 °C, which is consistent with literature.[34] The slopes of the lines (dρ/dT) and R^2 values were calculated and included in Table 3-18.

Correction of elemental C, H, N, S composition (Table A. 7), n-heptane insoluble content (Table 3-19), TAN (Table A. 8), free radical concentration (Table A. 9) and metals content (Table A. 10) in contaminated bitumen did not involve the use of any theoretical models. These corrections were done on weight basis whose details can be found in Appendix A.

Table 3-19. Corrected *n*-Heptane Insoluble Content of Bitumen Before and After Reaction [a]

	x	s
untreated bitumen	19.3	4.1
B+W+S	22.2	1.8
B	15.6	3.6
B+W	23.2	1.3
B+S	15.0	1.4

[a] Average (x) and sample standard deviation (s) of corrected values of each individual measurement in Table 12.

3.4. Discussion

3.4.1. Difference in Conversion Due to Phase Composition.

Statistical analysis of the corrected results (Table 3-17, Table 3-18, Table 3-19 and Tables A.7-A.10) was performed to test whether the changes observed in the corrected viscosity values were statistically significant or not. The statistical tests used are briefly described in Appendix A. In each case, the probability value (*p*) was calculated and compared with the level of significance, chosen as 0.05, in this study. Based on the statistical tests, the following changes were observed as significant or non-significant.

a) The reaction of bitumen on its own (B) caused the viscosity of bitumen to decrease compared to the untreated bitumen ($p < 0.05$). As shown in Table 3-17, the mean viscosity of bitumen from B, measured at 40 °C, was about 12% lower than the mean viscosity of the untreated bitumen, 21.4 ± 0.3 Pa.s compared to 24.4 ± 0.3 Pa.s in the feed. While the viscosity of bitumen decreased when it was treated alone, treatment of bitumen in the presence of solids, or water,

or both the solids and water (reactions B+S, B+W, B+W+S) resulted in a product with higher viscosity. Differences among the bitumen viscosities of B+S, B+W and B+W+S reactions were not statistically significant ($p > 0.1$). In the current work, no significant changes among the characteristics of the viscosity-temperature relationship of the samples were observed. In addition, the results obtained from the direct thermal treatment of bitumen froth as a whole (Appendix C) revealed a noticeable increase in viscosity (Table C. 1.), a trend that was directionally consistent with the observations made in the B+W+S reaction conducted in microreactors.

b) Changes in the densities among samples, indicated by Table 3-18, were non-significant ($p > 0.05$) when different thermal treatments were used. Large standard deviations were introduced by the density correction formula for solids in bitumen, making the differences in the density values non-significant. No meaningful changes were observed in the slopes $d\rho/dT$ as well.

c) As shown in Table 3-11 (phase contamination corrected values in Table A. 7. in Appendix A), significant changes in the H/C ratio were observed between the untreated bitumen and treated bitumen samples (B, B+W, B+S), whereas changes in N/C and S/C among samples were non-significant. However, the H/C ratios of untreated bitumen and bitumen from B+W+S are not significantly different ($p > 0.05$), possibly due to the larger variation in the carbon content of the B+W+S bitumen. Although significant changes in H/C could not be observed among the treated bitumen samples, the H/C ratio increased upon thermal treatment in the presence of water or solids compared to the untreated bitumen.

d) Results of the paired t-tests indicated that the *n*-heptane insoluble content of bitumen (Table 3-19) from B+S was significantly lower ($p < 0.05$) compared to the *n*-heptane insoluble content

of bitumen samples from B+W+S and B+W. The remaining changes were non-significant as the standard deviation for untreated bitumen and product of reaction 'B' were high.

e) Significant differences ($p < 0.05$) in the TAN values (Table 3-13, with phase contamination corrected values in Table A. 8 in Appendix A) were observed between the untreated bitumen and all of the treated bitumen samples (B, B+W+S, B+W and B+S) that were higher. The TAN value of bitumen from B+W+S reaction is also meaningfully higher than the bitumen from B and B+W reactions (at a significance level 0.05). Therefore, the samples can be divided into three groups based on their TAN values: (a) untreated bitumen, (b) B, B+W, B+S bitumen samples and (c) B+W+S bitumen sample. The TAN values of (a) < (b) < (c). In conclusion, the TAN of bitumen increased upon thermal treatment at 250 °C compared to the untreated bitumen, and was highest for the hydrothermally treated bitumen in the presence of solids.

f) According to the paired t-tests, the free radical concentration of bitumen samples (Table 3-14, with phase contamination corrected values in Table A. 9 in Appendix A) followed the order: untreated bitumen < B+W+S < B+S. This trend indicates that the presence of solids during thermal treatment of bitumen contributed to an increase in the free radical concentration, and in the presence of water the effect of solids decreased. Changes due to other reactions were found to be non-significant ($p > 0.05$). Although the g-value can provide information related to the composition of the bitumen sample,[19] changes in g-values in the current work were not significant ($p>0.05$).

g) As shown in Table 3-15 (phase contamination corrected values in Table A.10 in Appendix A), V is the most abundant metal present in untreated bitumen, followed by Si and Ni. About the changes, the first observation was that the metal content in untreated bitumen was greater than the metal content in the treated bitumen from B+W+S reaction for all the metals analyzed. This

indicates that the hydrothermal treatment of bitumen (B+W+S) at 250 °C results in metal removal in bitumen. Secondly, the metal content in the product of B+W was greater than that in the product of B+W+S in all the samples for all the metals analyzed, which would indicate that the solids might be promoting metal reduction in thermal treatment process. In addition, comparing the concentration of metals between the B+S and B+W reactions, the metal content in the B+S bitumen product was less than that in the bitumen product of reaction B+W for most metals analyzed, except for Mg, Mn and Na. Therefore, the mineral solids appear to be playing a major role in metal reduction during thermal treatment at 250 °C, both in the presence and absence of water.

The outcome of the statistical analysis of bitumen properties to find meaningful differences as a result of the different phase composition of samples is summarized in Table 3-20.

Table 3-20. Statistically Meaningful Trends of Bitumen Properties after Different Thermal Treatments

Property	Statistically Significant Trends	No Meaningful Differences
Viscosity	B < Untreated bitumen < B+S, B+W, B+W+S	B+S-B+W, B+W-B+W+S, B+S-B+W+S
H/C Ratio	Untreated bitumen < Treated Bitumen Samples	All of the treated bitumen samples
n-Heptane Insoluble Content	B+S < B+W, B+W+S	Untreated Bitumen-Treated Samples, B-B+W, B-B+S, B-B+W+S, B+W-B+W+S
TAN	Untreated Bitumen < B, B+W, B+S < B+W+S	B-B+W, B-B+S, B+W-B+S

Free Radical Concentration	Untreated Bitumen < B+W+S < B+S	Untreated Bitumen-B, Untreated Bitumen-B+W, B-B+W, B-B+S, B-B+W+S, B+W+S-B+W, B+W-B+S
Metal Content [a]	Untreated Bitumen > B+W+S B+W > B+W+S	_ [b]

[a] Only significant trends valid for all metals are listed

[b] Influenced by the metal

3.4.2. Influence of Reaction Environment on Bitumen Properties.

In this section, possible reasons contributing to the changes observed in the bitumen properties are discussed. In most cases, further investigation is necessary to test these interpretations.

3.4.2.1. Changes in Viscosity.

The decrease in the viscosity of bitumen treated alone at 250 °C was also observed in the work by Yañez Jaramillo and De Klerk,[14] in the investigation of viscosity changes in Cold Lake bitumen upon thermal conversion between 150 and 300 °C. In their work, the viscosity of bitumen measured at 40 °C decreased from 88 to 4.4 Pa.s upon thermal treatment at 250 °C for 2 h, and it was noted that the change in viscosity with reaction time was not a monotonous decrease. The viscosity decrease at the same conditions in this work was less; viscosity decreased from 24.4 to 21.4 Pa.s at 40 °C (Table 3-17).

Why is it then that the viscosity of the bitumen increased during thermal conversion in the presence of water and solids? In an attempt to answer this question, several possible explanations were evaluated.

(i) An increase in viscosity in the presence of water can occur due to dissolution of lighter oil components into water during the treatment, making the oil phase heavier, and thus more viscous. Water soluble components would be those containing polar functional groups such as -OH, -NH$_2$ and COOH, and their solubility in water would depend on properties such as pH, temperature and ionic strength. With increase in temperature, the aqueous solubility of organic components is expected to increase.[35] Moreover, at the slightly alkaline pH of the froth, 8.3 (Table 3-16), solubility of low molecular mass carboxylic acids in the aqueous phase is expected to be higher due to formation of the polar carboxylate groups.[36] However, the conductivity of the aqueous phase (Table 3-16), which is a measure of dissolved ionic material, did not increase after thermal treatment in the presence of water. There was no experimental support for this hypothesis.

(ii) Upon heating in the presence of water, some of the esters and anhydrides in bitumen are expected to hydrolyze to form carboxylic acids.[37] The carboxylic acids could then be neutralized by the basic compounds in water to form carboxylate salts. If the multivalent cations form crosslinks or bridges between the carboxylates as reported in literature,[38,39] then that would increase the molecular mass of the salt, decrease its water solubility and promote viscosity increase. However, no significant change in the pH or increase in conductivity of the treated aqueous samples compared to the untreated froth water (Table 3-16) was noticed to support these hypotheses.

(iii) When solids are present, interactions between the water and/or bitumen are expected to be affected due to adsorption of species in bitumen on the mineral surface. Participation of cations such as Ca^{2+}, Fe^{3+} and Al^{3+} in the cation-bridging and adsorption mechanisms is reported in literature.[40] Although the concentration of these ions in the aqueous phases of the B+W and

B+W+S reaction products was less compared to that in the untreated froth water as shown in Table 3-16, Table 3-15 provides no support for this.

(iv) In the absence of water, solids might be able to affect the viscosity of bitumen by catalyzing addition reactions. Participation of clay minerals in reactions involving organic compounds is reported in literature.[41-44] Polymerization of styrene (C_8H_8) catalyzed by kaolinite is reported,[44] which is an example of how a mineral interacts with an organic compound and catalyzes addition reactions. A reaction mechanism having both free radical and cationic characteristics was proposed by Solomon,[44] for the polymerization of styrene, in which the Lewis acid sites and transition metal species in the higher valency state (e.g. Fe^{3+}) can initiate an electron transfer from styrene to the clay mineral forming a radical-cation intermediate. Free radical generation by transition metal ions like Fe^{2+}/Fe^{3+} and their role in catalyzing liquid-phase oxidation of organic compounds are also reported in literature,[45] that are possible ways in which the minerals can participate in reactions. In principle, ions in solution capable of such redox reactions could also lead to radical generation. Directionally, adsorption and addition reactions on the surface of minerals should have decreased the viscosity of the liquid by removing such species from the liquid phase. This was not observed. However, the potential increase in free radical content from interaction with minerals in solids or dissolved in the water was found (Table 3-14). The increase in viscosity is also consistent with formation of additional heavier material. The possibility of some reactions caused by the minerals could therefore not be discounted.

(v) In commercial applications, acidic surfaces are of importance in the interaction between solids and hydrocarbons. Acid sites in silica-alumina catalysts promote polymerization of polycyclic and heterocylic aromatic hydrocarbons in catalytic cracking reactions, causing an increase in the molecular weight of hydrocarbon mixtures.[46] A similar type of behavior by the acidic minerals in

froth could be a reason for the viscosity increase observed. However, this presupposes that the acidic minerals are present in their acidic form, which appears unlikely at the alkaline conditions of the froth. Such an explanation also assumes that the products from polymerization will desorb and redissolve in the bitumen. This appeared unlikely.

(vi) In the same context, when the water is present in addition to solids, it can act as a Lewis base and compete with organic compounds for the Lewis acid sites on the clay mineral which are responsible for polymerization of compounds like styrene.[44] Evidence for deactivation of clay catalysts applied in the polymerization of styrene, due to presence of moisture, is available in literature.[42] Acid sites on clays are also activated before using them as catalysts in chemical reactions by heating the clays at temperatures greater than 100 °C to remove the free and bound water.[42] However, in the current study, no significant difference was observed in the products of B+W+S and B+S, to indicate an influence of the aqueous phase on the activity of mineral solids. It is unlikely that Lewis acid catalyzed mineral activity affected the reactions responsible for increasing viscosity.

The results obtained from this direct thermal treatment of bitumen froth as a whole revealed a noticeable increase in viscosity, a trend that was directionally consistent with the observations made in the B+W+S reaction conducted in microreactors at 250°C for 2 hours. Further details and data regarding this experiment can be found in the dedicated appendix section.

In conclusion, the viscosity of bitumen increased upon thermal treatment in the presence of water and solids at 250 °C, and various potential hypotheses for the role of water and solids, responsible for viscosity increase, were evaluated using the available results. Dissolution of lighter oil components containing polar functional groups into water, formation of carboxylate ions by hydrolysis of esters and anhydrides in bitumen and their crosslinking by multivalent cations, free

radical polymerization and acid-catalyzed addition reactions on the surface of mineral solids, are all possible reasons for the observed increase in the viscosity of bitumen upon thermal treatment in the presence of water and solids. However, most of these hypotheses had no experimental support. Free radical addition reactions catalyzed by solids, followed by desorption and dissolution of addition products in bitumen, was the only explanation that could not be discounted.

3.4.2.2. Changes in H/C Ratio.

Compared to the untreated bitumen, the H/C ratio increased upon thermal treatment, irrespective of the second phase present (Table 3-11).

In thermal conversion processes, chemical changes in bitumen occur through thermal cracking, and the chemistry of these reactions follows a free radical mechanism. Although the temperature used in this study (250 °C) is too low to produce coke, the reactions involving hydrogen transfer do take place.[15] Any light products that may have formed during the reaction were likely to be more hydrogen rich than the bulk liquid, which would have caused a slight decrease in H/C ratio, not the increase that was observed.

Adsorption of asphaltenes on the surface of mineral solids is widely reported in literature.[47-50] Although asphaltenes are a solubility class, they are generally characterized by high aromaticity (low H/C ratio).[1] Rejection of some asphaltenes and coke precursors to the solids phase by adsorption would also increase the H/C ratio of bitumen. However, no significant difference in the H/C ratio of the bitumen treated alone and the bitumen treated in the presence of solids was observed, indicating that the increase in H/C ratio of the B+S bitumen product compared to untreated bitumen is probably related only to the progression of thermal conversion rather than to the presence of solids. Yet, for the H/C to increase, apart from analytical uncertainty, there must

have been some way in which more carbon rich material was removed from the product that was common to all thermally treated samples.

3.4.2.3. Changes in *n*-Heptane Insoluble Content.

As mentioned in Table 3-20, the *n*-heptane insoluble content of bitumen from B+S reaction was significantly lower compared to that of the bitumen samples from B+W+S and B+W reactions. It appears as though the presence of water in thermal treatment influenced the *n*-heptane insoluble content of the bitumen product.

According to literature, water droplets dispersed in diluted bitumen can be surrounded by a film of irreversibly adsorbed surface-active species from bitumen, forming clusters.[51] Such clusters of water droplets in diluted bitumen can be separated out during filtration, adding to the *n*-heptane insoluble content of bitumen. Among all the bitumen products analyzed, only the products of reactions B+W+S and B+W contained residual water, as shown in Table 3-7. This residual water could form *n*-heptane insoluble material in bitumen as explained before.

If this hypothesis is true, significant differences in the *n*-heptane insoluble content of bitumen would be observed between the reactions performed in the presence of water (B+W+S and B+W) and the reactions in the absence of water (B and B+S). But due to high standard deviation of the product of reaction 'B' (Table 3-19), the differences in the *n*-heptane insoluble content between reaction B and the reactions in the presence of water (B+W+S and B+W) were non-significant ($p > 0.05$), providing no experimental support for this hypothesis. Differently put, compared to the reaction of bitumen on its own, the presence of water in the mixture did not cause a statistically significant increase in *n*-heptane insoluble content as one would anticipate if water droplets were encapsulated by *n*-heptane insoluble material.

It is worthwhile pointing out that the *n*-heptane insoluble content (Table 3-19), did not correlate with the viscosity (Table 3-17). Despite the lower n-heptane insoluble content of the B+S product, it had the highest viscosity.

3.4.2.4. Changes in TAN.

In this work the TAN increased with thermal treatment and was highest after thermal treatment in the presence of both water and solids. Acidic hydrolysis of esters can be promoted in the presence of water and acidic surface of solids acting as a catalyst, forming new carboxylic acid groups.[52] Such a reaction would increase the TAN of bitumen. However, this reaction is reversible,[52] and the reverse reaction (esterification) is also acid-catalyzed.[37,43]

On the other hand, base-catalyzed hydrolysis of esters is also reported in literature,[52] which is a possible reaction mechanism promoted by the bases in froth. However, the end products of the base-catalyzed hydrolysis of an ester are a carboxylate ion (not carboxylic acid) and an alcohol. Due to the resonance stability of the carboxylate ion, it has little tendency to react with alcohol. Therefore, the base catalyzed hydrolysis of esters is an irreversible reaction, and is not expected to have resulted in a decrease in pH, but may have caused the increase in the TAN of bitumen.[53] The ASTM D664 states that salts react if their hydrolysis constants are larger than 10^{-9},[53] and in the absence of evidence to the contrary, the contribution of carboxylates to TAN cannot be ruled out.

3.4.2.5. Changes in Free Radical Content.

In this work, the average g-values of the untreated and treated bitumen samples (Table 3-14) were in the range 2.0007-2.0030, which is typical of carbon-centered organic free radicals.[54,55] The reaction environment did not have an effect on the nature of the free radicals, only on their concentration.

Solids contributed to an increase in the free radical concentration of bitumen after thermal treatment. According to literature, clay minerals possess electron donating and accepting properties, by which they can create radical ions when interacting with organic compounds.[44] In this way, new radicals can be generated by solids or dissolved redox capable metal ions during thermal reactions as discussed in section 4.4.2.1.

3.4.2.6. Changes in Metal Content.

As mentioned in Section 4.4.1, the metal content of bitumen decreased somewhat upon hydrothermal treatment, and from the results, solids appear to be playing a dominant role in reducing the metal content in bitumen. At the same time it should be noted that the change in concentration of Fe, Ni, and V, was limited and of the order 10%.

3.5. Conclusions

The objective of this work was to investigate whether treatment of bitumen froth, i.e. in the presence of both water and mineral solids resulted in bitumen upgrading and in what ways the presence or absence of water and/or mineral solids affected the conversion of bitumen.

It was found that direct treatment of the bitumen froth at 250 °C did not lead to upgrading of the bitumen. Treatment at such low severity conditions was beneficial only when converting the bitumen on its own. The following conclusions could be drawn about the impact of water and mineral solids.

(a) The increase in bitumen viscosity due to the presence of mineral solids and/or water was accompanied by a slight increase in free radical content. Directionally these observations indicated an increase in heavier product formation. There was some experimental support for an explanation

based on ions that could generate additional free radicals by redox reactions and increase radical addition, although no specific proof of this was provided by the study.

(b) The increase in total acid number (TAN) without a concomitant increase in pH was tentatively explained in terms of base-assisted hydrolysis of esters and anhydrides. The extent of these reactions increased with the presence of mineral solids and water.

(c) The lack of impact of mineral solids and water on some properties, as well as the impact on a few properties, such as increase in H/C ratio, decrease in metal content, and increase in *n*-heptane insoluble content, was noted, but was left unexplained.

3.6. References

(1)   Gray, M. R. *Upgrading Oilsands Bitumen and Heavy Oil*; Pica Pica Press: Edmonton, Canada, 2015; p 473.

(2)   Letcher, T. M. Unconventional Oil: Oilsands. *Future Energy: Improved, Sustainable and Clean Options for our Planet*, 3rd ed.; Elsevier: Amsterdam, Netherlands, 2020; pp 49–65.

(3)   Masliyah, J.; Zhou, Z. J.; Xu, Z.; Czarnecki, J.; Hamza, H. Understanding Water-Based Bitumen Extraction from Athabasca Oil Sands. *Can. J. Chem. Eng.* **2004**, *82* (4), 628–654.

(4)   Rao, F.; Liu, Q. Froth Treatment in Athabasca Oil Sands Bitumen Recovery Process: A Review. *Energy Fuels* **2013**, *27* (12), 7199–7207.

(5)   Romanova, U. G.; Yarranton, H. W.; Schramm, L. L.; Shelfantook, W. E. Investigation of Oil Sands Froth Treatment. *Can. J. Chem. Eng.* **2004**, *82* (4), 710–721.

(6)   Feng, X.; Behles, J. A. Understanding the Demulsification of Water-in-Diluted Bitumen Froth Emulsions. *Energy Fuels* **2015**, *29*, 4616−4623.

(7)   Chen, Q.; Stricek, I.; Cao, M.; Gray, M. R.; Liu, Q. Influence of Hydrothermal Treatment on Filterability of Fine Solids in Bitumen Froth. *Fuel* **2016**, *180*, 314–323.

(8)   Fan, H. F.; Liu, Y. J.; Zhong, L. G. Studies on the Synergetic Effects of Mineral and Steam on the Composition Changes of Heavy Oils. *Energy Fuels* **2001**, *15* (6), 1475–1479.

(9)   Wu, C.; Lei, G. L.; Yao, C. J.; Sun, K. J.; Gai, P.Y.; Cao, Y. B. Mechanism for Reducing the Viscosity of Extra-Heavy Oil by Aquathermolysis with an Amphiphilic Catalyst. *J. Fuel Chem. Technol.* **2010**, *38* (6), 684–690.

(10)   Sankey, B. M.; Maa, P. S.; Bearden, R., Jr. Conversion of the Organic Component from Tar Sands to Lower Boiling Products. U.S. Patent 5,795,464, August 18, 1998.

(11)   Canıaz, R. O.; Arca, S.; Yaşar, M.; Erkey, C. Refinery Bitumen and Domestic Unconventional Heavy Oil Upgrading in Supercritical Water. *J. Supercrit. Fluids* **2019**, *152*, 104569.

(12)   Morimoto, M.; Sugimoto, Y.; Saotome, Y.; Sato, S.; Takanohashi, T. Effect of Supercritical Water on Upgrading Reaction of Oil Sand Bitumen. *J. Supercrit. Fluids* **2010**, *55* (1), 223–231.

(13)   Liu, C. T. Aquathermolysis of Heavy Oil Model Compounds. *Adv. Mater. Res.* **2011**, *236-238*, 732–735.

(14)   Yañez Jaramillo, L. M.; De Klerk, A. Partial Upgrading of Bitumen by Thermal Conversion at 150–300° C. *Energy Fuels* **2018**, *32* (3), 3299–3311.

(15)   Naghizada, N.; Prado, G. H. C.; De Klerk, A. Uncatalyzed Hydrogen Transfer during 100–250 °C Conversion of Asphaltenes. *Energy Fuels* **2017**, *31* (7), 6800–6811.

(16). Osborne, N.S.; Stimson, H.F.; Fiock, E.F.; Ginnings, D.C. The Pressure of Saturated Water Vapor in the Range 100° to 374° C. *Bur. Stand. J. Res.* **1933**, *10* (2), 155–188.

(17)   Carbognani, L.; Roa-Fuentes, L. C.; Diaz, L.; Berezinski, J.; Carbognani-Arambarri, L.; Pereira-Almao, P. Reliable Determination of Water Contents of Bitumen and Vacuum

Residua via Coulometric Karl Fischer Titration Using Tetrahydrofuran. *Pet. Sci. Technol.* **2014**, *32* (5), 602–609.

(18)   Chauhan, G.; De Klerk, A. Dissolution Methods for the Quantification of Metals in Oil Sands Bitumen. *Energy Fuels* **2020**, *34* (3), 2870–2879.

(19)   Tannous, J. H.; De Klerk, A. Quantification of the Free Radical Content of Oilsands Bitumen Fractions. *Energy Fuels* **2019**, *33* (8), 7083–7093.

(20)   Zachariah, A.; De Klerk, A. Thermal Conversion Regimes for Oilsands Bitumen. *Energy Fuels* **2016**, *30* (1), 239–248.

(21)   Wang, L.; Zachariah, A.; Yang, S.; Prasad, V.; De Klerk, A. Visbreaking Oilsands-Derived Bitumen in the Temperature Range of 340–400° C. *Energy Fuels* **2014**, *28* (8), 5014–5022.

(22)   Rutgers, I. R. Relative Viscosity and Concentration. *Rheol. Acta* **1962,** *2* (4), 305–348.

(23)   Montoya Sanchez, N.; De Klerk, A. Viscosity Mixing Rules for Bitumen at 1–10 wt % Solvent Dilution When Only Viscosity and Density Are Known. *Energy Fuels* **2020,** *34,* 8227−8238.

(24)   Poletto, M.; Joseph, D. D. Effective Density and Viscosity of a Suspension. *J. Rheol.* **1995**, *39* (2), 323–343.

(25)   Wen, J.; Zhang, J.; Wei, M. Effective Viscosity Prediction of Crude Oil-Water Mixtures with High Water Fraction. *J. Pet. Sci. Eng.* **2016**, *147*, 760–770.

(26)   Sefton, E.; Sinton, D. Evaluation of Selected Viscosity Prediction Models for Water in Bitumen Emulsions. *J. Pet. Sci. Eng.* **2010**, *72*, 128–133.

(27)   Pabst, W. Fundamental Considerations on Suspension Rheology. *Ceram.-Silik.* **2004**, *48* (1), 6–13.

(28)   Pal, R. New Generalized Viscosity Model for Non-Colloidal Suspensions and Emulsions.

Fluids **2020,** *5* (3), 150.

(29)   Pavlik, M. The Dependence of Suspension Viscosity on Particle Size, Shear Rate, and

Solvent Viscosity. M.S. Thesis, DePaul University, Chicago, IL, 2009.

(30)   Sherman, P. The Viscosity of Emulsions. *Rheol. Acta* **1962**, *2* (1), 74–82.

(31)   Shi, S.; Wang, Y.; Liu, Y.; Wang, L. A New Method for Calculating the Viscosity of W/O

and O/W Emulsion. *J. Pet. Sci. Eng.* **2018,** *171*, 928–937.

(32)   Barnea, E.; Mizrahi, J. A Generalized Approach to the Fluid Dynamics of Particulate

Systems: Part 1. General Correlation for Fluidization and Sedimentation in Solid

Multiparticle Systems. *Chem. Eng. J.* **1973,** *5* (2), 171–189.

(33)   Bullard, J. W.; Pauli, A. T.; Garboczi, E. J.; Martys, N. S. A Comparison of Viscosity–

Concentration Relationships for Emulsions. *J. Colloid Interface Sci.* **2009,** *330* (1), 186–

193.

(34)   Nourozieh, H.; Kariznovi, M.; Abedi, J. Density and Viscosity of Athabasca Bitumen

Samples at Temperatures up to 200C and Pressures up to 10 MPa. *SPE Reservoir Eval.*

Eng. **2015,** *18* (03), 375–386.

(35)   Black, S.; Muller, F. On the Effect of Temperature on Aqueous Solubility of Organic

Solids. *Org. Process Res. Dev.* **2010,** *14* (3), 661–665.

(36)   *Thermodynamic and transport properties of organic salts* (IUPAC Chem. Data Ser. 28);

Franzosini, P., Sanesi, M. Eds.; Pergamon Press: Oxford, 1980.

(37)   Loudon, M. The Chemistry of Carboxylic Acid Derivatives. *Organic Chemistry*, 5th ed.;

Roberts and Company Publishers: Greenwood Village, CO, 2009; pp 1004–1015.

(38)   Joseph, J. T.; Forrai, T. R. Effect of Exchangeable Cations on Liquefaction of Low Rank

Coals. *Fuel* **1992,** *71* (1), 75–80.

(39) van Bodegom, B.; van Veen, J. A. R.; van Kessel, G. M. M.; Sinnige-Nijssen, M. W. A;

Stuiver, H. C. M. Action of Solvents on Coal at Low Temperatures: 1. Low-Rank Coals.

Fuel **1984,** *63* (3), 346–354.

(40) Adegoroye, A.; Wang, L.; Omotoso, O.; Xu, Z.; Masliyah, J. Characterization of Organic-

Coated Solids Isolated from Different Oil Sands. *Can. J. Chem. Eng.* **2010**, *88* (3), 462–

470.

(41) Soma, Y.; Soma, M. Chemical Reactions of Organic Compounds on Clay Surfaces.

Environ. Health Perspect. **1989,** *83*, 205–214.

(42) Bittles, J.A.; Chaudhuri, A.K.; Benson, S.W. Clay-Catalyzed Reactions of Olefins. II.

Catalyst Acidity and Mechanism. *J. Polym. Sci., Part A: Gen. Pap.* **1964**, *2* (4), 1847–

1862.

(43) Nagendrappa, G. Organic Synthesis using Clay Catalysts Clays for 'Green Chemistry'.

Reson **2002,** *7* (1), 64–77.

(44) Solomon, D. H. Clay Minerals as Electron Acceptors and/or Electron Donors in Organic

Reactions. *Clays Clay Miner.* **1968,** *16* (1), 31–39.

(45) Denisov, E. T.; Denisova, T. G.; Pokidova, T. S. *Handbook of Free Radical Initiators*;

John Wiley & Sons, Inc: Hoboken, NJ, 2003; pp 591–653.

(46) Appleby, W. G.; Gibson, J. W.; Good, G. M. Coke Formation in Catalytic Cracking. *Ind.

Eng. Chem. Process Des. Dev.* **1962,** *1* (2), 102–110.

(47) Pernyeszi, T.; Patzkó, Á.; Berkesi, O.; Dékány, I. Asphaltene Adsorption on Clays and

Crude Oil Reservoir Rocks. *Colloids Surf., A* **1998**, *137* (1-3), 373–384.

(48) Dubey, S. T.; Waxman, M. H. Asphaltene Adsorption and Desorption from Mineral

Surfaces. *SPE Reservoir Eng.* **1991,** *6* (03), 389–395.

(49)   González, G.; Moreira, M. B. C. The adsorption of asphaltenes and resins on various

minerals. In *Asphaltenes and Asphalts, 1*; Yen, T.F., Chilingarian, G.V., Eds.; Elsevier

Science B.V.: Amsterdam, Netherlands, 1994; 40, pp. 207–231.

(50)   Briones, A. M. Asphaltene Adsorption on Different Solid Surfaces from Organic Solvents.

M.S. Thesis, University of Alberta, Edmonton, Canada, 2020.

(51)   Yang, F. Bitumen Fractions Responsible for Stabilizing Water in Oil Emulsions. Ph.D.

Dissertation, University of Alberta, Edmonton, Canada, 2016.

(52)   Moo-Young, M. Substrate Hydrolysis: Methods, Mechanism, and Industrial Applications

of Substrate Hydrolysis. In *Comprehensive Biotechnology*; Webb, C.; Elsevier:

Amsterdam, Netherlands, 2011; pp 103–118.

(53)   ASTM International. *D664-18e2 Standard Test Method for Acid Number of Petroleum

Products by Potentiometric Titration;* West Conshohocken, PA, 2018.

(54)   Jia, H.; Zhao, S.; Nulaji, G.; Tao, K.; Wang, F.; Sharma, V. K.; Wang, C. Environmentally

Persistent Free Radicals in Soils of Past Coking Sites: Distribution and

Stabilization. *Environ. Sci. Technol.* **2017**, *51* (11), 6000–6008.

(55)   Robinson, J. W.; Frame, E. M. S.; Frame, G. M. II. *Undergraduate instrumental analysis*.

CRC Press: Boca Raton, FL, 2014; p 21.

Chapter 4. Free Radical and Cationic Addition Due to Clay Minerals Found in Bitumen Froth at 250 °C Probed with Use of α-Methylstyrene and 1-Octene

Abstract

Following previous evidence that hydrothermal treatment of bitumen froth does not lead to bitumen upgrading at 250 °C and promotes viscosity increase, the current study explores the free radical and cationic reactivity of the clay minerals found in bitumen froth in promoting heavier material formation through addition reactions. The current investigation employed α-methylstyrene (AMS) and 1-octene as probe molecules instead of bitumen froth, and their conversion at 250 °C in the presence of the clay minerals kaolinite and illite was studied in batch reactors. Thermal conversion of AMS and 1-octene at 250 °C in the absence of minerals was observed to be low. In the presence of the clay minerals the conversion of AMS and 1-octene not only increased, but reactions such as dimerization of AMS, and 1-octene and toluene (used as solvent) alkylation were mainly promoted leading to heavier product formation. Double bond isomerization of 1-octene and cumene formation from AMS were side reactions that were also promoted by the clay minerals. Suppression of mineral related conversion by pyridine, and selectivity to different reaction products that enabled differentiation between free radical and cationic reaction pathways, indicated that the mineral related conversion was predominantly cationic in nature. Using the reactions in the presence of minerals and pyridine as surrogates for alkaline bitumen froth, it was concluded that even under alkaline conditions, minerals could promote heavier material formation through cationic addition.

Keywords: Hydrothermal treatment, bitumen froth, cationic addition, free radical addition, clay minerals

4.1. Introduction

Bitumen froth is the product of the hot water extraction process of mined oilsands, and it contains about 60 wt% bitumen, 30 wt% water and 10 wt% mineral solids.[1] In current industrial practice the bitumen is separated from the froth before the bitumen is upgraded.[2] Some researchers investigated direct thermal conversion of the bitumen froth and upgrading of bitumen in the presence of water and mineral solids, also called hydrothermal treatment.[3-6] Upgrading of the froth to improve bitumen properties and facilitate separation was reported to be successful over the temperature range 300–420 °C.[4] Yet, at 250 °C, hydrothermal treatment of bitumen froth did not lead to bitumen upgrading and promoted viscosity increase.[3]

In the previous work, thermal conversion of bitumen at 250 °C in the presence of solids alone increased the viscosity of bitumen by about 5 times its original viscosity, accompanied by an increase in the free radical concentration of bitumen.[3] On the other hand, when the bitumen was treated on its own, these changes were not observed.[3,7,8] Generally, heavier fractions of bitumen have a high viscosity, and also contain more free radicals.[9-12] It is therefore hypothesized that minerals promote formation of heavier material in bitumen at 250 °C, which would be consistent with the increase in the measured viscosity and free radical content of the product.

Solids in the bitumen froth are composed of the clay minerals kaolinite and illite, which constitute about 40-70 wt% of the minerals fraction.[4,5] Other minerals identified in the bitumen froth are quartz, pyrite, rutile, calcite, siderite, dolomite, muscovite, magnesite, hematite, maghemite, anatase and microcline.[3-5] Under the conditions of hydrothermal treatment process, it is possible that different minerals respond in a different manner. Upon heating, decomposition of minerals, e.g. decomposition of pyrite into pyrrhotite and H_2S,[5,13,14] or changes in the crystal structures of

minerals can occur,[15] that may influence their reactivity. However, such changes were reported mostly for minerals at temperatures above 400 °C,[15-18] and are not likely to occur at 250 °C.

The focus of this work is on the role of clay minerals in the bitumen froth in promoting addition reactions. There are several potential pathways:

(i) Redox reactions leading to free radical addition

(ii) Acid catalyzed addition

According to literature, clay minerals exhibit redox behavior.[19-24] The electrochemical activity of clay minerals is generally attributed to the structurally bound iron (Fe), which is present in the majority of clay minerals.[22,23] It was pointed out that the electron donating and electron accepting properties of iron containing clay minerals can convert an organic molecule to a radical anion or radical cation respectively.[19]

Under ambient conditions, formation of phenoxyl-type radicals by adsorption of phenol on Fe(III)-Montmorillonite was observed by Nwosu, et al.[24] A change in the oxidation state of Fe (reduction of Fe^{3+} to Fe^{2+}) was also observed by Nwosu, et al.[24] using X-ray absorption near-edge structure (XANES) spectroscopy and X-ray photoemission spectroscopy (XPS), indicating an electron transfer from phenol to the Fe(III)-Montmorillonite. Thus, redox reactions leading to the formation of reactive radical intermediates could offer a plausible explanation for the increase in heavier material through addition reactions.

Clays may also function as Bronsted acids or Lewis acids or both, and initiate cationic addition of organic compounds through formation of a carbocation. The Bronsted acidity of clays can arise from the dissociation of intercalated water molecules that are coordinated to cations, or due to the hydroxyl groups in specific sites in the lattice structure, or at the crystal edges which dissociate

into reactive protons.[25,26] The Lewis acid character of clays arises due to Fe^{3+} and Al^{3+} present at the crystal edges.[25,26] However, in the case of bitumen froth, the pH of the froth is slightly alkaline (pH ~ 8.3).[3] Exchangeable base cations such as Ca^{2+}, Mg^{2+}, K^+ and Na^+ would counteract the acidity of clays. Therefore, cationic addition catalyzed by clays appears to offer a plausible, but less likely explanation at the alkaline conditions of the bitumen froth.

The objective of this work is to investigate in what way the solids in bitumen froth promote heavier material formation through addition reactions. To facilitate analysis and interpretation, α-methyl styrene (AMS) and 1-octene were used as model compounds, since these two compounds have different propensity for free radical and cationic addition. These probe molecules were not selected to represent bitumen, but rather to interrogate the reaction pathways that were speculated to be active in bitumen during froth treatment.

In the current work, the conversion of AMS and 1-octene in the presence of natural clays kaolinite and illite was studied. Control reactions in which the α-methyl styrene/1-octene were treated in the absence of mineral solids were performed to identify the contribution of pure thermal conversion. The present work also benefited from previous investigations that employed α-methyl styrene (AMS) and 1-octene.[27-34]

Additionally, the possible reasons for the occurrence of addition reactions in the presence of mineral solids were explored. To distinguish between the contributions of free radical and cationic additions, a base (pyridine) was used to attenuate cationic addition. The side reactions taking place in parallel to the formation of addition products (e.g. rearrangement or isomerization reactions) were considered as they could provide useful information about the reaction pathway (free radical/carbocation).

4.2. Experimental

4.2.1. Materials.

Natural kaolinite and illite shale were used in this study as minerals. Details of the suppliers and product identifiers can be found in Table 4-1. The illite shale (500 g) was ground into a fine powder by using a SPEX SamplePrep ShatterBox 8530 ring and puck mill (115 VAC/60Hz) located in the Department of Earth and Atmospheric Sciences at University of Alberta. Kaolinite was supplied as a powder and did not require mechanical size reduction. Pictures of the minerals and their characterization information are given in Figure B. 1, Table B. 1 and Figure B. 2 in Appendix B. Other chemicals and cylinder gases used in this study are also listed in Table 4-1.

Table 4-1. Minerals, Chemicals and Cylinder Gases used in this Study

Compound	Formula	CASRN ^{a}	Purity (%) ^{b}	Supplier
		Minerals		
Kaolinite	$Al_2O_3 \cdot 2SiO_2 \cdot 2H_2O$	1318-74-7		Sigma-Aldrich
Illite Shale				Avantor (VWR)
		Chemicals		
α-Methylstyrene	C_9H_{10}	98-83-9	99	Sigma-Aldrich
1-Octene	C_8H_{16}	111-66-0	> 99	Acros Organics
Toluene, Certified ACS	C_7H_8	108-88-3	≥ 99.5	Fisher Scientific

Pyridine, Spectrophotometric Grade	C_5H_5N	110-86-1	≥ 99	Sigma-Aldrich
Cylinder Gases				
Nitrogen	N_2	7727-37-9	99.999	Praxair
Helium	He	7440-59-7	> 99	Praxair
Synthetic Air	O_2 / N_2	132259-10-0	> 99.9999	Praxair
Hydrogen	H_2	1333-74-0	99.999	Praxair

[a] CASRN = Chemical Abstracts Services registry number.

[b] This is the purity guaranteed by the supplier.

4.2.2. Equipment and Procedure.

Reactions were performed in micro batch reactors made of stainless steel (Type 316). The length and internal diameter of the micro batch reactors were 15.2 cm and 1.8 cm respectively, and the total length of the reactor tubing connected to the reactor body was 70 cm. Pictures of these reactors can be found in Figure B. 3 in Appendix B. These reactors were supplied by Swagelok and consisted of a thermocouple and pressure gauge to measure the temperature and pressure respectively inside the reactor.

For each reaction, the reactants were weighed and added into an 8 ml clear borosilicate glass vial, which was then placed inside the reactor using forceps. The purpose of using glass vials was to prevent contamination of the reaction mixture by the reactor side walls. The types of reactions performed and the amounts of reactants (g) used in each reaction are mentioned in Table 4-2.

As shown in Table 4-2, the reactions performed in this study can be grouped into three sets, one of them involving α-methylstyrene (AMS) and another involving 1-octene (OCT). Toluene was used as the solvent in these reactions. The third set of reactions are the control reactions that do not contain α-methylstyrene or 1-octene but performed to study the effect of heating only toluene and pyridine on their own, and toluene in the presence of kaolinite and illite. A total of 16 reactions were performed in duplicates. To understand the role of the minerals (kaolinite and illite) in promoting addition reactions, AMS and 1-Octene were individually treated in the presence of these minerals. Pyridine was used in some of the reactions to study the contribution of cationic addition in the conversion of the model compounds used in this study to their addition products. By adding pyridine, the acidity associated with the clay minerals would be suppressed, thereby inhibiting cationic addition reactions promoted by the acid sites.

After loading the micro batch reactors, a gas leak test was conducted and the reactors were pressurized with nitrogen. An initial pressure of 4.5 MPa, measured at room temperature, was used in all the reactions. The micro batch reactors were then placed in an Omega Fluidized Bath FSB-3 fluidized sand bath heater, and heated to 250 °C. Reactions in this study were conducted at 250 °C for a duration of 2 h, which was the time measured from the point at which the internal temperature in the reactors reached 250 °C. The reaction time of 2 h was chosen based on the previous study on hydrothermal froth treatment at 250 °C, where physical and chemical changes in bitumen were observed upon thermal treatment for a duration of 2 h.[3]

The final pressure at the reaction temperature (250 °C) for all the reactions was 7 MPa. At the end of the reactions, the reactors were removed from the sand bath and allowed to cool down. After reaching room temperature, the reactors were depressurized, and the masses of the solid-liquid mixture and the gas stream were noted down. The solids were allowed to settle and the top layer

(supernatant) was transferred to another glass container. The liquid found outside the glass vial was combined with the supernatant and the weights of wet solids and liquid products thus obtained were recorded. The liquid products were filtered using a 0.22 μm syringe filter to remove any suspended solids present, and used for analyses.

Table 4-2. Masses of Reactants Used and Type of Reactions Performed at 250 °C

Reaction Type	Identifier	Mass of Reactants (g) [a]			
		Toluene	AMS/OCT	Mineral	Pyridine
Toluene	T	3±0.006	-	-	-
Pyridine	P	-	-	-	3±0.005
Toluene + Kaolinite	T+K	3±0.005	-	0.6±0.001	-
Toluene + Illite	T+I	3±0.004	-	0.6±0.001	-
α-Methylstyrene + Toluene	AMS+T	3±0.002	0.6±0.003	-	-
α-Methylstyrene + Toluene + Kaolinite	AMS+T+K	3±0.002	0.6±0.001	0.6±0.002	-
α-Methylstyrene + Toluene + Illite	AMS+T+I	3±0.004	0.6±0.004	0.6±0.004	-
α-Methylstyrene + Toluene + Pyridine	AMS+T+P	3±0.005	0.6±0.005	-	0.01±0.002
α-Methylstyrene + Toluene + Pyridine + Kaolinite	AMS+T+P+K	3±0.001	0.6±0.005	0.6±0.003	0.01±0.000
α-Methylstyrene + Toluene + Pyridine + Illite	AMS+T+P+I	3±0.004	0.6±0.002	0.6±0.003	0.01±0.002

1-Octene + Toluene	OCT+T	3±0.004	0.6±0.002	-	-
1-Octene + Toluene + Kaolinite	OCT+T+K	3±0.003	0.6±0.002	0.6±0.004	-
1-Octene + Toluene + Illite	OCT+T+I	3±0.02	0.6±0.003	0.6±0.004	-
1- Octene + Toluene + Pyridine	OCT+T+P	3±0.05	0.6±0.004	-	0.01±0.000
1-Octene + Toluene + Pyridine + Kaolinite	OCT+T+P+K	3±0.05	0.6±0.000	0.6±0.005	0.01±0.003
1-Octene + Toluene + Pyridine + Illite	OCT+T+P+I	3±0.006	0.6±0.004	0.6±0.001	0.01±0.000

[a] Average±Standard Deviation of reactions performed in duplicate.

4.2.3. Analyses.

Thermogravimetric analysis of wet solids separated from the reaction products was performed using Mettler Toledo TGA/DSC-1. This analysis was performed to take into consideration the amount of organic substances retained by solids while reporting conversion of AMS and 1-octene. The solids were heated in a 70 μL alumina crucible from 25°C to 900°C, at a rate of 10 °C/min, in the presence of air flowing at a rate of 100 ml/min. The flow of gas was controlled using a Mettler Toledo GC 10 gas controller. This analysis was also conducted with the untreated kaolinite and illite minerals, originally used in the experiments, to measure the mass loss from purely inorganic mineral matter upon heating. After analyzing the treated solids, the effective mass loss was

calculated and reported as the amount of organic material associated with the solids upon reaction. Further, the amounts of AMS and 1-octene retained by solids were calculated.

In order to calculate the conversion of AMS and 1-octene in the reactions, the concentration (wt %) of these compounds in the reaction products was measured using gas chromatography with flame ionization detector (GC-FID). An Agilent 7890A GC connected to an FID Detector was used for this analysis, and separation was performed with a HP-PONA column of dimensions 50 m x 0.2 mm x 0.5 μm (length x inner diameter x film thickness). Helium flowing at constant rate of 1 ml min^{-1} was used as the carrier gas. The GC oven temperature program was initiated at 36 °C, at which the oven was held for 6 min. Then, the temperature was raised to 325 °C at a rate of 20 °C min^{-1} and the final hold time was about 10 min. The analysis was carried out by diluting about 0.1 g of the reaction products with about 7 g of toluene. For quantification, calibration curves were generated (Figure B. 4 in Appendix B) using mixtures of toluene and AMS/1-octene. Different concentrations of AMS/1-octene (5-20 wt %) were prepared using toluene as a solvent, and approximately 0.1 g of these mixtures was ultimately diluted with approximately 7 g of toluene before injecting into the GC.

Gas chromatography-mass spectrometry (GC-MS) was used to identify the reaction products. For this analysis, an Agilent Model 7820A GC system was used, and the GC was connected to a Model 5977E MS detector. A HP-PONA column of dimensions 50 m x 0.2 mm x 0.5 μm (length x inner diameter x film thickness) was used to perform separation. Helium flowing at a constant rate of 0.6 ml min^{-1} was used as the carrier gas. The GC oven temperature program was initiated at 36 °C, at which the oven was held for 6 min. Then, the temperature was raised to 250 °C at a rate of 6.4 °C min^{-1}, with isothermal sections at 63 °C (held for 3 min), 73 °C (held for 3 min) and 177 °C (held for 5 min). The reason for using an elaborate temperature program was to achieve a better

separation of poorly resolved peaks observed when a more simple and faster method was used such as in the GC-FID analysis. The analysis was carried out by diluting about 0.05 g of the analyte with about 1.45 g of toluene (dilution factor of 30). The temperature of the transfer line connecting the GC column to the ion source of the MS detector was maintained at 325 °C, and the ion source temperature was set at 230 °C. Compounds present in the reaction products were identified by comparing their mass spectra with those in the National Institute of Standards and Technology (NIST) mass spectral library through the NIST MS Search 2.0 program.   These compounds should only be seen as an indication of the nature of the products as their true identity has not been confirmed using commercial standards. Peak areas of the identified compounds were obtained using OriginPro 2022 v.9.9.0.225 software by integration. These peak areas were multiplied by the dilution factor to ignore the effect of sample dilution during analysis. The final peak areas obtained in this manner were used to semi-quantitatively compare the abundances of the compounds identified in the product mixtures of different reactions.

Characterization of acid sites in the mineral solids was done using diffuse reflectance infrared Fourier transform spectroscopy (DRIFTS). A diffuse infrared (IR) accessory supplied by Pike Technology was mounted on an ABB MB3000 Fourier transform infrared (FTIR) spectrometer. The diffuse IR accessory consisted of a sample holder which had a gas inlet line, gas outlet line, and cooling water inlet and outlet lines on the exterior side. The interior side of the sample holder had a circular area with a pedestal for holding the sample crucibles. A temperature controller was also attached to the sample holder, and a TempPro software was used to operate the temperature in the sample chamber from a computer that was connected to the FTIR instrument and the temperature controller. Analysis was conducted with a mixture of ~5 mg mineral powder and ~5 mg of potassium bromide (KBr), mixed with a spatula and loaded into a DiffusIR HC ceramic

porous cup (part number 162-4251) supplied by Pike Technologies. The IR spectra were collected using a Horizon MB software. Before collecting sample spectra, a blank spectrum was recorded using plain KBr. First, the solids were heated to 100 °C in an inert (nitrogen) atmosphere and held for 1 h at that temperature to remove any adsorbed water. Next, pyridine adsorption on the solids was performed at 30 °C for 1 h by passing nitrogen gas through a tube containing liquid pyridine and then through the sample chamber. The sample was then heated to 100 °C for 10 min to remove any physisorbed pyridine, after which it was allowed to cool down to the room temperature. An IR spectrum of the pyridine-adsorbed solids was then collected and compared with the spectrum of the raw solids (recorded at room temperature in nitrogen atmosphere) which were not exposed to pyridine. If the pyridine was adsorbed on the Bronsted acid and Lewis acids of the solids, the corresponding peaks would appear in the IR spectrum, indicating the presence of Bronsted and Lewis acid sites in solids. A step-wise desorption of pyridine from froth solids was performed under nitrogen flow at the temperatures 100 °C, 150 °C, 250 °C and 350 °C, in the same order, to examine the strength of the acid sites. In each step, the solids were heated to the desorption temperature and held for 10 min, before allowing them to cool down to room temperature to record a spectrum.

Measurement of weights related to the GC-MS and GC-FID analyses was conducted using a Mettler Toledo ME 204 analytical balance. The maximum capacity of this balance was 220 g and its readability was 0.0001 g. For TGA and DRIFTS analyses, a Mettler Toledo XS105 DualRange balance was used for weighing substances. The capacity and readability of this scale were 41 g and 0.01 mg respectively in the fine range, and 120 g and 0.1 mg respectively in the full range.

4.3. Results

4.3.1. Material balance.

Material Balance for each type of reaction performed in this study using AMS or 1-octene is given in Table 4-3. The overall material balance in these reactions was found to be >97 % on average on the total feed basis. In the reaction containing mineral solids, the liquid and solid material was collected and weighed together after reaction. The gas feed was calculated by subtracting the weight of the reactors before pressurizing with nitrogen gas from the final weight of the reactors after pressurizing with nitrogen and conducting a leak test. In some cases (e.g. OCT), gas bubbles appeared in the product mixture, indicating that some gas may be dissolved in the liquid phase, increasing its weight. The trapped gas was removed by ultrasonication of the samples for about 1 h at room temperature. There was no visible change in the appearance of the liquid and solid phases due to reaction.

Table 4-3. Material Balance for Thermal Treatment

	wt % (on total feed basis) [a]											
	Feed						Product					
	Solid		Liquid		Gas		Solid+Liquid		Gas		Total	
Reaction	x	s	x	s	x	s	x	s	x	s	x	s
T	0.0	0.0	54.6	1.4	45.4	1.4	51.3	1.2	46.3	0.1	97.6	1.1
P	0.0	0.0	51.0	1.0	49.0	1.0	54.8	1.0	43.0	0.2	97.8	1.1
T+K	10.2	0.3	50.9	1.2	38.9	1.5	57.5	2.9	39.7	2.7	97.2	0.2
T+I	10.0	0.2	50.0	1.2	39.9	1.4	55.5	0.1	41.6	1.0	97.2	0.9
AMS+T	0.0	0.0	57.3	1.3	42.7	1.3	54.9	0.3	42.7	0.9	97.6	0.7
AMS+T +K	9.2	0.4	56.5	2.5	34.2	2.9	64.6	2.8	33.1	2.4	97.7	0.4

	x	s	x	s	x	s	x	s	x	s	x	s
AMS+T+I	9.5	0.005	57.0	0.3	33.4	0.3	63.9	0.3	34.4	0.2	98.2	0.5
AMS+T+P	0.0	0.0	59.7	0.7	40.3	0.7	58.8	0.4	39.5	1.9	98.3	1.5
AMS+T+P+K	9.0	0.2	54.6	1.4	36.4	1.5	59.6	0.5	40.0	0.1	99.6	0.4
AMS+T+P+I	9.3	0.002	54.8	0.3	35.9	0.3	58.9	0.5	39.2	0.2	98.1	0.6
OCT+T	0.0	0.0	56.5	3.7	43.4	3.4	59.3	0.4	39.1	2.0	98.3	1.6
OCT+T+K	9.4	0.4	56.8	1.9	33.8	2.2	61.1	2.2	37.7	1.2	98.8	0.9
OCT+T+I	9.1	0.3	54.5	1.6	36.4	1.8	60.2	0.4	38.3	0.2	98.5	0.6
OCT+T+P	0.0	0.0	59.2	1.4	40.8	1.4	57.9	2.3	40.8	1.4	98.7	0.9
OCT+T+P+K	8.7	0.02	54.0	0.6	37.3	0.6	57.8	0.6	41.5	0.4	99.4	0.2
OCT+T+P+I	9.6	0.2	58.3	1.3	32.1	1.5	60.4	0.3	38.2	0.4	98.6	0.1

[a] Average (x) and standard deviation (s) calculated for reactions performed in duplicate

4.3.2. Organic Matter Retained by the Solids.

After reactions, it may be possible that some organic components remain trapped in pores and adsorbed on the surface of the mineral solids. Adsorption of AMS and/or 1-octene on solids would impact their conversion calculation. Therefore, the amount of organic matter associated with the treated solids was determined by measuring the mass lost upon heating the treated solids (Y wt %) in the temperature range 25-900 °C. As the untreated minerals kaolinite and illite underwent a mass loss (X wt %) upon heating in the same temperature range, the effective mass loss (wt%) was

calculated using Eq 4-1. The effective mass loss is an indicator of the organic content associated with the treated solids. The measured mass loss values of the untreated solids (X wt%) and treated solids (Y wt%), as well as the calculated effective mass loss (wt %) of the treated solids are listed in Table 4-4.

$$Effective\ Mass\ Loss\ (wt\ \%) = \frac{(Y - X)}{(100 - X)} \times 100 \qquad \text{Eq 4-1.}$$

X= Measured Mass Loss of Untreated Mineral (wt %)

Y= Measured Mass Loss of Treated Solids (wt %)

According to Table 4-4, the effective mass loss of the treated solids in the reactions AMS+T+K and AMS+T+I was significantly greater than the other two types of reactions performed with AMS in the presence of pyridine. Similarly, the effective mass loss from the reactions OCT+T+K and OCT+T+I was significantly greater than other reactions of 1-octene performed in the presence of pyridine.

Table 4-4. Mass Loss (wt %) over the Temperature Range 25-900 °C in Air Atmosphere

	Measured Mass Loss of Untreated Mineral (wt %) [a]	
	x	s
Untreated Kaolinite	11.1	0.04
Untreated Illite	5.3	0.04

153

Reaction	Measured Mass Loss of Treated Solids (wt %) [b]		Effective Mass Loss (wt %) [b]	
	x	s	x	s
AMS+T+K	35.4	0.5	27.4	0.6
AMS+T+I	18.0	0.3	13.5	0.4
AMS+T+P+K	13.7	0.3	3.0	0.3
AMS+T+P+I	7.1	0.1	1.9	0.2
OCT+T+K	37.0	0.1	29.2	0.1
OCT+T+I	9.5	0.2	4.5	0.2
OCT+T+P+K	12.3	0.3	1.4	0.3
OCT+T+P+I	6.3	0.03	1.1	0.03

[a] Average (x) and standard deviation (s) of minerals analyzed in triplicate

[b] Average (x) and standard deviation (s) of reactions in duplicate

4.3.3. AMS and 1-Octene Conversion.

The initial concentration of AMS and 1-octene in the untreated reaction mixtures, and the final concentration of AMS and 1-octene in the liquid product phase obtained from each reaction (determined using GC-FID) are listed in Table 4-5. The final concentrations of AMS and 1-octene after reactions, and the effective mass loss of the treated solids (Table 4-4) were used to calculate the conversion of AMS and 1-octene in the reactions, which is also displayed in Table 4-5. The equations used in the conversion calculation are given in Table B. 2 of Appendix B.

As shown in Table 4-5, the contribution of self-reaction of AMS was low (~0.2 %), which was anticipated.[31] At the same conditions, the ~88 % conversion of AMS in the reactions AMS+T+K and AMS+T+I indicates the role of the clay minerals in promoting conversion of AMS into other

compounds. Further, addition of pyridine to the reactions of AMS performed in the presence of solids (AMS+T+P+K and AMS+T+P+I) affected the interaction between the minerals and AMS, resulting in a lower conversion of AMS (< 15 %).

Table 4-5. Initial and Final Concentrations (wt %) of AMS and 1-Octene in the Reactions and their Reaction Conversion (%) [a]

Reaction	Initial Concentration (wt %)		Final Concentration [b] (wt %)		Conversion (%)	
	x	s	x	s	x	s
AMS+T	16.9	0.1	17.7	0.6	0.2	0.1
AMS+T+K	17.0	<0.1	2.1	0.1	88.0	0.5
AMS+T+I	16.8	0.1	2.0	<0.1	88.9	0.2
AMS+T+P	16.7	0.1	15.6	0.2	7.9	1.3
AMS+T+P+K	16.7	0.1	16.4	<0.1	10.0	0.4
AMS+T+P+I	16.8	<0.1	15.8	0.1	15.1	0.7
OCT+T	16.7	0.1	15.2	1.0	4.8	0.2
OCT+T+K	16.7	0.1	5.1	0.1	70.8	0.1
OCT+T+I	16.6	<0.1	7.1	0.1	60.9	<0.1
OCT+T+P	16.7	0.1	17.1	0.2	0.0	<0.1
OCT+T+P+K	16.5	0.2	16.5	0.2	8.7	1.3
OCT+T+P+I	16.6	0.1	14.9	0.1	20.1	0.1

[a] Average (x) and standard deviation (s) of reactions in duplicate

[b] In liquid product

Similar trends were observed in the reactions containing 1-octene. Conversion during the self-reaction of 1-octene was low (~5 %). A higher conversion of 1-octene was obtained at the same

conditions when the minerals were present in the reactions OCT+T+K and OCT+T+I (about 71 %

and 61 % respectively), indicating that the mineral solids influenced the reactivity of 1-octene and

promoted its transformation into other reaction products. Further, the effect of minerals on the

conversion of 1-octene was not as high when pyridine was added to the reaction mixtures of

OCT+T+P+K and OCT+T+P+I, during which the average conversion of 1-octene was about 9 %

and 20 % respectively.

4.3.4. Identification of Organic Compounds in the Reactants and Products.

Reaction products obtained in the presence of clay minerals were analyzed using GC-MS to obtain

information about the nature of compounds formed during thermal conversion of AMS and 1-

octene in the presence of minerals. However, the interpretation of the role of solids in the addition

product formation from AMS and 1-octene would be incomplete and unclear without the GC-MS

analysis of the reactants, and products formed in the control reactions. Any of the compounds

identified in the untreated chemicals used as raw materials in the reactions or those formed in the

control reactions, that are also identified in the reactions of AMS and 1-octene in the presence of

minerals, must be disregarded during interpretation to clearly determine the nature of compounds

formed only from the interaction between AMS/1-octene and the clay minerals (with and without

addition of pyridine).

Therefore, the GC-MS analysis of the raw materials used in the reactions (toluene, AMS, 1-octene

and pyridine) was performed to determine the nature of impurities present in these chemicals.

Further, products obtained in the control reactions with toluene and pyridine (T, P, T+K, T+I) and

products from the control reactions of AMS and 1-octene performed in the absence of minerals

(AMS+T, OCT+T, AMS+T+P, OCT+T+P) were analyzed.

4.3.4.1. Analysis of Reactants

In this section the GC-MS results of the reactants used in the reactions are presented. Toluene was not only used in the reactants but was also used as a solvent for all the samples analyzed. The compounds identified in toluene (untreated) are listed in Table 4-6 along with the chemical formulae of the compounds. These peaks were present in all the samples that were analyzed including reactants and products. While the major impurities appear to be ethyl benzene and xylenes, there were various other compounds present in toluene like the cyclic isomers of C_8H_{16} etc.

Table 4-6. Compounds Identified in Reactants through GC–MS [a]

| Toluene | | Peak Area [c] | |
Compound	Chemical Formula	x ($\times 10^4$)	s ($\times 10^2$)
Toluene	C_7H_8	110000	50
Ethyl Benzene	C_8H_{10}	41	7
m-Xylene	C_8H_{10}	14	2
p-Xylene	C_8H_{10}	17	6
Cyclohexane, 1,3-dimethyl-	C_8H_{16}	14	6
Cyclopentane, 1-ethyl-3-methyl-	C_8H_{16}	6	5
Cyclopentane, propyl-	C_8H_{16}	10	5
Cyclohexane, ethyl-	C_8H_{16}	17	4
Heptane, 2-methyl-	C_8H_{18}	15	7
Hexane, 3-ethyl-	C_8H_{18}	12	5
AMS [b]		Peak Area [c]	
Compound	Chemical Formula	x ($\times 10^4$)	s ($\times 10^2$)
AMS	C_9H_{10}	13000	7
Butenyl Benzene	$C_{10}H_{12}$	36	8
C_4-Benzene	$C_{10}H_{14}$	5	6
1-Octene [b]		Peak Area [c]	
Compound	Chemical Formula	x ($\times 10^4$)	s ($\times 10^2$)
1-Octene	C_8H_{16}	6900	6

Compound	Chemical Formula	x $(\times 10^4)$	s $(\times 10^2)$
Heptane, 3-methylene-	C_8H_{16}	70	4
Octane	C_8H_{18}	25	5
Pyridine [b]			
		Peak Area [c]	
Compound	Chemical Formula	x $(\times 10^4)$	s $(\times 10^2)$
Pyridine	C_5H_5N	6100	8

[a] These compounds should only be seen as an indication of the nature of the products as their true identity has not been confirmed using commercial standards

[b] Compounds identified in toluene are not listed to avoid duplication of data

[c] Average (x) and standard deviation (s) of duplicate samples

Similarly, the compounds identified in AMS, 1-octene and pyridine chemicals used in the reactions are also given in Table 4-6. In the case of pyridine on its own, no additional hydrocarbon compounds were identified during the analysis. The peak areas of the compounds are also listed in Table 4-6 to indicate the relative abundances of these compounds in the chemicals.

4.3.4.2. Analysis of Products from Control Reactions with Toluene and Pyridine

As toluene and pyridine were used in the reactions, analysis of the products of T, P, T+K, T+I reactions was performed to know whether heating toluene (in the presence and absence of minerals) and pyridine would form any new compounds. If any of these compounds are identified in the products of thermal conversion of AMS or 1-octene they could be disregarded during interpretation to determine the nature of compounds resulting from heating only AMS and 1-octene.

Table 4-7. Compounds Identified in the Products of Control Reactions through GC–MS [a,b,c]

| Compound | Chemical Formula | Peak Area [d] | | | | | |
| | | T | | T+K | | T+I | |
		x ($\times 10^4$)	s ($\times 10^2$)	x ($\times 10^4$)	s ($\times 10^2$)	x ($\times 10^4$)	s ($\times 10^2$)
Naphthalene, 2-methyl-	$C_{11}H_{10}$	- [e]	- [e]	6	6	3	5
2 Carbon Alkylated Diphenyls	$C_{14}H_{14}$	1	3	41	5	36	6
	$C_{14}H_{14}$	- [e]	- [e]	40	7	31	6
	$C_{14}H_{14}$	32	3	43	5	33	3
3 Carbon Alkylated Diphenyls	$C_{15}H_{16}$	- [e]	- [e]	1	2	- [e]	- [e]
	$C_{15}H_{16}$	- [e]	- [e]	1	5	- [e]	- [e]
	$C_{15}H_{16}$	- [e]	- [e]	0.4	3	- [e]	- [e]

[a] These compounds should only be seen as an indication of the nature of the products as their true identity has not been confirmed using commercial standards

[b] Compounds identified in toluene (Table 4-6) are not listed to avoid duplication of data

[c] Reaction Temperature = 250 °C, Reaction Time = 2 h

[d] Average (x) and standard deviation (s) of reactions in duplicate

[e] Not detected

It appears that toluene that was used as solvent is not completely inert when heated at 250 °C, forming a minor amount of new compounds as shown in Table 4-7. According to Table 4-7, when toluene was heated on its own, compounds having a general molecular formula $C_{14}H_{14}$ were detected, while those with a general molecular formula $C_{11}H_{10}$, $C_{14}H_{14}$ and $C_{15}H_{16}$ were detected in the presence of minerals. These compounds consisted of two rings either fused together or connected by a carbon chain of one or two carbon atoms. More compounds appeared when kaolinite was present in the reaction, and the amounts of identified compounds also seemed to be

higher in the case of T+K compared to other reactions. Additionally, no new compounds were identified in the product of self-reaction of pyridine.

4.3.4.3. Analysis of Products from Thermal Conversion of AMS

Compounds formed upon thermally treating AMS are shown in Table 4-8. The major products identified in the reactions of AMS were the AMS dimers ($C_{18}H_{20}$). Based on the cumulative peak areas of the AMS dimers in different reactions containing minerals, it can be said that the mineral solids promoted addition reactions in the system containing AMS at the conditions used in this study. Although AMS heated on its own at 250 °C, in the absence of minerals, still seemed to form a dimer as the major product, the conversion is low (around 0.2%) as indicated in Table 4-5.

Overall, three types of AMS dimers (D_1, D_2, D_3) were formed in this study as shown in Table 4-8, although their true isomeric identity was not confirmed. The fragment at $m/z = 236$ was common in all the three spectra (Figure B. 5 in Appendix B), indicating that they were isomers of AMS dimer. Electron impact fragmentation of D_1 and D_2 liberated C_3-alkylbenzene fragments, evidenced by strong 118 ($C_9H_{10}^+$) and 119 ($C_9H_{11}^+$) m/z signals respectively in the mass spectra. The mass spectrum of D_3 had a different fragmentation pattern and one that did not involve liberation of a C_3-alkylbenzene fragment.

On comparing the cumulative peak areas of the AMS dimers in different reactions containing minerals, it was found that addition of pyridine in the reactions did not result in the formation of as much AMS dimer as the reactions performed without pyridine. Moreover, in the reactions containing minerals, the selectivity for the formation of the dimers seemed to be influenced by the presence or absence of pyridine in the reaction system. For example, the selectivity for the formation of D_1, D_2 and D_3 in the reactions without pyridine (AMS+T+K and AMS+T+I) followed

the order $D_1>D_2$ (D_3 was not detected), whereas in the reactions with pyridine (AMS+T+P+K and AMS+T+P+I) the selectivity was in the order $D_2>D_1>D_3$.

Table 4-8. Compounds Identified in the Products of Thermal Conversion of AMS through GC–MS [a,b,c]

Compound	Chemical Formula	Peak Area [d]											
		AMS+T		AMS+T+ K		AMS+T+ I		AMS+T+ P		AMS+T+ P+K		AMS+T+ P+I	
		x $\times 10^4$	s $\times 10^2$	x $\times 10^4$	s $\times 10^2$	x $\times 10^4$	s $\times 10^2$	x $\times 10^4$	s $\times 10^2$	x $\times 10^4$	s $\times 10^2$	x $\times 10^4$	s $\times 10^2$
Benzene	C_6H_6	3	6	2	7	3	4	1	5	3	6	3	4
Styrene	C_8H_8	5	5	1	3	2	3	7	7	3	6	3	6
Ethyl Benzene	C_8H_{10}	44	3	43	6	43	7	43	5	44	8	43	9
Benzene, (1-methylethyl)- (Cumene)	C_9H_{12}	3	4	41	2	47	6	2	3	5	6	7	6
Butenyl Benzene [e]	$C_{10}H_{12}$	8	7	1	7	0.3	6	6	6	2	4	1	4
2 Carbon Alkylated Diphenyl [f]	$C_{14}H_{14}$	-[g]	-[g]	1	6	7	5	-[g]	-[g]	-[g]	-[g]	-[g]	-[g]
4 Carbon Alkylated Diphenyl	$C_{16}H_{18}$	5	4	2	7	7	8	6	7	4	5	4	5
5 Carbon Alkylated Diphenyl	$C_{17}H_{20}$	3	5	-[g]	-[g]	-[g]	-[g]	-[g]	-[g]	-[g]	-[g]	-[g]	-[g]
AMS Dimer (D1)	$C_{18}H_{20}$	-[g]	-[g]	3790	6	3900	6	-[g]	-[g]	35	6	440	7
AMS Dimer (D2)	$C_{18}H_{20}$	-[g]	-[g]	77	69	41	7	-[g]	-[g]	319	9	713	6
AMS Dimer (D3)	$C_{18}H_{20}$	62	5	-[g]	-[g]	-[g]	-[g]	55	3	26	5	13	6

[a] These compounds should only be seen as an indication of the nature of the products as their true identity has not been confirmed using commercial standards

[b] Reaction Temperature $= 250\ °C$, Reaction Time $= 2$ h

[c] Compounds identified in toluene (Table 4-6) are not listed (except Ethyl Benzene) to avoid duplication of data

Formation of side products such as benzene (C_6H_6), styrene (C_8H_8) and cumene (C_9H_{12}) was also observed in all the reaction products. Among them, the increasing peak areas of cumene in the reactions AMS+T+K and AMS+T+I compared to other reactions stood out, indicating that the solids likely promoted hydrogen disproportionation of AMS. This tendency was suppressed when pyridine was added to the system containing minerals.

Further, two ring aromatics of general formula $C_{16}H_{18}$ and $C_{17}H_{20}$ were also identified in the reactions as shown in Table 4-8.

4.3.4.4. Analysis of Products from Thermal Conversion of 1-Octene

Several compounds were identified in the products of thermal conversion of 1-octene at 250 °C, as shown in Table 4-9. The major products were the $C_{15}H_{24}$ isomers which were alkylated toluene structures. The formation of most of these isomers was favored in the presence of minerals, without the addition of pyridine. Although the octene dimer ($C_{16}H_{32}$) which appeared in the OCT+T reaction was not detected in the reactions containing minerals, higher peak areas of the $C_{15}H_{24}$ compounds provide evidence that minerals used in this study promoted the formation of heavier components by olefin-aromatic alkylation (Friedel-Crafts alkylation).

In addition, it was interesting to identify straight-chain double bond stereoisomers of octene (C_8H_{16}) in the reaction products. Once again, these compounds were more pronounced in the products of OCT+T+K and OCT+T+I reactions than OCT+T, implying that the minerals likely

promoted linear chain double bond isomerization of 1-octene. Moreover, the formation of these compounds seemed to be suppressed by the addition of pyridine (OCT+T+P+K and OCT+T+P+I).

Further, the $C_{14}H_{14}$ and $C_{15}H_{16}$ compounds that were identified in the control reactions with toluene (Table 4-7) also appeared in the products of reactions that consisted of minerals as shown in Table 4-9. These products were hardly formed in the reactions performed in the presence of pyridine.

Table 4-9. Compounds Identified in the Products of Thermal Conversion of 1-Octene through GC–MS [a,b,c]

Compound	Chemical Formula	Peak Area [d]											
		OCT+T		OCT+T+ K		OCT+T+ I		OCT+T+ P		OCT+T+ P+K		OCT+T+ P+I	
		x ×10^4	s ×10^2	x ×10^4	s ×10	x ×10^4	s ×10	x ×10^4	s ×10^2	x ×10^4	s ×10^2	x ×10^4	s ×10^2
Heptane, 3-methylene-[e]	C_8H_{16}	8	6	2	7	3	6	6	5	5	8	5	7
4-Octene (E)	C_8H_{16}	1	6	3	6	7	6	-[g]	-[g]	1	6	-[g]	-[g]
4-Octene (Z)	C_8H_{16}	1	6	5	8	14	8	0.1	3	2	7	4	6
Octane [e]	C_8H_{18}	7	7	6	9	7	6	9	5	7	7	6	3
2-Octene (E)	C_8H_{16}	-[g]	-[g]	1	4	2	10	-[g]	-[g]	-[g]	-[g]	-[g]	-[g]
3-Octene (Z)	C_8H_{16}	-[g]	-[g]	27	8	42	5	-[g]	-[g]	-[g]	-[g]	8	2
2-Octene (Z)	C_8H_{16}	-[g]	-[g]	11	6	21	8	-[g]	-[g]	7	7	12	1
2 Carbon	$C_{14}H_{14}$	-[g]	-[g]	7	6	7	5	-[g]	-[g]	1	6	2	2
Alkylated	$C_{14}H_{14}$	-[g]	-[g]	-[g]	-[g]	5	4	-[g]	-[g]	0.5	6	2	3
Diphenyls [f]	$C_{14}H_{14}$	-[g]	-[g]	-[g]	-[g]	-[g]	-[g]	-[g]	-[g]	0.4	4	1	2
3 Carbon	$C_{15}H_{16}$	-[g]	-[g]	2	3	-[g]	-[g]	-[g]	-[g]	-[g]	-[g]	-[g]	-[g]
Alkylated	$C_{15}H_{16}$	-[g]	-[g]	4	6	-[g]	-[g]	-[g]	-[g]	-[g]	-[g]	-[g]	-[g]
Diphenyls [f]	$C_{15}H_{16}$	-[g]	-[g]	2	7	-[g]	-[g]	-[g]	-[g]	-[g]	-[g]	-[g]	-[g]
	$C_{15}H_{24}$	-[g]	-[g]	1697	11	1079	6	-[g]	-[g]	-[g]	-[g]	-[g]	-[g]
9 Carbon	$C_{15}H_{24}$	-[g]	-[g]	-[g]	-[g]	-[g]	-[g]	1	6	1	6	4	6
Alkylated	$C_{15}H_{24}$	-[g]	-[g]	1271	6	798	7	-[g]	-[g]	-[g]	-[g]	-[g]	-[g]
Benzenes	$C_{15}H_{24}$	-[g]	-[g]	665	5	540	9	-[g]	-[g]	-[g]	-[g]	-[g]	-[g]
	$C_{15}H_{24}$	3	4	34	4	38	7	1	2	18	5	20	2
Hexadecene	$C_{16}H_{32}$	2	5	-[g]	-[g]	-[g]	-[g]	-[g]	-[g]	-[g]	-[g]	-[g]	-[g]

^{a} These compounds should only be seen as an indication of the nature of the products as their true identity has not been confirmed using commercial standards

^{b} Reaction Temperature = 250 °C, Reaction Time = 2 h

^{c} Compounds identified in toluene (Table 4-6) are not listed to avoid duplication of data

^{d} Average (x) and standard deviation (s) of reactions in duplicate

^{e} Present in 1-Octene Chemical (Table 4-6)

^{f} Formed in the control reactions (Table 4-7)

^{g} Not detected

4.3.5. Lewis and Bronsted Acid Sites in the Minerals.

As mentioned earlier, raw solids kaolinite and illite were exposed to pyridine vapors at room temperature to identify the Bronsted acid and Lewis acid complexes formed on the surface of solids. The DRIFTS spectra of kaolinite and illite obtained before and after pyridine adsorption are given in Figure 4-1.

As shown in Figure 4-1, peaks corresponding to the wavenumbers 1550 cm^{-1}, 1450-1455 cm^{-1} and 1489 cm^{-1} which were barely noticeable in the spectra of raw kaolinite and illite, were identified on the pyridine-adsorbed mineral solids. These peaks are generally attributed to the Bronsted acid-bound pyridinium cation (1550 cm^{-1}), Lewis acid-bound pyridine (1450-1455 cm^{-1}) and both the types of species (1489 cm^{-1}),[35] indicating that the minerals used in this study contained both the Bronsted and Lewis acid sites.
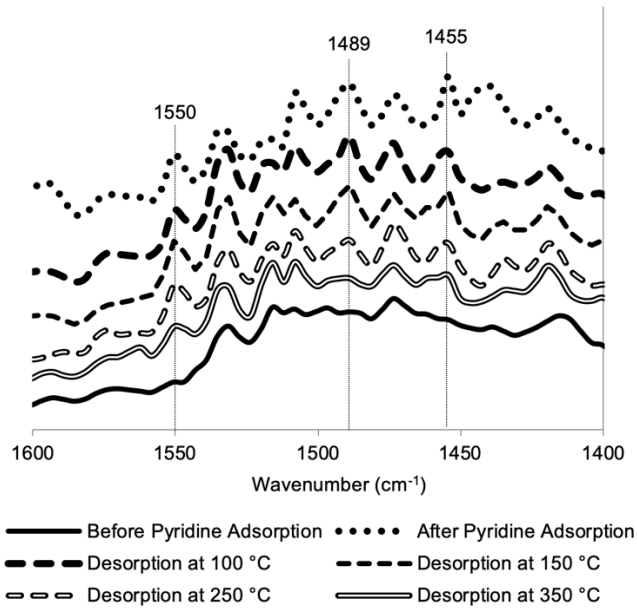
(a)
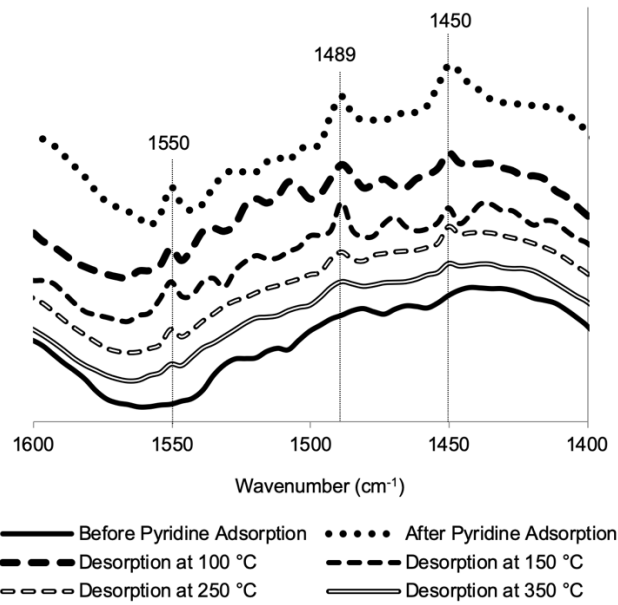
(b)

Figure 4-1. DRIFTS Spectra of (a) Kaolinite (b) Illite Before and After Pyridine Adsorption

Further, the intensity of the peaks decreased as the temperature was raised from 100 °C to 350 °C. Desorption of pyridine from stronger Bronsted and Lewis acid sites occurs at higher temperatures and the final intensities at 350 °C still remained greater than those for the raw minerals, indicating the strength of the acid sites in these minerals.

Quantification of acid sites by Ammonia-Temperature Programmed Desorption analysis in the temperature range 25-400 °C indicated that the total amount of acid sites in the minerals used was about 40 μmol NH_3/g, as indicated in Table B. 1 in Appendix B.

4.4. Discussion

4.4.1. Addition Reaction Chemistry of AMS and 1-Octene

As the primary focus of this work is on the addition reactions, the formation of the major addition products observed in the reactions of AMS and 1-octene are discussed in this section, and plausible explanations for the changes occurring in the presence of mineral solids are given.

The largest molecules detected in the GC-MS analysis in the current study were the AMS dimers ($C_{18}H_{20}$) and 1-octene dimer ($C_{16}H_{32}$), as indicated in Table 4-8 and Table 4-9 respectively. Although one cannot rule out the possibility of heavier products, the absence of trimers that was within the detection capability of the analytical method employed indicates that it is unlikely that heavier products formed.

The characteristics of free radical and/or cation mediated reactions that could perhaps lead to the formation of some of the-addition products identified are explored.

4.4.1.1. Dimerization of AMS.

In the current study, the major products identified in the reactions of AMS were the AMS dimers ($C_{18}H_{20}$). Self-reaction of AMS did not yield significant amounts of AMS dimers, as the overall reaction conversion itself was ~0.2 %. Further, addition of pyridine to the reaction system not containing any minerals (AMS+T+P) did not influence the dimer formation as shown in Table 4-8. These results agree with the literature in which AMS was reported to show weak polymerization when reacted on its own.[29,36]

In the studies of Uzcátegui, et al.[36] and Naghizada, et al.,[11] self-reaction of AMS at 250 ° C did not result in dimers, when performed in the solvents pentane and diphenylether respectively. In some other studies, despite the poor ability of AMS to polymerize, formation of AMS dimers was noted when treated in bulk.[30,37] In the current study, the formation of a minor amount of AMS dimer D_3 in the reaction AMS+T performed in the absence of solids could be explained by a free radical reaction mechanism. The initiation of the radical reaction between toluene and AMS is speculated to occur due to the action of toluene. Benzyl radicals could be formed from toluene upon heating as shown in Eq 4-2., which could in turn initiate the formation of cumyl radicals from AMS as shown in Eq 4-3. These cumyl radicals can further propagate and add to AMS leading to the formation of AMS dimer as shown in Eq 4-4. and Eq 4-5.

$$\text{Toluene } [C_6H_5CH_3] \rightarrow C_6H_5CH_2{}^\bullet + H^\bullet \qquad\qquad \text{Eq 4-2.}$$

$$H^\bullet + \text{AMS } [C_6H_5C(CH_3)=CH_2] \ \rightarrow \ \text{Cumyl Radical } [C_6H_5C(CH_3)_2{}^\bullet] \qquad\qquad \text{Eq 4-3.}$$

$$\text{Cumyl Radical} + \text{AMS} \rightarrow \ C_6H_5C(CH_3)_2CH_2C(CH_3)(C_6H_5)^\bullet \qquad\qquad \text{Eq 4-4.}$$

$$C_6H_5C(CH_3)_2CH_2C(CH_3)(C_6H_5)^\bullet \rightarrow H^\bullet + \text{AMS Dimer } [C_{18}H_{20}] \qquad \text{Eq 4-5.}$$
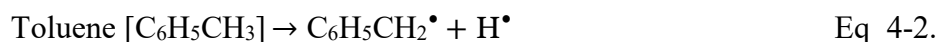
The generation of benzyl radicals from toluene is also supported by Table 4-7, in which toluene when heated on its own at 250 ° C in the absence of solids formed a minor amount of bibenzyl ($C_{14}H_{14}$) type of compounds, which could have occurred through the reactions shown in Eq 4-2. and Eq 4-6. The C-H bond of the methyl group in toluene, whose bond dissociation energy (375.0 $\pm$ 8.4 kJ/mol) is about 100 kJ/mol less than the ring C-H bond ($\sim$ 473.5 kJ/mol) and also less than the C-C bond between the phenyl and methyl groups of toluene ($\sim$ 427 kJ/mol), is the weakest bond in the molecule.[38-41] Upon cleavage of the C-H bond of the methyl group in toluene, a resonance-stabilized benzylic radical is generated as shown in Eq 4-2.

$$2\ C_6H_5CH_2^\bullet \rightarrow C_{14}H_{14} \qquad \text{Eq 4-6.}$$

In literature, mechanisms for self-initiation of monomers like styrene, which readily undergo spontaneous thermal initiation even in the absence of an initiator, are reported.[42] Although AMS does not readily undergo spontaneous thermal polymerization like styrene, self-initiation of AMS through a bimolecular reaction generating monoradicals, as shown in Eq 4-7., could still occur.

$$2\ (C_6H_5)(C_3H_5) \rightarrow\ (C_6H_5)(C_3H_6)^\bullet + (C_6H_5)(C_3H_4)^\bullet \qquad \text{Eq 4-7.}$$
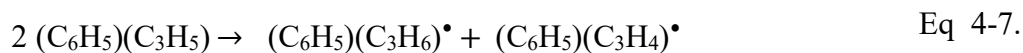
In the current study, formation of AMS dimers was promoted in the presence of both types of mineral solids, as shown by the peak areas of the dimers D_1 and D_2 in Table 4-8. Although the true isomeric identity of the dimers D_1 and D_2 was not confirmed, based on the most probable hits from the MS library search of the spectra, and the literature on mass-fragmentation patterns of AMS dimers, the structures of D_1 and D_2 corresponded to those in Figure 4-2(a) and Figure 4-2(b) respectively.[37] This tentative assignment is congruent with the electron impact fragmentation that

resulted in dominant C_3-alkylbenzene fragments (Figure B. 5 in Appendix B). The sequence of elution of the dimers in the current study was also the same as that noticed in the work by Kauffmann, et al.,[37] for the same properties of the stationary phase. D_3 appears to be a cyclic saturated dimer as shown in Figure 4-2(c). This assignment is also congruent with the electron impact mass spectrum (Figure B. 5).
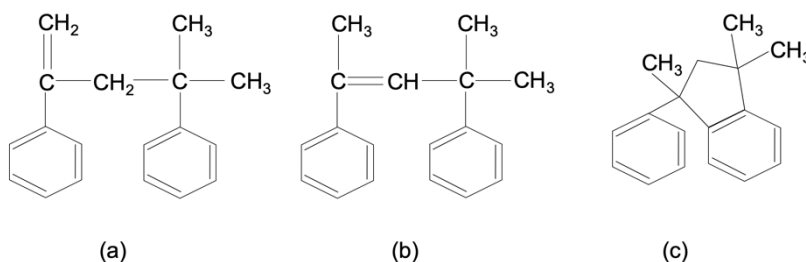
Figure 4-2. Tentative Structures of AMS Dimers (a) D_1 (b) D_2 (c) D_3 in this Study

In literature, both the free radical and cationic addition reaction mechanisms for the formation of saturated and unsaturated dimers were proposed.[28,30,31,37,43,44] These studies were either conducted in the presence of a free radical initiator, or cationic initiators consisting of Bronsted and Lewis acid sites (e.g. ion-exchanged clays). The proposed mechanisms for both cationic and free radical dimerization contain the initiation, propagation and termination steps. For AMS, the most stable primary reactive intermediate (radical or carbocation) formed during initiation would be on the tertiary carbon.

Figure 4-3 depicts the cationic dimerization of AMS to form both unsaturated and cyclic saturated dimers, as reported in literature.[28,31,43,45] A dimeric cation is formed during the propagation step, following which the abstraction of H^+ from the dimeric cation would lead to the termination of the process, resulting in isomeric AMS dimers. In Figure 4-3, the typical linear head-to-tail addition

of AMS units is shown, along with the intramolecular cyclization to form an indane skeleton. Similar mechanisms were reported for the free radical dimerization of AMS.[37,45]

According to literature, the solvent system, the type of initiator and the reaction conditions such as temperature used in the reactions would influence the product selectivity and conversion of AMS dimerization.[27,28,30,36,44,46] For example, cationic polymerization reactions performed in non-polar solvents, similar to toluene in the current study, mostly favored the formation of AMS dimers as opposed to polar solvents. It was said that the polar solvents could reduce the contact between the active sites in clays and the monomer due to preferential adsorption of the polar molecules from the solvent onto the mineral surface, thereby affecting reaction rate and conversion.[27,28] In this study, toluene is not expected to contribute to such a situation. Another common example of the reaction conditions influencing AMS dimerization was the increase in the yield of saturated AMS dimer during cationic polymerization at higher temperatures (>100 ° C).[28,46]
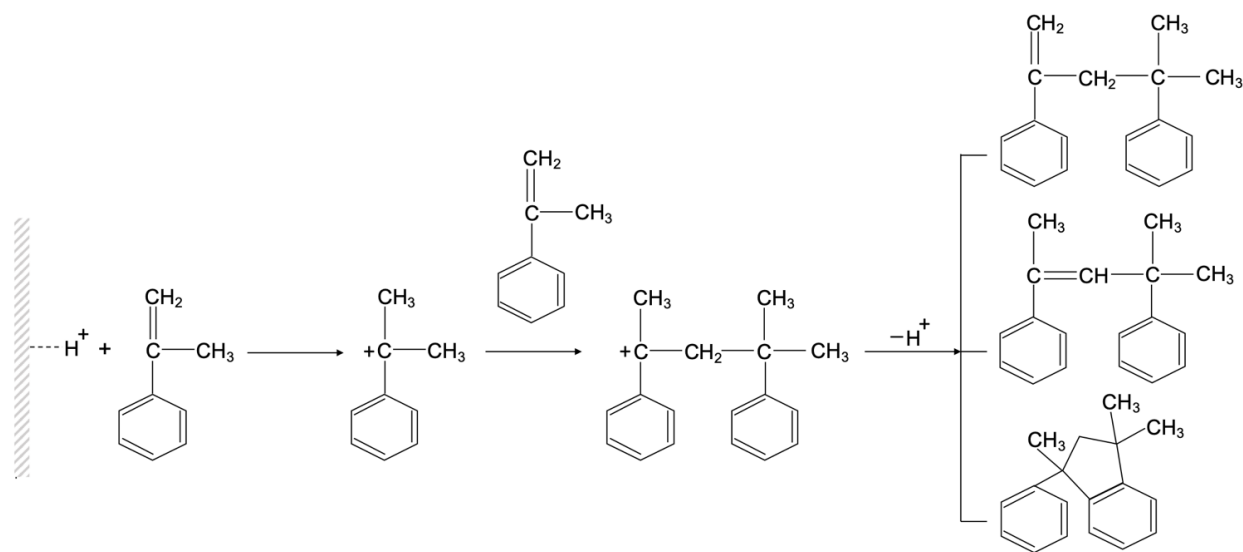
Figure 4-3. Cationic Dimerization of AMS

Despite the similarities between free radical and cationic dimerization of AMS, it was found in the current study that the overall abundance of the AMS dimers (indicated by the cumulative peak areas) decreased upon addition of pyridine for both types of minerals used, as shown in Table 4-8. Addition of pyridine would inhibit cationic addition of AMS by deactivating the acid sites on the mineral surface. Therefore, it appears that cationic addition is the primary reaction pathway leading to the formation of AMS dimers in the presence of the minerals.

On the other hand, D_3 is the product of thermal dimerization and based on the peak areas in Table 4-8, its formation was suppressed in the presence of minerals. Thermal formation of D_3 was also little affected by the addition of pyridine. Therefore, a higher level of radical reactivity doesn't seem to occur in the presence of minerals compared to the absence of minerals. Kauffmann, et al.[37] made a compelling argument that the tricyclic dimers can be produced thermally and by photo-initiation. At the same time, it was indicated in literature that the formation of the tricyclic dimer could be suppressed during cationic dimerization.[28] Thus, it appears that D_1 and D_2 are the bicyclic dimers, whereas D_3 is the tricyclic dimer, as indicated in Figure 4-2.

The tendency for AMS to predominantly homopolymerize via cationic pathway is also supported by literature, in which it is well established that AMS shows weak polymerization phenomena by free radical mechanisms.[37,47] The slow rate and poor yields in the free radical polymerization of AMS in the previous studies were attributed to the low ceiling temperature (61 °C) of AMS, above which depropagation (release of the monomer) would become more pronounced.[37,44,47] Hence, homopolymerization of AMS is usually carried out through ionic polymerization.[47]

Further, in Table 4-8, comparison of the peak areas of D_1 and D_2 in the reactions containing the same type of mineral (kaolinite or illite) indicates that addition of pyridine influenced the dimer

selectivity. Suppression of D_1 relative to D_2 upon addition of pyridine could suggest that the acid-catalyzed double bond isomerization of D_2 to D_1, originally promoted by the acid sites in solids in the reactions AMS+T+K and AMS+T+I, was suppressed by the addition of pyridine.

Because of the selectivity profile of D_1-D_3 in the AMS dimerization and the suppression by pyridine, it can be concluded that free radical addition took place only to a minor extent compared to cationic addition in the presence of minerals.

4.4.1.2. Formation of 9-Carbon Alkylated Benzenes from 1-Octene.

The 9-carbon alkylated benzenes ($C_{15}H_{24}$) were the major products formed during the conversion of 1-octene in toluene at 250 °C as shown in Table 4-9. These compounds are most likely the products of reaction between 1-octene and toluene.

In the reaction OCT+T, the free radical pathway to the formation of 9-carbon alkylated benzenes must proceed by the addition of the benzylic radical (Eq 4-2.) to the double bond in octene, or by combination of the benzylic and octyl free radicals. In the addition reaction between the benzylic radical and octene, a secondary radical intermediate like $(C_6H_5)(CH_2-CH_2-CH^\bullet(C_6H_{13}))$ would form, which is less stable compared to a benzylic radical. Due to the stability of the benzylic radical, the free radical mechanisms for the formation of octyl toluene, that are mentioned above, would mostly not be favored which is likely the reason why the thermal formation of 9-Carbon Alkylated Benzenes was low, as shown in Table 4-9.

The 9-carbon alkylated benzenes increased in significant amounts when both types of minerals used in this study were present in the reactions, and the formation of a majority of these alkylated benzenes was suppressed upon addition of pyridine to the reaction system as shown in Table 4-9.

These changes are also reflected in the overall conversion of 1-octene in the reactions (Table 4-5), where the conversion increased significantly in the presence of minerals compared to the reactions performed in their absence, and a significant drop in the conversion was noticed upon addition of pyridine in the reactions. These observations indicate that minerals likely promoted cationic addition of 1-octene to toluene (alkylation) resulting in higher molecular weight compounds, which was likely suppressed due to the interaction between pyridine and the acid sites in minerals.

Friedel-Crafts-type alkylation reactions between olefins and aromatic compounds such as benzene and toluene in the presence of an acid catalyst are widely reported in literature.[48-57] Such reactions have been reported to generate isomers of alkylated aromatics, as well as polyalkylated aromatic compounds.[48,52,53] These alkylations are usually carried out in the presence of mineral acids such as H_2SO_4, HF, and H_3PO_4, Lewis acids such as $AlCl_3$ and BF_3, or solid acids such as zeolites, clays, and sulfonic ion-exchange resins.[47,48,54]

In the current study, different isomers of the 9-carbon alkylated benzenes ($C_{15}H_{24}$) seemed to form. Lachter, et al.[49] explained the formation of ortho, para and meta variants of 2-, 3-, 4- octyl-toluene isomers ($C_{15}H_{24}$) in the reaction of toluene with 1-octene using a carbocation mechanism. In the presence of acid sites, addition of a secondary carbocation formed from 1-octene and possible migration along the chain by hydride shift, can generate 2-, 3-, 4- octyl-toluene compounds as shown in Figure 4-4.[49] As linear double bond isomers of octene were also identified in the reactions of the current study (discussed in more detail in Section 4.2.2.), they could combine with toluene to result in such $C_{15}H_{24}$ isomers. Further, methyl shift in the olefin structure could result in a more stable tertiary carbocation, causing different branched isomers of $C_{15}H_{24}$ to form. Table 4-9

showed little evidence of skeletal isomerization of octenes. It is therefore unlikely that the $C_{15}H_{24}$ isomers formed contained branched alkyl chains.

In addition to monoalkylated aromatic compounds, polyalkylated aromatic compounds were also identified in some studies. For instance, the formation of mono-, di- and tri- alkylated benzenes upon reaction of benzene with 1-hexene in the presence of acidic ion exchange resins was reported in literature.[48] There are two competing phenomena that affects the likelihood of further alkylation. The addition of an electron donating alkyl group to an aromatic ring could activate the ring for further alkylation compared to the unalkylated ring. Steric crowding due to alkylation makes it more difficult for the alkylated aromatic to interact with alkyl carbocations for further alkylation. In the current study, however, dialkylated or trialkylated variants of octyl toluene were not detected.
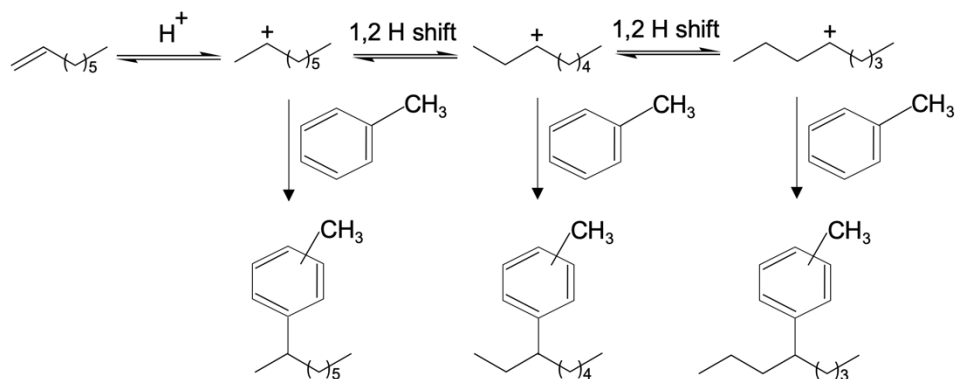
Figure 4-4. Alkylation of Toluene with 1-Octene in the Presence of Acid Catalyst. Reprinted from Ref.49. Copyright (2000), with permission from Elsevier.

4.4.2. Side Reactions of AMS and 1-Octene

In this section, formation of some of the side products observed in the reactions of AMS and 1-octene are discussed, and plausible explanations for the changes occurring in the presence of

mineral solids are given. The characteristics of free radical and/or cation mediated reactions that could perhaps lead to some of these changes are explored.

4.4.2.1. Hydrogen Transfer Reactions to form Cumene from AMS.

In the current study, cumene was identified in the products of AMS conversion. As cumene was not identified in any of the reactants used (Table 4-6), it would indicate that cumene was formed during the reactions. Treatment of AMS in toluene at 250 ° C (AMS+T) at the conditions used in this study resulted in the formation of a small amount of cumene, as shown in Table 4-8, even though no cumene was detected in the study by Uzcátegui, et al.[36] where AMS was treated at 250 ° C in pentane. A possible reason for this is the generation of cumyl radicals (Eq 4-3.) in the presence of toluene, ultimately leading to the formation of cumene.

In the presence of minerals, the concentration of cumene increased for the reactions AMS+T+K and AMS+T+I as shown in Table 4-8. In the previous studies, both cumene and AMS dimers were formed from AMS similar to what was observed in the current study, when AMS was treated with free radical sources at temperatures above 200 ° C.[11,36] The selectivity to form cumene varied with the reaction conditions such as temperature, reaction time and the ratio of free radical source to AMS in the reaction mixture, and steric effects.[11] In these studies, formation of cumene was explained by free radical mechanisms that involved hydrogen transfer. Hydrogen disproportionation of cumyl radicals can result in the formation of cumene.

In the current study, however, the acidic properties of the solids seem to be primarily responsible for the cumene formation in the presence of minerals. Even though the concentration of cumene increased in the presence of minerals for the reactions AMS+T+K and AMS+T+I, a similar increase was not observed in the reactions AMS+T+P+K and AMS+T+P+I, containing pyridine.

These results indicate that a cationic mechanism might be dominating the conversion of AMS to cumene over the free radical pathway in the presence of mineral solids.

In literature, there is evidence that hydrogen transfer of olefins could occur in the presence of acid catalysts.[58-60] Mayr, et al.[59] proposed reaction schemes for hydride transfer processes between carbocations and unsaturated hydrocarbons. It was said that during propagation, the addition of a carbocation to the double bond of an unsaturated compound is often accompanied by a hydrogen transfer reaction, as shown in Figure 4-5. The stability of the carbocation intermediates formed in both the reactions is expected to influence the competition between them. However, in the current study, the exact cationic surface reaction mechanism for the formation of cumene from AMS is not clear.
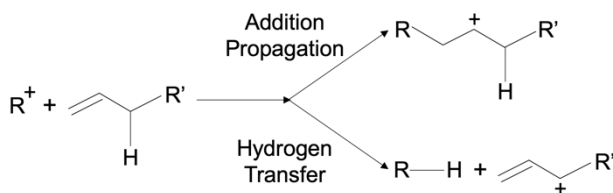
Figure 4-5. Addition Propagation vs. Hydrogen Abstraction during Carbocation Reactions with Olefins. Reproduced from Ref.59. Copyright [2002] American Chemical Society.

4.4.2.2. Linear Double Bond Isomerization of Octene.

While alkylated benzene compounds ($C_{15}H_{24}$) were the major products formed in the thermal treatment of 1-octene in toluene, double bond isomers of *n*-octene were identified as the side products, as indicated in Table 4-9.

Comparing the peak areas in Table 4-9, the reaction OCT+T resulted in minor amounts of fewer number of *n*-octene isomers, whereas the clay minerals appeared to promote the linear double bond

isomeration of octene in the reactions OCT+T+K and OCT+T+I. These reactions, performed in the presence of minerals, resulted in higher number of *n*-octene isomers of higher concentration compared to other reactions of 1-octene. In the presence of pyridine (OCT+T+P+K and OCT+T+P+I reactions), the *n*-octene isomers were lower in amounts than the reactions of the corresponding mineral type performed without pyridine (OCT+T+K and OCT+T+I). Therefore, cationic isomerization promoted by the acidity of the mineral solids appears to be the primary reaction pathway leading to linear double bond isomerization of octene at 250 °C.

In literature, the double bond isomerization of C_4+ olefins, catalyzed by Bronsted and Lewis acid sites, has been reported.[34,61-65]. Figure 4-6 shows the linear double bond isomerization of octene in the presence of Bronsted acid sites. In clays, the hydroxyl groups in specific sites in the lattice structure, or at the crystal edges could act as Bronsted acid sites and dissociate into reactive protons. [25,26] In Figure 4-6, it is shown how the position of the carbocation changes through a hydride shift.
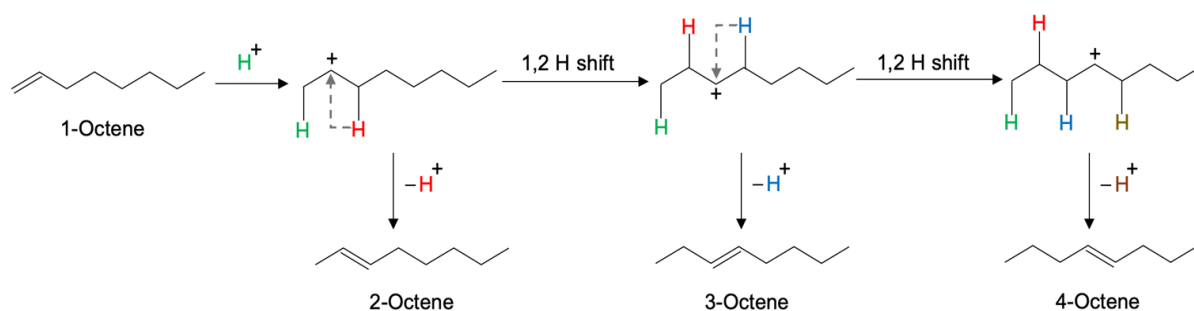
Figure 4-6. Linear Double Bond Isomerization of *n*-Octene Catalyzed by Bronsted Acidity

Double bond migration of olefins was also reported to occur on different Lewis acid catalysts.[63,64] The reaction mechanisms for double bond isomerization on the Lewis acid sites of the clay minerals proceed through a coordinatively unsaturated intermediate, but the intermediate is formed

differently. Figure 4-7 illustrates how a coordinatively unsaturated intermediate is formed leading to positional isomerization of the double bond through coordination with the aluminium species. The coordinatively unsaturated aluminium sites act as Lewis acid sites in a clay mineral and facilitate 1,3 hydride shift of the allylic hydrogen. Some researchers also suggested hydrogen addition-abstraction and 'hydrogen switch' mechanisms in which double bond migration occurred through simultaneous addition of a hydrogen furnished by the silica-alumina catalyst and release of hydrogen from another carbon, yielding an isomer.[64, 66]
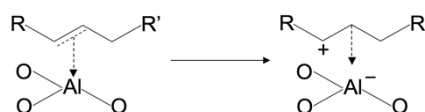
Figure 4-7. Formation of Coordinatively Unsaturated Intermediate from Olefins by Lewis

Acid Sites (For Simplicity the Bonding is Shown as Localized)

In this study, stereoisomers (E and Z configurations) of n-octene were formed. At the experimental conditions used in the current study, the selectivity to Z isomers exceeded the selectivity to E isomers, as indicated by the peak areas in Table 4-9. According to literature, generation of Z-isomers is less thermodynamically favorable compared to the generation of E-isomers, as the Z-alkenes are usually less stable than the E-alkenes.[67] Many catalysts do not offer significant control over stereoselectivity in alkene isomerization, giving E/Z ratios of isomers in the range of 2 to 5.[67] The higher Z-isomer selectivity during double bond isomerization suggests that the surface intermediate is subject to constraints that favor the Z-isomers over the E-isomers, instead of a 'free' carbocation as suggested by Figure 4-6.

Reactions such as oligomerization, alkylation and cracking compete with isomerization, and the reaction selectivity is said to depend on the reaction temperature and strength of acid sites on the

catalyst surface.[34,48,57,62,63] For example, oligomerization is slow on weak acid sites and is favored at higher temperatures compared to isomerization reactions.[34,62] On the other hand, it was found in literature that double bond migration could still occur on higher number of weak acid sites.[34,62,63]

In this work, formation of alkylated toluene products was favored over isomerization of octene (Table 4-9). In addition to the above factors mentioned, the aromatic to olefin molar ratio is another possible factor for higher selectivity towards alkylation over other side reactions. In a study reporting increased selectivity for toluene alkylation with 1-hexene over the double bond isomerization and dimerization products, the behavior was attributed to the usage of higher toluene to 1-hexene molar ratio.[48] In industry, an aromatic to alkene molar ratio of 6 to 8 is typically used for alkylation to reduce side reactions such as isomerization and oligomerization of alkenes.[48] In the current study, the toluene to 1-octene molar ratio used was ~6.1 which probably contributed to increased selectivity for the octyl-toluene products compared to the 1-octene isomers.

Skeletal isomerization could occur through methyl or alkyl group shift instead of the hydride shift to give branching. It is reported in literature that skeletal isomerization of C_5+ *n*-olefins is easier compared to the lighter ones, because the reaction could proceed through the formation of a more stable secondary carbocation via a protonated cyclopropane intermediate compared to the formation of a less stable primary carbocation in the case of C_4 olefins.[34,68] However, Table 4-9 showed little evidence of skeletal isomerization of octenes.

Additionally, in literature, cracking of C_7+ olefins was said to be facile compared to C_6 and lighter olefins, and cracking of 1-octene occurred at temperatures greater than 200 °C over a solid acid catalyst.[34] Further, the cracking propensity was said to increase due to increase in branching through skeletal isomerization.[34] However, no cracking products in the range C_{2-7} were identified

in the present study. The reasons for observing little skeletal isomers and oligomers, and no evidence of cracking products of octene in the reactions conducted in the current study are not clear. They might be related to the characteristics of the acid sites in the minerals used in this study, Bronsted acid strength in particular, as well as the reaction conditions.

Considering the role of a free radical pathway in the reactions of 1-octene discussed above, the poor reactivity of 1-octene through free radical mechanisms was attributed to the allylic degradative chain transfer in α-olefins in literature.[69] This type of autoinhibition reaction in 1-octene would result in the formation of octane and a stable radical (Eq 4-8.). However, there is unambiguous experimental support for this reaction in this study, as octane was present as an impurity in the 1-octene chemical used in the reactions (Table 4-6), and its peak area in the reaction products did not indicate an increase in its concentration upon reaction.

$$CH_3CH^{\bullet}(C_6H_{13}) + CH_2=CH(C_6H_{13}) \rightarrow$$

$$CH_3CH_2(C_6H_{13}) + CH_2=CH(CH)^{\bullet}(C_5H_{11})$$

Eq 4-8.
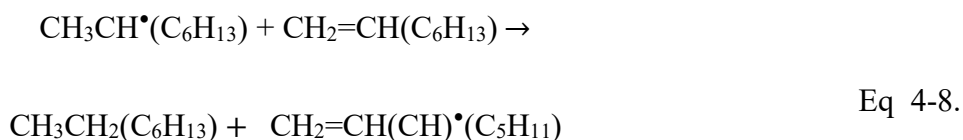
4.4.3. Implications for Hydrothermal Froth Treatment

The current study provides evidence that clay minerals in the bitumen froth are capable of promoting heavier material formation through acid-catalyzed addition reactions. This behavior could be relevant to the thermal treatment of bitumen froth (called hydrothermal treatment), during which the clay minerals could interact with the organic species in bitumen, promoting addition reactions in the froth.

Minerals in bitumen froth experience an alkaline environment,[3] that can be related to the experiments with organic-mineral mixtures in the presence of pyridine in the current study. Water

molecules may also compete with the organic compounds for the acid sites on mineral surfaces,[19] that are responsible for cationic addition. Even in the presence of pyridine, some conversion of the probe molecules to addition products through dimerization and aromatic alkylation were noticed in the present study, suggesting that the clay minerals could still promote heavier material formation at the alkaline conditions of the froth during hydrothermal froth treatment. In this study, the results of AMS dimerization indicated that clay minerals primarily promoted cationic addition reactions at alkaline conditions. However, no clear evidence was found to support the claim that the minerals could promote free radical addition reactions during hydrothermal froth treatment.

Increase in the amounts of heavier compounds could be one of the reasons for the increase in the viscosity of bitumen during hydrothermal treatment of bitumen froth at 250 °C observed in a previous study.[3] Therefore, if any of the potential benefits of this process are to be realized, it would be necessary to operate the hydrothermal froth treatment process at temperatures higher than 250 °C. In terms of engineering application, to achieve a temperature higher than 250 °C, a furnace would be required.

Besides addition reactions, the current study also indicates the possible occurrence of other types of reactions, such as isomerization and transfer hydrogenation, that could be promoted by the clay minerals during hydrothermal froth treatment.

The current study was limited to kaolinite and illite minerals and the role of other types of minerals present in bitumen froth in the chemistry of the thermal conversion of bitumen froth is still left to be investigated. The impact of persistent free radical in bitumen, which may affect the relative contribution of carbocation versus free radical chemistry was also not explored in this study.

4.5. Conclusions

The objective of this work was to understand the nature of the reactions (cationic vs. free radical) promoted by the solids in bitumen froth that potentially lead to heavier material formation during hydrothermal forth treatment at 250 °C. α-Methylstyrene (AMS) and 1-octene instead of bitumen froth were used as probe molecules to conduct this investigation, and their thermal conversion in the presence of clay minerals kaolinite and illite was studied.

The following conclusions were drawn based on the product analysis:

(a) When comparing reactions performed in the presence and absence of minerals (koalinite and illite), the presence of minerals caused an increase in the conversion of AMS from 0.2 % to 88 %, and an increase in the conversion of 1-octene from 4.8 % to 61-71 %. The overall contribution of thermal conversion was therefore minor compared to that of mineral related conversion.

(b) The mineral related conversion was predominantly cationic in nature. This was concluded following on the demonstrated suppression of mineral related conversion by pyridine, as well as the nature of some reaction products that enabled differentiation between free radical and cationic reaction pathways. The selectivity to different AMS dimers, double bond isomers of 1-octene, and isomers of 1-octene and toluene (used as solvent) alkylation were useful reactions for distinguishing between radical and cationic pathways.

(c) Experiments in the presence of minerals and pyridine were employed as surrogates for alkaline bitumen froth. Although the model reactions did not account for the complexity of bitumen froth, the present investigation nevertheless showed that cationic addition could take place at 250 °C. In the presence of minerals, even under alkaline conditions, cationic addition was the dominant reaction pathway.

4.6. References

(1) Rao, F.; Liu, Q. Froth Treatment in Athabasca Oil Sands Bitumen Recovery Process: A Review. *Energy Fuels* **2013**, *27* (12), 7199–7207.

(2) Van Der Merwe, S; Hann, T. Process for Integration of Paraffinic Froth Treatment Hub and a Bitumen Ore Mining and Extraction Facility. U.S. Patent 9,546,323, January 17, 2017.

(3) Turuga, A. S. S.; De Klerk, A. Hydrothermal Treatment of Bitumen Froth: Impact of Mineral Solids and Water on Bitumen Properties. *Energy Fuels* **2021**, *35*, 17536–17550.

(4) Chen, Q.; Stricek, I.; Cao, M.; Gray, M. R.; Liu, Q. Influence of Hydrothermal Treatment on Filterability of Fine Solids in Bitumen Froth. *Fuel* **2016**, *180*, 314–323.

(5) Zhao, J.; Liu, Q.; Gray, M. R. Characterization of Fine Solids in Athabasca Bitumen Froth Before and After Hydrothermal Treatment. *Energy Fuels* **2016**, *30* (3), 1965–1971.

(6) Sankey, B. M.; Maa, P. S.; Bearden, R., Jr. Conversion of the Organic Component from Tar Sands to Lower Boiling Products. U.S. Patent 5,795,464, August 18, 1998.

(7) Yañez Jaramillo, L. M.; De Klerk, A. Partial Upgrading of Bitumen by Thermal Conversion at 150–300° C. *Energy Fuels* **2018**, *32* (3), 3299–3311.

(8) Qu, X.; Li, Y.; Li, S.; Wang, J.; Xu, H.; Li, Z. Thermal Cracking, Aquathermolysis, and their Upgrading Effects of Mackay River Oil Sand. *J. Petrol. Sci. Eng.* **2021**, *201*, 108473.

(9) Gray, M. R. *Upgrading Oilsands Bitumen and Heavy Oil*; Pica Pica Press: Edmonton, Canada, 2015; pp 72–78.

(10) Tannous, J. H.; De Klerk, A. Quantification of the Free Radical Content of Oilsands Bitumen Fractions. *Energy Fuels* **2019**, *33* (8), 7083–7093.

(11) Naghizada, N.; Prado, G. H. C.; De Klerk, A. Uncatalyzed Hydrogen Transfer during 100–250 °C Conversion of Asphaltenes. *Energy Fuels* **2017**, *31* (7), 6800–6811.

(12) Alili, A.S.; Siddiquee, M. N.; De Klerk, A. Origin of Free Radical Persistence in Asphaltenes: Cage Effect and Steric Protection. *Energy Fuels* **2020**, *34* (1), 348–359.

(13) Gryglewicz, G.; Wilk, P.; Yperman, J.; Franco, D.V.; Maes, I. I.; Mullens, J.; Van Poucke, L. C. Interaction of the Organic Matrix with Pyrite during Pyrolysis of a High-Sulfur Bituminous Coal. *Fuel* **1996**, *75* (13), 1499–1504.

(14) Lambert, J. M.; Simkovich, G.; Walker, P. L. The Kinetics and Mechanism of the Pyrite-to-Pyrrhotite Transformation. *Metall. Mater. Trans. B* **1998**, *29* (2), 385–396.

(15) Ringdalen, E. Changes in Quartz During Heating and the Possible Effects on Si Production. *JOM* **2015**, *67* (2), 484–492.

(16) Insley, H.; Ewell, R. H. Thermal Behavior of the Kaolin Minerals. *J. Res. Natl. Bur. Stand.* **1935**, *14* (5), 615–627.

(17) Dubrawski, J. V. Thermal Decomposition of Some Siderite-Magnesite Minerals using DSC. *J. Therm. Anal. Calorim.* **1991**, *37* (6), 1213–1221.

(18) Rat'ko, A. I.; Ivanets, A. I.; Kulak, A. I.; Morozov, E. A.; Sakhar, I. O. Thermal Decomposition of Natural Dolomite. *Inorg. Mater.* **2011**, *47* (12), 1372–1377.

(19) Solomon, D. H. Clay Minerals as Electron Acceptors and/or Electron Donors in Organic Reactions. *Clays Clay Miner.* **1968**, *16* (1), 31–39.

(20) Worasith, N.; Ninlaphurk, S.; Mungpayaban, H.; Wen, D.; Goodman, B. A. Characterization of Paramagnetic Centres in Clay Minerals and Free Radical Surface Reactions by EPR Spectroscopy. In *Clays and Clay Minerals: Geological Origin, Mechanical Properties and Industrial Applications*, Wesley, L. R.; Eds.; Nova Science Publ.: New York, NY, 2014; pp 336–359

(21) Hoving, A. L.; Sander, M.; Bruggeman, C.; Behrends, T. Redox Properties of Clay-Rich Sediments as Assessed by Mediated Electrochemical Analysis: Separating Pyrite, Siderite and Structural Fe in Clay Minerals. *Chem. Geol.* **2017**, *457*, 149–161.

(22) Gorski, C. A.; Aeschbacher, M.; Soltermann, D.; Voegelin, A.; Baeyens, B.; Marques Fernandes, M.; Hofstetter, T. B.; Sander, M. Redox Properties of Structural Fe in Clay Minerals. 1. Electrochemical Quantification of Electron-Donating and -Accepting Capacities of Smectites. *Environ. Sci. Technol.* **2012**, *46* (17), 9360–9368.

(23) Pentráková, L.; Su, K.; Pentrák., M.; Stucki, J. W. A Review of Microbial Redox Interactions with Structural Fe in Clay Minerals. *Clay Miner.* **2013**, *48* (3), 543–560.

(24) Nwosu, U. G.; Roy, A.; Dela Cruz, A. L. N.; Dellinger, B.; Cook, R. Formation of Environmentally Persistent Free Radical (EPFR) in Iron (III) Cation-Exchanged Smectite Clay. *Environ. Sci.: Processes Impacts* **2016**, *18* (1), 42–50.

(25) Nagendrappa, G. Organic Synthesis Using Clay Catalysts. *Reson.* **2002**, *7* (1), 64–77.

(26) Soma, Y.; Soma, M. Chemical Reactions of Organic Compounds on Clay Surfaces. *Environ. Health Perspect.* **1989**, *83*, 205–214.

(27) Moulkheir, A.; Harrane, A.; Belbachir, M. Maghnite-H$^+$, a Solid Catalyst for the Cationic Polymerization of α-Methylstyrene. *J. Appl. Polym. Sci.* **2008**, *109* (3), 1476–1479.

(28) Chaudhuri, B.; Sharma, M. M. Some Novel Aspects of Dimerization of α-Methylstyrene with Acidic Ion-Exchange Resins, Clays and Other Acidic Materials as Catalysts. *Ind. Eng. Chem. Res.* **1989**, *28* (12), 1757–1763.

(29) Hersberger, A. B.; Reid, J. C.; Heiligmann, R. G. Polymerization of Alpha-Methylstyrene. *Ind. Eng. Chem*. **1945**, *37* (11), 1073–1078.

(30) Lin, S. Y.; Tseng, J. M.; Lin, Y. F.; Huang, W. T.; Shu, C. M. Comparison of Thermal Polymerization Mechanisms for α-Methylstyrene and Trans-β-Methylstyrene. *J. Therm. Anal. Calorim.* **2008**, *93* (1), 257 267.

(31) Ayat, M.; Bensaada, N.; Belbachir, M.; Harrane, A.; Meghabar, R. Synthesis and Characterization of Poly (α-Methylstyrene) by Cationic Polymerization Using a New Solid Ecological Catalyst. *Orient. J. Chem.* **2015**, *31*, 2115–2123.

(32) Andrekanic, R. A.; Salek, J. S.; Mulhall, S. E.; Bubnov, Y. V. Polymerization of Alpha Methylstyrene. U.S. Patent 6,649,716, November 18, 2003.

(33) Bringué, R.; Cadenas, M.; Fité, C.; Iborra, M.; Cunill, F. Study of the Oligomerization of 1-Octene Catalyzed by Macroreticular Ion-Exchange Resins. *Chem. Eng. J.* **2012**, *207*, 226–234.

(34) De Klerk, A. Oligomerization of 1-Hexene and 1-Octene Over Solid Acid Catalysts. *Ind. Eng. Chem. Res.* **2005**, *44* (11), 3887–3893.

(35) Brown, D. R.; Rhodes, C. N. Brønsted and Lewis Acid Catalysis with Ion-Exchanged Clays. *Catal. Lett.* **1997**, *45* (1), 35–40.

(36) Uzcátegui, G.; Fong, S. Y.; De Klerk, A. Cracked Naphtha Reactivity: Effect of Free Radical Reactions. *Energy Fuels* **2018**, *32* (5), 5812–5823.

(37) Kauffmann, H. F.; Harms, H.; Olaj, O. F. Ground-State Dynamics of α-Methylstyrene. I. Thermally Induced Oligomerization in Bulk. *J. Polym. Sci., Polym. Chem. Ed.* **1982**, *20* (10), 2943–2967.

(38) Luo, Y. R. *Handbook of Bond Dissociation Energies in Organic Compounds*; CRC Press: Boca Raton, FL, 2003; p 31.

(39) Tian, M.; McCormick, R. L.; Luecke, J.; De Jong, E.; Van Der Waal, J. C.; Van Klink, G. P. M.; Boot, M. D. Anti-Knock Quality of Sugar Derived Levulinic Esters and Cyclic Ethers. *Fuel* **2017**, *202*, 414–425.

(40) Nam, P. C.; Nguyen, M. T.; Chandra, A. K. The C−H and α(C− X) Bond Dissociation Enthalpies of Toluene, C_6H_5-CH_2X (X= F, Cl), and Their Substituted Derivatives: A DFT Study. *J. Phys. Chem. A* **2005**, *109* (45), 10342–10347.

(41) Genco, J. I.; Duke, F. R.; Griffel, M.; Jennings, L. D. *The (C-H) Bond Dissociation Energy in the Methyl Group of Toluene;* Technical Report Number ISC-746; U.S. Atomic Energy Commission, Technical Information, March 1956.

(42) Elroy, I. Polymerization of Alpha-Methylstyrene at High Pressures. Ph.D. Dissertation, Imperial College London, UK, 1961.

(43) Zhao, X. A Kinetic Study of the Hydrogenation and Dimerization of Styrene and α-Methylstyrene on Ni-Mo-S Catalyst. M.S. Thesis, The University of British Columbia, Vancouver, Canada, 2015.

(44) Mehta B. J. Synthesis and Analysis of Dimers of Alpha-Methylstyrene. M.A. Thesis, Western Michigan University, Kalamazoo, MI, 1975.

(45) Gridnev, A. A. Kinetics of Alpha-Methylstyrene Oligomerization by Catalytic Chain Transfer. *J. Polym. Sci., Part A: Polym. Chem.* **2002**, *40* (9), 1366–1376.

(46) Rustamov, M. I.; Seidov, N. M.; Ibragimov, K. D.; Mamedbeili, E. G. Dimerization of α-Methylstyrene in the Presence of Mordenite, Aimed at Preparation of Transformer Oils. *Russ. J. Appl. Chem.* **2009**, *82* (2), 317–322.

(47) Jozaghkar, M. R.; Ziaee, F.; Azar, A. S. Investigation of Poly (α-Methyl Styrene) Tacticity Synthesized by Photo-Polymerization. *Polym. Bull.* **2021**, *78* (9), 5303–5314.

(48) Cadenas, M.; Bringué, R.; Fité, C.; Iborra, M.; Ramírez, E.; Cunill, F. Alkylation of Toluene with 1-Hexene Over Macroreticular Ion-Exchange Resins. *Appl. Catal., A* **2014**, *485*, 143–148.

(49) Lachter, E. R.; San Gil, R. A. D. S.; Tabak, D.; Costa, V. G.; Chaves, C. P. S.; Dos Santos, J. A. Alkylation of Toluene with Aliphatic Alcohols and 1-Octene Catalyzed by Cation-Exchange Resins. *React. Funct. Polym.* **2000**, *44* (1), 1–7.

(50) Liu, Y.; Xu, L.; Xu, B.; Li, Z.; Jia, L.; Guo, W. Toluene Alkylation with 1-Octene Over Supported Heteropoly Acids on MCM-41 Catalysts. *J. Mol. Catal. A: Chem.* **2009**, *297* (2), 86–92.

(51) Pu, X.; Liu, N. W.; Jiang, Z. H.; Shi, L. Acidic and Catalytic Properties of Modified Clay for Removing Trace Olefin from Aromatics and Its Industrial Test. *Ind. Eng. Chem. Res.* **2012**, *51* (43), 13891–13896.

(52) McCaulay, D. A.; Lien, A. P. Effect of Acid Strength on Alkylation of Arenes with Olefins. I. *m*-Xylene with Ethylene. *J. Am. Chem. Soc.* **1955**, *77* (7), 1803–1804.

(53) Hojabri, F. Gas-Phase Catalytic Alkylation of Aromatic Hydrocarbons. *J. Appl. Chem. Biotechnol.* **1971**, *21* (3), 87–89.

(54) Török, B.; Schäfer, C.; Kokel, A. Friedel-Crafts and Related Reactions Catalyzed by Solid Acids. *Heterogeneous Catalysis in Sustainable Synthesis*; Elsevier: Amsterdam, Netherlands, 2021; pp 317–378.

(55) Guo, Y.; Du, X.; Liu, L.; Dong, Y.; Lei, Z. Reaction Mechanism of Benzene Alkylation with Propylene Catalyzed by HZSM-5 Zeolite and H-Beta Zeolite. *Mater. Today Commun.* **2021**, *26*, 101757.

(56) Geatti, A.; Lenarda, M.; Storaro, L.; Ganzerla, R.; Perissinotto, M. Solid Acid Catalysts from Clays: Cumene Synthesis by Benzene Alkylation with Propene Catalyzed by Cation Exchanged Aluminum Pillared Clays. *J. Mol. Catal. A: Chem.* **1997**, *121* (1), 111–118.

(57) Sadovnikov, A. A.; Arapova, O. V.; Russo, V.; Maximov, A. L.; Murzin, D. Y.; Naranov, E. R. Synergy of Acidity and Morphology of Micro-/Mesoporous Materials in the Solid-Acid Alkylation of Toluene with 1-Decene. *Ind. Eng. Chem. Res.* **2022**, *61* (5), 1994–2009.

(58) Kubokawa, Y. Desorption of Olefins from Silica—Alumina Catalysts. *J. Phys. Chem.* **1965**, *69* (8), 2676–2679.

(59) Mayr, H.; Lang, G.; Ofial, A. R. Reactions of Carbocations with Unsaturated Hydrocarbons: Electrophilic Alkylation or Hydride Abstraction? *J. Am. Chem. Soc.* **2002**, *124* (15), 4076–4083.

(60) Müller, S.; Liu, Y.; Kirchberger, F. M.; Tonigold, M.; Sanchez-Sanchez, M.; Lercher, J. A. Hydrogen Transfer Pathways during Zeolite Catalyzed Methanol Conversion to Hydrocarbons. *J. Am. Chem. Soc.* **2016**, *138* (49), 15994–16003.

(61) Bruno, J. E. Double-Bond Isomerization of Long Chain Olefins. M.S. Thesis, Louisiana State University and Agricultural and Mechanical College, Baton Rouge, LA, 2012.

(62) Bruno, J. E.; Dooley, K. M. Double-Bond Isomerization of Hexadecenes with Solid Acid Catalysts. *Appl. Catal., A* **2015**, *497*, 176–183.

(3) Park, Y. K.; Kim, S. J.; You, N.; Cho, J.; Lee, S. J.; Lee, J. H.; Jeon, J. K. MoO$_3$/SiO$_2$ Catalysts for Double Bond Migration of 2-Butene. *J. Ind. Eng. Chem.* **2011**, *17* (2), 186–190.

(64) Yi, F.; Cao, J. P.; Xu, D.; Tao, Z.; Hu, C.; Bai, Y.; Zhao, G.; Chen, H.; Yang, Y.; Li, Y. Mechanisms of Double-Bond Migration Reactions of Pentene Isomers on Different Lewis Acids. *Appl. Surf. Sci.* **2022**, *589*, 152970.

(65) Yi, F.; He, P.; Chen, H.; He, Y.; Tao, Z.; Li, T.; Zhao, G.; Yun, Y.; Wen, X.; Yang, Y.; Li, Y. Mechanisms of Double-Bond Isomerization Reactions of *n*-Butene on Different Lewis Acids. *ACS Catal.* **2021**, *11* (17), 11293–11304.

(66) Gerberich, H. R.; Hall, W. K. Studies of the Hydrogen Held by Solids: IX. The Hydroxyl Groups of Alumina and Silica-Alumina as Sites for the Isomerization of Butene. *J. Catal.* **1966**, *5* (1), 99–110.

(67) Larsen, C. R.; Erdogan, G.; Grotjahn, D. B. General Catalyst Control of the Monoisomerization of 1-Alkenes to *trans*-2-Alkenes. *J. Am. Chem. Soc.* **2014**, *136* (4), 1226–1229.

(68) Benazzi, E.; Travers, C.; Gnep, N. S.; Andy, P.; Guisnet. M. Selective Skeletal Butene Isomerization Through a Bimolecular Mechanism. *Oil Gas Sci. Technol.* **1999**, *54* (1), 23–28.

(69) Rudin, A.; Choi, P. Free-Radical Polymerization. *The Elements of Polymer Science and Engineering*, 3rd ed.; Academic Press: Waltham, MA, 2013; pp 341–389.

Chapter 5. Conclusions

5.1. Introduction

Bitumen extracted from mined oil sands in the form of bitumen froth is further separated from the water and mineral solids using solvent-based froth treatment processes. The resultant bitumen product still needs to be diluted or upgraded to reach the viscosity targets for pipeline transport. In this thesis, application of temperatures that are much higher than the operating temperatures of the commercial solvent-based froth treatment processes (30-85 °C), as a potential way to achieve partial bitumen upgrading was investigated.

A temperature of 250 °C was chosen for this work, as steam, which is the basic utility in an oil and gas processing plant, can be used to supply heat for the process, without requiring a new furnace. Based on evidence in literature that bitumen on its own can undergo some conversion and macroscopic changes even at temperatures as low as 200 °C, it was of interest to evaluate the impact of mineral solids and water, present in the bitumen froth, on the physical and chemical changes in bitumen during thermal treatment of bitumen froth, also known as hydrothermal treatment.

Further, this thesis also dealt with understanding the role of mineral matter in the conversion chemistry. Clay minerals, kaolinite and illite, which constitute about 40-70 wt% of the total solids in bitumen froth, were chosen for this work. The types of reactions promoted by these clay minerals, and their selectivity to different reaction products was studied. Clay minerals, in general, are known for both their redox and acidic properties, making free radical and cationic pathways possible. However, due to the alkaline conditions of the bitumen froth, it was relevant to determine

whether minerals caused free radical and cationic reactions and whether the free radical pathway was preferred over the cationic pathway.

5.2. Major Conclusions and Insights

5.2.1. Hydrothermal Treatment of Bitumen Froth at 250 °C

The study on hydrothermal treatment of bitumen froth at 250 °C found that the process is not capable of partially upgrading bitumen at the study conditions. As a result of treating bitumen in the presence of water and mineral solids, the viscosity and total acid number (TAN) of bitumen increased compared to the bitumen treated on its own and untreated bitumen. As TAN is an important property that indicates the potential for corrosion problems in crude oil refineries, increasing the TAN of bitumen would mean increasing the corrosive nature of the product and decreasing the product's value. On the other hand, increasing the viscosity of bitumen product would increase the need for dilution or other strategies to enable pipeline transportation of bitumen. Therefore, these changes are directionally opposite to what is required in partial upgrading of bitumen.

The increase in the TAN of bitumen without an accompanying decrease in the pH upon hydrothermal treatment was tentatively explained by base-catalyzed hydrolysis of esters and anhydrides, promoted by the bases in the froth. Unlike acidic hydrolysis, which is reversible and produces a carboxylic acid, the base-catalyzed hydrolysis is irreversible and produces a carboxylate ion that can likely increase TAN without decreasing the pH, as observed in the pH measurements in this study.

The increase in bitumen viscosity due to thermal treatment in the presence of water and/or mineral solids, that was empirically observed in this work, is a different observation from what was

anticipated based on the past work on thermal conversion of heavy oils and bitumen. Of the potential explanations considered, generation of free radicals from the interaction of organic components with minerals through redox reactions, and radical addition reactions leading to heavier material formation offered a plausible explanation for the observed increase in the viscosity of bitumen. This explanation was also consistent with the increase in the free radical concentration of bitumen that was noted after hydrothermal treatment and treatment in the presence of only mineral solids, compared to the untreated bitumen.

Although the main objective of this work was not to investigate the separation characteristics of the hydrothermal treatment process, separation of solids and water from the bitumen froth is the primary purpose of the oilsands froth treatment processes. In this work, solvent (toluene) dilution and separation methods, including centrifugation, vacuum filtration and rotary evaporation, were used to separate the solids and water from the feed, and product mixtures obtained after thermal treatment. Comparing the residual solids and water content in the diluted bitumen (~5 wt % toluene) samples produced from untreated froth and hydrothermally treated bitumen froth after using similar separation procedures, no additional benefit in terms of froth separation was noticed from using the hydrothermal treatment of bitumen froth at the study conditions.

Phase contamination of bitumen samples made it challenging for determining the true impact of thermal conversion of bitumen in the presence of water and/or mineral solids on the bitumen properties in this study. As no such work was previously performed with the bitumen froth that required correction of bitumen properties for the presence of toluene (organic solvent), water and mineral solids, all in the same mixture, a new challenge was presented in this work for studying thermal changes in bitumen froth quantitatively. The study brought together theoretical concepts

of suspensions, emulsions and organic-solvent bitumen mixtures, to correct the properties of contaminated bitumen samples and shed new light on the effect of hydrothermal treatment.

To conclude, this portion of the thesis explored a new way of partial bitumen upgrading, called hydrothermal froth treatment, with anticipated benefits. However, the investigation found that the process was not beneficial at the study conditions and several changes in the properties of bitumen were observed that were contrary to what is required from a partial upgrading technology. The main contribution of this applied research study was evaluation of the modified froth treatment process from concept to rejection, which led to questions on the reactive behavior of mineral solids in bitumen froth that were fundamental to the field, and were explored in the next part of the thesis.

5.2.2. Probing Free Radical and Cationic Reactivity of Clay Minerals using α-Methyl Styrene (AMS) and 1-Octene

This part of the thesis attempted to examine the fundamental chemistry that was speculated to occur in the hydrothermal treatment of bitumen froth in the presence of clay minerals, that would be responsible for heavier material formation and the increase in the viscosity of bitumen that was observed in the first part of the thesis. Understanding the chemistry of the process is crucial for any process development. In this case, knowledge of the reaction chemistry between mineral solids and hydrocarbons, and how the chemistry affects the bitumen properties is important for the future development of high temperature application of bitumen froth treatment processes.

Clay minerals constitute 40-70 wt% of the total solids in bitumen froth, and are generally known for their redox and acidic properties. This study explored whether the major clay minerals in bitumen froth, kaolinite and illite, can promote free radical addition reactions and cationic (acid-catalyzed) addition reactions of organic compounds. Due to the alkaline nature of the bitumen

froth, it was relevant to investigate whether the free radical reaction pathway would be preferred over the cationic pathway.

This study was conducted using AMS and 1-octene as probe molecules instead of bitumen froth. Conversion of the probe molecules in the absence of minerals at 250 °C was low, and was explained using free radical mechanisms of self-initiation or bimolecular initiation by the action of toluene. It was found that the clay minerals kaolinite and illite, present in the bitumen froth, promoted the formation of heavier molecules at 250 °C. This was concluded based on the increase in the peak areas of the AMS dimers ($C_{18}H_{20}$) and 9-carbon alkylated benzenes ($C_{15}H_{24}$) from the GC-MS chromatograms of the products of AMS and 1-octene conversion respectively in the presence of the minerals compared to their absence. Dimerization of AMS and alkylation of 1-octene and toluene (which was used as solvent in the reactions) were observed to be the major reactions during thermal conversion.

To distinguish between free radical addition and cationic addition, a set of experiments were performed with the probe molecules, clay minerals and pyridine. If the addition reactions were cation-mediated or acid-catalyzed, addition of a base like pyridine would reduce the effect of those reactions. In this work, the AMS dimerization and aromatic alkylation of 1-octene and toluene were suppressed upon addition of pyridine to the reaction systems, indicating that the addition reactions promoted by the clay minerals were cationic in nature. Comparison of the overall conversion and peak areas of the reaction products of AMS and 1-octene, as well as the selectivity profile of different isomers of AMS dimers, revealed that free radical addition took place only to a minor extent compared to cationic addition in the presence of minerals.

Even in the presence of a base like pyridine, some conversion of the probe molecules to addition products through dimerization and olefin-aromatic alkylation (Friedel−Crafts alkylation) was noticed. Selectivity profile of different isomers of AMS dimers in the reactions conducted in the presence of pyridine suggested that in the presence of the clay minerals, even under alkaline conditions, cationic addition was the dominant reaction pathway.

Besides addition products, formation of cumene from AMS and linear double bond stereo isomers from 1-octene in the presence of minerals were also noted. These side products decreased in amounts in the presence of pyridine in the reaction system, indicating that cationic conversion occurred.

In this work, thermal adsorption and desorption tests with the natural clay minerals using pyridine and ammonia vapors confirmed the presence of both Bronsted acid and Lewis acid sites on the mineral surface. The minerals appeared to retain some of the acid-bound pyridine complexes even during thermal desorption at 250 °C and 350 °C, indicating their acidic strength.

To conclude, this portion of the thesis explored the fundamental reaction mechanisms by which the clay minerals in bitumen froth interact with organic compounds and promote addition reactions. The main finding of this study was showing that the clay minerals can promote addition reactions at 250 °C, even under alkaline conditions, and that the mineral-related conversion was predominantly cationic in nature. Besides addition reactions, the possible occurrence of other types of reactions, such as isomerization and transfer hydrogenation, that could be promoted by the clay minerals during hydrothermal froth treatment was also indicated by this study.

5.3. Recommended Future Work

5.3.1. Role of Water in the Conversion Chemistry

Hydrothermal treatment of bitumen froth at 250 °C caused the viscosity of bitumen to increase compared to both the untreated bitumen and bitumen treated on its own at 250 °C. As the treatment of bitumen with only water at 250 °C also led to a viscosity increase, the contribution of water to the viscosity changes cannot be ignored. Further, water also appeared to play a dominant role in increasing the *n*-heptane insoluble content of bitumen during thermal conversion. The chemistry of hydrothermal froth treatment process is incomplete without understanding the role of process water during bitumen conversion. In literature, there appears to be a disagreement between aspects of the physical and chemical role of water in the conversion chemistry. Further investigation is needed to shed light on the participation of water in the reaction chemistry, and the solubility effects of water in influencing the partitioning of molecules in the bulk organic liquid to different phases.

The following questions are recommended for future research:

(a) What are the physical and/or chemical mechanisms by which water participates in the bitumen conversion chemistry (e.g. hydrogen transfer reactions), more specifically in this case, in increasing the bitumen viscosity at 250 °C?

(b) What role does water play as a solvent in modifying conversion chemistry, by affecting the solubility of polar organic components present in bitumen and promoting their partitioning between phases?

5.3.2. Base-Catalyzed Hydrolysis Leading to Increase in TAN

In this work, the TAN of bitumen increased upon hydrothermal treatment of bitumen froth at 250 °C. Base-catalyzed hydrolysis of esters and anhydrides promoted by the bases in water seemed to be a plausible explanation for the observed increase in TAN of bitumen. Due to the irreversible nature of base-catalyzed hydrolysis reaction, the product is a carboxylate, which has a negative ion on its hydrophilic end and the hydrocarbon chain as its hydrophobic tail. These carboxylates may behave as surfactants and contribute to the stability of emulsions, making separation difficult. As the main purpose of a froth treatment process is to overcome the challenge of water-in-oil emulsions present in the bitumen froth and facilitate phase separation, it would be relevant to investigate this aspect.

The following question is recommended for future research:

(a) How does the chemistry contributing to a change in the TAN of bitumen during hydrothermal treatment affect the stability of water-in-oil emulsions in bitumen froth and phase separation?

5.3.3. Performing Hydrothermal Treatment at Higher Temperature

In this work, treating bitumen froth at 250 °C did not prove to be beneficial for bitumen upgrading. Is performing thermal treatment of bitumen froth at a higher temperature (> 250 °C) then a potential solution to achieving partial bitumen upgrading?

The following questions are recommended in this line of research:

(a) What is the operating temperature range in which the cracking reactions dominate over the addition reactions in the hydrothermal froth treatment process, which contribute to viscosity reduction in bitumen?

(b) Do clay minerals function as catalysts for cracking reactions at higher temperatures, by promoting formation of carbocations, which undergo scission of C−C bonds and rearrangement processes, similar to the role of solid acid catalysts (e.g. zeolites) in the catalytic cracking process?

(c) Can increased catalytic benefit be obtained by combining acidification of bitumen froth with thermal treatment at higher temperatures, due to increased acidity of clays? If yes, using what type of acids and in what concentrations can the benefits be observed? Additionally, can the benefits of metal removal obtained through acid treatment of bitumen reported in literature be observed in the current process?

As mentioned earlier, a furnace would be required to supply heat for the reaction at higher temperatures, increasing the cost of the process. Therefore, the process would be economically viable only if the high temperature operation causes reasonable partial bitumen upgrading and enhancement of separation efficiency, which result in economic benefits that exceed its operating and equipment costs.

In the case of acidification, in addition to having access to a fresh supply of acid or technology for regeneration of spent acid, additional safety measures must be taken to prevent corrosion issues – e.g. usage of corrosion resistant reactor materials. These added features are expected to drive up costs.

5.3.4. Changes in the H/C Ratio of Bitumen

In this work, compared to the untreated bitumen, an increase in the hydrogen-to-carbon ratio (H/C ratio) of bitumen was noticed upon thermal treatment at 250°C, irrespective of the second phase present. There must have been some way in which more carbon rich material was removed from

the product that was common to all thermally treated samples. H/C ratio is an important property of bitumen. The higher the H/C ratio, the more valuable the bitumen. It would therefore be useful to know what caused an increase in the H/C ratio during thermal treatment at 250°C. This was not investigated in the current thesis and is recommended for future research.

The following question is recommended for future research:

(a) What is the mechanism of carbon rejection that occurs during thermal treatment of bitumen at 250°C, which contributes to an increase in the H/C ratio of bitumen?

5.3.5. Effect of Reaction Chemistry on Solids Separation

The current work explored in what ways the mineral solids (clay minerals) affect the reaction chemistry. It is anticipated that the reaction chemistry in turn affects how the solids interact with the froth and their separation efficiency during hydrothermal froth treatment. Previously, some work was carried out to study the wettability alteration of solids on hydrothermal treatment and the influence on their filterability. However, different mineral solids might respond differently to the reaction chemistry. As separation of solids from bitumen is one of the important requirements of froth treatment, it is important to understand the relationship between hydrothermal conversion of bitumen froth and the separation characteristics of different minerals in the bitumen froth.

The following questions are recommended for future research:

(a) What is the relationship between the degree of thermal conversion and the surface wettability alteration of different types of minerals in bitumen froth such as oxides (e.g. silica, rutile), carbonates (e.g. calcite, dolomite), clay minerals (e.g. kaolinite, illite), pyrite, etc.? Can the wettability characteristics of minerals be correlated with the chemical characteristics of thermally treated bitumen (e.g. SARA composition)?

5.3.6. Investigation of the Influence of Emulsified Water in Bitumen Froth Treatment

In this study, experiments were performed using bitumen (B), water (W), and solids (S) separated from bitumen froth, examining the properties of the resulting bitumen products in four distinct reactions: B, B+W, B+S, and B+W+S. Valuable insights were obtained regarding the impact of water and/or solids addition on bitumen properties. However, it is essential to acknowledge that bitumen froth contains emulsified water, which can differ significantly from the water added separately in the B+W and B+W+S reactions. The presence of emulsified water may introduce complexities related to interfacial area and interaction dynamics not addressed in this study. Thus, future investigations should include experiments treating bitumen froth without separation to better understand how emulsified water affects bitumen properties. This will enhance understanding of water's role in real-world bitumen froth treatment scenarios.

5.3.7. Incorporating Real Froth Solids in Model Compound and Clay Mineral Experiments

In the investigation of potential reaction pathways for organic compounds in the presence of clay minerals during hydrothermal froth treatment, experiments were conducted using model compounds, α-methyl styrene and 1-octene, in the presence of purely inorganic clay minerals, kaolinite and illite, procured from suppliers without any organic matter contamination. However, it should be noted that in real bitumen froth, these clay minerals are naturally coated with organic matter. This organic coating introduces significant complexity, potentially modifying the interaction dynamics between organic compounds and clay minerals. To gain a more comprehensive insight into hydrothermal froth treatment, future experiments with real froth solids are recommended, allowing for the examination of the organic-inorganic interactions inherent to authentic bitumen froth scenarios.

5.3.8. Energy and Environmental Impact of Elevated-Temperature Bitumen Froth Treatment

While the current study has explored elevated-temperature bitumen froth treatment, it is essential to acknowledge that a comprehensive energy and environmental impact assessment was not within the scope of this research. Therefore, future investigations should prioritize conducting a thorough life cycle assessment (LCA) or environmental impact assessment (EIA) to accurately quantify the energy and environmental implications of the modified process.

The following questions are recommended for future research:

(a) What are the energy-related consequences of adopting a higher operating temperature (250 °C) compared to conventional froth treatment processes (30-85 °C), including the potential for increased energy consumption and the possibility of enhanced bitumen separation efficiency?

(b) How do the environmental implications of the modified froth treatment process, specifically the exclusion of hydrocarbon solvents and the direct heating of froth at 250 °C, contribute to reduced environmental impact, particularly in terms of volatile organic compounds (VOCs) emissions and addressing concerns related to tailings pond ?

Bibliography

Acevedo, S.; Castro, A.; Negrin, J. G.; Fernández, A.; Escobar, G.; Piscitelli, V.; Delolme, F.; Dessalces, G. Relations Between Asphaltene Structures and Their Physical and Chemical Properties: The Rosary-Type Structure. *Energy Fuels* **2007**, *21* (4), 2165–2175.

Adegoroye, A.; Uhlik, P.; Omotoso, O.; Xu, Z.; Masliyah, J. A Comprehensive Analysis of Organic Matter Removal from Clay-Sized Minerals Extracted from Oil Sands Using Low Temperature Ashing and Hydrogen Peroxide. *Energy Fuels* **2009**, *23* (7), 3716–3720.

Adegoroye, A.; Wang, L.; Omotoso, O.; Xu, Z.; Masliyah, J. Characterization of Organic-Coated Solids Isolated from Different Oil Sands. *Can. J. Chem. Eng.* **2010**, *88* (3), 462–470.

Alili, A.S.; Siddiquee, M. N.; De Klerk, A. Origin of Free Radical Persistence in Asphaltenes: Cage Effect and Steric Protection. *Energy Fuels* **2020**, *34* (1), 348–359.

Allen, E. W. Process Water Treatment in Canada's Oil Sands Industry: I. Target Pollutants and Treatment Objectives. *J. Environ. Eng. Sci.* **2008**, *7* (2), 123–138.

Al-Muntaser, A. A.; Varfolomeev, M. A. Suwaid, M. A.; Yuan, C.; Chemodanov, A. E.; Feoktistov, D. A.; Rakhmatullin, I. Z.; Abbas, M.; Domínguez-Álvarez, E.; Akhmadiyarov, A. A.; Klochkov, V. V.; Amerkhanov, M. I. Hydrothermal Upgrading of Heavy Oil in the Presence of Water at Sub-Critical, Near-Critical and Supercritical Conditions. *J. Pet. Sci. Eng.* **2020**, *184*, 106592.

Alshareef, A. H.; Scherer, A.; Tan, X.; Azyat, K.; Stryker, J. M.; Tykwinski, R. R.; Gray, M. R. Formation of Archipelago Structures During Thermal Cracking Implicates a Chemical Mechanism for the Formation of Petroleum Asphaltenes. *Energy Fuels* **2011**, *25* (5), 2130–2136.

Andrekanic, R. A.; Salek, J. S.; Mulhall, S. E.; Bubnov, Y. V. Polymerization of Alpha Methylstyrene. U.S. Patent 6,649,716, November 18, 2003.

An, J.; Bagnell, L.; Cablewski, T.; Strauss, C. R.; Trainor, R.W. Applications of High-Temperature Aqueous Media for Synthetic Organic Reactions. *J. Org. Chem* **1997**, *62* (8), 2505–2511.

Appleby, W. G.; Gibson, J. W.; Good, G. M. Coke Formation in Catalytic Cracking. *Ind. Eng. Chem. Process Des. Dev.* **1962,** *1* (2), 102–110.

Araújo, J. H. D.; Silva, N. F. D.; Acchar, W.; Gomes, U. U. Thermal Decomposition of Illite. *Mater. Res.* **2004**, *7*, 359–361.

Arcelus-Arrillaga, P.; Pinilla, J. L.; Hellgardt, K.; Millan, M. Application of Water in Hydrothermal Conditions for Upgrading Heavy Oils: A Review. *Energy Fuels* **2017**, *31* (5), 4571–4587.

ASTM International. *D664-18e2 Standard Test Method for Acid Number of Petroleum Products by Potentiometric Titration;* West Conshohocken, PA, 2018.

Aveyard, R.; Binks, B. P.; Clint, J. H. Emulsions Stabilised Solely by Colloidal Particles. *Adv. Colloid Interface Sci.* **2003**, *100-102*, 503–546.

Axelson, D. E.; Mikula, R. J.; Potoczny, Z. M. Characterization of Oil Sands Mineral Components and Clay-Organic Complexes. *Fuel Sci. Technol. Int.* **1989**, *7* (5–6), 659–673.

Ayat, M.; Bensaada, N.; Belbachir, M.; Harrane, A.; Meghabar, R. Synthesis and Characterization of Poly (α-Methylstyrene) by Cationic Polymerization Using a New Solid Ecological Catalyst. *Orient. J. Chem.* **2015**, *31*, 2115–2123.

Bakhtiari, M. T. Role of Sodium Hydroxide in Bitumen Extraction: Production of Natural Surfactants and Slime Coating. Ph.D. Dissertation, University of Alberta, Edmonton, Canada, 2015.

Bandura, L.; Woszuk, A.; Kołodyńska, D.; Franus, W. Application of Mineral Sorbents for Removal of Petroleum Substances: A Review. *Miner.* **2017**, *7* (3), 37.

Barnea, E.; Mizrahi, J. A Generalized Approach to the Fluid Dynamics of Particulate Systems: Part 1. General Correlation for Fluidization and Sedimentation in Solid Multiparticle Systems. *Chem. Eng. J.* **1973,** *5* (2), 171–189.

Bichard, J. A. *Oil Sands Composition and Behaviour Research*; AOSTRA Technical Publication Series, No. 4; Canada, 1987; p 9–2.

Binks, B. P.; Lumsdon, S. O. Influence of Particle Wettability on the Type and Stability of Surfactant-Free Emulsions. *Langmuir* **2000**, *16* (23), 8622–8631.

Binks, B. P.; Lumsdon, S. O. Pickering Emulsions Stabilized by Monodisperse Latex Particles: Effects of Particle Size. *Langmuir* **2001**, *17* (15), 4540–4547.

Bittles, J.A.; Chaudhuri, A.K.; Benson, S.W. Clay-Catalyzed Reactions of Olefins. II. Catalyst Acidity and Mechanism. *J. Polym. Sci., Part A: Gen. Pap.* **1964**, *2* (4), 1847–1862.

Black, S.; Muller, F. On the Effect of Temperature on Aqueous Solubility of Organic Solids. *Org. Process Res. Dev.* **2010,** *14* (3), 661–665.

Bringué, R.; Cadenas, M.; Fité, C.; Iborra, M.; Cunill, F. Study of the Oligomerization of 1-Octene Catalyzed by Macroreticular Ion-Exchange Resins. *Chem. Eng. J.* **2012**, *207*, 226–234.

Briones, A. M. Asphaltene Adsorption on Different Solid Surfaces from Organic Solvents. M.S. Thesis, University of Alberta, Edmonton, Canada, 2020.

Brown, D. R.; Rhodes, C. N. Brønsted and Lewis Acid Catalysis with Ion-Exchanged Clays. *Catal. Lett.* **1997**, *45* (1), 35–40.

Bruno, J. E.; Dooley, K. M. Double-Bond Isomerization of Hexadecenes with Solid Acid Catalysts. *Appl. Catal., A* **2015**, *497*, 176–183.

Bruno, J. E. Double-Bond Isomerization of Long Chain Olefins. M.S. Thesis, Louisiana State University and Agricultural and Mechanical College, Baton Rouge, LA, 2012.

Bullard, J. W.; Pauli, A. T.; Garboczi, E. J.; Martys, N. S. A Comparison of Viscosity–Concentration Relationships for Emulsions. *J. Colloid Interface Sci.* **2009,** *330* (1), 186–193.

Byrappa, K.; Adschiri, T. Hydrothermal Technology for Nanotechnology. *Prog. Cryst. Growth Charact. Mater.* **2007**, *53* (2), 117–166.

Cadenas, M.; Bringué, R.; Fité, C.; Iborra, M.; Ramírez, E.; Cunill, F. Alkylation of Toluene with 1-Hexene Over Macroreticular Ion-Exchange Resins. *Appl. Catal., A* **2014**, *485*, 143–148.

Canıaz, R. O.; Arca, S.; Yaşar, M.; Erkey, C. Refinery Bitumen and Domestic Unconventional Heavy Oil Upgrading in Supercritical Water. *J. Supercrit. Fluids* **2019**, *152*, 104569.

Canıaz, R. O.; Erkey, C. Process Intensification for Heavy Oil Upgrading Using Supercritical Water. *Chem. Eng. Res. Des.* **2014**, *92* (10), 1845–1863.

Carbognani, L.; González, M. F.; Lopez-Linares, F.; Stull, C. S.; Pereira-Almao, P. Selective Adsorption of Thermal Cracked Heavy Molecules. *Energy Fuels* **2008**, *22* (3), 1739–1746.

Carbognani, L.; Roa-Fuentes, L. C.; Diaz, L.; Berezinski, J.; Carbognani-Arambarri, L.; Pereira-Almao, P. Reliable Determination of Water Contents of Bitumen and Vacuum Residua via Coulometric Karl Fischer Titration Using Tetrahydrofuran. *Pet. Sci. Technol.* **2014**, *32* (5), 602–609.

Castillo, J.; De Klerk, A. Visbreaking of Deasphalted Oil from Bitumen at 280–400° C. *Energy Fuels* **2018**, *33* (1), 159–175.

Chacón-Patiño, M. L.; Rowland, S. M.; Rodgers, R. P. The Compositional and Structural Continuum of Petroleum from Light Distillates to Asphaltenes: The Boduszynski Continuum Theory as Revealed by FT-ICR Mass Spectrometry. In *The Boduszynski Continuum: Contributions to the Understanding of the Molecular Composition of Petroleum;* Ovalles, C.; Moir, M. E.; ACS Symposium Series 1282; American Chemical Society: Washington DC, USA, 2018; pp 113–171.

Chaudhuri, B.; Sharma, M. M. Some Novel Aspects of Dimerization of α-Methylstyrene with Acidic Ion-Exchange Resins, Clays and Other Acidic Materials as Catalysts. *Ind. Eng. Chem. Res.* **1989**, *28* (12), 1757–1763.

Chauhan, G.; De Klerk, A. Dissolution Methods for the Quantification of Metals in Oil Sands Bitumen. *Energy Fuels* **2020**, *34* (3), 2870–2879.

Chen, Q.; Gray, M. R.; Liu, Q. Irreversible Adsorption of Asphaltenes on Kaolinite: Influence of Dehydroxylation. *Energy Fuels* **2017**, *31* (9), 9328–9336.

Chen, Q.; Liu, Q. Bitumen Coating on Oil Sands Clay Minerals: A Review. *Energy Fuels* **2019**, *33* (7), 5933–5943.

Chen, Q. Organically-Modified Clay Minerals in Oil Sands: Characterization and Effect of Hydrothermal Treatment. Ph.D. Dissertation, University of Alberta, Edmonton, Canada, 2017.

Chen, Q.; Stricek, I.; Cao, M.; Gray, M. R.; Liu, Q. Influence of Hydrothermal Treatment on Filterability of Fine Solids in Bitumen Froth. *Fuel* **2016**, *180*, 314–323.

Cortés, F. B.; Mejía, J. M.; Ruiz, M. A.; Benjumea, P.; Riffel, D. B. Sorption Of Asphaltenes onto Nanoparticles of Nickel Oxide Supported on Nanoparticulated Silica Gel. *Energy Fuels* **2012**, *26* (3), 1725–1730.

Couillard, M.; Tyo, D. D.; Kingston, D. M.; Patarachao, B.; Zborowski, A.; Ng, S.; Mercier, P. H. J. Structure and Mineralogy of Hydrophilic and Biwettable Sub-2 μm Clay Aggregates in Oil Sands Bitumen Froth. *Miner.* **2020**, *10* (11), 1040.

Cui, X.; Su, H. Y.; Chen, R.; Yu, L.; Dong, J.; Ma, C.; Wang, S.; Li, J.; Yang, F.; Xiao, J.; Zhang, M.; Ma, D.; Deng, D.; Zhang, D. H.; Tian, Z.; Bao, X. Room-Temperature Electrochemical Water–Gas Shift Reaction for High Purity Hydrogen Production. *Nat. Commun.* **2019**, *10* (86), 1–8.

Czarnecki, J.; Masliyah, J.; Xu, Z.; Dabros, M. *Handbook on Theory and Practice of Bitumen Recovery from Athabasca Oil Sands - Volume 2: Industrial Practice*; Kingsley Knowledge Publishing: 2013; p 214.

Das, S. Critical Review of Water Radiolysis Processes, Dissociation Products, and Possible Impacts on the Local Environment: A Geochemist's Perspective. *Aust. J. Chem.* **2013**, *66* (5), 522–529.

De Klerk, A. Oligomerization of 1-Hexene and 1-Octene Over Solid Acid Catalysts. *Ind. Eng. Chem. Res.* **2005**, *44* (11), 3887–3893.

De Klerk, A. Processing Unconventional Oil: Partial Upgrading of Oilsands Bitumen. *Energy Fuels* **2021**, *35* (18), 14343–14360.

De Klerk, A. Thermal Conversion Modeling of Visbreaking at Temperatures Below 400°C. *Energy Fuels* **2020**, *34* (12), 15285–15298.

De Klerk, A. Unconventional Oil: Oilsands. In *Future Energy: Improved, Sustainable and Clean Options for Our Planet*, 3rd ed.; Letcher, T. M., Eds.; Elsevier: Amsterdam, Netherlands, 2020; pp 49–65.

Denisov, E. T.; Denisova, T. G.; Pokidova, T. S. *Handbook of Free Radical Initiators*; John Wiley & Sons, Inc: Hoboken, NJ, 2003; pp 591–653.

DeZutter, C. B.; Horner, J. H.; Newcomb, M. Rate Constants for 1, 5-and 1, 6-Hydrogen Atom Transfer Teactions of Mono-, Di-, and Tri-Aryl-Substituted Donors, Models for Hydrogen Atom Transfers in Polyunsaturated Fatty Acid Radicals. *J. Phys. Chem. A* **2008**, *112* (9), 1891–1896.

Djimasbe, R.; Varfolomeev, M. A.; Kadyrov, R. I.; Davletshin, R. R. Khasanova, N. M.; Saar, F. D.; Al-Muntaser, A. A.; Suwaid, M. A.; Mukhamedyarova, A. N. Intensification of Hydrothermal

Treatment Process of Oil Shale in the Supercritical Water Using Hydrogen Donor Solvents. *J. Supercrit. Fluids* **2022**, *191*, 105764.

D'Souza, A. S.; Pantano, C.G. Mechanisms for Silanol Formation on Amorphous Silica Fracture Surfaces. *J. Am. Chem. Soc.* **1999**, *82* (5), 1289–1293.

Dubey, S. T.; Waxman, M. H. Asphaltene Adsorption and Desorption from Mineral Surfaces. *SPE Reservoir Eng.* **1991,** *6* (03), 389–395.

Dubrawski, J. V. Thermal Decomposition of Some Siderite-Magnesite Minerals using DSC. *J. Therm. Anal. Calorim.* **1991**, *37* (6), 1213–1221.

Elroy, I. Polymerization of Alpha-Methylstyrene at High Pressures. Ph.D. Dissertation, Imperial College London, UK, 1961. *Energy Fact Book 2021-2022*; ISSN 2370-3105; Natural Resources Canada; Canada, 2021; pp 96–146.

Estacio, S. G.; Couto, P. C. D.; Guedes, R. C.; Cabral, B. J. C.; Simões, J. A. M. Homolytic Dissociation in Hydrogen-Bonding Liquids: Energetics of the Phenol O–H Bond in Methanol and the Water O–H Bond in Water. *Theor. Chem. Acc.* **2004**, *112*, 282–289.

Fan, H. F.; Liu, Y. J.; Zhong, L. G. Studies on the Synergetic Effects of Mineral and Steam on the Composition Changes of Heavy Oils. *Energy Fuels* **2001**, *15* (6), 1475–1479.

Fan, H.; Zhang, Y.; Lin, Y. The Catalytic Effects of Minerals on Aquathermolysis of Heavy Oils. *Fuel* **2004**, *83*(14–15), 2035–2039.

Feng, X.; Behles, J. A. Understanding the Demulsification of Water-in-Diluted Bitumen Froth Emulsions. *Energy Fuels* **2015**, *29* (7), 4616–4623.

Flury, C.; Afacan, A.; Tamiz Bakhtiari, M.; Sjoblom, J.; Xu, Z. Effect of Caustic Type on Bitumen Extraction from Canadian Oil Sands. *Energy Fuels* **2014**, *28* (1), 431–438.

Fox, M. A.; Whitesell, J. K. Substitution Alpha to Carbonyl Groups: Enolate Anions and Enols as Nucleophiles. In *Organic Chemistry*, 3rd ed.; Eds.; Jones and Bartlett Publishers: Sudbury, Massachusetts, 2004; p 651.

Franco, C.; Patiño, E.; Benjumea, P.; Ruiz, M. A.; Cortés, F. B. Kinetic and Thermodynamic Equilibrium of Asphaltenes Sorption onto Nanoparticles of Nickel Oxide Supported on Nanoparticulated Alumina. *Fuel* **2013**, *105*, 408–414.

Geatti, A.; Lenarda, M.; Storaro, L.; Ganzerla, R.; Perissinotto, M. Solid Acid Catalysts from Clays: Cumene Synthesis by Benzene Alkylation with Propene Catalyzed by Cation Exchanged Aluminum Pillared Clays. *J. Mol. Catal. A: Chem.* **1997**, *121* (1), 111–118.

Genco, J. I.; Duke, F. R.; Griffel, M.; Jennings, L. D. *The (C-H) Bond Dissociation Energy in the Methyl Group of Toluene;* Technical Report Number ISC-746; U.S. Atomic Energy Commission, Technical Information, March 1956.

Gerberich, H. R.; Hall, W. K. Studies of the Hydrogen Held by Solids: IX. The Hydroxyl Groups of Alumina and Silica-Alumina as Sites for the Isomerization of Butene. *J. Catal.* **1966**, *5* (1), 99–110.

Giraldo, J.; Nassar, N. N.; Benjumea, P.; Pereira-Almao, P.; Cortés, F. B. Modeling and Prediction of Asphaltene Adsorption Isotherms using Polanyi's Modified Theory. *Energy Fuels* **2013**, *27* (6), 2908–2914.

Golchin, A.; Baldock, J. A.; Oades, J. M. A Model Linking Organic Matter Decomposition, Chemistry, and Aggregate Dynamics. In *Soil Processes and the Carbon Cycle*, 1st ed.; Lal, R.; Kimble, J. M.; Follett, R. F.; Stewart, B. A., Eds.; CRC Press: Boca Raton, FL, 1998; pp 245–266.

González, G.; Moreira, M. B. C. The adsorption of asphaltenes and resins on various minerals. In *Asphaltenes and Asphalts, 1*; Yen, T.F., Chilingarian, G.V., Eds.; Elsevier Science B.V.: Amsterdam, Netherlands, 1994; 40, pp. 207–231.

Gorski, C. A.; Aeschbacher, M.; Soltermann, D.; Voegelin, A.; Baeyens, B.; Marques Fernandes, M.; Hofstetter, T. B.; Sander, M. Redox Properties of Structural Fe in Clay Minerals. 1. Electrochemical Quantification of Electron-Donating and -Accepting Capacities of Smectites. *Environ. Sci. Technol.* **2012**, *46* (17), 9360–9368.

Gray. M. R. Fundamentals of Partial Upgrading of Bitumen. *Energy Fuels* **2019**, *33* (8), 6843–6856.

Gray, M. R. *Upgrading Oilsands Bitumen and Heavy Oil*; Pica Pica Press: Edmonton, Canada, 2015; pp 2–477.

Gridnev, A. A. Kinetics of Alpha-Methylstyrene Oligomerization by Catalytic Chain Transfer. *J. Polym. Sci., Part A: Polym. Chem.* **2002**, *40* (9), 1366–1376.

Gryglewicz, G.; Wilk, P.; Yperman, J.; Franco, D.V.; Maes, I. I.; Mullens, J.; Van Poucke, L. C. Interaction of the Organic Matrix with Pyrite during Pyrolysis of a High-Sulfur Bituminous Coal. *Fuel* **1996**, *75* (13), 1499–1504.

Gu, G.; Zhang, L.; Xu, Z.; Masliyah, J. Novel Bitumen Froth Cleaning Device and Rag Layer Characterization. *Energy Fuels* **2007**, *21* (6), 3462–3468.

Guo, Y.; Du, X.; Liu, L.; Dong, Y.; Lei, Z. Reaction Mechanism of Benzene Alkylation with Propylene Catalyzed by HZSM-5 Zeolite and H-Beta Zeolite. *Mater. Today Commun.* **2021**, *26*, 101757.

Hao, H.; Li, L.; Yuan, Z.; Patra, P.; Somasundaran, P. Adsorption Differences of Sodium Oleate on Siderite and Hematite. *Miner. Eng.* **2019**, *137*, 10–18.

Han, L.; Zhang, R.; Bi, J. Experimental Investigation of High-Temperature Coal Tar Upgrading in Supercritical Water. *Fuel Process. Technol.* **2009**, *90* (2), 292–300.

Hersberger, A. B.; Reid, J. C.; Heiligmann, R. G. Polymerization of Alpha-Methylstyrene. *Ind. Eng. Chem*. **1945**, *37* (11), 1073–1078.

Hojabri, F. Gas-Phase Catalytic Alkylation of Aromatic Hydrocarbons. *J. Appl. Chem. Biotechnol.* **1971**, *21* (3), 87–89.

Hollerbach, A. Influence of Biodegradation on the Chemical Composition of Heavy Oil and Bitumen. In *Exploration for Heavy Crude Oil and Natural Bitumen*; Meyer, R. F.; AAPG Studies in Geology Series No. 25; American Association of Petroleum Geologists: Tulsa, OK, 1987; pp 243–248.

Holzapfel, W.B. Effect of Pressure and Temperature on the Conductivity and Ionic Dissociation of Water up to 100 Kbar and 1000°C. *J. Chem. Phys.* **1969**, *50* (10), 4424–4428.

Hoving, A. L.; Sander, M.; Bruggeman, C.; Behrends, T. Redox Properties of Clay-Rich Sediments as Assessed by Mediated Electrochemical Analysis: Separating Pyrite, Siderite and Structural Fe in Clay Minerals. *Chem. Geol.* **2017**, *457*, 149–161.

Hristova, E. J.; Stoyanov, S. R. Bitumen Froth Treatment in the Transition Region Between Paraffinic and Naphthenic Process Conditions. *Fuel* **2021**, *286*, 119385.

Insley, H.; Ewell, R. H. Thermal Behavior of the Kaolin Minerals. *J. Res. Natl. Bur. Stand.* **1935**, *14* (5), 615–627.

Jia, H.; Zhao, S.; Nulaji, G.; Tao, K.; Wang, F.; Sharma, V. K.; Wang, C. Environmentally Persistent Free Radicals in Soils of Past Coking Sites: Distribution and Stabilization. *Environ. Sci. Technol.* **2017**, *51* (11), 6000–6008.

Jiang, T.; Hirasaki, G. J.; Miller, C. A.; Ng, S. Effects of Clay Wettability and Process Variables on Separation of Diluted Bitumen Emulsion. *Energy Fuels* **2011**, *25* (2), 545–554.

Joseph, J. T.; Forrai, T. R. Effect of Exchangeable Cations on Liquefaction of Low Rank Coals. *Fuel* **1992**, *71* (1), 75–80.

Jozaghkar, M. R.; Ziaee, F.; Azar, A. S. Investigation of Poly (α-Methyl Styrene) Tacticity Synthesized by Photo-Polymerization. *Polym. Bull.* **2021**, *78* (9), 5303–5314.

Kaminsky, H. A. W.; Etsell, T. H.; Ivey, D. G.; Omotoso, O. Distribution of Clay Minerals in the Process Streams Produced by the Extraction of Bitumen from Athabasca Oil Sands. *Can. J. Chem. Eng.* **2009**, *87* (1), 85–93.

Katritzky, A. R.; Lapucha, A. R.; Murugan, R.; Luxem, F. J.; Siskin, M.; Brons, G. Aqueous High-Temperature Chemistry of Carbo-and Heterocycles. 1. Introduction and Reaction of 3-Pyridylmethanol, Pyridine-3-Carboxaldehyde, and Pyridine-3-Carboxylic Acid. *Energy Fuels* **1990**, *4* (5), 493–498.

Kauffmann, H. F.; Harms, H.; Olaj, O. F. Ground-State Dynamics of α-Methylstyrene. I. Thermally Induced Oligomerization in Bulk. *J. Polym. Sci., Polym. Chem. Ed.* **1982**, *20* (10), 2943–2967.

Kloet, J. V.; Schramm, L. L.; Shelfantook, B. The Influence of Bituminous Froth Components on Water-in-Oil Emulsion Stability as Determined by the Micropipette Technique. *Colloids Surf., A* **2001**, *192* (1–3), 15–24.

Kjonaas, R. A.; Mattingly, S. P. Acid-Catalyzed Isomerization of Carvone to Carvacrol. *J. Chem. Educ.* **2005**, *82* (12), 1813.

Kotlyar, L. S.; Sparks, B. D.; Woods, J. R.; Chung, K. H. Solids Associated with the Asphaltene Fraction of Oil Sands Bitumen. *Energy Fuels* **1999**, *13* (2), 346–350.

Kubokawa, Y. Desorption of Olefins from Silica—Alumina Catalysts. *J. Phys. Chem.* **1965**, *69* (8), 2676–2679.

Lachter, E. R.; San Gil, R. A. D. S.; Tabak, D.; Costa, V. G.; Chaves, C. P. S.; Dos Santos, J. A. Alkylation of Toluene with Aliphatic Alcohols and 1-Octene Catalyzed by Cation-Exchange Resins. *React. Funct. Polym.* **2000**, *44* (1), 1–7.

Lambert, J. F.; Poncelet, G. Acidity in Pillared Clays: Origin and Catalytic Manifestations. *Top. Catal.* **1997**, *4* (1–2), 43–56.

Lambert, J. M., Jr.; Simkovich, G.; Walker, P. L., Jr.; The Kinetics and Mechanism of the Pyrite-to-Pyrrhotite Transformation. *Metall. Mater. Trans. B* **1998**, *29* (2), 385–396.

Lanin, S. N.; Vlasenko, E. V.; Kovaleva, N. V.; Zung, F. T. The Adsorption Properties of Titanium Dioxide. *Russ. J. Phys. Chem. A* **2008**, *82* (12), 2152–2155.

Larsen, C. R.; Erdogan, G.; Grotjahn, D. B. General Catalyst Control of the Monoisomerization of 1-Alkenes to *trans*-2-Alkenes. *J. Am. Chem. Soc.* **2014**, *136* (4), 1226–1229.

Letcher, T. M. Unconventional Oil: Oilsands. *Future Energy: Improved, Sustainable and Clean Options for our Planet*, 3rd ed.; Elsevier: Amsterdam, Netherlands, 2020; pp 49–65.

Lin, S. Y.; Tseng, J. M.; Lin, Y. F.; Huang, W. T.; Shu, C. M. Comparison of Thermal Polymerization Mechanisms for α-Methylstyrene and Trans-β-Methylstyrene. *J. Therm. Anal. Calorim.* **2008**, *93* (1), 257 267.

Liu, C. T. Aquathermolysis of Heavy Oil Model Compounds. *Adv. Mater. Res.* **2011**, *236-238*, 732–735.

Liu, D.; Yuan, P.; Liu, H.; Cai, J.; Tan, D.; He, H.; Zhu, J.; Chen, T. Quantitative Characterization of the Solid Acidity of Montmorillonite using Combined FTIR And TPD Based on the NH_3 Adsorption System. *Appl. Clay Sci.* **2013**, *80*, 407–412.

Liu, J.; Xu, Z.; Masliyah, J. Role of Fine Clays in Bitumen Extraction from Oil Sands. *AIChE J.* **2004**, *50* (8), 1917–1927.

Liu, X. Alkenes and Alkynes. *Organic Chemistry I;* Kwantlen Polytechnic University: Surrey, Canada, 2021; pp 332–366.

Liu, Y.; Xu, L.; Xu, B.; Li, Z.; Jia, L.; Guo, W. Toluene Alkylation with 1-Octene Over Supported Heteropoly Acids on MCM-41 Catalysts. *J. Mol. Catal. A: Chem.* **2009**, *297* (2), 86–92.

Liu, Z.; Li, Y.; Yu, F.; Zhu, J.; Xu, L. Co-Pyrolysis of Oil Sand Bitumen with Lignocellulosic Biomass Under Hydrothermal Conditions. *Chem. Eng. Sci.* **2019**, *199*, 417–425.

Li, X.; Bai, Y.; Sui, H.; He, L. Understanding Desorption of Oil Fractions from Mineral Surfaces. *Fuel* **2018**, *232*, 257–266.

Lopez-Linares, F.; Carbognani, L.; Stull, C. S.; Pereira-Almao, P.; Spencer, R. J. Adsorption of Virgin and Visbroken Residue Asphaltenes over Solid Surfaces. 1. Kaolin, Smectite Clay Minerals, and Athabasca Siltstone. *Energy Fuels* **2009**, *23* (4), 1901–1908.

Loudon, M. The Chemistry of Carboxylic Acid Derivatives. *Organic Chemistry*, 5th ed.; Roberts and Company Publishers: Greenwood Village, CO, 2009; pp 1004–1015.

Luo, Y. R. *Handbook of Bond Dissociation Energies in Organic Compounds*; CRC Press: Boca Raton, FL, 2003; p 31.

Ma, J.; Yang, Y.; Li, X.; Sui, H.; He, L. Mechanisms on the Stability and Instability of Water-in-Oil Emulsion Stabilized by Interfacially Active Asphaltenes: Role of Hydrogen Bonding Reconstructing. *Fuel* **2021**, *297*, 120763.

Mamonov, A.; Aslanidis, P.; Fazilani, N.; Puntervold, T.; Strand, S. Influence of Sandstone Mineralogy on the Adsorption of Polar Crude Oil Components and Its Effect on Wettability. *Energy Fuels* **2022**, *36* (18), 10785–10793.

Marriott, P. R.; Perkins, M. J.; Griller, D. Spin Trapping for Hydroxyl in Water: A Kinetic Evaluation of Two Popular Traps. *Can. J. Chem.* **1980**, *58* (8), 803–807.

Masliyah, J.; Czarnecki, J.; Xu, Z. *Handbook on Theory and Practice of Bitumen Recovery from Athabasca Oil Sands - Volume 1: Theoretical Basis*; Kingsley Knowledge Publishing: 2011; pp 177–192.

Masliyah, J.; Zhou, Z. J.; Xu, Z.; Czarnecki, J.; Hamza, H. Understanding Water-Based Bitumen Extraction from Athabasca Oil Sands. *Can. J. Chem. Eng.* **2004**, *82* (4), 628–654.

Mayr, H.; Lang, G.; Ofial, A. R. Reactions of Carbocations with Unsaturated Hydrocarbons: Electrophilic Alkylation or Hydride Abstraction? *J. Am. Chem. Soc.* **2002**, *124* (15), 4076–4083.

McCaulay, D. A.; Lien, A. P. Effect of Acid Strength on Alkylation of Arenes with Olefins. I. *m*-Xylene with Ethylene. *J. Am. Chem. Soc.* **1955**, *77* (7), 1803–1804.

Mehta B. J. Synthesis and Analysis of Dimers of Alpha-Methylstyrene. M.A. Thesis, Western Michigan University, Kalamazoo, MI, 1975.

Mikula1, R. J.; Axelson, D. E.; Sheeran, D. Mineral Matter and Clay-Organic Complexes in Oil Sands Extraction Processes. *Fuel Sci. Technol. Int* **1993**, *11* (12), 1695–1729.

Moir, M. E. Asphaltenes, what art thou? Asphaltenes and the Boduszynski Continuum. In *The Boduszynski Continuum: Contributions to the Understanding of the Molecular Composition of Petroleum*; Ovalles, C.; Moir, M. E.; ACS Symposium Series 1282; American Chemical Society: Washington DC, USA, 2018; pp 3–24.

Mohammed, M.; Babadagli, T. Wettability Alteration: A Comprehensive Review of Materials/Methods and Testing the Selected Ones on Heavy-Oil Containing Oil-Wet Systems. *Adv. Colloid Interface Sci.* **2015**, *220*, 54–77.

Montoya Sanchez, N.; De Klerk, A. Viscosity Mixing Rules for Bitumen at 1–10 wt % Solvent Dilution When Only Viscosity and Density Are Known. *Energy Fuels* **2020,** *34,* 8227−8238.

Moo-Young, M. Substrate Hydrolysis: Methods, Mechanism, and Industrial Applications of Substrate Hydrolysis. In *Comprehensive Biotechnology*; Webb, C.; Elsevier: Amsterdam, Netherlands, 2011; pp 103–118.

Morimoto, M.; Sugimoto, Y.; Sato, S.; Takanohashi, T. Bitumen Cracking in Supercritical Water Upflow. *Energy Fuels* **2014**, *28* (2), 858–861.

Morimoto, M.; Sugimoto, Y.; Saotome, Y.; Sato, S.; Takanohashi, T. Effect of Supercritical Water on Upgrading Reaction of Oil Sand Bitumen. *J. Supercrit. Fluids* **2010**, *55* (1), 223–231.

Moulkheir, A.; Harrane, A.; Belbachir, M. Maghnite-H$^+$, a Solid Catalyst for the Cationic Polymerization of α-Methylstyrene. *J. Appl. Polym. Sci.* **2008**, *109* (3), 1476–1479.

Mullins, O. C.; Sabbah, H.; Eyssautier, J.; Pomerantz, A. E.; Barré, L.; Andrews, A. B.; Ruiz-Morales, Y.; Mostowfi, F.; McFarlane, R.; Goual, L.; Lepkowicz, R. Advances in asphaltene science and the Yen–Mullins model. *Energy Fuels* **2012**, *26* (7), 3986–4003.

Müller, S.; Liu, Y.; Kirchberger, F. M.; Tonigold, M.; Sanchez-Sanchez, M.; Lercher, J. A. Hydrogen Transfer Pathways during Zeolite Catalyzed Methanol Conversion to Hydrocarbons. *J. Am. Chem. Soc.* **2016**, *138* (49), 15994–16003.

Mundle, S. O.; Kluger, R. Decarboxylation via Addition of Water to a Carboxyl Group: Acid Catalysis of Pyrrole-2-Carboxylic Acid. *J. Am. Chem. Soc.* **2009**, *131* (33), 11674–11675.

Murray, H. H. Overview—Clay Mineral Applications. *Appl. Clay Sci.* **1991**, *5* (5-6), 379–395.

Nagendrappa, G. Organic Synthesis Using Clay Catalysts. *Reson.* **2002**, *7* (1), 64–77.

Naghizada, N.; Prado, G. H. C.; De Klerk, A. Uncatalyzed Hydrogen Transfer during 100–250 °C Conversion of Asphaltenes. *Energy Fuels* **2017**, *31* (7), 6800–6811.

Nam, P. C.; Nguyen, M. T.; Chandra, A. K. The C−H and α(C− X) Bond Dissociation Enthalpies of Toluene, C_6H_5-CH_2X (X= F, Cl), and Their Substituted Derivatives: A DFT Study. *J. Phys. Chem. A* **2005**, *109* (45), 10342–10347.

Nassar, N. N. Asphaltene Adsorption onto Alumina Nanoparticles: Kinetics and Thermodynamic Studies. *Energy Fuels* **2010**, *24* (8), 4116–4122.

Nhieu, P.; Liu, Q.; Gray, M. R. Role of Water and Fine Solids in Onset of Coke Formation During Bitumen Cracking. *Fuel* **2016**, *166*, 152–156.

Nourozieh, H.; Kariznovi, M.; Abedi, J. Density and Viscosity of Athabasca Bitumen Samples at Temperatures up to 200C and Pressures up to 10 MPa. *SPE Reservoir Eval. Eng.* **2015,** *18* (03), 375–386.

Nwosu, U. G.; Roy, A.; Dela Cruz, A. L. N.; Dellinger, B.; Cook, R. Formation of Environmentally Persistent Free Radical (EPFR) in Iron (III) Cation-Exchanged Smectite Clay. *Environ. Sci.: Processes Impacts* **2016**, *18* (1), 42–50.

Ollinger, J. On Mimicking Nano-particulate Behaviors of Asphaltenes in Solution and at Interfaces. M.S. Thesis, University of Alberta, Edmonton, Canada, 2015.

Osborne, N.S.; Stimson, H.F.; Fiock, E.F.; Ginnings, D.C. The Pressure of Saturated Water Vapor in the Range 100° to 374° C. *Bur. Stand. J. Res.* **1933**, *10* (2), 155–188.

Pabst, W. Fundamental Considerations on Suspension Rheology. *Ceram.-Silik.* **2004**, *48* (1), 6–13.

Pal, R. New Generalized Viscosity Model for Non-Colloidal Suspensions and Emulsions. *Fluids* **2020,** *5* (3), 150.

Park, Y. K.; Kim, S. J.; You, N.; Cho, J.; Lee, S. J.; Lee, J. H.; Jeon, J. K. MoO_3/SiO_2 Catalysts for Double Bond Migration of 2-Butene. *J. Ind. Eng. Chem.* **2011**, *17* (2), 186–190.

Pavlik, M. The Dependence of Suspension Viscosity on Particle Size, Shear Rate, and Solvent Viscosity. M.S. Thesis, DePaul University, Chicago, IL, 2009.

Pavlovic, I.; Knez, Z.; Skerget, M. Hydrothermal Reactions of Agricultural and Food Processing Wastes in Sub-and Supercritical Water: A Review of Fundamentals, Mechanisms, and State of Research. *J. Agric. Food Chem.* **2013**, *61* (34), 8003–8025.

Payan, F.; De Klerk, A. Hydrogen Transfer in Asphaltenes and Bitumen at 250° C. *Energy Fuels* **2018**, *32* (9), 9340–9348.

Pentráková, L.; Su, K.; Pentrák., M.; Stucki, J. W. A Review of Microbial Redox Interactions with Structural Fe in Clay Minerals. *Clay Miner.* **2013**, *48* (3), 543–560.

Pernyeszi, T.; Patzkó, Á.; Berkesi, O.; Dékány, I. Asphaltene Adsorption on Clays and Crude Oil Reservoir Rocks. *Colloids Surf., A* **1998,** *137* (1-3), 373–384.

Pignatello, J. J. Soil Organic Matter as a Nanoporous Sorbent of Organic Pollutants. *Adv. Colloid Interface Sci.* **1998**, *76–77*, 445–467.

Poindexter, M. K.; Marsh, S. C. Inorganic Solid Content Governs Water-in-Crude Oil Emulsion Stability Predictions. *Energy Fuels* **2009**, *23* (3), 1258–1268.

Poletto, M.; Joseph, D. D. Effective Density and Viscosity of a Suspension. *J. Rheol.* **1995**, *39* (2), 323–343.

Pu, X.; Liu, N. W.; Jiang, Z. H.; Shi, L. Acidic and Catalytic Properties of Modified Clay for Removing Trace Olefin from Aromatics and Its Industrial Test. *Ind. Eng. Chem. Res.* **2012**, *51* (43), 13891–13896.

Qu, X.; Li, Y.; Li, S.; Wang, J.; Xu, H.; Li, Z. Thermal Cracking, Aquathermolysis, and their Upgrading Effects of Mackay River Oil Sand. *J. Petrol. Sci. Eng.* **2021**, *201*, 108473.

Rakhmatullin, I. Z.; Efimov, S. V.; Klochkov, A. V.; Gnezdilov, O. I.; Varfolomeev, M. A.; Klochkov, V. V. NMR Chemical Shifts of Carbon Atoms and Characteristic Shift Ranges in the Oil Sample. Pet. Res. **2022**, *7* (2), 269–274.

Rao, F.; Liu, Q. Froth Treatment in Athabasca Oil Sands Bitumen Recovery Process: A Review. *Energy Fuels* **2013**, *27* (12), 7199–7207.

Rat'ko, A. I.; Ivanets, A. I.; Kulak, A. I.; Morozov, E. A.; Sakhar, I. O. Thermal Decomposition of Natural Dolomite. *Inorg. Mater.* **2011**, *47* (12), 1372–1377.

Reausser College of Natural Resources, UC Berkeley. Chemical Formulae for Minerals and Gems. https://nature.berkeley.edu/classes/eps2/wisc/mineral.html (accessed April 17, 2023).

Ren, S.; Dang-Vu, T.; Zhao, H.; Long, J.; Xu, Z.; Masliyah, J. Effect of Weathering on Surface Characteristics of Solids and Bitumen from Oil Sands. *Energy Fuels* **2009**, *23* (1), 334–341.

Ringdalen, E. Changes in Quartz During Heating and the Possible Effects on Si Production. *JOM* **2015**, *67* (2), 484–492.

Robinson, J. W.; Frame, E. M. S.; Frame, G. M. II. *Undergraduate instrumental analysis*. CRC Press: Boca Raton, FL, 2014; p 21.

Rocha, J. A.; Baydak, E. N.; Yarranton, H. W. What Fraction of the Asphaltenes Stabilizes Water-in-Bitumen Emulsions? *Energy Fuels* **2018**, *32* (2), 1440–1450.

Romanova, U. G.; Valinasab, M.; Stasiuk, E. N.; Yarranton, H. W.; Schramm, L. L.; Shelfantook, W. E. The Effect of Oil Sands Bitumen Extraction Conditions on Froth Treatment Performance. *J. Can. Pet. Technol.* **2006**, *45* (09), 36–45.

Romanova, U. G.; Yarranton, H. W.; Schramm, L. L.; Shelfantook, W. E. Investigation of Oil Sands Froth Treatment. *Can. J. Chem. Eng.* **2004**, *82* (4), 710–721.

Roostaei, M.; Hosseini, S. A.; Soroush, M.; Velayati, A.; Alkouh, A.; Mahmoudi, M.; Ghalambor, A.; Fattahpour, V. Comparison of Various Particle-Size Distribution-Measurement Methods. *SPE Reservoir Eval. Eng.* **2020**, *23* (04), 1159–1179.

Rudin, A.; Choi, P. Free-Radical Polymerization. *The Elements of Polymer Science and Engineering*, 3rd ed.; Academic Press: Waltham, MA, 2013; pp 341–389. Ruiz-Morales, Y.; Mullins, O. C. Polycyclic Aromatic Hydrocarbons of Asphaltenes Analyzed by Molecular Orbital Calculations with Optical Spectroscopy. *Energy Fuels* **2007**, *21* (1), 256–265.

Rustamov, M. I.; Seidov, N. M.; Ibragimov, K. D.; Mamedbeili, E. G. Dimerization of α-Methylstyrene in the Presence of Mordenite, Aimed at Preparation of Transformer Oils. *Russ. J. Appl. Chem.* **2009**, *82* (2), 317–322.

Rutgers, I. R. Relative Viscosity and Concentration. *Rheol. Acta* **1962,** *2* (4), 305–348.

Sabbah, H.; Morrow, A. L.; Pomerantz, A. E.; Zare, R. N. Evidence for Island Structures as the Dominant Architecture of Asphaltenes. *Energy Fuels* **2011**, *25* (4), 1597–1604.

Sadovnikov, A. A.; Arapova, O. V.; Russo, V.; Maximov, A. L.; Murzin, D. Y.; Naranov, E. R. Synergy of Acidity and Morphology of Micro-/Mesoporous Materials in the Solid-Acid Alkylation of Toluene with 1-Decene. *Ind. Eng. Chem. Res.* **2022**, *61* (5), 1994–2009.

Sankey, B. M.; Maa, P. S.; Bearden, R., Jr. Conversion of the Organic Component from Tar Sands to Lower Boiling Products. U.S. Patent 5,795,464, August 18, 1998.

Sefton, E.; Sinton, D. Evaluation of Selected Viscosity Prediction Models for Water in Bitumen Emulsions. *J. Pet. Sci. Eng.* **2010**, *72*, 128–133.

Shelfantook, W. E. A Perspective on the Selection of Froth Treatment Processes. *Can. J. Chem. Eng.* **2004**, *82* (4), 704–709.

Sherman, P. The Viscosity of Emulsions. *Rheol. Acta* **1962**, *2* (1), 74–82.

Shiley, R. H.; Konopka, K. L.; Hinckley, C. C; Smith, G. V.; Twardowska, H.; Saporoschenko, M. *Effect of Some Metal Chlorides on the Transformation of Pyrite to Pyrrhotite*. Technical Report Number PB-82-255506; Illinois Department of Energy and Natural Resources, August 1982.

Shi, S.; Wang, Y.; Liu, Y.; Wang, L. A New Method for Calculating the Viscosity of W/O and O/W Emulsion. *J. Pet. Sci. Eng.* **2018,** *171*, 928–937.

Singh, M. B.; Rampal, N.; Malani, A. Structural Behavior of Isolated Asphaltene Molecules at the Oil–Water Interface. *Energy Fuels* **2018**, *32* (8), 8259–8267.

Siskin, M.; Brons, G.; Katritzky, A. R.; Murugan, R. Aqueous Organic Chemistry. 2. Crosslinked Cyclohexyl Phenyl Compounds. *Energy Fuels* **1990**, *4* (5), 482–488.

Siskin, M.; Brons, G.; Vaughn, S. N.; Katritzky, A. R.; Balasubramanian, M. Aqueous Organic Chemistry. 3. Aquathermolysis: Reactivity of Ethers and Esters. *Energy Fuels* **1990**, *4* (5), 488–492.

Siskin, M.; Katritzky, A. R. Reactivity of Organic Compounds in Superheated Water: General Background. *Chem. Rev.* **2001**, *101* (4), 825–836.

Solomon, D. H. Clay Minerals as Electron Acceptors and/or Electron Donors in Organic Reactions. *Clays Clay Miner*. **1968**, *16* (1), 31–39.

Solomon, D. H. Clay Minerals as Electron Acceptors and/or Electron Donors in Organic Reactions. *Clays Clay Miner.* **1968**, *16* (1), 31–39.

Soma, Y.; Soma, M. Chemical Reactions of Organic Compounds on Clay Surfaces. *Environ. Health Perspect.* **1989**, *83*, 205–214.

Speight, J. G. Petroleum Asphaltenes - Part 1: Asphaltenes, Resins and the Structure of Petroleum. *Oil Gas Sci. Technol.* **2004**, *59* (5), 467–477.

Statistical Review of World Energy - All Data, 1965-2021. *BP Statistical Review of World Energy* [Online]; London, 2022. https://www.bp.com/en/global/corporate/energy-economics/statistical-review-of-world-energy.html (accessed Nov 5, 2022).

Stewart, I.; Whiteway, S. G.; Cleyle, P. J.; Caley, W. F. Decomposition of Pyrite in a Coal Matrix During the Pyrolysis of Coal. In *Mineral Matter and Ash in Coal*; Vorres, K. S., Eds.; ACS Symposium Series; American Chemical Society: Washington, DC, 1986; Vol. 301, pp 485–499.

Stoffyn-Egli, P.; Lee, K. Formation and Characterization of Oil–Mineral Aggregates. *Spill Sci. Technol. Bull.* **2002**, *8* (1), 31–44.

Strausz, O. P.; Lown, E. M. 2003. *The Chemistry of Alberta Oil Sands, Bitumens and Heavy Oils*; Alberta Energy Research Institute: Calgary, Canada, 2003; pp 24–636.

Subramanian, S.; Simon, S.; Gao, B.; Sjöblom, J. Asphaltene Fractionation Based on Adsorption onto Calcium Carbonate: Part 1. Characterization of Sub-Fractions and QCM-D Measurements. *Colloids Surf., A* **2016**, *495*, 136–148.

Tannous, J. H.; De Klerk, A. Quantification of the Free Radical Content of Oilsands Bitumen Fractions. *Energy Fuels* **2019**, *33* (8), 7083–7093.

Tekin, K.; Karagöz, S.; Bektaş, S. A Review of Hydrothermal Biomass Processing. *Renewable Sustainable Energy Rev*. **2014**, *40*, 673–687.

Telmadarreie, T.; Berton, P.; Bryant, S. L. Treatment of Water-in-Oil Emulsions Produced by Thermal Oil Recovery Techniques: Review of Methods and Challenges. *Fuel* **2022**, *330*, 125551.

Tian, M.; McCormick, R. L.; Luecke, J.; De Jong, E.; Van Der Waal, J. C.; Van Klink, G. P. M.; Boot, M. D. Anti-Knock Quality of Sugar Derived Levulinic Esters and Cyclic Ethers. *Fuel* **2017**, *202*, 414–425.

Thermodynamic and transport properties of organic salts (IUPAC Chem. Data Ser. 28); Franzosini, P., Sanesi, M. Eds.; Pergamon Press: Oxford, 1980.

Thomas, M. M.; Clouse, J. A.; Longo, J. M. Adsorption of Organic Compounds on Carbonate Minerals: 1. Model Compounds and Their Influence on Mineral Wettability. *Chem. Geol.* **1993**, *109* (1–4), 201–213.

Török, B.; Schäfer, C.; Kokel, A. Friedel-Crafts and Related Reactions Catalyzed by Solid Acids. *Heterogeneous Catalysis in Sustainable Synthesis*; Elsevier: Amsterdam, Netherlands, 2021; pp 317–378.

Tumanyan, B. P.; Petrukhina, N. Y. N.; Kayukova, G. P.; Nurgaliev, D. K.; Foss, L. E.; Romanov, G. V. Aquathermolysis of Crude Oils and Natural Bitumen: Chemistry, Catalysts and Prospects for Industrial Implementation. *Russ. Chem. Rev.* **2015**, *84* (11), 1145.

Turuga, A. S. S. Effect of Solvent Deasphalting Process on the Properties of Deasphalted Oil and Asphaltenes from Bitumen. M.S. Thesis, University of Alberta, Edmonton, Canada, 2017.

Tu, Y.; Kingston, D.; Kung, J.; Kotlyar, L. S.; Sparks, B. D.; Chung, K. H. Adsorption of Pentane Insoluble Organic Matter from Oilsands Bitumen onto Clay Surfaces. *Pet. Sci. Technol.* **2006**, *24* (3–4), 327–338.

University of South Alabama. Mineral Chemical Groups and Formulae for Rock Forming Minerals. https://www.southalabama.edu/geography/allison/GY111/MineralFormulaTable.pdf (accessed April 17, 2023).

Uzcátegui, G.; Fong, S. Y.; De Klerk, A. Cracked Naphtha Reactivity: Effect of Free Radical Reactions. *Energy Fuels* **2018**, *32* (5), 5812–5823.

van Bodegom, B.; van Veen, J. A. R.; van Kessel, G. M. M.; Sinnige-Nijssen, M. W. A; Stuiver, H. C. M. Action of Solvents on Coal at Low Temperatures: 1. Low-Rank Coals. *Fuel* **1984,** *63* (3), 346–354.

Van Der Merwe, S.; Diep, J. K. Q.; Shariati, M. R.; Hann, T. Process and System for Solvent Addition to Bitumen Froth. U.S. Patent 10,041,005, Aug 7, 2018.

Van Der Merwe, S; Hann, T. Process for Integration of Paraffinic Froth Treatment Hub and a Bitumen Ore Mining and Extraction Facility. U.S. Patent 9,546,323, January 17, 2017.

Velayati, A.; Habibi, A.; Nikrityuk, P.; Tang, T.; Zeng, H. Emulsions in Bitumen Froth Treatment and Methods for Demulsification and Fines Removal in Naphthenic Froth Treatment: Review and Perspectives. *Energy Fuels* **2022**, *36* (16), 8607–8623.

Vilcáez, J.; Watanabe, M.; Watanabe, N.; Kishita, A.; Adschiri, T. Hydrothermal Extractive Upgrading of Bitumen Without Coke Formation. *Fuel* **2012**, *102*, 379–385.

Vinoth Kumar, K. C.; Jani Subha, T. FT-IR Spectroscopic Analysis of Seasonal Impact of Mineral Assemblage in Coastal Soil Samples and its Structural Study. *Int. J. Adv. Sci. Res. Manage.* **2019**, *4* (4), 245–252.

Wang, D.; Qiao, C.; Zhao, Z.; Yang, W.; Chen, H.; Yin, T.; Yan, Z.; Wu, M.; Mao, X.; Santander, C.; Liu, Q.; Liu, Q.; Nikrityuk, P. A.; Tang, T.; Zeng, Hongbo. Understanding the Properties of

Bitumen Froth from Oil Sands Surface Mining and Treatment of Water-in-Oil Emulsions. *Energy Fuels* **2021**, *35* (24), 20079–20091.

Wang, H.; Li, C.; Peng, Z.; Zhang, S. Characterization and Thermal Behavior of Kaolin. *J. Therm. Anal. Calorim.* **2011**, *105* (1), 157–160.

Wang, L.; Zachariah, A.; Yang, S.; Prasad, V.; De Klerk, A. Visbreaking Oilsands-Derived Bitumen in the Temperature Range of 340–400° C. *Energy Fuels* **2014**, *28* (8), 5014–5022.

Wen, J.; Zhang, J.; Wei, M. Effective Viscosity Prediction of Crude Oil-Water Mixtures with High Water Fraction. *J. Pet. Sci. Eng.* **2016**, *147*, 760–770.

Wiehe, I. A. A Phase-Separation Kinetic Model for Coke Formation. *Ind. Eng. Chem. Res.* **1993**, *32* (11), 2447–2454.

Worasith, N.; Ninlaphurk, S.; Mungpayaban, H.; Wen, D.; Goodman, B. A. Characterization of Paramagnetic Centres in Clay Minerals and Free Radical Surface Reactions by EPR Spectroscopy. In *Clays and Clay Minerals: Geological Origin, Mechanical Properties and Industrial Applications*, Wesley, L. R.; Eds.; Nova Science Publ.: New York, NY, 2014; pp 336–359.

Worasith, N.; Ninlaphurk, S.; Mungpayaban, H.; Wen, D.; Goodman, B. A. Characterization of Paramagnetic Centres in Clay Minerals and Free Radical Surface Reactions by EPR Spectroscopy. In *Clays and Clay Minerals: Geological Origin, Mechanical Properties and Industrial Applications*, Wesley, L. R.; Eds.; Nova Science Publ.: New York, NY, 2014; pp 336–359.

Wu, C.; Lei, G. L.; Yao, C. J.; Sun, K. J.; Gai, P.Y.; Cao, Y. B. Mechanism for Reducing the Viscosity of Extra-Heavy Oil by Aquathermolysis with an Amphiphilic Catalyst. *J. Fuel Chem. Technol.* **2010**, *38* (6), 684–690.

Wypych, F.; De Freitas, R. A. Clay minerals: Classification, structure, and properties. In *Clay Minerals and Synthetic Analogous as Emulsifiers of Pickering Emulsions*; Developments in Clay Science; Elsevier: Amsterdam, Netherlands, 2022; Vol. 10, pp 3–35.

Xu, Y. Asphaltene Precipitation in Paraffinic Froth Treatment: Effects of Solvent and Temperature. *Energy Fuels* **2017**, *32* (3), 2801–2810.

Yañez Jaramillo, L. M.; De Klerk, A. Is Solubility Classification a Meaningful Measure in Thermal Conversion?. *Energy Fuels* **2022**, *36* (16), 8649–8662.

Yañez Jaramillo, L. M.; De Klerk, A. Partial Upgrading of Bitumen by Thermal Conversion at 150–300° C. *Energy Fuels* **2018**, *32* (3), 3299–3311.

Yang, F. Bitumen Fractions Responsible for Stabilizing Water in Oil Emulsions. Ph.D. Dissertation, University of Alberta, Edmonton, Canada, 2016.

Yan, N.; Masliyah, J. H. Effect of pH on Adsorption and Desorption of Clay Particles at Oil–Water Interface. *J. Colloid Interface Sci.* **1996**, *181* (1), 20–27.

Yi, F.; Cao, J. P.; Xu, D.; Tao, Z.; Hu, C.; Bai, Y.; Zhao, G.; Chen, H.; Yang, Y.; Li, Y. Mechanisms of Double-Bond Migration Reactions of Pentene Isomers on Different Lewis Acids. *Appl. Surf. Sci.* **2022**, *589*, 152970.

Yi, F.; He, P.; Chen, H.; He, Y.; Tao, Z.; Li, T.; Zhao, G.; Yun, Y.; Wen, X.; Yang, Y.; Li, Y. Mechanisms of Double-Bond Isomerization Reactions of *n*-Butene on Different Lewis Acids. *ACS Catal.* **2021**, *11* (17), 11293–11304.

Yu, X.; Zhai, C.; Jing, Y.; Sang, S.; Wang, Y.; Regenauer-Lieb, K.; Sun, Y. Investigation of the Temperature Dependence of the Chemical–Mechanical Properties of the Wufeng–Longmaxi Shale. *ACS Omega* **2022**, *7* (49), 44689–44697.

Zachariah, A.; De Klerk, A. Partial Upgrading of Bitumen: Impact of Solvent Deasphalting and Visbreaking Sequence. *Energy Fuels* **2017**, *31* (9), 9374–9380.

Zachariah, A.; De Klerk, A. Thermal Conversion Regimes for Oilsands Bitumen. *Energy Fuels* **2016**, *30* (1), 239–248.

Zhang, H.; Sun, Z.; Hu, Y. H. Steam Reforming of Methane: Current States of Catalyst Design and Process Upgrading. *Renewable Sustainable Energy Rev.* **2021**, *149*, 111330.

Zhang, X.; Liu, Y.; Fan, Y.; Che, H. Effects of Reservoir Minerals and Chemical Agents on Aquathermolysis of Heavy Oil During Steam Injection. *China Pet. Process. Petrochem. Technol.* **2010**, *12* (3), 25–31.

Zhao, H.; Dang-Vu, T.; Long, J.; Xu, Z.; Masliyah, J. H. Role of Bicarbonate Ions in Oil Sands Extraction Systems with a Poor Processing Ore. *J. Dispers. Sci. Technol.* **2009**, *30* (6), 809–822.

Zhao, J.; Liu, Q.; Gray, M. R. Characterization of Fine Solids in Athabasca Bitumen Froth Before and After Hydrothermal Treatment. *Energy Fuels* **2016**, *30* (3), 1965–1971.

Zhao, X. A Kinetic Study of the Hydrogenation and Dimerization of Styrene and α-Methylstyrene on Ni-Mo-S Catalyst. M.S. Thesis, The University of British Columbia, Vancouver, Canada, 2015.

Zhao, Y.; Wei, F. Simultaneous Removal of Asphaltenes and Water from Water-in-Bitumen Emulsion: I. Fundamental Development. *Fuel Process. Technol.* **2008**, *89* (10), 933–940.

Zhong, J.; Wang, P.; Zhang, Y.; Yan, Y.; Hu, S.; Zhang, J. Adsorption Mechanism of Oil Components on Water-Wet Mineral Surface: A Molecular Dynamics Simulation Study. *Energy* **2013**, *59*, 295–300.

Benazzi, E.; Travers, C.; Gnep, N. S.; Andy, P.; Guisnet. M. Selective Skeletal Butene Isomerization Through a Bimolecular Mechanism. *Oil Gas Sci. Technol.* **1999**, *54* (1), 23–28.

Appendices

Appendix A. Supporting Information for Chapter 3.

A.1. Photos of Micro Batch Reactors:

(a)   (b)

**Figure A. 1.** Photos of Micro Batch Reactors used in (a) Reactions B, B+S, B+W+S

(b) Reaction B+W

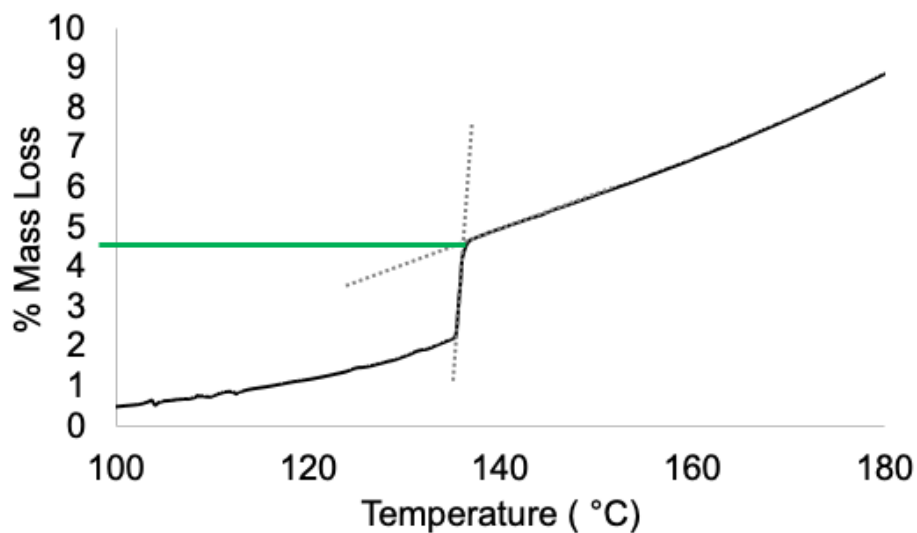### A.1. Estimation of Residual Toluene in Bitumen-Toluene Mixtures:

In bitumen samples containing toluene, as in the current study, the toluene content can be estimated using simulated distillation (simdis) and thermogravimetric analysis (TGA). This was tested by spiking Athabasca bitumen with known amounts of toluene. In the boiling point vs. percentage recovery of bitumen-toluene mixture obtained in simdis as shown in Figure A. 2.(a), the region between 100 and 200 °C is of interest. Until around 110 °C, the simdis curve is almost vertical or parallel to y-axis, as represented by the dotted line at 110 °C. At temperature around 110 °C, a change in the shape of the curve was observed. Above 150 °C, the percentage recovery increases almost linearly with respect to the boiling point until 200 °C, as represented by the other dotted

line. The point of intersection of the two dotted lines (indicated by the green line) coincided with the toluene content (wt %) in the bitumen sample (In Figure A. 2.(a) this amount was equal to ~4.65 wt %).

The same was estimated in TGA of Athabasca bitumen-toluene mixtures as shown in Figure A. 2.(b). The shape of the TGA curve shown in Figure A. 2.(b) is different from that of the simdis curve shown in Figure A. 2.(a). In TGA, a sharp rise in the percentage mass lost was observed between 120 and 140 °C, as indicated by the dotted line in Figure A. 2.(b) after which the shape of the curve changes, as indicated by the other dotted line. The point where the curve changes shape from the sharp rise, or at which the two dotted lines intersect (indicated by the green line) coincided with the amount of toluene (wt %) in the bitumen sample. (In Figure A. 2.(b) this amount was also equal to ~4.65 wt %).
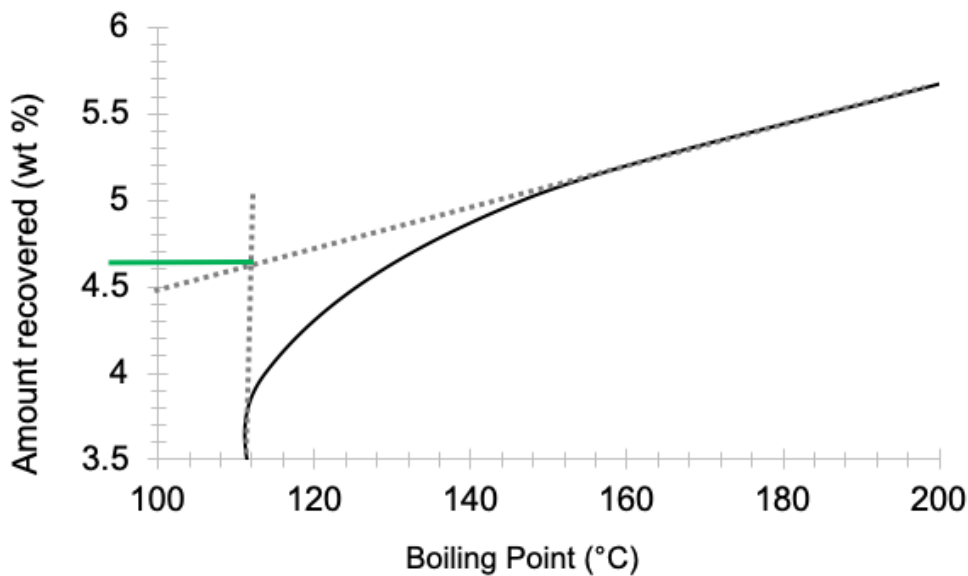
(a)

(b)

Figure A. 2. Determination of Residual Toluene in a Bitumen-Toluene Mixture containing

~4.7 wt % toluene using (a) Simdis and (b) TGA

A.2. Mineral Characterization by X-Ray Diffraction:

The mineral composition of solids in froth was determined by the Department of Earth and Atmospheric Sciences, University of Alberta. A ~ 2.5 g aliquot of the mineral solids sample was ground under 100% ethanol for 5 minutes in a McCrone micronizing mill using synthetic agate pellets. Micronized aliquots were air dried and later analyzed on a Rigaku Ultima IV powder X-ray diffractometer (XRD), which is equipped with a cobalt X-ray source that was operated at 38 mA and 38 kV. The X-ray wavelengths (Å) (Table A. 1.) and instrument specifications are as follows:

Table A. 1. X-ray Wavelengths

Anode	Wavelength (Å)		
Co	Kα1 (100)	Kα2 (50)	Kβ1
	1.78900	1.79283	1.62083

- Focusing Geometry: Bragg-Brentano Mode

- Detector: D/teX Ultra with Fe Filter (K-beta filter)

- Slit sizes used:

  - Divergence Slit - 2/3deg

  - Divergence Height Limiting Slit - 10mm

  - Scattering slit - open

  - Receiving Slit - open

The samples were mounted in a 2 mm deep alumina well, and the XRD patterns were collected from 5–80° 2θ range, using a sampling width of 0.02° 2θ, at a speed of 1.2° 2θ/min. Qualitative phase identification was achieved using the EVA V4.3.0.1. (Bruker) and JADE 9.6 (Rigaku) software packages, and quantification was performed using the Bruker AXS TOPAS v5 software.

Qualitative XRD: Qualitative phase identification was performed using the EVA (Bruker) and JADE (Rigaku) software packages. Mineral phases were identified with respect to the International Center for Diffraction Data Powder Diffraction File 4+ (ICDD PDF4+) database.

Quantitative XRD: Rietveld refinements of the XRD data were performed to determine mineral abundances with Bruker AXS TOPAS v5 software.[1-3] Unit cell parameters were calibrated using the NIST certified standard reference material SRM 660b, consisting of lanthanum hexaboride (LaB$_6$). These parameters were refined and the fundamental parameters approach to peak fitting was utilized for all phases.[4] During refinement, a Rietveld-compatible structureless fitting analysis was used to model the peaks of kaolinite to account for the turbostratic stacking disorder.[5,6] The Pawley/Internal-standard method,[6,7] was applied to generate a peaks phase kaolinite with a pattern collected from the Clay Minerals Society's Source Clay KGa-2 kaolinite. This peaks phase was used to make a partial or no known crystal structure (PONKCS) phase by refinement of a pattern

collected from a mixture of KGa-2 kaolinite and synthetic corundum (50%–50% (wt/wt)) using the method of Scarlett and Madsen.[5]

Table A. 2. contains the mineralogical composition of the froth solids, determined by quantitative XRD analysis. As mentioned in the Chapter 3, the solids contained organic matter, whose weight is not considered in the calculation of the mineral distribution of solids. In other words, the amount of each mineral (wt %) was calculated on the basis of total amount of minerals in the solids. Quartz and kaolinite were identified as the major minerals in the froth solids, constituting 79% of the total mineral content on weight basis.

Table A. 2. Mineralogical Composition of Solids

Mineral	Chemical Formula	wt % [a]
Quartz	SiO_2	53.3
Anatase	TiO_2	2.5
Magnesite	$MgCO_3$	0.7
Calcite	$CaCO_3$	0.8
Muscovite-2*M1*	$KAl_2(AlSi_3O_{10})(OH)_2$	6.1
Microcline	$KAlSi_3O_8$	2.2
Pyrite	FeS_2	2.2
Rutile	TiO_2	3.6
Siderite	$FeCO_3$	2.1
Dolomite	$CaMg(CO_3)_2$	0.8
Kaolinite	$Al_2Si_2O_5(OH)_4$	25.6

[a] Only a single measurement was performed

A.3. Water Analysis

The characterization of water phase isolated from froth is given in Table A. 3. The major cations and anions generally present in the connate water of oil sands and process water, such as sodium, potassium, calcium, magnesium, chloride, sulfate, phosphate, nitrite and nitrate were analyzed.

Ion-exchange reactions and dissolution are two ways in which some of the components present in the bitumen and solid phases can enter the aqueous phase. Therefore, in addition to the elements mentioned above, additional elements that are expected to be present in untreated bitumen such as Cu, Fe, Ni, V, Mn and Zn were also analyzed. Analysis of the elements found in the minerals in froth such as Al and Ti was also performed.

Table A. 3. Characterization of Water Phase Isolated from Bitumen Froth [a]

Element	Units	x	s
Al	µg/g	1	0.02
B	µg/g	- [b]	- [b]
Ca	µg/g	8	0.02
Cu	µg/g	- [c]	- [c]
Fe	µg/g	4	1
K	µg/g	0.3	0
Mg	µg/g	6	0.01
Mn	µg/g	0	0
Na	µg/g	722	2
Ni	µg/g	0.1	0
Si	µg/g	- [b]	- [b]
Ti	µg/g	0.1	0.02
V	µg/g	0.02	0
Zn	µg/g	- [c]	- [c]
NH_4-N	mg/L	1	- [d]
SO_4-S	mg/L	52	- [d]
NO_2-N	µg/L	81	- [d]
PO_4-P	µg/L	53	- [d]
Cl^-	mg/L	812	- [d]
TON [e]	µg/L	143	- [d]
pH		8.3	0.1

| Conductivity | mS/cm | 1.7 | 0.5 |

[a] Analysis of three samples; average (x) and standard deviation (s)

[b] Elements absent in the calibration standard

[c] Below Detection Limit

[d] Only a single measurement was performed

[e] Sum of NO_2-N and NO_3-N. NO_3-N can be obtained by calculation

The cations were analyzed using ICP-OES, and the procedure is similar to that followed for the treated water samples that is given in the Chapter 3. Anions NH_4-N, SO_4-S, NO_2-N, PO_4-P, Cl- and total organic nitrogen (TON) in the water samples were analyzed by the Natural Resources Analytical Laboratory at University of Alberta using a Thermo Gallery Plus Beermaster Autoanalyzer. Beer-Lambert law was applied to obtain the concentration of the analyte in the sample from the measured light absorbances of colored complexes that were formed upon reaction between the samples and reagents.

As shown in Table A. 3., sodium and chloride were the major ions in the aqueous phase, present in concentrations greater than 700 ppm and 800 ppm respectively. The concentrations of Ca, Mg and Fe were between 5 and 10 ppm, and the rest of the cations were less than 1 ppm in concentration. Among the anions, the concentration of sulfates, phosphates, nitrites and nitrates was greater than 50 ppm. The water was slightly alkaline with a pH around 8.3.

A.4. Viscosity and Density Correction of Bitumen-Solid, Bitumen-Water and Bitumen-Organic Solvent Mixtures:

In the current study, Eq A. 1-Eq A. 3 listed in Table A. 4. were used in the same sequence to calculate the viscosity of continuous phase in each case (η_{b+t+w}, η_{b+t}, η_b) and finally obtain the viscosity of pure bitumen (η_b). As the maximum value for the solids concentration ($\emptyset_s$) in the contaminated bitumen samples was ~0.003, Einstein's relation for the prediction of viscosity of dilute suspensions, generally valid for $\emptyset_s \leq 0.02$,[8] was applied. For this correction, the solids were assumed to be rigid and non-interacting spherical particles. The Einstein's relation for suspensions can be extended to dilute emulsions. In this work, the maximum value for the volume fraction of water ($\emptyset_w$) in the liquid mixture was ~0.004. Under an assumption that the water droplets are perfectly spherical, the distance between them is very large compared to their diameter, and no interaction occurs, the Einstein's relation was applied to correct the viscosity of the water-diluted bitumen emulsion. Further, Miadonye's mixing rule was applied to the bitumen-toluene mixture in order to calculate the viscosity of pure bitumen. This correlation is applicable to single-phase, Newtonian liquid mixtures and was found to give a better viscosity estimation for bitumen-toluene mixtures at the temperatures used in this study.[9]

Table A. 4. Viscosity Correction Methods for Contaminated Bitumen Samples used in this study [a]

Viscosity Correction for	Type of Mixture	Author/Method	Equation	
Solids	Suspension	Einstein	$\eta_{r_1} = (1+2.5\emptyset_s)$ $\eta_{r_1} = \dfrac{\eta_m}{\eta_{b+t+w}}$ $\emptyset_s = w_s \times \dfrac{\rho_m}{\rho_s}$	Eq A. 1
Water	Emulsions	Einstein	$\eta_{r_2} = (1+2.5\emptyset_w)$ $\eta_{r_2} = \dfrac{\eta_{b+t+w}}{\eta_{b+t}}$ $\emptyset_w = w_w \times \dfrac{\rho_{b+t+w}}{\rho_w}$	Eq A. 2
Toluene	Bitumen-Organic Solvent	Miadonye	$v_{b+t} = \exp\left(\exp\left(\alpha(1-w_t{}^n)\right) + \ln(v_t) - 1\right)$ $\alpha = \ln\left(\ln(v_b) - \ln(v_t) + 1\right)$ $n = \dfrac{v_t}{0.9029v_t + 0.1351}$ $v_{b+t} = \dfrac{\eta_{b+t}}{\rho_{b+t}} \times 10^6$ $\eta_b = \dfrac{v_b \times \rho_b}{10^6}$	Eq A. 3

[a] List of symbols used: η_{r_1}, relative viscosity of suspension; η_{r_2}, relative viscosity of water-in-oil emulsion; η_m, measured dynamic viscosity of contaminated bitumen sample (Pa.s.); η_{b+t+w}, dynamic viscosity of bitumen, toluene and water mixture (Pa.s.); η_{b+t}, dynamic viscosity of bitumen and toluene mixture (Pa.s.); η_b, dynamic viscosity of bitumen (Pa.s.); v_{b+t}, kinematic viscosity of bitumen and toluene mixture (cSt); v_t, kinematic viscosity of toluene (cSt); v_b, kinematic viscosity of bitumen (cSt); ρ_m, measured density of contaminated bitumen sample (kg/m³); ρ_s, density of solids (kg/m³); ρ_{b+t+w}, density of bitumen, toluene and water mixture (kg/m³); ρ_w, density of water (kg/m³); ρ_{b+t}, density of bitumen and toluene mixture (kg/m³); ρ_b, density of bitumen (kg/m³); w_s, mass fraction of solids in contaminated bitumen sample; w_w, mass fraction water in bitumen, toluene and water mixture; w_t, mass fraction of toluene in bitumen and toluene mixture; $\emptyset_s$, volume fraction of solids in the contaminated bitumen sample; $\emptyset_w$, volume fraction of water in bitumen, toluene and water mixture.

In the above equations, the densities ρ_{b+t+w} and ρ_b were obtained at different temperatures from the calculations in Table A. 6. of this document. As the density correction for water was ignored, same values were used for ρ_{b+t+w} and ρ_{b+t} for the viscosity correction. The average density of froth solids (ρ_s) used in this study was determined as 2253 kg/m³ applying the technique of water displacement. The values of density of water (ρ_w)[10] and kinematic viscosity of toluene (v_t) used in the calculations are given in Table A.5.

v_t was calculated from Eq A. 4, for which the density and dynamic viscosity of toluene (ρ_t and η_t respectively) were calculated at different temperatures (T in units K) from Eq A. 5 and Eq A. 6 respectively. These equations for determining the density and viscosity of toluene at different temperatures were developed by Krall, et al.[11]

$$v_t(cSt) = \frac{\eta_t\,(Pa.s.)}{\rho_t\left(\frac{kg}{m^3}\right)} \times 10^6 \qquad \text{Eq A. 4}$$

$$\rho_t\left(\frac{kg}{m^3}\right) = 1103.15 - 0.68109(T) - 0.4228 \times 10^{-3}(T)^2 \qquad \text{Eq A. 5}$$

$$\eta_t = 12.977182 \times \exp\left(\frac{0.036136}{T^0} + \frac{0.061266}{T^{o3}}\right)$$
$$\times \left[\frac{\rho_0}{1 - \rho_0(0.271276 + 0.048892(T^0))}\right] \qquad \text{Eq A. 6}$$

$$\rho_0 = \frac{\rho_t}{290.2} \;;\; T^0 = \frac{T}{593.91}$$

Table A. 5. Properties of Water and Toluene at 20 °C, 40 °C and 60 °C

Property	Symbol	20 °C	40 °C	60 °C
Density of Water (kg/m³)	ρ_w	998.2	992.2	983.2
Dynamic Viscosity of Toluene (Pa.s.)	η_t	5.92E-04	4.69E-04	3.82E-04
Density of Toluene (kg/m³)	ρ_t	867.2	848.4	829.3
Kinematic Viscosity of Toluene (cSt)	v_t	0.68	0.55	0.46

The equations used for correction of densities of contaminated bitumen samples are shown in Table A. 6. The mean density formula for suspensions, reported in literature,[12] was used in the estimation of liquid mixture (bitumen + toluene + water) density. Correction of density for the presence of water in bitumen from the B+W ($\emptyset_w$) ~ 0.004) and B+W+S ($\emptyset_w$) ~ 0.003) reactions was not performed as theoretical models for the prediction of density of emulsions with the parameters available in this work were not found in literature. The liquid density obtained after correction for presence of solids was directly corrected for the presence of toluene, under an assumption that no volume change occurred upon mixing (ideal mixing). The equation used for correction of toluene served well in previous studies for estimating the densities of mixtures containing Athabasca bitumen and aromatic solvents (such as toluene and xylene) in the concentration and temperature ranges used in this study, suggesting that ideal mixing would be a good approximation in these systems.[9,13]

Table A. 6. Density Correction Methods for Contaminated Bitumen Samples used in this study [a]

Viscosity Correction for	Type of Mixture	Method	Equation	
Solids	Suspension	Mean density	$\rho_m = \rho_{b+t+w}(1 - \emptyset_s) + \rho_s\emptyset_s$ $\emptyset_s = w_s \times \dfrac{\rho_m}{\rho_s}$	Eq A. 7
Toluene	Bitumen-Organic Solvent	No volume change	$\rho_{b+t+w} = \dfrac{1}{\dfrac{w_t}{\rho_t} + \dfrac{1 - w_t}{\rho_b}}$	Eq A. 8

[a] List of symbols used: ρ_m, measured density of contaminated bitumen sample (kg/m^3); ρ_s, density of solids (kg/m^3); ρ_{b+t+w}, density of bitumen, toluene and water mixture (kg/m^3); ρ_t, density of toluene (kg/m^3); ρ_b, density of bitumen (kg/m^3); w_s, mass fraction of solids in contaminated bitumen sample; w_t, mass fraction of toluene in bitumen and toluene mixture; $\emptyset_s$, volume fraction of solids in the contaminated bitumen sample.

A.5. Correction of Other Properties:

Elemental (C, H, N, S) Composition. The amounts of water (source of hydrogen) and toluene (source of carbon and hydrogen) in the contaminated bitumen samples were considered to calculate the actual amounts of C, H, N and S in contaminated bitumen samples. These values were then converted to wt % on bitumen weight basis (Table A. 7.). In this correction, the amounts of sulfur and carbon originating from the combustion of pyrite and carbonates in the froth solids were neglected due to their negligible quantities according to Table A. 2.

Table A. 7. Elemental (C, H, N, S) Composition (wt %) and Molar element ratios of Bitumen

Before and After Reaction [a]

Bitumen Sample	C		H		N		S	
	x	s	x	s	x	s	x	s
untreated bitumen	83.72	0.24	10.28	0.03	0.55	0.002	4.82	0.01
B+W+S	84.92	1.29	10.57	0.24	0.54	0.01	5.17	0.09
B	84.38	0.91	10.63	0.17	0.52	0.01	5.13	0.23
B+W	82.57	0.47	10.47	0.01	0.53	0.01	5.16	0.03
B+S	84.49	0.92	10.61	0.11	0.54	0.03	5.09	0.34
Bitumen Sample	H/C		N/C		S/C	
	x	s	x	s	x	s
untreated bitumen	1.47	0.00000	0.006	0.00000	0.022	0.00000
B+W+S	1.49	0.01	0.005	0.00004	0.023	0.0001
B	1.51	0.01	0.005	0.00004	0.023	0.0008
B+W	1.52	0.01	0.006	0.00003	0.023	0.0003
B+S	1.51	0.001	0.005	0.00033	0.023	0.0018

[a] Average (x) and sample standard deviation (s) of corrected values of each individual measurement in Table 3-11 of Chapter 3.

***n*-heptane insoluble content.** The effective n-heptane insoluble content in bitumen was calculated by subtracting the amounts of residual mineral solids in the samples from the measured n-heptane insoluble content values given in Table 3-12 of Chapter 3. This is because precipitation of asphaltenes using n-heptane would also result in the precipitation of *n*-heptane insoluble inorganic material present in the contaminated bitumen sample. The calculated result was then expressed as wt % on the basis of bitumen weight as shown in Table 3-19 of Chapter 3.

Total Acid Number (TAN), Free Radical Concentration and Metal Content. The corrected values of TAN (mg KOH/g), free radical concentration (spins/g) and metal content (µg/g), all expressed on bitumen weight basis, can be found in Table A. 8., Table A. 9. And Table A.10. respectively.

Table A. 8. Corrected Total Acid Number (TAN) of Bitumen Before and After Reaction

Bitumen Sample	TAN (mg KOH/g) [a]	
	x	s
untreated bitumen	4.0	0.2
B+W+S	5.2	0.2
B	4.6	0.1
B+W	4.6	0.1
B+S	4.7	0.1

[a] Average (x) and sample standard deviation (s) of corrected values of each individual measurement in Table 3-13 of Chapter 3.

Table A. 9. Corrected Free Radical Content (spins/g) in Bitumen Before and After Reaction

Bitumen Sample	Free Radical Content (spins/g) [a]	
	x	s
untreated bitumen	3.2×10^{17}	1.1×10^{16}
B+W+S	3.6×10^{17}	3.8×10^{15}
B	3.4×10^{17}	7.3×10^{16}
B+W	3.9×10^{17}	7.0×10^{16}
B+S	4.5×10^{17}	7.0×10^{15}

[a] Average (x) and sample standard deviation (s) of corrected values of each individual measurement in Table 3-14 of Chapter 3.

Table A. 10. Corrected Metal Concentration ($\mu g/g$) in Bitumen Before and After Reaction [a]

Element	Untreated bitumen		B+W+S		B		B+W		B+S	
	x	s	x	s	x	s	x	s	x	s
Al	68.53	0.21	44.98	0.73	68.06	1.18	49.39	0.18	47.21	0.54
B	14.09	0.07	3.66	0.08	13.09	0.24	11.30	0.08	3.72	0.05
Ca	13.85	0.05	8.65	0.14	13.23	0.25	13.57	0.06	13.43	0.16
Cu	2.39	0.01	0.55	0.01	1.96	0.03	0.74	0.01	0.52	0.01
Fe	53.49	0.17	40.19	0.63	54.17	0.95	44.01	0.15	38.03	0.44
K	$-^{b}$	$-^{b}$	$-^{b}$	$-^{b}$	$-^{b}$	$-^{b}$	$-^{b}$	$-^{b}$	$-^{b}$	$-^{b}$
Mg	8.60	0.03	6.36	0.10	8.01	0.14	6.61	0.03	9.62	0.11
Mn	1.43	0.00	0.82	0.01	1.37	0.02	0.92	0.00	2.86	0.03
Na	48.71	0.16	22.30	0.37	47.68	0.84	23.12	0.08	37.34	0.44
Ni	103.87	0.32	86.43	1.33	106.38	1.87	99.53	0.35	104.56	1.21
P	1.43	0.02	$-^{c}$	$-^{c}$	$-^{c}$	$-^{c}$	$-^{c}$	$-^{c}$	$-^{c}$	$-^{c}$
Si	105.78	0.36	70.29	1.15	104.2	1.84	78.16	0.30	72.42	0.84
Ti	15.04	0.04	11.08	0.17	14.91	0.26	12.17	0.04	11.69	0.13
V	254.06	0.77	213.67	3.26	254.03	4.43	237.69	0.82	244.89	2.80
Zn	2.15	0.01	1.85	0.03	2.21	0.04	2.54	0.01	2.60	0.03

[a] Average (x) and sample standard deviation (s) of corrected values of each individual measurement in Table 3-15 of Chapter 3.

A.6. Statistical Analysis of Bitumen Properties.

First, an analysis of variance (ANOVA) single factor test was performed to test for the equality of all means (null hypothesis: all means are the same; alternative hypothesis: two or more means are different). The null hypothesis was rejected when a probably value or p-value ≤ 0.05 was obtained. Next, a t-test (combined with an F-test to determine if the variances were equal) was used to test each pair of means separately. In addition, the Tukey's honestly significant difference (HSD) test, a single step multiple comparison procedure, was also used to test the pairwise differences of all means in a single-step, thus controlling the probability of making Type 1 errors.

Acknowledgements

A.7. References

(1) Bish, D. L.; Howard, S. A. Quantitative Phase Analysis using the Rietveld Method. *J. Appl. Crystallogr.* **1988**, *21* (2), 86−91.

(2) Hill, R. J.; Howard, C. J. Quantitative Phase Analysis from Neutron Powder Diffraction Data using the Rietveld Method. *J. Appl. Crystallogr.* **1987**, *20* (6), 467−474.

(3) Rietveld, H. M. A Profile Refinement Method for Nuclear and Magnetic Structures. *J. Appl. Crystallogr.* **1969**, *2* (2), 65−71.

(4) Cheary, R. W.; Coelho, A. A Fundamental Parameters Approach to X-ray Line-Profile Fitting. *J. Appl. Crystallogr.* **1992**, *25* (2), pp.109−121.

(5) Scarlett, N. V. Y.; Madsen, I. C. Quantification of Phases with Partial or No Known Crystal Structures. *Powder Diffr.* **2006**, *21* (4), 278−284.

(6) Wilson, S. A.; Raudsepp, M.; and Dipple, G.M. Verifying and Quantifying Carbon Fixation in Minerals from Serpentine-Rich Mine Tailings using the Rietveld Method with X-ray Powder Diffraction Data. *Am. Mineral.* **2006**, *91* (8-9), 1331−1341

(7) Turvey, C. C.; Hamilton, J. L.; Wilson, S. A. Comparison of Rietveld-Compatible Structureless Fitting Analysis Methods for Accurate Quantification of Carbon Dioxide Fixation in Ultramafic Mine Tailings. *Am. Mineral.* **2018**, *103* (10), 1649−1662.

(8) Rutgers, I. R. Relative Viscosity and Concentration. *Rheol. Acta* **1962**, *2* (4), 305–348.

(9) Montoya Sanchez, N.; De Klerk, A. Viscosity Mixing Rules for Bitumen at 1–10 wt % Solvent

Dilution When Only Viscosity and Density Are Known. *Energy Fuels* **2020**, *34*, 8227−8238.

(10) Crittenden, J. C.; Trussell, R. R.; Hand, D.W.; Howe, K.J.; Tchobanoglous, G. MWH's Water Treatment: Principles and Design, Third Edition; John Wiley & Sons, Inc: Hoboken, NJ, 2012; pp 1861–1862.

(11) Krall, A.H.; Sengers, J.V.; Kestin, J. Viscosity of Liquid Toluene at Temperatures from 25 to 150. Degree. C and at Pressures up to 30 MPa. *J. Chem. Eng. Data* **1992**, *37* (3), 349−355.

(12) Poletto, M.; Joseph, D. D. Effective Density and Viscosity of a Suspension. *J. Rheol.* **1995**, *39* (2), 323–343.

(13) Guan, J.G.; Kariznovi, M.; Nourozieh, H.; Abedi, J. Density and Viscosity for Mixtures of Athabasca Bitumen and Aromatic Solvents. *J. Chem. Eng. Data* **2013**, *58* (3), 611–624.

Appendix B. Supporting Information for Chapter 4.

B.1. Minerals used in this Study – Kaolinite and Illite:

The minerals kaolinite and illite used in this study are shown in Figure B. 1.

(a)   (b)   (c)
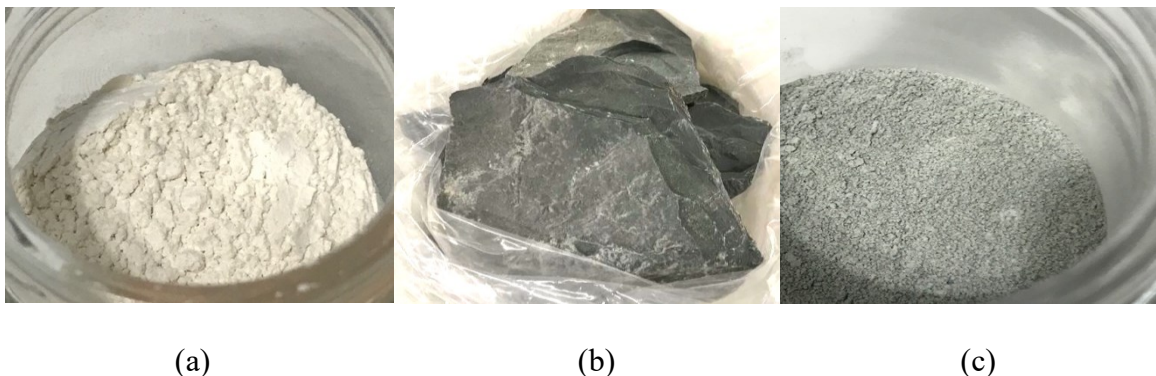
Figure B. 1. Minerals used in this study (a) Kaolinite (b) Illite Shale (c) Powdered Illite

Some of their characteristics, namely the specific surface area, pore size, pore volume, amount of acid sites, particle size and composition are summarized in Table B. 1. The Brunauer-Emmet-Teller (BET) specific surface area, pore size distribution (PSD) and pore volume were determined using nitrogen gas adsorption analysis based on BET theory (for specific surface area) and Density functional theory (DFT)/Monte-Carlo theory (for PSD and cumulative pore volume). The analysis was performed in the nanoFAB facility at University of Alberta using the Autosorb 1MP surface area analyzer (Quantachrome Instruments). ~0.5 g of mineral powder, which was previously dried in an oven at 100 °C was outgassed at 150 °C for 3 h, after which the surface area and pore size were determined using 7 BET, 20 adsorption and 20 desorption points. The N_2 adsorption isotherms were used to determine the specific surface area and the N_2 desorption isotherms were used to determine the pore size distribution and pore volume.

The amount of acid sites on the solids was measured by performing an ammonia-temperature programmed desorption (NH_3-TPD) analysis using a ChemBET TPR/TPD Quantachrome

instrument which consisted of a thermal conductivity detector. About 0.25 g of mineral sample was loaded into a U-shaped quartz cell and a small lump of glass wool was inserted into one stem of the quartz cell, to avoid lighter particles from being carried away by the gas flow. A thermocouple was placed into the sample cell to measure the temperature in the cell. The sample cell which was placed in the sample holder inside a furnace. The TPRWin software was used for gas switching, temperature programming and recording the signals. At first, sample outgassing was performed by heating the sample to a temperature of 400 °C at the rate of 25 °C/min under helium flow (75 ml/min), to remove any trapped gas or water vapor. The furnace was then allowed to cool down to 40 °C and adsorption of ammonia was conducted by passing ammonia gas (75 ml/min) over the sample for a duration of 40 min. Helium was then purged into the sample cell for 40 min to remove any physically adsorbed ammonia from the sample. The TPD analysis was then initiated by heating the sample to 400 °C at the rate of 10 °C/min under helium flow (75 ml/min). The total area under the TPD curve was obtained by integration using an OriginPro 2022 v.9.9.0.225 software. Using the calibration curve generated by the peak areas of known pulses of ammonia manually injected into the instrument, the total amount of acid sites on the minerals was calculated.

The particle size analysis was performed using the Beckman Coulter LS 13320 laser particle size analyzer by following the international standard ISO 13320:2009. The mineral powders were dispersed in a solution containing 1 % sodium hexametaphosphate (Calgon) by soaking them overnight. The mineral slurries were transferred to the laser particle size analyzer instrument and continuously pumped through an optical cell with deionized water. Laser was shone through the cell, and the intensity of diffracted light was recorded at different angles over a 1-2 min acquisition time. Using the principle of laser diffraction and Fraunhofer light scattering theory, the distribution

of sample particles across 127 size classes from 0.4 – 2000 μm was calculated. Additionally, a second optical cell using polarization intensity differential scattering was simultaneously used to determine particle sizes in the range 0.017 – 0.400 μm, resulting in a total particle size range 0.017 – 2000 μm. Table B. 1. contains the size distribution of the mineral particles of both kaolinite and illite with respect to the cumulative volume percent.

Scanning electron microscopy with energy dispersive X-ray spectroscopy (SEM-EDX) and X-ray diffraction (XRD) analyses of kaolinite and illite were conducted at the Department of Earth and Atmospheric Sciences, University of Alberta. The elemental composition estimated by SEM-EDX is included in Table B. 1., and the XRD patterns of the minerals are shown in Figure B. 2.

Table B. 1. Characteristics of Minerals used in this Study

Mineral	BET Surface Area ($m^2\,g^{-1}$)	Pore Size ($\times 10^{-8}$ m) (Mode)	Cumulative Pore Volume ($\times 10^{-5}\,m^3\,kg^{-1}$)	Amount of Acid Sites (μmol NH_3/g)
Kaolinite	7.37	2.38	3.92	40
Illite	15.69	0.51	2.56	37
Particle Size Distribution				
		Particle Diameter (μm<)		
% Cumulative Volume	Kaolinite		Illite	
10	1.18		1.93	
25	3.06		7.31	
50	6.53		87.05	
75	12.06		401.27	
90	19.77		815.33	

Mineral Composition [a]			
Kaolinite		Illite	
Impurity	%	Impurity	General Formula
Fe_2O_3	~0.5	Quartz [b]	SiO_2
TiO_2	~0.4	Pyrite [c]	FeS_2
K_2O	~1.8	Biotite [c]	$K(Mg,Fe)_3AlSi_3O_{10}(OH)_2$
Na_2O	~0.1	Apatite [c]	$Ca_5(F,Cl,OH)(PO_4)_3$
		Clinochlore [b]	$(Mg,Fe)_5Al(Si_3Al)O_{10}(OH)_8$
		Phengite [b]	$KAl_{1.5}(Mg,Fe)_{0.5}(Al_{0.5}Si_{3.5}O_{10})(OH)_2$
		Rutile [c]	TiO_2
		Smectite [c]	-

Elemental Composition (wt %) [d]				
	Kaolinite		Illite	
Element	x	s	x	s
Al	20.6	2.9	11.4	0.8
Si	23.4	1.9	29.8	2.7
O	54.0	3.5	47.7	3.0
Na	- [e]	- [e]	0.2	0.1
K	1.9	2.4	5.6	0.4
Mg	- [e]	- [e]	1.5	0.03
Fe	- [e]	- [e]	3.4	0.2
Ti	- [e]	- [e]	0.5	0.1

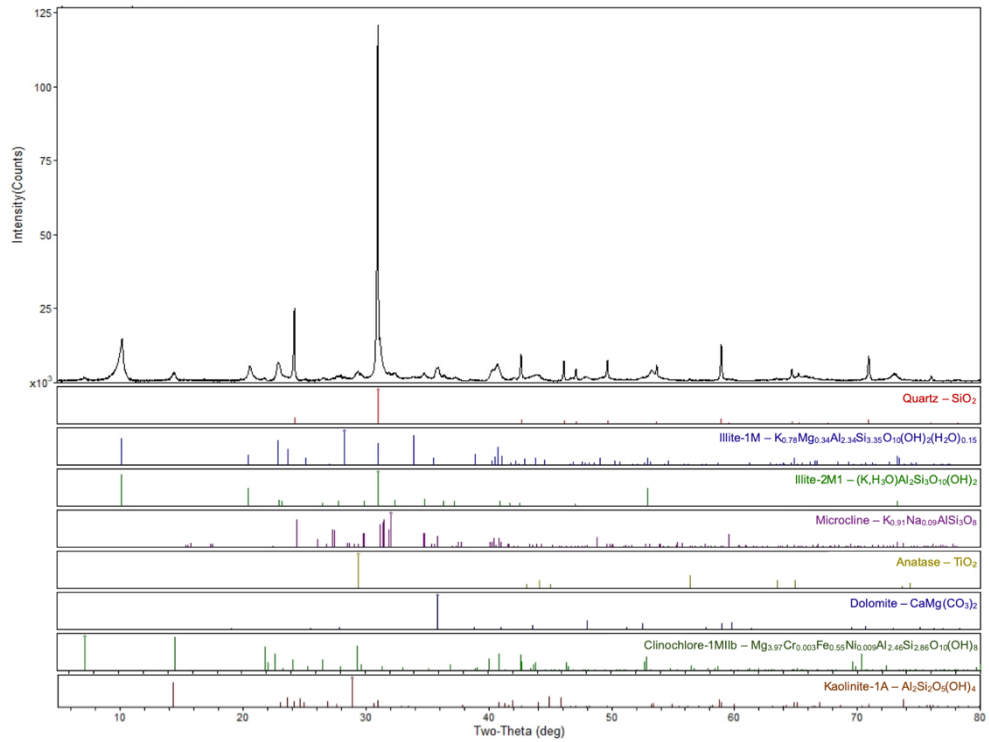[a] Supplier Information

[b] >0.5 vol %

[c] <0.5 vol %

[d] Average (x) and standard deviation (s) of four measurements
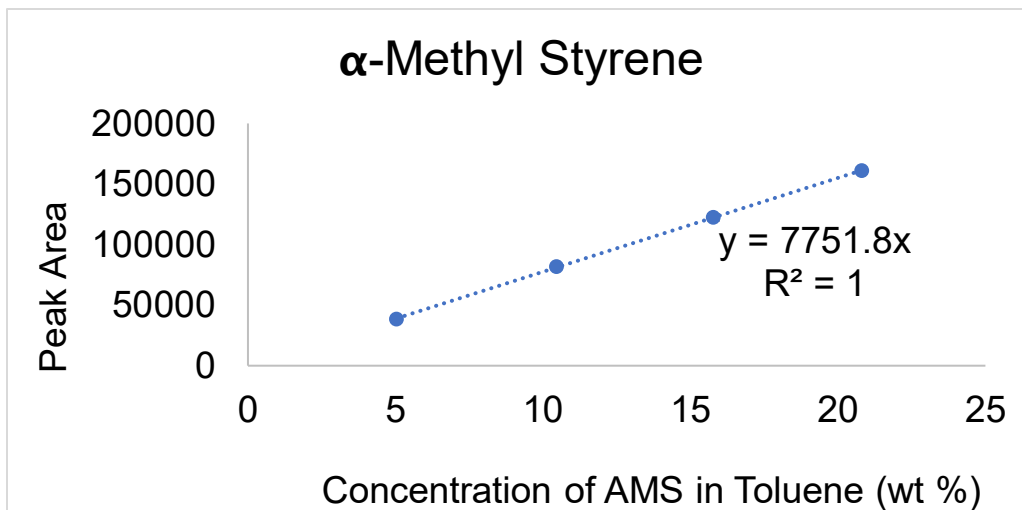
[e] Not detected
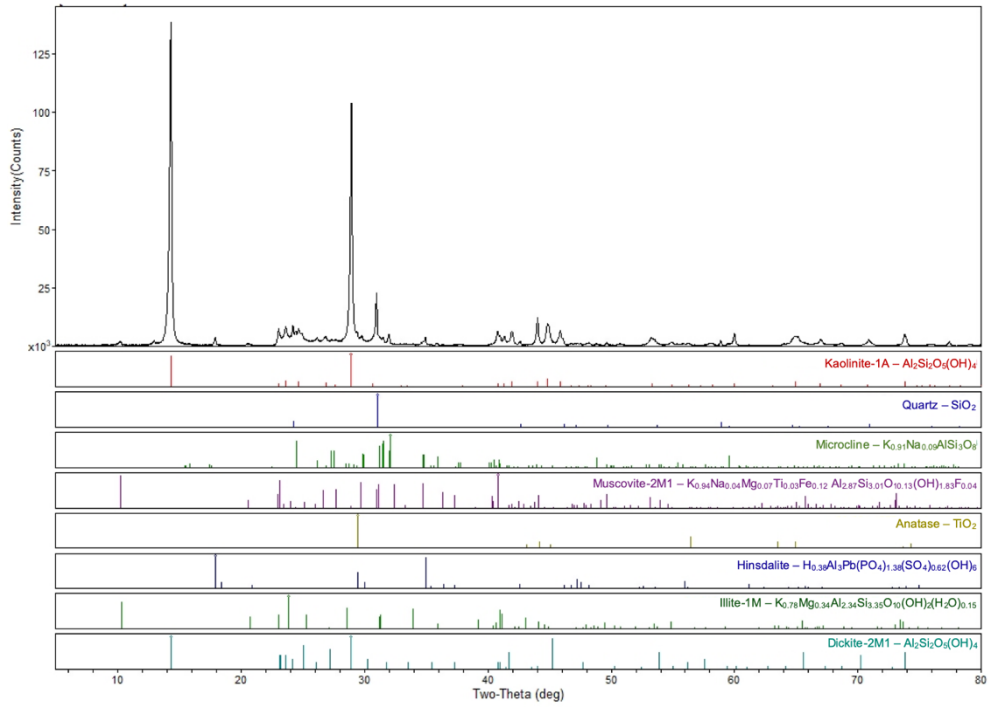
(a)

(b)

Figure B. 2. XRD Patterns of Minerals used in this Study (a) Kaolinite (b) Illite
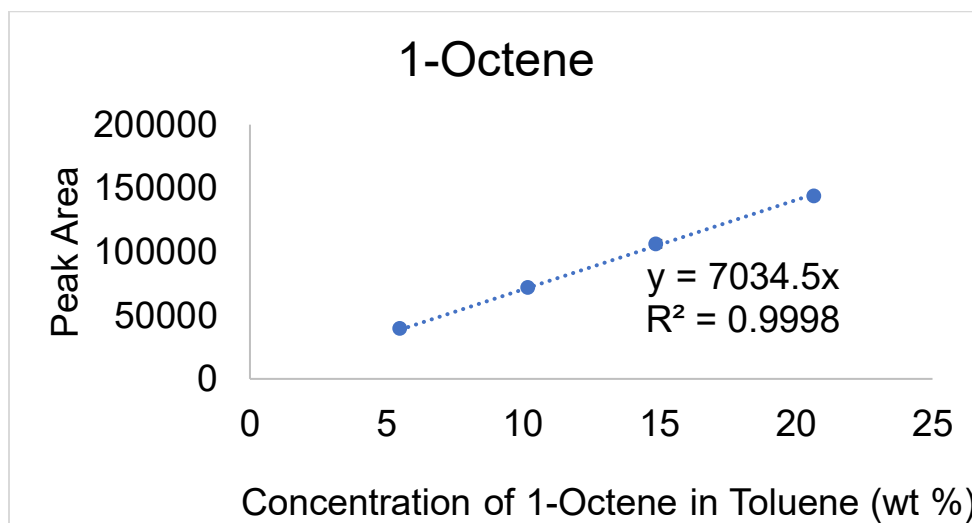
B.2. Pictures of the Micro Batch Reactor:

Figure B. 3. Photos of the Micro Batch Reactor

B.3. GC-FID Calibrations Curves:

(a)

(b)

**Figure B. 4.** Calibration Curves of **α**-Methyl Styrene (AMS) and 1-Octene in Toluene

B.4. Calculation of Liquid Conversion and AMS and 1-Octene in the Reactions:

Table B. 2. Equations for Calculating the Liquid Conversion of AMS/1-Octene (X_i) in the

Reactions [a]

Equation	
$$w_{i\,Product} = \frac{C_{i\,Product} \times (l_{Product} + l_{Solids})}{100}$$	Eq B. 1
$$l_{Solids} = \left(\frac{C_{OM\,Solids} \times w_{Wet\,Solids}}{100} \right)$$	Eq B. 2
$$w_{Wet\,Solids} = \frac{w_{Dry\,Solids}}{\left(1 - \frac{C_{OM\,Solids}}{100} \right)}$$	Eq B. 3
$$l_{Product} = (l + s)_{Product} - w_{Wet\,Solids}$$	Eq B. 4
$$X_i = \left(\frac{w_{i\,Reactant} - w_{i\,Product}}{w_{i\,Reactant}} \right) \times 100$$	Eq B. 5

[a] List of symbols used: $w_{i\,Product}$, mass of AMS/1-octene in the liquid product (g); $C_{i\,Product}$, concentration of AMS/1-octene in the reaction product determined by GC-FID (individual values from Table 4-5) (wt %); $l_{Product}$, mass of the liquid product collected after reaction (g); l_{Solids}, mass of liquid retained by the mineral solids (g); $C_{OM\,Solids}$, percentage mass of organic material retained by the mineral solids after reaction determined by TGA (individual values from Table 4-4) (wt %); $w_{Wet\,Solids}$, mass of wet mineral solids separated from the reaction product (g); $w_{Dry\,Solids}$, mass of dry mineral solids used for the reaction (individual values from Table 4-2) (g); $(l + s)_{Product}$, liquid and solid product mixture from the reaction (g); X_i, liquid conversion of AMS/1-octene (%); $w_{i\,Reactant}$, mass of AMS/1-octene used in the reaction feed (individual values from Table 4-2) (g)
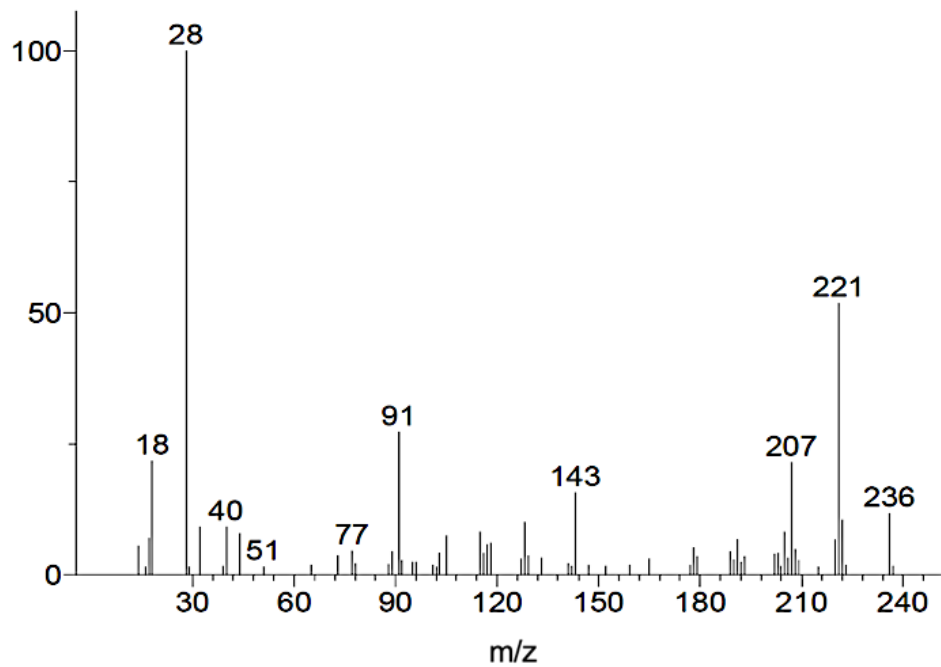
# B.5. Mass Spectra of AMS Dimers ($C_{18}H_{20}$)

(a)

(b)
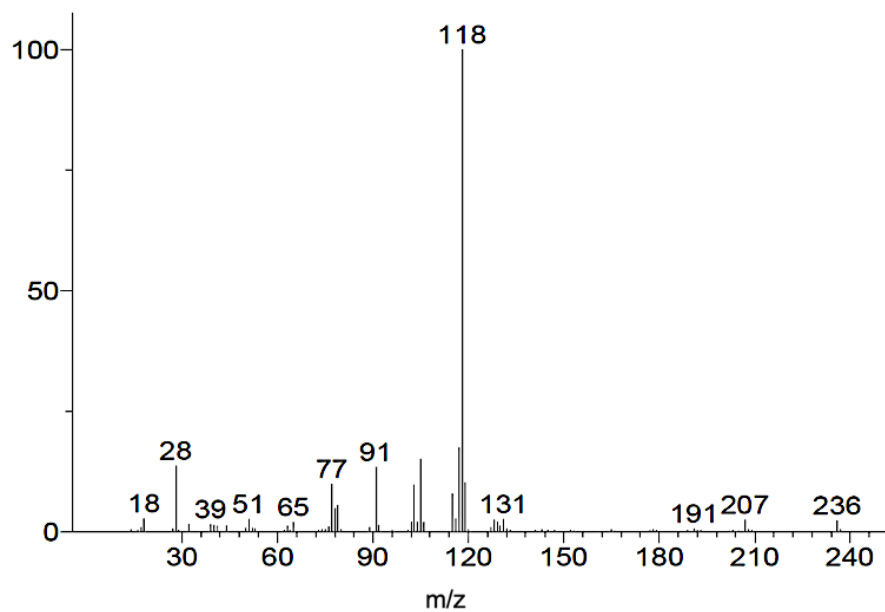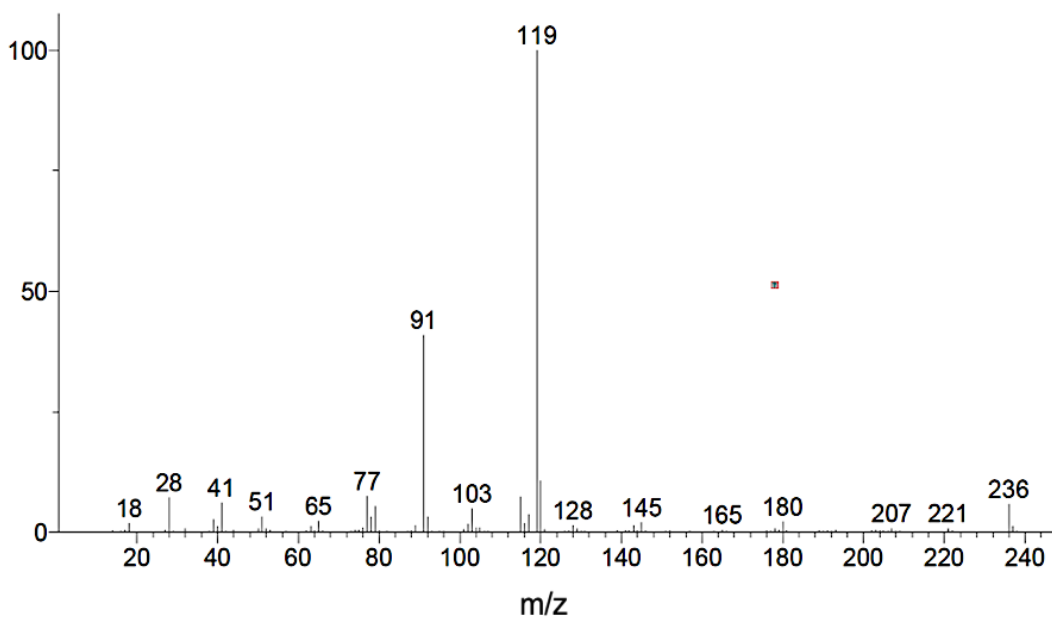
Figure B. 5. Mass Spectra of AMS Dimers (a) D_1 (b) D_2 (c) D_3

Appendix C.

A 2-liter container filled with industrial bitumen froth was subjected to a pre-heating process within a water bath set at 60 °C for a duration of 30 min. Prior to transferring it into the reactor, the froth was stirred with a spatula. For the subsequent reaction, 990 g of bitumen froth was utilized. The experimental setup consisted of a Parr 4572 HP/HT 1.8 L reactor, designed to hold pressure up to 34.5 MPa at 500 ºC, coupled to an arrangement of 316 stainless steel condensers with collection tanks (Figure C. 1.). A Specview software allowed the temperature of the reactor to be adjusted, as well as the program of the heating and cooling sequences.
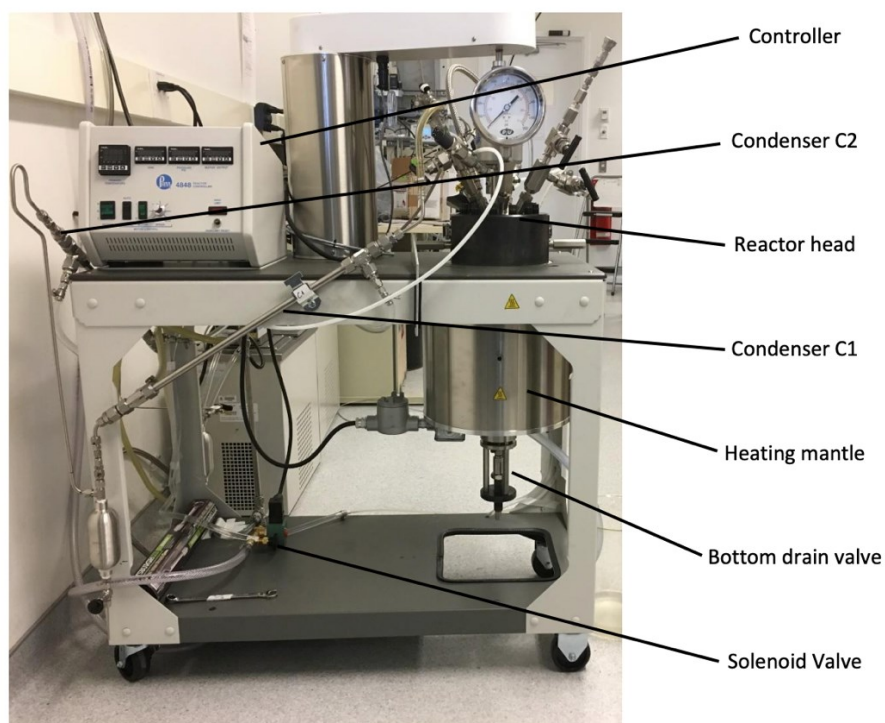
Figure C. 1. Main Parts of the Bitumen Froth Treatment Reactor Setup

Thermal treatment of bitumen froth was carried out at a reaction temperature of 250°C, and the reaction proceeded for 5 hours, starting when the reactor reached the 250 °C temperature. The

reactor was initially pressurized at 1.5 MPa of N_2. After reaction, the system was cooled to 200 °C, temperature at which water was separated by venting and subsequent condensation using the condensers-collection tanks arrangement. The time taken to cool from 250 °C to 200 °C varied from 5 min to 35 min among the experiments. These differences in the cooling time could have some implications when interpreting the data.

Post-reaction, the reactor was cooled down to room temperature. The pressure transducer, the head of the stirrer and all condensers are cooled down using water chillers. In addition, a line of distilled water was connected to the internal serpentine to cool down the contents of the reactor. About 1568 g of toluene was added to recover the bitumen-solids product mixture from the bottom drain valve of the reactor. To eliminate the solids, centrifugation and vacuum filtration techniques were applied, using conditions similar to those detailed in Chapter 3. The added toluene was then retrieved through rotary evaporation, employing conditions involving a temperature of 60°C, a rotational speed of 80 rpm, and an absolute pressure of 7.7 kPa. The overall material balance for these experiments was approximately 97%.

Viscosity measurements were carried out on untreated bitumen from the raw bitumen froth and the bitumen obtained after the thermal treatment at 250 °C. These measurements were conducted at temperatures of 25 °C, 40 °C, and 60 °C, employing a shear rate of 10 s^{-1} (as shown in Table C. 1.). Upon comparing the viscosity of untreated bitumen with that of treated bitumen at different temperatures in Table C. 1., it becomes evident that subjecting the bitumen froth to direct thermal treatment at 250°C resulted in an increase in bitumen viscosity when compared to the raw bitumen present in the bitumen froth. This directional change in viscosity aligns with the viscosity increase observed in the B+W+S reaction in Chapter 3.

Table C. 1. Viscosity (Pa.s) of the Bitumen Samples measured at 25 °C, 40 °C and 60 °C before and after reaction [a] (1 Pa.s = 1000 cP)

Bitumen Sample	25 °C		40 °C		60 °C	
	x	s	x	s	x	s
untreated bitumen	80.9	0.01	15.1	0.002	2.6	0.002
treated bitumen	235.2	0.3	33.7	0.01	4.3	0.003

[a] Average (x) and sample standard deviation (s) of measurements in triplicate.